The Rustico Inlet Study, PEI - Field Results

by

C. L. Amos(1), C. Anderson (2) and M. LeCouturier(3)

(1) Geological Survey of Canada
(2) Challenger Oceanography, Dartmouth
(3) Southampton University, UK

The Rustico Inlet Study, PEI - Field Results

by

Carl L. Amos[1] Carl Anderson[2] and Magali LeCouturier[3]

1. Geological Survey of Canada - Atlantic
Bedford Institute of Oceanography
Dartmouth, Nova Scotia, CANADA
2. Challenger Oceanography
Novalea Drive Dartmouth, Nova Scotia, CANADA
3. Department of Oceanography
The University, Southampton, UK

EXECUTIVE SUMMARY

A field program was undertaken during July, 1997 in order to make in situ measurements of currents, waves, seabed sediments, and seabed stability in Rustico Bay. These measurements were considered essential for purposes of calibration of (1) a hydrodynamic numerical model (Baird and Associates, 1990), and (2) a sediment transport numerical model (Li and Amos, 1996); these models are to be used in order to predict (1) the effects of removal of the Robinson's Island causeway on infill of the navigation channel to North Rustico, and (2) sedimentation patterns in Rustico Bay. In order for the models to be accurate, recent input data (on bathymetry, tidal elevation, sedimentation constants and coefficients, bottom sediment distribution, and turbidity) were needed, as well as good, independent calibration data sets (on tidal currents, tidal elevation, and sedimentation rates). The field program was carried out in parallel with a bathymetric survey of the region in order to furnish a recent set of water depths to the hydrodynamic model. As well, a coring program was undertaken in order to define the long-term evolution of the Bay which will provide information on conditions before the causeway was built. Finally, water quality measurements were made by Acadia University. These results are reported separately (Brylinsky, 1997)

This report describes the initial results of a field program in Rustico Bay during July, 1997. The work was mobilized from North Rustico and encompassed measurements made throughout the Wheatley and Hunter river estuaries. The following data were collected in this study: current speed and water elevation measures at four sites for 19 days; current speed and water elevation measures either side of the bridge/causeways at the heads of the Hunter and Wheatley river estuaries for a period of 5 days; 15 Sea Carousel deployments made throughout the Wheatley and Hunter river estuaries; 15 seabed camera stations at the Sea Carousel sites; and water turbidity measures at four sites in the bay.

Full data sets of good quality were recovered from all instruments. Water elevation showed a neap/spring cycle of tides. These tides showed a strong diurnal inequality at spring tides with similar patterns in tidal flow. Strong residual flows were apparent which appear anomalous. The source of these may be calibration errors in the flow sensors which are being investigated at present.

Rustico Bay seabed is composed of sand at the mouth and mud at the central and inner parts. The Bay is characterized by two regions of mud deposition located mid way up-estuary on the eastern flanks of both the Wheatley and Hunter river estuaries. These regions have the greatest susceptibility to resuspension, and contain the highest fines (silt and clay), and organic contents. Post-causeway deposition in these regions is in excess of 10 cm, in other regions deposition appears to be about 6 cm since causeway construction (based on Catscan analyses of syringe cores).

The clarity of the water was very low due to the presence of chlorophyll in suspension. As a result, the seabed was visible in bottom photographs only at the outer stations (R7, R8, R9, and

R15). The photographs show a transition from a mud bed with abundant shell fragments and inhabited by sea grasses, to a sandy/gravelly one dominated by current ripples. The most important result of the photo survey is that the seabed in Rustico Bay is highly variable in composition and faunal density, and that sea grasses appear to play a strong role in the stabilization of the seabed (see front cover).

All the required data sets and sedimentation parameters for simulation of sedimentation patterns in Rustico Bay have been compiled and provide a valuable suite of data for accurate simulation. These will be used in the next phase of the work, which is to combine the output from the calibrated Baird hydrodynamic model with the sediment transport model (SEDTRANS96) of the Geological Survey of Canada.

This work was undertaken during the height of the summer. We cannot be sure of the processes and bed responses during the winter (under ice cover) or during the changes in season. In particular, the impact of waves appears to be critical to the distribution of sediments yet we do not have sufficient data to accurately simulate these effects, nor is the theory well enough advanced to make such predictions as yet. Consequently, it is vital to develop a first-hand experience in the processes and responses of Rustico Bay and to understand how these may be linked through time. This and the accompanying studies provide us with this insight.

FRONT COVER

A photography of the seabed in the Wheatley river estuary taken during this survey. It shows the highly dense eel grass which dominates the shallower, muddier portions of the Bay.

LIST OF CONTENTS

4

1.0 INTRODUCTION

A study was undertaken on behalf of Parks Canada to provide a calibrated numerical simulation of the Hunter and Wheatley river estuaries, PEI. The numerical simulation of the estuaries were for the purposes of (1) defining the effects of removal of a causeway joining mainland PEI to Robinsons Island (the original mouth of the Wheatley river estuary) on the stability of the navigation channel to North Rustico; and (2) to determine the change in flushing of the Wheatley river estuary through removal of the causeway. A model for this purpose was developed by W.F. Baird and Associates (1990) and the predictions indicated that the removal of the causeway would have little effect on either issue. It was not possible to be sure of the results of the model because of (1) lack of good modern-day bathymetry of the region, (2) lack of long term current measurements and water level elevation within the estuaries, and (3) lack of in situ measures on the constants and coefficients that govern the sediment transport and benthic flux of material. The purpose of this study was to collect the baseline calibration data (Figure 1.1) with which to calibrate the hydrodynamic model of Baird and Associates (*ibid*) and to set up and run a 2-D finite difference model of sediment transport in Rustico Bay in order to re-assess the impact of the causeway and the consequences of various remediation alternatives.

A 2-week field program was undertaken during July, 1997 aboard the MV Mosey Boy in order to collect the required data base. This program comprised the following operations:

- 15 Sea Carousel deployments to determine the erodibility and sedimentation parameters of the seabed

- 4 InterOcean current meter moorings for (1) long term monitoring (19 days), and (2) short term monitoring (either side of the Oysterbed and Rustico causeway bridges)

- seabed camera deployments to assess the diversity of each Sea Carousel site

- box coring/syringe coring to determine the grain size and physical properties of the seabed at each Sea Carousel site

- 3 Cyclops deployments for (1) long-term monitoring (19 days) of turbidity within the water column

- vibrocoring at each of the Sea Carousel sites to determine the net sedimentation since causeway construction (reported separately by K. Edwardson and R. Cranston, Geological Survey of Canada, Atlantic)

- O_2 profiling of the topmost 30 mm of the sediment column

- CTD profiling at each Sea Carousel station as reference information (reported by Brylinsky, 1997)

- Bulk sediment samples for settling experiments in Lab Carousel (undertaken at Institut Maurice Lamontagne, Mont Joli, Quebec)

2.0 METHODS

Most of the sedimentation/erosion parameters needed to simulate sediment transport in Rustico Bay may be determined from time-series of measurements using the Sea Carousel and Lab Carousel. We sub-divide these parameters into: (1) cohesive (muddy); and (2) non-cohesive (sandy) responses. Both of these responses were expected to be evident in Rustico Bay.

The effects of consolidation and the deposition threshold cannot, at present, be determined using this instrument, and so are determined on bulk samples placed within a laboratory equivalent of the Sea Carousel called Lab Carousel. The sedimentation parameters vary spatially and so a series of 15 stations were established in order to map this variation.

2.1 Definitions of seabed erodibility and stability

The stability of sandy beds and the methods by which sand transport may be calculated is reviewed by Li and Amos (1995). In order to simulate accurately this transport we need to quantify the following parameters:

- **threshold for traction (surface creep), τ_{sc} (Pa);** this defines the beginning of sand motion. It is usually defined visually as the continuous motion of 10 grains or by extrapolation of sand transport flux to zero. Traction is evident as the generation of ripples which migrate in the direction of sand movement;

- **threshold for saltation/suspension, τ_{ss} (Pa);** this defines the decay of ripples and the beginning of sand motion into the water column from the bed. Sand moves over the bed in a series of jumps i.e. in saltation;

- **threshold for sheet flow, τ_s (Pa);** this defines the motion of the bed as a liquefied traction carpet without the presence of bedforms. It usually defines the reference concentration of sand in suspension which decreases upwards through the water column;

- **bedload transport rate as a function of applied bed stress, SED$_b$ (kg/m/s);** this defines the mass transport rate per unit width per unit time (kg/m/s) moving along the bed with grain-to-grain contact; this is calculated from the video imagery which gives bedform height (H), bedform wave length (L), and bedform migration rate (D$_r$). The mass transport rate (G$_s$) as bedload = **0.5 ρ_b H.D$_r$**, where ρ_b is the sand bulk density (determined from Catscan analyses);

- **suspension profile with height above the bed;** this defines the distribution of material suspended in the vertical, and is necessary in order to compute the suspended sediment transport rate. It is also a measure of turbidity, and the suspended mass. This parameter

6

may be used as a proxy for organic carbon suspension, nutrient fluxes, and O_2 balance of the water column;

- **suspended sediment flux (kg/m/s);** the depth integration of the suspension profile times the mean flow velocity (kg/m/s); it is determined from the OBS measures of suspended sediment concentration per unit volume times the mean current speed (U): SSC.U kg/m/s; and

- **bedform type;** this defines the type and size of ripples (in sand) or scour patterns (in mud). It is used as an input parameter in the estimation of bed shear stresses and defines the bed roughness (Li and Amos, 1995).

Erodibility of cohesive bed sediment may be defined as the ablation of that bed due to hydrodynamic forces. By contrast, stability may be defined as the resistance of a bed to hydrodynamic forces. The stability of cohesive sediment is often expressed as a single index: the erosion threshold. This index defines the resistance of the bed surface to fluid motion, but does not take into account what takes place once the erosion process has begun, nor does it account for the rate of change in strength with time and the duration over which the erosion event prevails once initiated. Furthermore, bed stability is the time-product of the upward (erosional) and downward (sedimentation) benthic fluxes, and so we must also account for the type of bed erosion (Villaret and Paulic, 1986), the nature (size, shape, and density) of the eroded material, and the associated sedimentation properties (mass settling rate, ballistic momentum flux, and mode of transport). The evolution of a cohesive bed is the sum of the responses to all stabilizing and destabilizing forces applied to that bed. The stabilizing forces impact the sedimentation character of a bed sediment; the destabilizing forces influence the erodibility of that bed. We may describe the erosion character of a bed in terms of the following attributes:

- **the erosion threshold (cohesion), $\tau_c(0)$ (in Pa);** interpreted as the point at which the surface of the bed begins to erode. There are several criteria by which this threshold is defined. In the past we choose to express it as the intercept of the sediment failure envelop with the sediment surface (Amos *et al.*, 1992b). In this report, we define it as the value of bed stress at which the suspended sediment concentration reaches ambient values in a regression plot of SSC and stress (Sutherland, 1996). As a proxy to erodibility, $\tau_c(0)$ is rather poor because of the large variations in strength just below the surface layer. Indeed, some contend that an erosion threshold doesn't exist;

- **the erosion threshold as a function of sediment depth, $\tau_c(z)$ (in Pa);** interpreted as the sediment failure envelope. It defines the changes in sediment strength (to fluid erosion) throughout the erosion process. It is based on the assumption that, at an applied bed shear stress (τ_o), bed erosion will stop when the bed has eroded to a depth (z) wherein the strength equals the applied stress: $\tau_c(z) = \tau_o$ (Mehta and Partheniades, 1982). By definition, therefore, it is applicable to type I erosion only; that is, asymptotically decaying erosion with time;

7

► **the friction coefficient, φ (in degrees)**; adapted from Terzaghi and Peck (1967) is: $\varphi = \tan^{-1}(\tau_c(z)/\sigma')$. Depth is transformed to an effective stress (σ') from a knowledge of sediment bulk density (ρ_b): $\sigma' = \rho_b g z + U'$ where g is the gravitational force and U' is the ambient pore pressure (usually unknown, but assumed to be zero in this study). φ is used to define the relative stability of a bed, its consolidation state, and bed sedimentary macro-structure;

► **the peak erosion rate, E_p (in kg/m²/s)**, as a function of applied bed shear stress and eroded depth; erosion rate shows a distinct maximum within the first 60 seconds of an applied eroding stress. This peak then diminishes with time in a fashion that defines the erosion type;

► **the mean erosion rate, E_m (in kg/m²/s)**, as a function of applied bed shear stress and eroded depth; it is defined as a function of the difference in the starting and final SSC within any velocity increment: $E_m = \delta M/\delta t = (SSC_{end} - SSC_{start})V/\Delta t \alpha$, where M is the eroded dry mass, V is the Sea Carousel volume (0.218 m³), α is the flume bed area (0.87 m²) and Δt is the duration of the applied eroding bed shear stress;

► **the type of erosion** as a function of time (erosion type) and excess bed shear stress (in Pa); it may be either asymptotically diminishing with time (type I) or constant (type II). The two types of erosion results in vastly differing final SSC's as well as eroded depths. We suppose it is controlled by the change in bed strength with depth, but not enough information is available to accurately predict when either type of erosion will occur;

► **the size spectra and modes of transport** of material eroded from the bed: type I erosion is characterised by the release of flocs and small pellets (surface erosion), and the mode of transport is largely in suspension; whereas type II erosion occurs through the release of rip-up clasts and large (8 mm) aggregates (mass erosion). In this latter case, the mode of transport is largely through saltation and surface creep, with a significant portion of the eroded material moving within 2 cm of the bed. We presume that this bedload fraction has a large impact on the nature of the erosion process itself through the delivery of momentum to the bed. Also, sedimentation of material eroded in type II fashion will be much more rapid than that of material derived from type I erosion; and

► **the rate of change in the erosion threshold (Pa/s)**; this is a time-dependent attribute of the sediment which is largely unknown due to its complexity but largely the result of consolidation. We may chart its evolution in terms of changes in sediment bulk density with sediment depth and with time.

We define sedimentation character in terms of:

► **the deposition threshold, τ_d (Pa)**: that is, the applied stress at which material begins to drop back to the bed. It is dependent on SSC (through the influence on water density and viscosity), and the mass settling velocity of the particles in suspension (W_s). We determine

it in settling experiments within the Lab Carousel using "fresh" sediment and local seawater. We transform the mass settling equation of Krone (1962) as follows: $\delta M/\delta t = W_s SSC(1 - \tau_0/\tau_d)$; and $\tau_d = \tau_0/(1 - [\delta M/\delta t.1/SSC.W_s])$. τ_d cannot be determined using Sea Carousel at present because of the uncertainties resulting from dispersion (leakage). Consequently, it was determined within Lab Carousel using two bulk samples collected in Rustico Bay;

▸ **the mean mass deposition rate, D_m (kg/m^2/s)**; under an applied stress below the critical for deposition, we may determine D_m from the rate in change in SSC: $D_m = \delta M/\delta t = (SSC_{start} - SSC_{end})V/\Delta t\alpha$. This can only be determined using Lab Carousel at the present time, and so was determined on the two bulk samples in Lab Carousel;

▸ **the still water mass settling velocity, W_s (m/s)**; measured at the end of each Sea Carousel erosion experiment, the still-water mass settling velocity may be defined as $D_m = \delta M/\delta t. = SSC_t.W_s (1 - \tau_0/\tau_d)$; where SSC_t is the mean suspended sediment concentration for the settling period under consideration. Thus $W_s = \delta M/\delta t. 1/SSC_t$,; and

▸ **the concentration decay constant, k (1/s)** usually defined from either $SSC(t) = k\ln(t) + b$, or from $SSC(t) = SSC_0 \exp(kt)$. A concentration half-life can be derived from this procedure.

2.2 Catscan analysis for bulk density

Bulk density was evaluated using x-ray computed tomography, which offers advantages over standard methods of analysis by being digital (yielding spectra of the Hounsfield Unit), three-dimensional, and able to resolve to a voxel volume of 0.06 mm^3 anywhere within the sample. The Hounsfield Unit (HU) for any voxel is defined as $HU = 1000(\mu_s - \mu_w)/\mu_w$, where μ_s and μ_w are the x-ray linear attenuation coefficients of sediment and fresh water, respectively. According to Beer's Law, μ_s is a function of sediment bulk density ρ_b. Thus for a constant photoelectric effect, HU should vary in direct proportion to ρ_b. To eliminate negative numbers, and to approximate bulk density, Orsi (1994) transformed HU into a computed tomographic number CT with the expression $CT = 1 + (HU/1000)$ so that air has $CT \approx 0$, water has $CT \approx 1$, and natural, fine-grained sediment has CT between 1 and 3. The transform from CT to fresh-water wet bulk density was: $\rho_b = 390 + 670(CT)$ kg/m^3; $r^2 = 0.992$; n = 11 (Amos *et al.* 1996).

Syringe cores were analysed in a frozen state, wet bulk densities were therefore corrected to equivalent densities at 25°C (the water temperature at the time of sampling) from the following relationship: $\rho_{b25} = \rho_{b0} (\rho_{25}/\rho_0)$, where ρ_{b25} = wet bulk density at 25°C, ρ_{b0} = wet bulk density at 0°C, ρ_{25} = water density at 25°C (1.026), and ρ_0 = water density at 0°C (1.000).

Sediment volume (V_s) is determined as: $V_s = (\rho_{b25} - \rho_{25})/(2650 - \rho_{25})$, that is the wet sediment bulk density minus the water density divided by the sediment buoyant density. Once V_s is known, porosity (η) can be found: $\eta = (1 - V_s)$, from which the dry weight bulk density (ρ_{bd25}) may be determined: $\rho_{bd25} = (1 - \eta\rho_b)$ and the water content (W) of the sediment is: $W = \eta\rho_{25}/(1 - \eta\rho_b)$.

9

3.0 INSTRUMENTATION

3.1 Sea Carousel instrumentation and deployment

Sea Carousel is a benthic annular flume designed for field use in subaqueous settings. The carousel is 1.0 m in radius with an annulus 0.15 m wide and 0.30 m high. It weighs approximately 150 kg in air and 40 kg in water and is made of aluminum (Figure 3.1.1a). Flow in the annulus is induced by rotating a movable lid which is driven by a 0.75 HP digital stepping motor that is powered from the surface (Figure 3.1.2a). Eight small paddles, spaced equidistantly beneath the lid, induce a flow of water in the annulus. The Carousel is equipped with three optical back scatter sensors (OBS's; Downing, 1983; Figure 3.1.3a). Two of these are located non-intrusively on the inner wall of the annulus at heights of 0.03 and 0.18 m above the skirt (the skirt is a horizontal flange situated around the outer wall of the annulus 0.04 m above the base; it was designed to standardize penetration of the flume into the seabed; Figure 3.1.1a). The third OBS detects ambient suspended sediment concentration outside the annulus, or it may be used to detect internal sediment concentration at a height between the other two. A Seapoint® fluorometer is installed at a height of 0.20 m above the bed in order to monitor chlorophyll through fluorescence (Figure 3.1.4a; instrument to left of Sontek). A sampling port, through which water samples may be drawn, is situated in the outer wall of the annulus at a height of 0.2 m above the skirt. It is used to calibrate the three sensors under well mixed conditions, for the calibration of the fluorometer, and for the collection of biological and chemical samples (Figure 3.1.4b). Water samples are pumped to the surface through the rubber tubing using a Gusher® foot-pump.

Mean flow within the Sea Carousel is determined from a relationship between azimuthal speed and lid rotation presented in Amos, *et al.* (1992a) and later verified in laboratory measurements made using a Laser-Doppler flow sensor (Fung, 1995). Mean tangential lid rotational speeds are detected through a shaft end-coder resting on the lid (Figure 3.1.2b). Tangential (U_y) and vertical (U_w) current speeds are also detected by a Marsh-McBirney® EM flow meter (model 512) situated *circa* 0.18 m above the bed. A Sontek® ADV current meter is also installed at a height of 0.15 m above the bed and mid-flow (Figure 3.1.4a). It logs three components of flow (azimuthal, radial, and vertical) at 25 Hz in 2 minute bursts midway through each speed increment. Controller boards for each sensor and necessary power (12 VDC) are derived from an underwater pod located above the annulus (Figure 3.1.1b). Output voltages from all sensors are digitized and transformed to scientific units on a Campbell Scientific® CR10 data logger and stored on a Campbell Scientific® SM192 storage module (storage capacity of 96,000 data values), also located in the underwater pod. The data logger is interrogated and programmed from the surface using a micro-computer linked to the data logger through an RS232 interface. Maximum sampling rate of all channels is approximately 2 Hz, whereas U_y and U_w may be logged at rates up to 10 Hz. All channels may be monitored and displayed on the surface computer allowing the operator to control experiments interactively. Bed shear stress is varied in time through a series of script commands issued to

the digital motor through a surface controller. The data stored from each deployment is downloaded at regular intervals through the RS232 cable throughout each experiment.

A window is located in the inner flume wall for purposes of observing and recording the mechanics of bed failure. Visual observations are made using a Sony® Handycam 8 mm video recorder model CCD-V11 held in an Amphibico®, Amphibian V11 underwater housing. Light is provided by two Amphibico® 75-Watt underwater lights powered from the surface. The housing has a lens that corrects for underwater geometric distortions and so is suitable for accurate image scaling. The camera images 30 frames/s. A co-axial cable connects the camera to a surface monitor for real-time detection. Sequential video images are digitized for particle trajectories at varying heights above the bed. From these, velocity profiles may be constructed. From such profiles, thicknesses of the logarithmic part of the benthic boundary layer may be determined and friction velocities computed. These latter values may then be compared with laboratory measures as a check.

The location, depth and survey date of the 15 Sea Carousel deployments described in this report are summarised in Table 3.1.1

STATION	DATE	LAT	LON	DEPTH
R1	15 July, 1997	46° 26.50'	63° 18.22'	3.8
R2	15 July, 1997	46° 24.40'	63° 14.83'	1.5
R3	16 July, 1997	46° 25.17'	63° 14.19'	2.1
R4	16 July, 1997	46° 23.34'	63° 14.13'	1.8
R5	17 July, 1997	46° 24.90'	63° 14.11'	2.3
R6	18 July, 1997	46° 25.51'	63° 13.81'	2.9
R7	18 July, 1997	46° 25.75'	63° 15.35'	4.2
R8	19 July, 1997	46° 26.10'	63° 18.16'	5.9
R9	20 July, 1997	46° 26.58'	63° 16.51'	4.8
R10	20 July, 1997	46° 25.97'	63° 18.95'	3.2
R11	21 July, 1997	46° 25.33'	63° 13.27'	3.8
R12	21 July, 1997	46° 26.01'	63° 18.55'	2.6
R13	22 July, 1997	46° 26.24'	63° 18.34'	2.6
R14	22 July, 1997	46° 26.83'	63° 18.11'	1.6

STATION	DATE	LAT	LON	DEPTH
R15	23 July, 1997	46° 27.19'	63° 17.70'	2.7

Table 3.1.1 A summary of the Sea Carousel stations undertaken in this study.

The deployment and operation of the Sea Carousel in this study were held as constant as possible for comparability. The Carousel was lowered to within 1 m of the bed. Thereafter it was lowered at a slow rate of 5-10 cm/s (subsequently found to be below the threshold for erosion). After landing, the Carousel data logger was initialized to log for about 10 minutes under still-water conditions. This initial period was used to determine the current meter zero offsets, and to clear the water of any material suspended by the instrument landing. The experiment consisted of subjecting the seabed to 13 increments of flow, each increment lasting 5 minutes. The instantaneous azimuthal current speeds were quite variable due to: (1) macro turbulence; (2) variations in lid speed; and (3) changes in bed roughness. Finally, the flow was stopped for a 10-minute period and still-water settling of eroded material was monitored. After retrieval of the Carousel, the site was marked with a red Grimsby float and fixed with GPS which was considered accurate to ± 50 m.

Motor settings (V) were used as the standard input to control flow in the Sea Carousel. These settings show a perfectly linear relationship to lid rotation (rot) of the form: $rot = 1.374 \times 10^{-4}(V) + 0.058$ m/s, $r^2 = 0.98$, $n = 13$ (Figure 4.1.16). The index azimuthal velocity (U_y) is also linearly related to motor setting in the form: $U_y = 7.89 \times 10^{-5}(V) + 0.03$ m/s. The clear-water friction velocity (U_*) is defined as: $U_* = 0.0557(rot)$, and bed shear stress (τ_o) is derived form $\tau_o = \rho U_*^2$.

The measured azimuthal horizontal (u) and vertical (w) current speeds are defined as: $u = (u_v - 212) * 0.007 + 0.65$ m/s, and $w = 0.007 * w_v$ m/s, where u_v and w_v are the EMCM voltage outputs for the horizontal and vertical sensors respectively.

The effect of the suspended sediments on the suppression of the bed shear stress is complex. It can cause fluid stress reduction through: (1) thickening of the viscous sub-layer; (2) consumption of momentum in maintaining material with finite W_s in suspension, and (3) fluid momentum transfer to accelerating saltating aggregates. Nominal experiments on this subject are inconclusive. Nevertheless, a stress reduction algorithm has been applied to our data on the basis of results in Amos *et al.* (1992a) and Li and Gust (in prep.). This algorithm is: $\sqrt{(\tau_s/\rho)} = \sqrt{(\tau_o/\rho)} - [0.2267(\log_{10}(SSC)).((\sqrt{(\tau_o/\rho)}/6.35))$ cm/s (evaluated for SSC in mg/L).

The raw data from Sea Carousel is processed in order to produce the calibrated plots for interpretation. The processing involves the following:

- define date and time for each record;

12

- read record and despike the data (± 2 standard deviations);

- time-average the 1Hz data (usually over 10 seconds);

- transform time-averaged OBS output to SSC (mg/L) and suspended mass (kg);

- transform current meter output to azimuthal and vertical flow (m/s);

- compute the clear water friction velocity (m/s) and bed shear stress (Pa);

- determine stress reduction due to SSC;

- compute fluid density and flow Reynolds number;

- determine lid rotational speed (m/s);

- compute diffusion rate out of flume (kg/s);

- compute corrected suspended mass (kg) and erosion rate (kg/m^2/s);

- compute mean eroded depth (mm);

- compute mass settling velocity (m/s) and equivalent particle diameter (m); and

- write output files for plotting results (*.asc; *.dia; *.set).

Estimates of bed shear stress have been made using ADV burst-sampled data (25 Hz) using the inertial-dissipation method (Stapleton and Huntley, 1995). The results of this work is well beyond the scope of this study and forms part of the post-graduate studies of a Ph.D. student currently working on the Rustico Bay study (Magali LeCouturier, Department of Oceanography, Southampton University, UK). The purpose of this work is to verify the estimates of bed shear stress made using other, simpler methods, and to assess changes in bed roughness throughout the Bay .

Bedload transport predominates at the sandy sites. The various parameters needed to model bedload transport are derived from the video measurements made in situ on the Sea Carousel. These include the onset of traction, the height, wavelength, and migration rates of ripples, and the onset of saltation and suspension. In the case of sand, the total load (traction + suspension) is the product of bedload derived from ripple migration and the suspended sediment flux derived from the product of the current meter and OBS outputs.

3.2. Current meter

Four InterOcean® S4 current meters were used in this project (Figure 3.2.1b). These meters are

equipped with sensors to monitor two horizontal components of flow and hydrostatic pressure. Note that these meters are not equipped with temperature and salinity sensors, so these data were not collected in this project. The current meters were programmed to log current speed and direction and hydrostatic pressure for 1 minute at 2 Hz each 30 minutes for the duration of the deployments. The meters were set to a height of 0.5 m above the seabed in a tubular aluminum frame ballasted with lead. A summary of the deployments of these meters is given in Table 3.2.1.

STATION	LAT	LON	RECORDS	START	END
RUSTICO1	46° 25.60'	63° 14.49'	906	1730/6July,1997	1400/25July,1997
RUSTICO2	46° 24.52'	63° 14.58'	856	1800/6July,1997	1330/24July,1997
RUSTICO3	46° 26.75'	63° 18.23'	915	1630/6July,1997	1730/25July,1997
RUSTICO4	46° 27.46'	63° 16.79'	858	1630/6July,1997	1330/24July,1997
RUSTICO6	46° 24.10'	63° 15.30'	385	1502/24July,1997	1502/1Aug,1997
RUSTICO7	46° 24.52'	63° 14.58'	384	1544/24July,1997	1514/1Aug,1997
RUSTICO8	46° 26.75'	63° 18.23'	334	1813/25July,1997	1643/1Aug,1997
RUSTICO9	46° 25.90'	63° 19.15'	331	1928/25July,1997	1628/1Aug,1997

Table 3.2.1 A summary table of the current meter deployments.

3.3 Bottom Camera

A submersible 35 mm still camera was used to photograph the seabed at each reference station in this survey. The camera was mounted on a tubular frame with a flash unit and a trigger weight release mechanism (Figure 3.2.1a). At each station, the camera was raised and lowered 6 times between pauses of 30 seconds to allow the flash to recharge. Colour, 100 ASA, print film was used in association with a daylight flash unit. Photographs covered an area about 1 x 1.5 m of the seabed and were taken at a height of about 1 m.

3.4 Cyclops

Three Cyclops' were used in this study. Cyclops is a self contained turbidity sensor (see Figure 3.2.1b, the Cyclops is clamped to the vertical part of the tubular frame with the active sensor lowermost). It logs backscatter within the water column and stores the intensity of backscatter on an Onset® data logger. Backscatter is logged using a Seapoint® Optical Backscatter Sensor mounted on the endcap of the underwater housing. The housing is mounted on a ballasted frame in order that the OBS is about 30 cm above the bed. A sediment trap is also attached to the frame in order to collect a sample to calibrate the OBS to mass concentration of suspended sediment.

14

The sensors were set up to log time-averaged turbidity each 72 seconds. The location and duration of deployment of the three Cyclops' are given in Table 3.4.1.

STATION	LAT	LON	START	END
CYCLOPS1	46° 25.60'	63° 14.49'	1053/6July,1997	1415/24July,1997
CYCLOPS2	46° 24.52'	63° 14.58'	1056/6July,1997	1308/24July,1997
CYCLOPS5	46° 26.79'	63° 16.40'	1058/6July,1997	1430/25July, 1997
CYCLOPS8	46° 26.75'	63° 18.23'	1811/25July,1997	1640/1Aug,1997

Table 3.4.1. A summary of the Cyclops deployments

3.5 Bottom sampling and grain size analyses

Bottom sediment samples were collected using a medium VanVeen grab sampler. Sub-samples were collected for: (1) grain size analysis and sediment textural analysis; (2) organic content (loss on ignition); and (3) bulk density profiles (through syringe coring). Oxygen profiles of the topmost 10 cm of the sediment column were also undertaken upon sample recovery. Bulk samples were also collected for later use in Lab Carousel in order to determine the deposition parameters.

4.0 RESULTS

Good results were obtained from 15 stations within the Wheatley and Hunter river estuaries. The time-series for each station are shown in Figures 4.1.1 to 4.1.15. A consistent time-series of flow was applied in each case. This corresponded to lid speeds of 0.084, 0.166, 0.249, 0.332, 0.416, 0.50, 0.58, 0.67, 0.75, 0.83, 1.00, 1.17 and 1.33 m/s. Each flow speed was held for 300 seconds. Acceleration rate was constant between each speed increment. The motor stalled for brief periods during early experiments due to overheating of the motor controller. This did not appear to affect the results.

The relationship between OBS output and SSC was determined from 14 samples pumped from the Sea Carousel at each increment of lid speed. The regressions of these results are plotted in Figures 4.1.17 and 4.1.18 for the upper (OBS1) and lower (OBS3) sensors respectively. In view of the overlap in results and the wide scatter at any station, a constant set of calibration equations were used for all stations. These took the form: $SSC1 = 2.06(OBS1) - 0.000428(OBS1^2) - b_1$ mg/L, and $SSC3 = 2.105(OBS3) - 0.000447(OBS3^2) - b_2$ mg/L, where b_1 and b_2 are offsets which depend on the ambient SSC in each case and so are site specific. Plots of corrected SSC and erosion rate (E) versus applied bed shear stress are given for each station in Figures 4.1.19 to 4.1.33. In almost all cases, SSC shows an increase in proportion with the logarithm of time. The data show little scatter, and so the derivation of erosion threshold (τ_c), using the regression of SSC with log time, is considered reliable to ± 0.05 Pa. The solid dots in each figure illustrate the

data which was used to determine the erosion threshold and erosion rates. The open dots are considered to be pre-erosion measurements.

4.1 Sea Carousel - Erosion thresholds and erosion rates

A clearly defined erosion threshold was evident at all stations. A summary of the results on erosion threshold is given in Table 4.1.1. All stations were on mud except for stations R8, R9 and R15 which were on sand and gravel. The erosion threshold of bottom sediments in the Wheatley river estuary showed a steady increase seaward from 0.11 Pa at the Oysterbed Bridge to 0.62 Pa at the sandy mouth (Figure 4.1.34). The Hunter river estuary was quite different in the distribution of erosion thresholds as no systematic trend was evident. The highest threshold of the survey (0.79 Pa) was found off Rustico Harbour navigation channel reflecting the coarsest grain size in this region. The difference in trends between the two estuaries implies that they are quite different in sedimentation character and circulation patterns, and so should be considered as two independent systems. However, the erosion thresholds in the Hunter river estuary was equivalent to the values in the central and inner Wheatley river estuary.

STATION	EROSION THRESHOLD (Pa)	MEAN DIAMETER(mm)	% FINES
R1	0.11	6.8×10^{-3}	85
R2	0.18	2.09×10^{-2}	59
R3	0.21	2.61×10^{-2}	46
R4	0.26	3.61×10^{-2}	41
R5	0.14	3.54×10^{-3}	96
R6	0.22	2.80×10^{-2}	48
R7	0.41	3.33×10^{-2}	38
R8	0.51	0.187	0.2
R9	0.62	0.252	0.2
R10	0.26	1.58×10^{-2}	61
R11	0.17	3.56×10^{-3}	96
R12	0.17	6.38×10^{-3}	85
R13	0.4	6.38×10^{-2}	26
R14	0.15	1.55×10^{-2}	64
R15	0.79	0.219	0.7

Table 4.1.1 A summary of the Sea Carousel results and sediment size.

There is a weak, positive relationship between erosion threshold and sediment bulk density (Figure 4.1.35) above a density of about 1200 kg/m^3. Below this density there appears to be no relationship between these two variables and the erosion threshold is constantly low. This trend is typical of both estuaries. Furthermore, there is an inverse relationship between erosion threshold and mud content to a maximum mud content of about 60% (Figure 4.1.36) which is also the same for both estuaries. Above 60% mud content the threshold is uniformly low at around 0.2 Pa. It follows that the regions of mud content above 60% have bulk densities below 1200 kg/m^3, and are highly susceptible to resuspension.

Regions of high mud content are found along the eastern flanks of the two estuaries and about mid-way between the mouths (Figure 4.1.37). This is unusual as most estuaries show a fining in bottom sediment towards the head of the estuary. Thus the regions of Rustico Bay that are the most susceptible to erosion are the easternmost parts of both the Wheatley and Hunter river estuaries.

Differences in seabed stability between the two estuaries appear due only to changes in seabed sediment composition. The lowest thresholds are found along the eastern flanks; the highest thresholds are associated with the sands situated at the mouths of the two estuaries.

The erosion rates of bottom sediment, once the erosion threshold has been exceeded, have been determined and the results for each station presented in Table 4.1.2. In all cases, erosion rate E showed a logarithmic increase with applied bed shear stress τ_o and so is predictable with relatively high confidence under unidirectional flows. The data on which the erosion rates are determined are plotted in Figures 4.1.19 to 4.1.33. The erosion rate constant, (a measure of the degree of erosion) was plotted against location within the estuary (Figure 4.1.34). The highest erosion potential is associated with the regions of high mud content i.e. the easternmost parts of the two estuaries.

STATION	EROSION RATE	r^2
R1	$E = 3.44 \times 10^{-3} + 3.80 \times 10^{-3} (\log_{10}\tau_o)$	0.95
R2	$E = 1.26 \times 10^{-3} + 1.86 \times 10^{-3} (\log_{10}\tau_o)$	0.92
R3	$E = 1.20 \times 10^{-3} + 1.63 \times 10^{-3} (\log_{10}\tau_o)$	0.97
R4	$E = 1.26 \times 10^{-3} + 2.02 \times 10^{-3} (\log_{10}\tau_o)$	0.98
R5	$E = 2.52 \times 10^{-3} + 2.62 \times 10^{-3} (\log_{10}\tau_o)$	0.97

STATION	EROSION RATE	r^2
R6	$E = 1.21 \times 10^{-3} + 1.83 \times 10^{-3} (\log_{10} \tau_o)$	0.86
R7	$E = 4.32 \times 10^{-3} + 1.11 \times 10^{-3} (\log_{10} \tau_o)$	0.95
R8	$E = 2.57 \times 10^{-3} + 9.38 \times 10^{-3} (\log_{10} \tau_o)$	0.93
R9	$E = 0.10 \times 10^{-3} + 0.51 \times 10^{-3} (\log_{10} \tau_o)$	0.87
R10	$E = 1.99 \times 10^{-3} + 3.24 \times 10^{-3} (\log_{10} \tau_o)$	0.99
R11	$E = 2.48 \times 10^{-3} + 3.10 \times 10^{-3} (\log_{10} \tau_o)$	0.98
R12	$E = 2.20 \times 10^{-3} + 2.74 \times 10^{-3} (\log_{10} \tau_o)$	0.98
R13	$E = 0.44 \times 10^{-3} + 1.43 \times 10^{-3} (\log_{10} \tau_o)$	0.90
R14	$E = 7.83 \times 10^{-5} + 2.01 \times 10^{-3} (\log_{10} \tau_o)$	0.96
R15	$E = 0.19 \times 10^{-3} + 1.82 \times 10^{-3} (\log_{10} \tau_o)$	0.84

Table 4.1.2. A summary of the erosion rates as a function of applied bed shear stress

In general, the erosion rate decreased seaward in both estuaries. Differences in E were about a factor of 3 between the inner and outer stations. The scatter in results in the Hunter river estuary were larger than those from the Wheatley suggesting a more complex depositional environment in the Hunter (Figure 4.1.35).

4.2 Sea Carousel - Mass settling, deposition rates and sediment size

The still water mass settling rate was determined for each station by analysis of SSC time-series during a 10 minute period at the end of each experimental run. Plots of these time-series for each station are shown in Figures 4.2.1 to 4.2.12. The sandy sites were not analyzed due the rapid settling of any sand in suspension, and the dominance of bedload transport. A summary of results is given in Table 4.2.1.

STATION	MEAN W_s (m/s)	MEAN diam (m)	SSC_o (mg/L)
R1	6.85×10^{-4}	5.85×10^{-5}	748
R2	5.09×10^{-4}	3.53×10^{-5}	317
R3	8.75×10^{-4}	6.41×10^{-5}	623

STATION	MEAN W_s (m/s)	MEAN diam (m)	SSC_o (mg/L)
R4	9.06×10^{-4}	5.89×10^{-5}	926
R5	8.13×10^{-4}	1.22×10^{-4}	735
R6	1.20×10^{-3}	9.26×10^{-5}	394
R7	1.12×10^{-3}	6.03×10^{-5}	588
R10	7.46×10^{-4}	8.52×10^{-5}	994
R11	1.05×10^{-3}	1.34×10^{-4}	377
R12	1.58×10^{-3}	1.31×10^{-4}	826
R13	8.75×10^{-4}	4.54×10^{-5}	674
R14	6.22×10^{-4}	7.89×10^{-5}	419

Table 4.2.1. A summary of the settling rates, mean particle diameters of settling material, and starting SSC, determined from Sea Carousel at the muddy sites.

Mass settling rate varies between 10^{-4} and 10^{-3} m/s, which is within the range of normal sedimentation rates in estuaries. The Wheatley river estuary shows a weak trend of increasing sedimentation rate from the head of the estuary seaward (Figure 4.2.13). Differences are of the order of a factor of two. There are no clear trends in the Hunter river estuary and sedimentation rates vary between the same limits as the Wheatley. The main control on sedimentation mass deposition is turbidity in the water column. This is seen from Figure 4.2.14 which shows the concentration decay constant (k) is linearly related to turbidity. W_s on the other hand is independent of suspended sediment concentration and has an estuary-wide average of 9.15×10^{-4} m/s (Figure 4.2.15).

The grain size of suspended material is derived based on the assumption that the density of the eroded aggregates is that of the bed from which they are derived. Based on this assumption we see that grain size generally diminishes with settling time: the largest grains settling first. Figure 4.2.2 shows the trend of settling of aggregates which start in the medium sand size range and end in the medium silt size range. Stations R5 and R12 are anomalous as the aggregate sizes are consistently in the fine sand range. This may be related to the effects of the aquaculture of mussels which produce pseudo-feces of around this size. The inference of this is that erosion takes place by release of the pseudo-feces from the bed. At station R12, this is associated with the highest settling rate measured in the Bay (1.58×10^{-3} m/s) which suggests that the mussels may help stabilize the bottom sediments of the Bay.

19

4.3 Bulk density and O_2 profiles

Bulk density profiles of the topmost 10 cm of sediment at each of the mud dominated stations were derived from Catscan analysis of frozen syringe cores collected from VanVeen grab samples. These profiles are plotted in Figures 4.3.1 to 4.3.12. The plots show the mean bulk density and the standard deviation of about 14,000 individual measures derived from each tomographic slice (1.5 mm). The standard deviation is thus a measure of the heterogeneity of the sediment, not the error in measurement. The bulk density of bed material ranges from about 1400 to 2000 kg/m³. This is higher than would be expected from recently deposited, muddy sediments (1000 - 1200 kg/m³) and suggests that the post-causeway rate of deposition has been low. Material of relatively low bulk density and relatively low standard deviation prevails near the surface. This we assume is related to post-causeway conditions. This layer is typically 6 cm thick at stations R2, R3, R4, R6 and R14 (a sedimentation rate of 0.2 cm/a). At stations R1, R5, R11 and R12 this layer is greater than 10 cm. At site R7 there appears to have been no sedimentation, while at station R13 only 1 cm of deposition appears to have taken place. The regions of relatively high sedimentation appear close to the sites of the mussel nets which suggests that sedimentation is enhanced by their presence. In almost all cases, the topmost 1 cm exhibits the largest gradient in bulk density; perhaps related to biological activity.

The surface bulk density is plotted with location in Figure 4.3.13. Notice that the lowest values are associated with the regions of highest mud content; that is in the easternmost parts of the two estuaries. Also notice that the bulk densities in the vicinity of the two causeway/bridges at the heads of the estuaries are relatively high, illustrating low sedimentation rates and perhaps even scour.

The distribution of oxygen throught the topmost sediment layer has been determined for each of the muddy stations. The plot of the results is shown in Figure 4.3.14. In general the bottom waters have an O_2 content of below 30% which is low for coastal waters (which usually are 100% saturated). A buffer layer is found in the tomost 3-5 mm of the sediment bed within which there is a rapid decrease in O_2 content to zero (reducing conditions). Below the buffer layer, the sediments are in O_2 deficit, meaning that any erosion of this material to the water column will result in depletion of O_2 in the water column.

4.4 Sea bed photography

The water clarity was extremely low during the period of this survey due to the abundance of photosynthesizing plankton. Consequently the inner stations were completely masked from view. Only stations R1, R7, R8, and R9 yielded images of the bed, and even here the green colouration of the water is evident. At station R1, the seabed is dominated by dense sea grass (Figure 4.4.1). At station R7, the bed is variable in roughness and composition. In Figure 4.4.2 we see variable, though abundant shell fragments including disarticulated oysters. Also evident is the presence of sea grass which has the effect of stabilizing the seabed. The variability in shell size and abundance is evident in Figure 4.4.3 while the variability in sea grass abundance is clear in Figure 4.4.4.

Station R8 is at the transition from a muddy to a sandy substrate, though sand dominates. Sea grass is evident in places, though the site is characterized by current-formed ripples in sand (Figure 4.4.5). The sand is largely devoid of shell material and sea grass disappears seaward. The presence of gravel, rounded cobbles, and large fragments of shell indicate that station R9 is a region of active scour (Figure 4.4.7). The site is extremely variable in sediment composition and benthic communities (Figure 4.4.8).

4.5 Current meter measurements

The S4 current meters were programmed to record pressure and current for 60 seconds at a sampling rate of 2 Hz every 30 minutes. These data were downloaded from the instruments immediately following recovery, and the manufacturer's calibrations were used to convert them to engineering units (depth h in meters, current speed r in cm/s, and direction d_{mag} in degrees relative to magnetic north). Further processing and plotting was performed in MATLAB.

All measurements recorded before and after a current meter was in place on the bottom were eliminated. Magnetic direction d_{mag} was converted to true direction d_N (relative true north) by subtracting the magnetic declination of 23.5° from d_{mag}. Current rate and true direction (r, d_N) were then resolved into eastward and northward velocity components (u, v).

The 30-minute vector mean current $(u, v)_{mean}$ and average sea level h_{mean} were calculated by averaging (u, v, h) over the 1-minute (120-sample) sampling periods and converting units to m/s. Mean current and direction $(r, d_N)_{mean}$ were then calculated from $(u, v)_{mean}$. The time t of each resulting observation was computed in hours from 00:00 1 July 1997, and data files were created containing $(u, v, h)_{mean}$ and t for each current meter deployment.

Time series plots of 30-minute mean depth and vector mean current, both as (r, d_N) and (u, v), are presented in Figures 4.5.1 through 4.5.8. Tidal variations in water depth h and current are evident, and both current direction and rate exhibit tidal variation. The offshore sea level time series (deployment rus4, Fig. 4.5.4) exhibits shifts in mean sea level around 8 July and 14 July. During the intervening time period (8-14 July), the current speed is anomalously low compared to the rest of the record. Also during this period, the current direction is restricted to the range 110-240°T, much less than during the prior and subsequent portions of the record. It is suspected that a shift in the position of the current meter mooring may be responsible for the change in mean sea level at rus4, although it is not clear how this may have also affected the current measurements.

The locations of the current meters are shown in Figure 1.1. Rus1 was situated in the central Wheatley river estuary; Rus2 was located in the inner Wheatley river estuary; Rus3 was the control site situated in the central Hunter river estuary; and Rus4 was placed immediately outside the entrance to Rustico Bay. These deployments were for 20 days each and were synchronous. Rus7 replaced Rus2 and was used to compare against Rus6 which was situated inside the Oysterbed Bridge. Rus8 replaced Rus3 and was used to compare with currents recorded at Rus9 which was located inside the Hunter river bridge.

Rus1 showed strong diurnal inequalities and associated inequalities in tidal flow. Peak tidal currents were 0.2 m/s and took place during spring tides . Peak neap tidal currents were typically 0.1 m/s. These peak tidal flows appeared to be to the east (flood dominated). The inequalities were greatest during spring tides. During neap tides the two tides were of equal magnitude. Large fluctuations in the currents were evident between 15 and 20 July. These fluctuations cannot be due to wind as the weather was settled for this period. Rus2 showed lower peak current speeds (being further landwards) which were a maximum of 0.1 m/s. The currents in central Hunter estuary were strongly linked to the tidal elevation and peaked during the flood period of the tide. As in the Wheatley, there was a strong diurnal inequality during spring tides and significant fluctuations of non-tidal origin throughout the period of deployment. Rus4 showed a period of drift and offset between 7 and 15 July. At other times, the currents were strongly diurnal due to the inequality of the tides. The currents here peaked at 0.3 m/s. The tide heights inside the two bridges (Rus6 and Rus9) were comparable to those recorded by those seawards (Rus7 and Rus8) and so no attenuance of the tidal wave by the bridges was noted. Tidal currents, on the other hand, were about 50% lower inside the bridge than outside.

4.6 Cyclops measurements

The data collected by the three Cyclops were of good quality, and the instruments collected data throughout the periods of deployment. The locations of the Cyclops are shown in Figure 1.1. The OBS's were calibrated against material collected in the sediment traps and the OBS voltage was transformed to SSC. The time-series of SSC are shown in Figure 4.6.1. The results indicate that during the first half of the deployment, tides were relatively small and little resuspension was taking place. During spring tides at stations 1 and 5, however, considerable resuspension took place to levels in excess of 150 mg/L (the saturation point of the sensors). At station 2 we see a steady increase in SSC probably diagnostic of increases in organic content of the water column.

4.7 Sediment grain size

Results of the sediment grain size analyses are given in Appendix 1. A plot of the mud content in bottom sediments is shown in Figure 4.1.37. The regions of mud deposition are to the east of each estuary (greater than 7 phi) and the transition from sand to mud (4 phi) is located near stations R7 and between R14 and R15 (Table 4.1.1). In general, the grain size of bottom sediment decreases towards the heads of the two estuaries, although the effects of the causeway/bridges can be seen at stations R10 and R2 as reversals in this general trend.

4.8 Settling parameters

The settling characteristics of sediments within Rustico Bay have been determined using the Lab Carousel using Gulf of St. Lawrence seawater and bulk samples collected at stations R11 and R12. These were considered representative of the muddier parts of the Wheatley and Hunter river estuaries respectively. The bulk samples were mixed at four concentrations for about 30 minutes at current speeds strong enough to maintain suspension, then the speed was reduced in small

increments each lasting 20 minutes. Within these increments the rate of change in suspension was recorded and the decay constant (k) derived. This constant was determined from the relationship : $SSC(t) = SSC_0 \exp(kt)$, A summary of the results is given in Table 4.8.1.

SAMPLE	STRESS(Pa)	DEPOSITION STRESS (Pa)	DECAY CONSTANT	SSC(mg/L)	r^2
R11-1-1	0.31	0.47	-9.11×10^{-5}	65	0.92
R11-1-2	0.23	--	-1.94×10^{-4}	66	0.92
R11-1-3	0.14	--	-2.60×10^{-4}	66	0.99
R11-1-4	0.03	--	-2.62×10^{-4}	66	0.99
R11-1-5	0.00	--	-1.49×10^{-4}	65	0.86
R11-2-1	0.39	0.40	-4.87×10^{-5}	150	0.63
R11-2-2	0.31	--	-6.05×10^{-5}	142	0.42
R11-2-3	0.23	--	-4.79×10^{-4}	145	0.97
R11-2-4	0.14	--	-8.33×10^{-4}	154	0.99
R11-2-5	0.03	--	-1.02×10^{-3}	160	0.99
R11-2-6	0.00	--	-6.30×10^{-4}	154	0.98
R11-3-1	0.39	0.37	-9.77×10^{-6}	368	0.04
R11-3-2	0.31	--	--	375	0.19
R11-3-3	0.23	--	-7.63×10^{-4}	374	0.96
R11-3-4	0.14	--	-1.99×10^{-3}	425	0.99
R11-3-5	0.03	--	-2.65×10^{-3}	391	0.97
R11-3-6	0.00	--	-1.94×10^{-3}	358	0.96
R11-4-1	0.39	0.35	-1.37×10^{-5}	606	0.22
R11-4-2	0.31	--	--	476	0.13
R11-4-3	0.23	--	-5.63×10^{-4}	633	0.97
R11-4-4	0.14	--	-2.38×10^{-3}	422	0.98
R11-4-5	0.03	--	-4.77×10^{-3}	553	0.98
R11-4-6	0.00	--	-6.09×10^{-3}	768	0.98

SAMPLE	STRESS(Pa)	DEPOSITION STRESS (Pa)	DECAY CONSTANT	SSC(mg/L)	r^2
R12-1-1	0.33	0.72	-2.68×10^{-4}	44	0.88
R12-1-2	0.28	--	-3.69×10^{-4}	41	0.90
R12-1-3	0.23	--	-4.66×10^{-4}	40	0.95
R12-1-4	0.18	--	-4.37×10^{-4}	40	0.91
R12-1-5	0.11	--	-5.16×10^{-4}	40	0.97
R12-1-6	0.00	--	-1.68×10^{-4}	40	0.79
R12-2-1	0.33	0.43	-7.83×10^{-5}	240	0.77
R12-2-2	0.28	--	-1.37×10^{-4}	236	0.91
R12-2-3	0.23	--	-2.66×10^{-4}	240	0.98
R12-2-4	0.18	--	-3.04×10^{-4}	237	0.99
R12-2-5	0.11	--	-2.95×10^{-4}	239	0.75
R12-2-6	0.00	--	-1.57×10^{-4}	243	0.95
R12-3-1	0.33	0.32	-2.08×10^{-5}	423	0.07
R12-3-2	0.28	--	-3.01×10^{-4}	403	0.87
R12-3-3	0.23	--	-7.17×10^{-4}	397	0.98
R12-3-4	0.18	--	-8.47×10^{-4}	400	0.98
R12-3-5	0.11	--	-9.52×10^{-4}	430	0.98
R12-3-6	0.00	--	-6.31×10^{-4}	400	0.95
R12-4-1	0.40	0.52	-6.68×10^{-5}	928	0.77
R12-4-2	0.32	--	-7.79×10^{-5}	953	0.70
R12-4-3	0.24	--	-4.36×10^{-4}	952	0.99
R12-4-4	0.15	--	-8.36×10^{-4}	1033	0.99
R12-4-5	0.04	--	-9.89×10^{-4}	969	0.97
R12-4-6	0.00	--	-8.54×10^{-4}	960	0.94

Table 4.8.1. A summary of the settling results from samples collected at sites R11 and R12. The

results are for differing sediment concentrations and differing flow speeds.

The time-series of the Lab Carousel settling experiments are given in Figures 4.8.1 to 4.8.8. As can be seen, mass deposition increases with increasing SSC and decreasing current speed. In Figures 4.8.9 to 4.8.16, the rate of change in SSC is plotted in log-linear form. Curiously, still water settling is lower than that of the lowest current speed (Figure 4.8.9). Although the trends are almost straight lines, some show complex patterns of settling indicating a more complex settling trend with time. In general, k varied inversely in a linear fashion with stress. Two examples are shown in Figures 4.8.17 and 4.8.18 for SSC's of 150 and 950 mg/L. k also varied linearly with SSC, although the form of the fit was quite different for the two samples analyzed (Figure 4.8.19). This relationship took the forms:

$$k_{11} = -6.77 \times 10^{-4} - 8.56 \times 10^{-6}(SSC_o)$$

$$k_{12} = -1.24 \times 10^{-4} - 8.00 \times 10^{-7}(SSC_o)$$

The deposition threshold has been determined by plotting k against applied shear stress, deriving the best-fit regression line, and solving for $k = 0$. These were derived for each concentration (Table 4.8.1). The mean values for R11 and R12 are $0.40 \pm 4.5 \times 10^{-2}$ Pa and 0.50 ± 0.15 Pa.

4.9 Bedload transport rates (SED_b)

Bedload transport rates have been determined from video results from stations R8 and R15, where the seabed was largely sand. These results are summarized in Table 4.9.1. Bedload transport took place by the generation of ripples between 1 and 2 cm in height. The threshold for bedload transport (τ_{sc}) was 0.39 Pa for station R8 and 0.42 Pa for station R15. These values are about double those determined from the Shields parameter (from SEDTRANS - 0.16 and 0.18 Pa respectively), and possibly reflect the use of a flatbed calibration of bed shear stress to applied flow over rough beds. The partitioning of shear stresses into skin friction and form drag is a discussion beyond the scope of this work. The transport rate (SED_b) increased with excess bed shear stress (τ) in a linear fashion in both cases studied in the form $SED_b = 0.0633(\tau_o - \tau_b)$; $r^2 = 0.92$ (Station R8) and $SED_b = 0.0166(\tau_o - \tau_{sc})$; $r^2 = 0.71$ (Station R15). The sand at station R15 is thus harder to move, which is in keeping with the coarser grain size at this site (see Table 4.1.1).

The suspension of sand takes place at critical stresses (τ_s) of 0.51 Pa at station R8 and 0.79 Pa at station R15. These values are about double those expected using the Bagnold criterion (from SEDTRANS - 0.23 and 0.36 respectively). Above these stress levels, sand moves into suspension and is transported as a suspended sediment flux. This has been determined for the Sea Carousel time series and is plotted in Figures 4.9.1 and 4.9.2. The bedload transport rates at station R8 are about an order of magnitude smaller than the suspended sand flux and so forms only a small part of the total load. The total transport (SED_t = bedload + suspended load) is shown in Figure 4.9.1b. Note that the total load increases as a linear function of excess bed shear stress in the form
: $\log_{10}(SED_t) = 0.400(\tau_o - \tau_{sc})$; $r^2 = 0.90$.

25

Figure 4.9.2 shows the sand transport results for station R9. Despite considerable scatter, there appears to be a linear relationship between suspended sand flux and excess shear stress: $\log_{10}$ $(\text{SED}_{t)} = -1.37 + 0.459(\tau_o - \tau_{sc})$; $r^2 = 0.60$. A similar trend was found in the N. Rustico navigation channel (R15) which is plotted in Figure 4.9.3.

STATION	TIME	MASS(kg/m/s)	STRESS (Pa)
8	1354	3.0×10^{-3}	0.55
8	1400	1.2×10^{-2}	0.67
8	1404	1.8×10^{-2}	0.76
8	1406	1.5×10^{-2}	0.8
8	1412	3.1×10^{-2}	0.98
8	1416	3.6×10^{-2}	1.2
15	1331	1.9×10^{-4}	0.45
15	1341	8.0×10^{-3}	0.74
15	1345	1.0×10^{-2}	0.94
15	1349	1.8×10^{-2}	1.18
15	1351	1.2×10^{-2}	1.2
15	1353	1.2×10^{-2}	1.2

Table 4.9.1 A summary of the bedload transport measurements made at stations R8 and R15

5.0 CONCLUSIONS AND RECOMMENDATIONS

A full complement of data has been gathered in the Rustico Bay system and will provide the basis for the set-up and calibration of a numerical simulation of the sediment transport pathways and flushing of the tidal waters of the Bay. This data set includes measurements of the tidal currents and water level throughout the system. The results indicate that the 1 m tides are very complex demonstrating a marked diurnal inequality especially during spring tides. The expectation of this is that the flood tide would be long and of low magnitude while the ebb would be short and of greater magnitude (thus enhancing flushing). The measured currents were not so clear cut and showed residuals which were inconclusive. The source of this problem is being investigated presently. One surprise of the study was the apparent lack of effect of the two bridge-causeways on the propagation of the tidal wave into the upper reaches of the Bay. Despite this, accelerated flow near the bridges is evident in bottom sediment type, and the presence of algae upstream

suggests that the bridges are having an impact on the passage of sediments and organic matter.

Cyclops was deployed alongside the current meters and 20 days of good records were recovered. The data showed that resuspension of bottom material took place during periods of wave activity and as a result the benthic flux of sediment, organics, nutrients, and toxins is an important contribution to the water quality of the Bay.

Sea Carousel was deployed at 15 stations throughout the Bay. The results showed a trend of increasing resistence to erosion from the head seawards. The thresholds for erosion and erosion rates have been well-defined and show a correlation with sediment mud content and bulk density of seabed material. The Hunter and Wheatley rivers show similar ranges in values although the spatial trends vary. This may reflect the distribution of aquaculture sites, which appears to enhance sedimentation.

Catscan analyses of syringe cores collected in the topmost 10 cm of the seabed suggest that post-causeway sedimentation has been generally less than 6 cm. This material appears to be higher in organic matter than the material below.

Bottom sediment samples from each Sea Carousel site have been analyzed for grain size. The distribution of muddy sediments is atypical. In most estuaries, mud content increases steadily headwards. Here, the highest mud content is found along the eastern margins of the two estuaries. This may reflect the effects of the bridge-causeways, or the aquaculture activities in the region.

Bottom photographs were masked by high chlorophyll in the water column. The bed was only visible at the sandy outer stations. Here, the presence of eel grass was evident if patchy, and the seabed composition was highly variable.

Sedimentation studies undertaken in Lab Carousel defined well the threshold for deposition, the mass settling rate and the decay constant for two muddy sediments (one from the Wheatley and one from the Hunter river estuary). The two samples were markedly different in their settling rates. The Wheatley river sediments appear to settle much faster than the Hunter counterparts. This together with the apparently different distribution in sediment properties between the two estuaries indicates that they should be considered as separate systems.

6.0 REFERENCES

Amos, C.L., Grant, J., Daborn, G.R. and Black, K. 1992a. Sea Carousel - a benthic annular flume. Estuarine, Coastal and Shelf Sciences 34: 557-577

Amos, C.L., Daborn, G.R., Christian, H.A. Atkinson, A. and Robertson, A. 1992b. In situ erosion measurements on fine-grained sediments from the Bay of Fundy. Marine Geology 108: 175-196.

Amos, C.L., Sutherland, T.F., Radzijewski, B. and Doucette, M. 1996. A rapid technique to

determine bulk density of fine-grained sediments by X-ray computed tomography. Journal of Sedimentary Research 66(5): 1023-1039.

W.F. Baird & Associates, Coastal Engineers Ltd. 1990. North Rustico Sediment transport study North Rustico, PEI. Submitted to Public Works Canada, Charlottetown, PEI: 60p.

Brylinsky, M. 1997. Data report for collection and analysis of field data for the environmental assessment of the removal of the Rustico Island causeway, Prince Edward Island. Acadian Centre for Estuarine Research Report: 24p.

Downing, J. P. 1983 An optical instrument for monitoring suspended particulates in ocean and laboratory. Proceedings of Oceans'83: 199-202.

Fung, A. 1995. Accurate calibration measurements of flow in Lab Carousel under varying lid rotations. Unpublished Contract Report 23420-5-M083 to Geological Survey of Canada.

Gibbs, R.J., Matthews, M.D. and Link, D.A. 1971. The relationship between sphere size and settling velocity. Journal of Sedimentary Petrology 41: 7-18.

Krone, R.B. 1962. Flume studies on the transport of sediment in esturial shoaling processes. Final Report Hydraulic Engineering Laboratory and Sanitary Engineering Research Laboratory. University of California, Berkeley.

Li, M. Z. and Amos, C.L. 1995. SEDTRANS92: a sediment transport model for continental shelves. Computers & Geosciences 4: 533-554.

Mehta, A.J. and Partheniades, E. 1982. Resuspension of deposited cohesive sediment beds. Eighteenth Conference Coastal Engineering: 1569-1588.

Stapleton, K.R. and Huntley, D.A. 1995. Seabed stress determination using the inertial dissipation method and the turbulent kinetic energy method. Earth Surface Processes and Landforms. 20: 807-815.

Sutherland, T.F. 1996. Biostabilization of estuarine subtidal sediments. Unpublished Ph.D. Thesis, Dalhousie University, Halifax: 179p.

Terzaghi, K. and Peck, R.B. 1967. Soil Mechanics in Engineering Practice. Publ. John Wiley & Sons, New York: 729p.

Villaret, C. and Paulic, M. 1986. Experiments on the erosion of deposited and placed cohesive sediments in an annular flume. Report to Coastal and Oceanographic Engineering Department, University of Florida, Gainesville.

7.0 ITINERARY

DATE	OPERATION
5 July, 1997	To N. Rustico - preparing current meter moorings
6 July	Deployment of 4 S4 current meter moorings in Rustico Bay
13 July	Arrive N. Rustico for major GSCA/ACadia field program
14 July	Mobilizing Mosey Boy, setting up shore-based laboratory
15 July	Stations R1 and R2
16 July	Station R3 and R4
17 July	Station R5
18 July	Station R6 and R7
19 July	Station R8
20 July	Station R9 and R10
21 July	Stations R11 and R12
22 July	Stations R13 and R14
23 July	Station R15; demobilizing Sea Carousel
24 July	Recovery of current meter moorings, download data; redeploy
25 July	Seabed camera statio
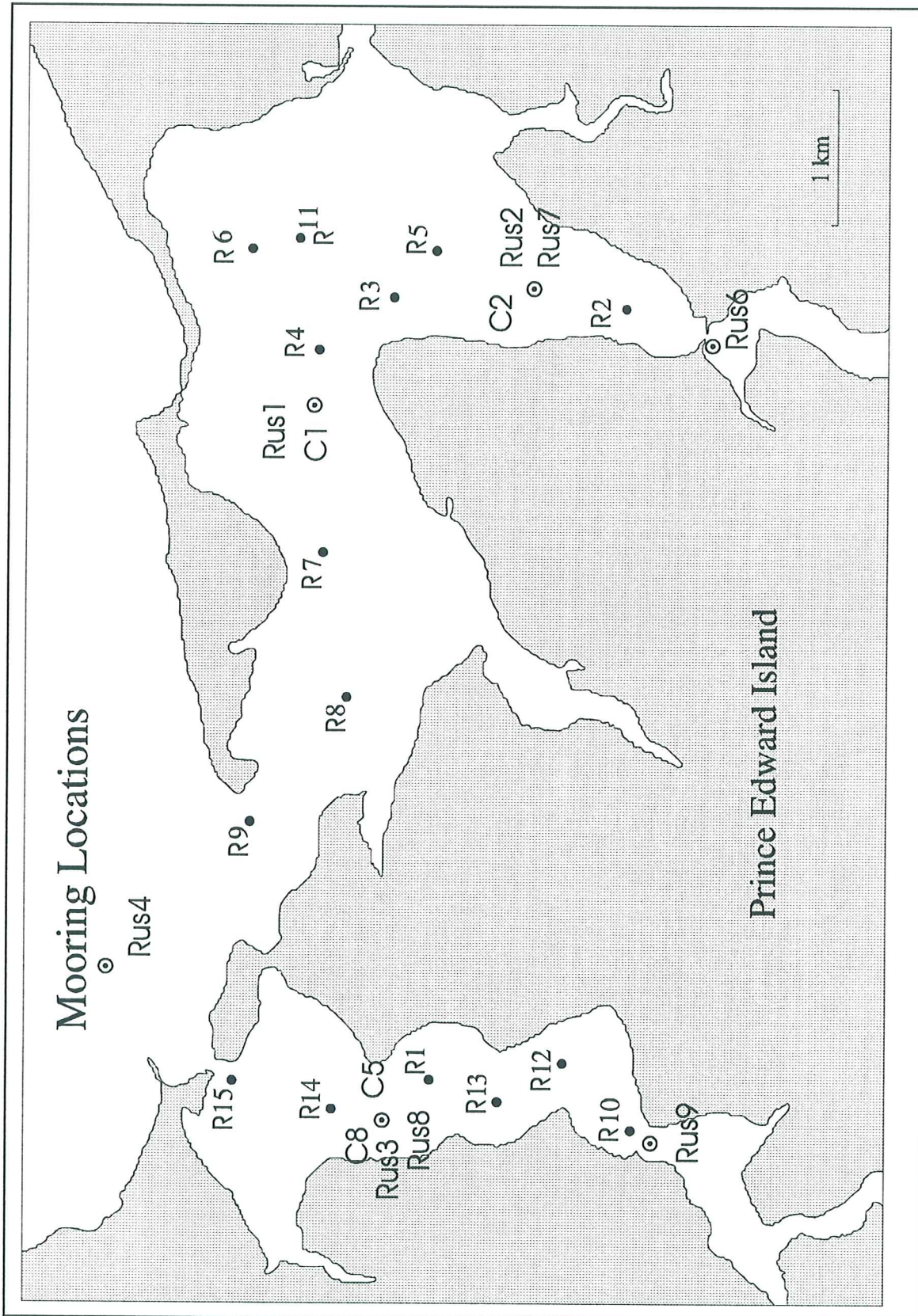
Figure 1.1. The study region of Rustico Bay showing the two estuaries surveyed: the Hunter river estuary and the Wheatley river estuary. The locations of the current meters (Rus), the Cyclops (C) and the Sea Carousel stations (R) are also shown.

Figure 3.1.1 A. The Sea Carousel benthic flume aboard Mosey Boy; B. the controller pod to Sea Carousel showing the underwater bulk heads and connectors for the three OBS sensors, the EM flow meter, the shaft-endcoder, the fluorometer and data communications.
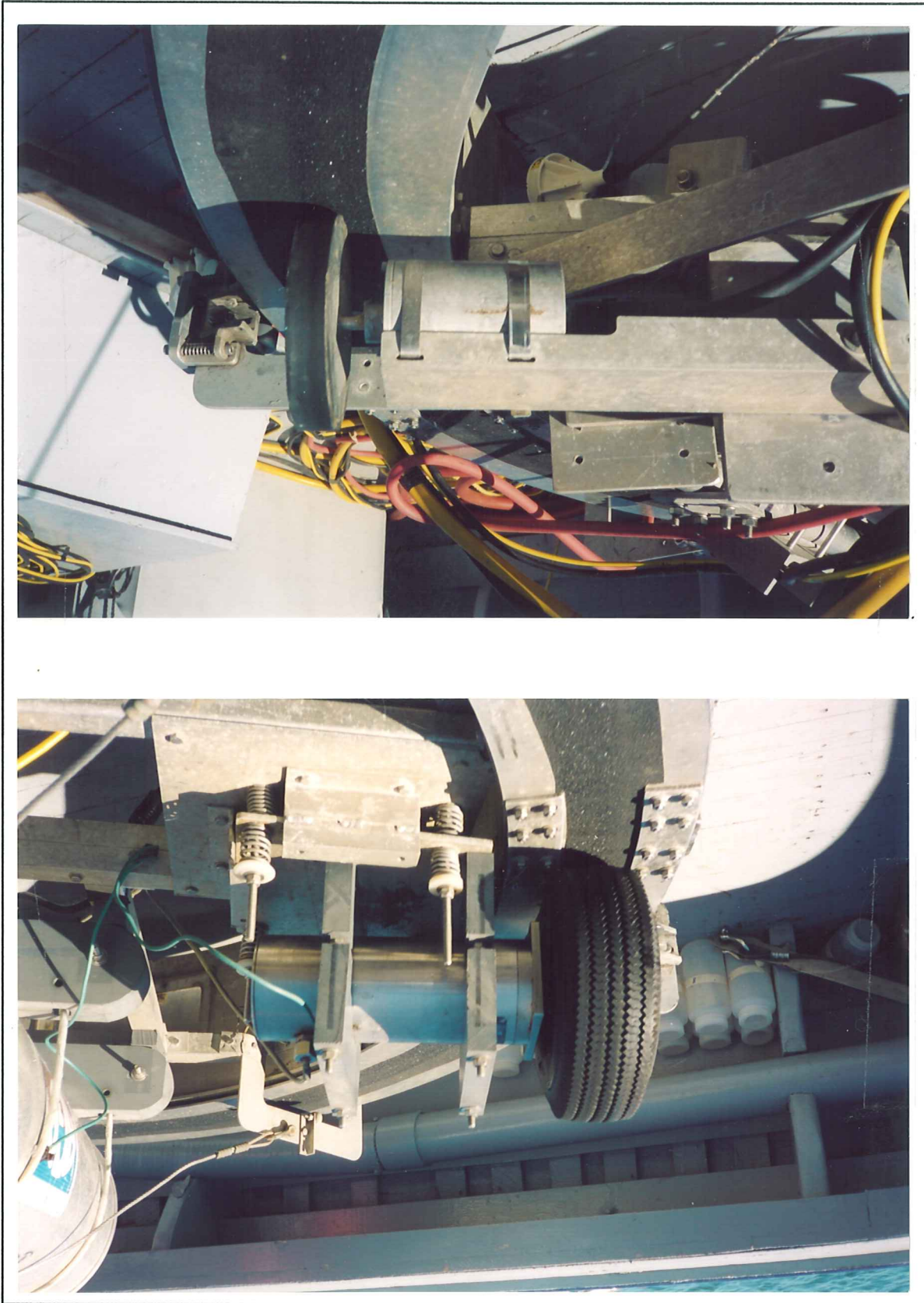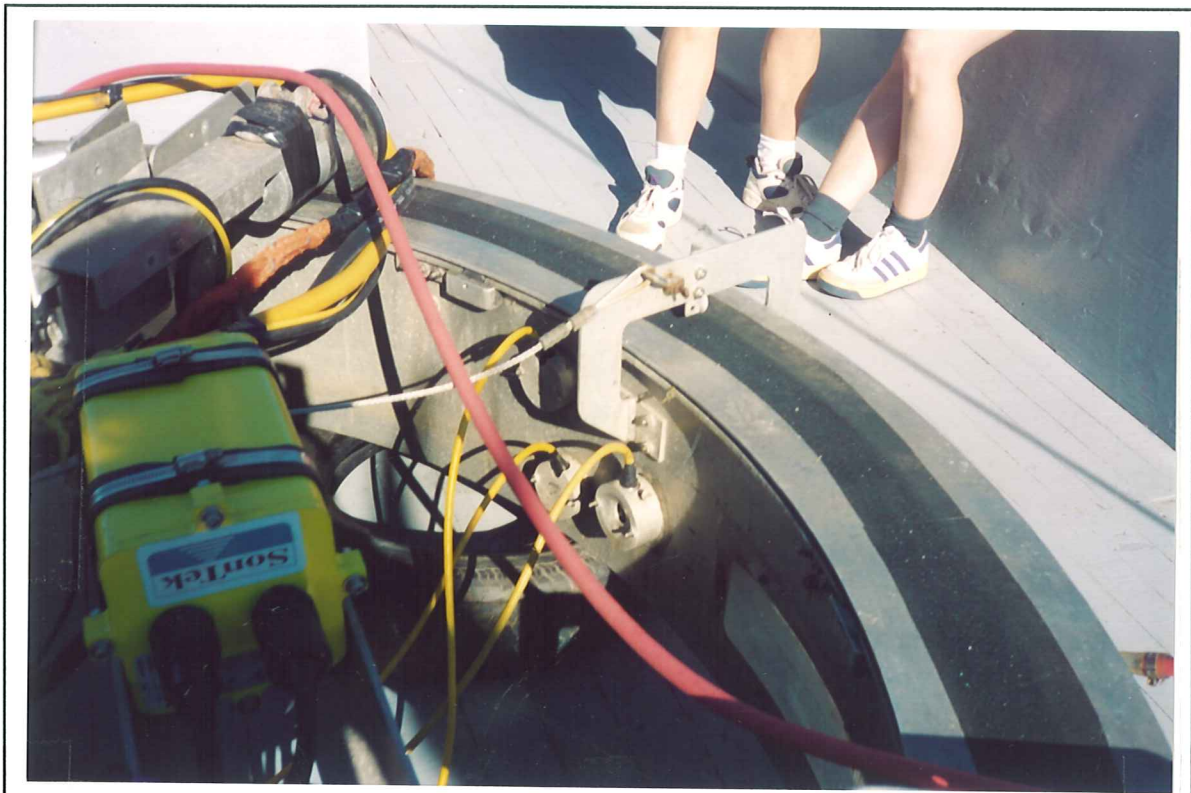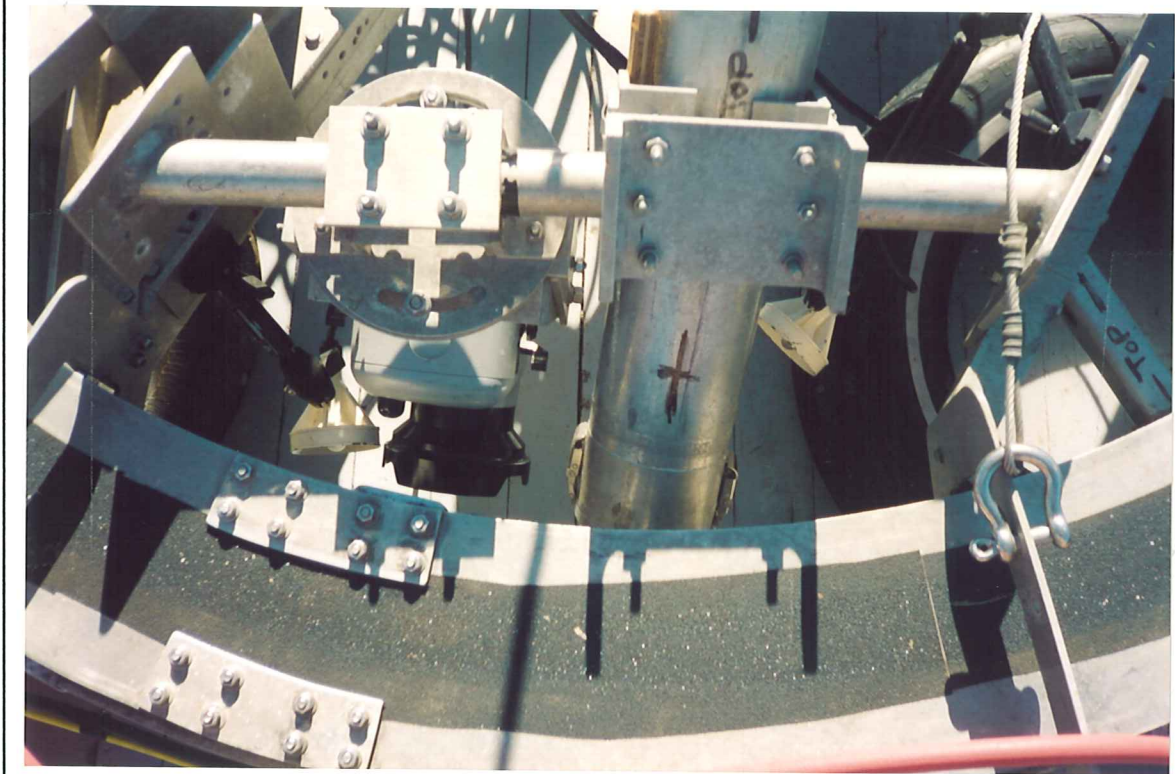
Figure 3.1.3 A. The OBS sensors mounted on the inner wall of the Sea Carousel; in the foreground is the controller to the Sontek ADV flow sensor. The red rubber hose is used for sampling waters from the flume during experiments; B. The Hi8 video camera and Amphibico housing (left) and VHS real time monitoring system positioned to see the bed through a window in the side of the flume.

33
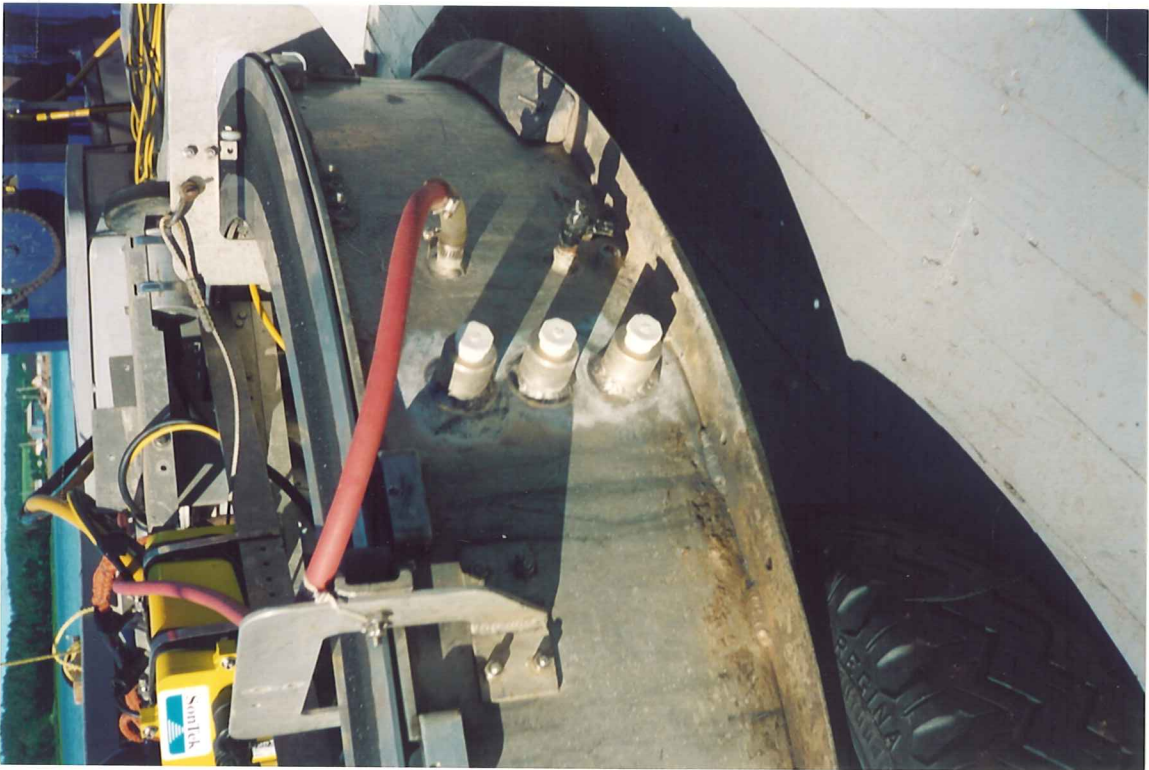
Figure 3.1.4 A. The sensor heads of the Sontek ADV current meter (yellow) and SeaPoint Fluorometer installed in the inner wall of the Sea Carousel; B. The sample port used in this study with three optional ports for sampling at varying heights above the bed. Also notice the lead ballast bolted to the skirt of the flume
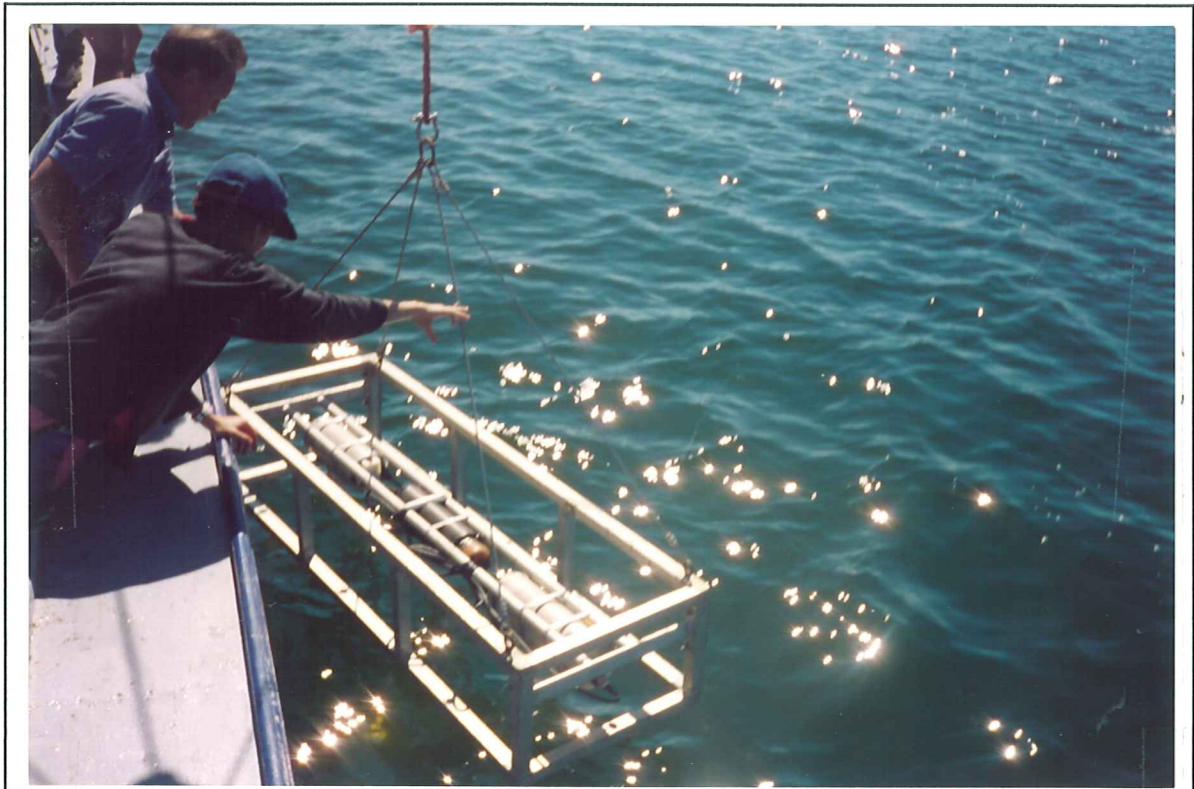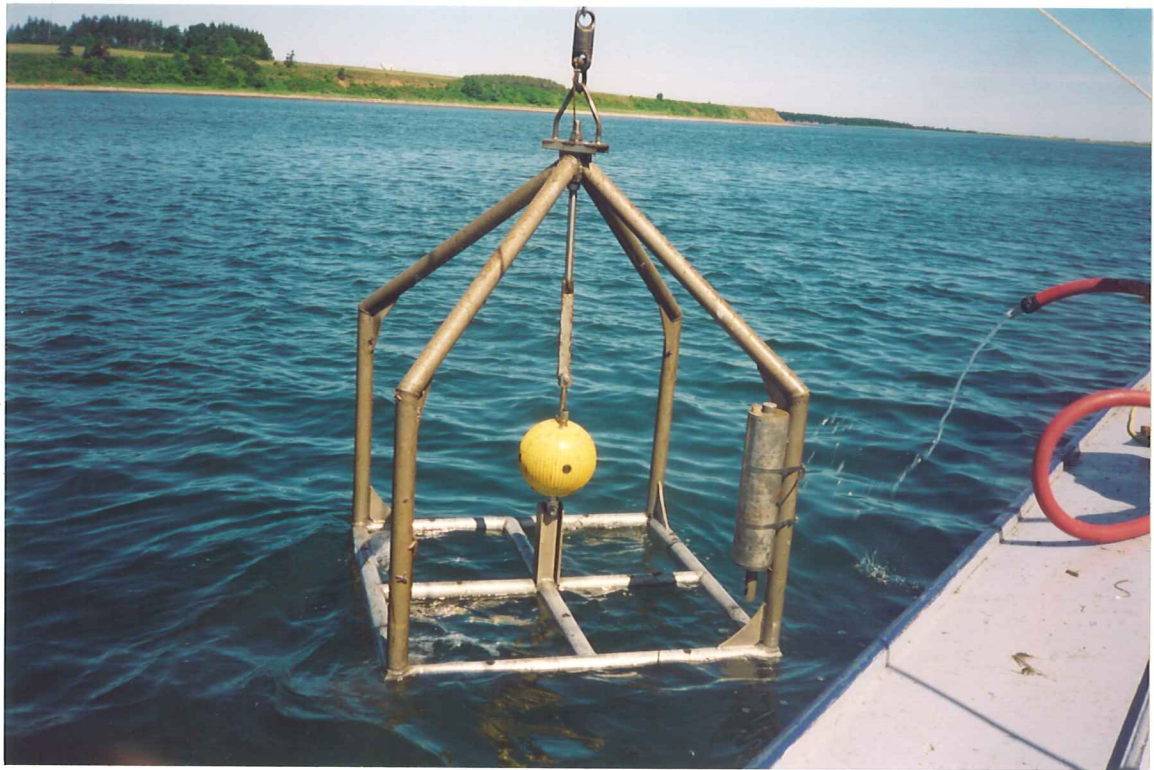
Figure 3.2.1A. The seabed camera (35 mm) used to photograph the seabed at each of the Sea Carousel stations. It is equipped with a flash and bottom trip weight; B. The S4 current meter (yellow ball) and Cyclops (strapped to upright) on a tubular frame being deployed.

SEA CAROUSEL - Rustico Bay, PEI

SITE R1 - 15 July, 1997
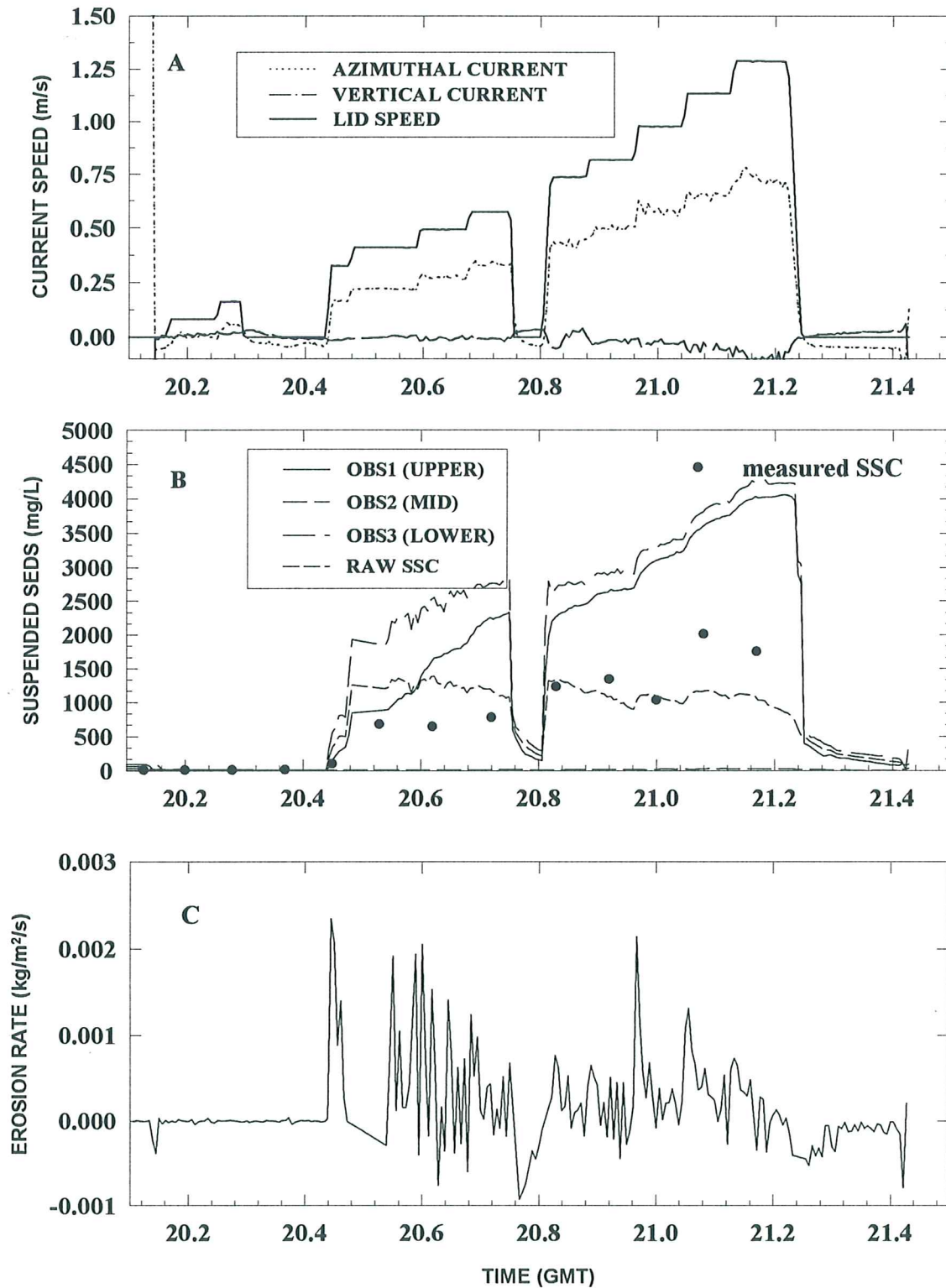
Figure 4.1.1. Time-series plots of results from Sea Carousel at station R1

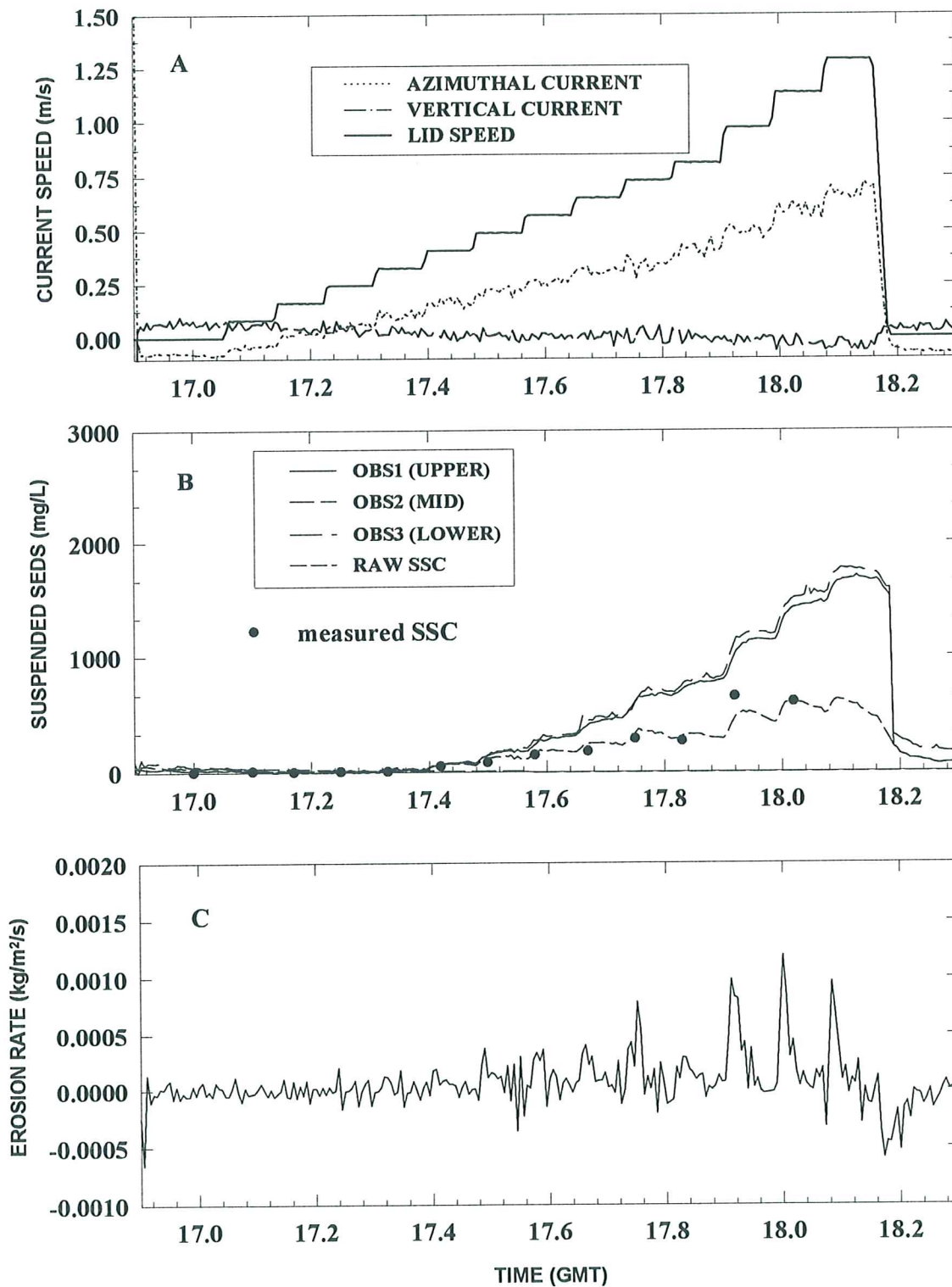# SEA CAROUSEL - Rustico Bay, PEI
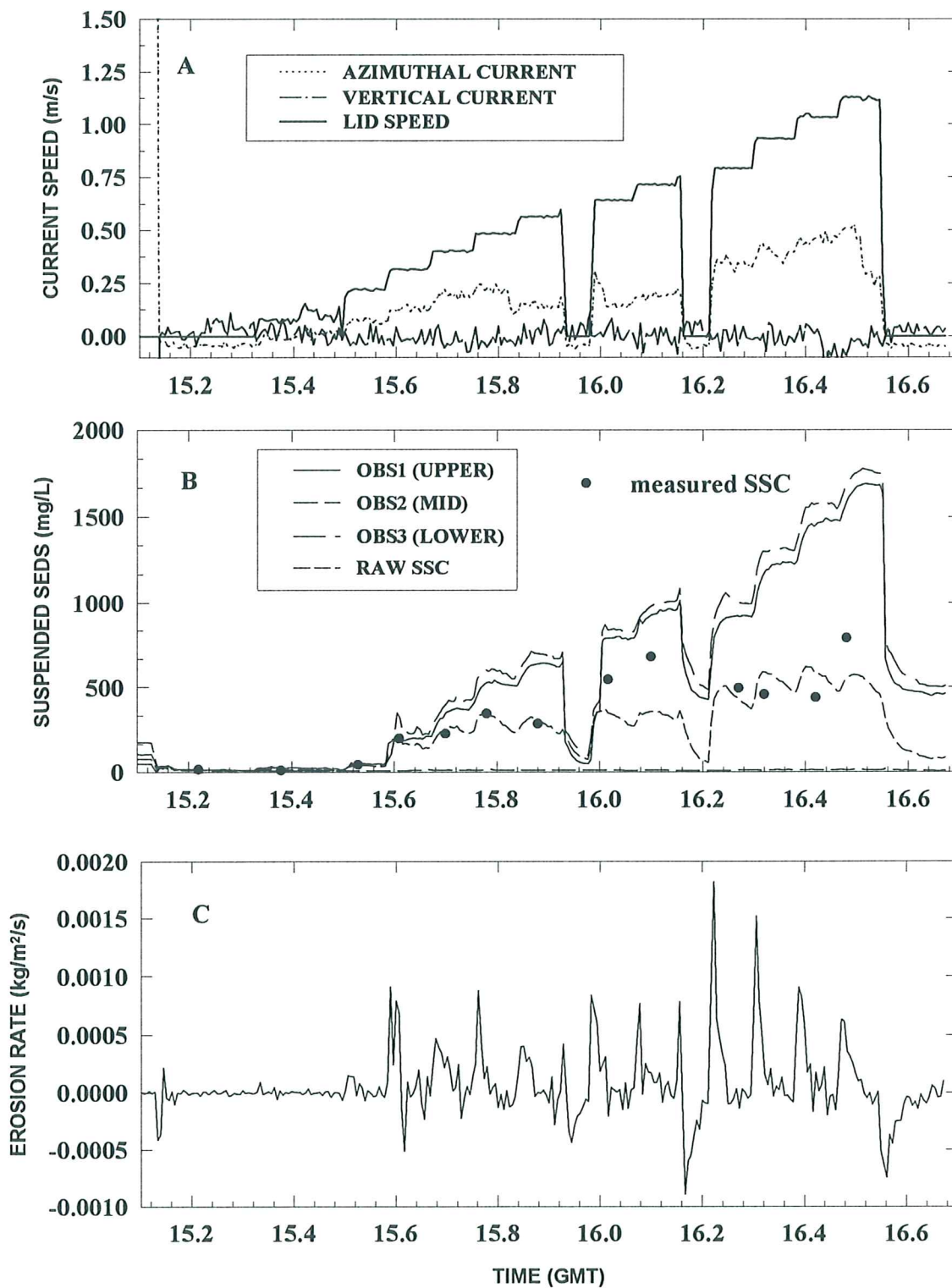
SITE R2 - 16 July, 1997

Figure 4.1.2. Time-series plots of results from Sea Carousel at station R2.

SEA CAROUSEL - Rustico Bay, PEI

SITE R3 - 16 July, 1997
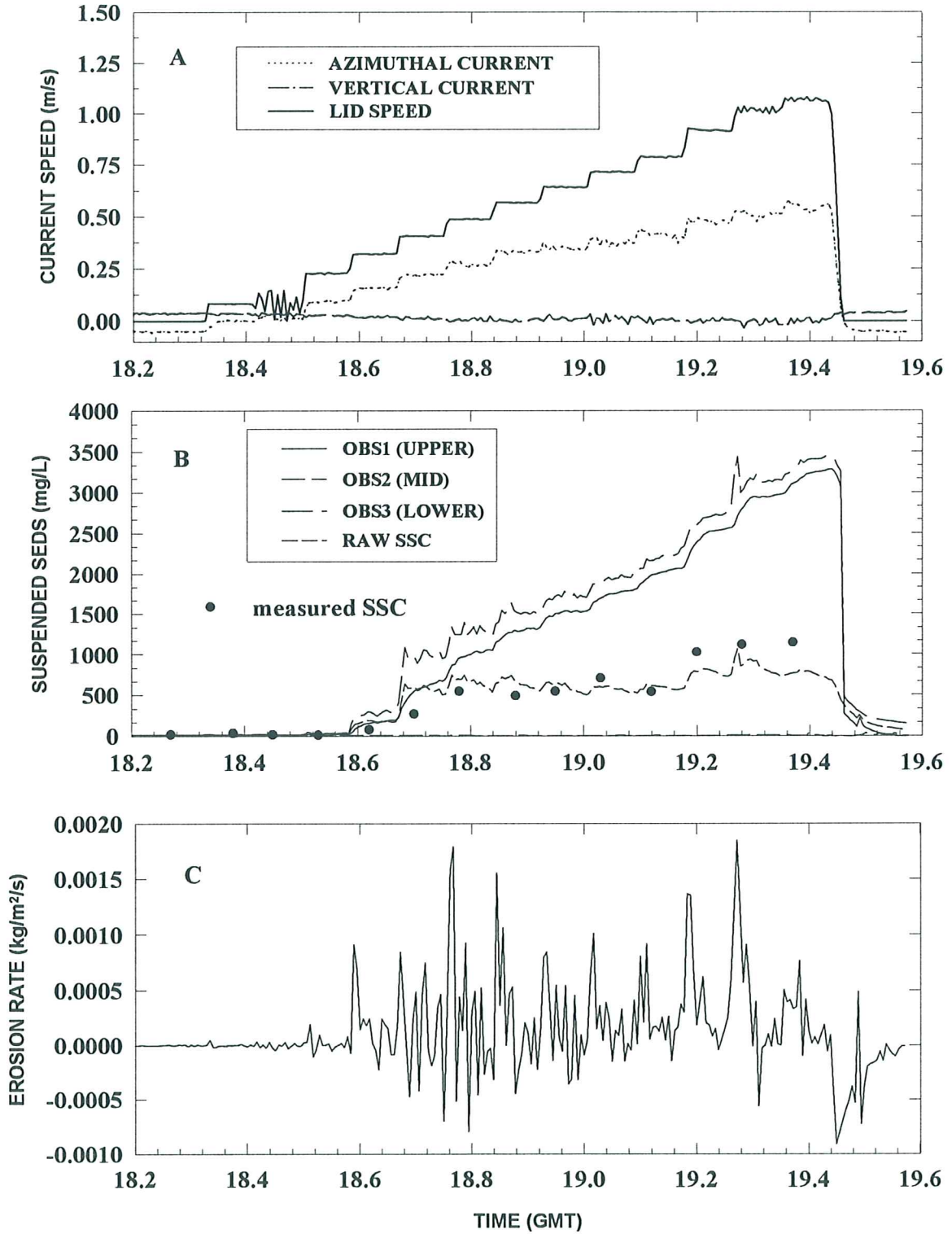
Figure 4.1.3. Time-series plots of results from Sea Carousel at station R3

SEA CAROUSEL - Rustico Bay, PEI
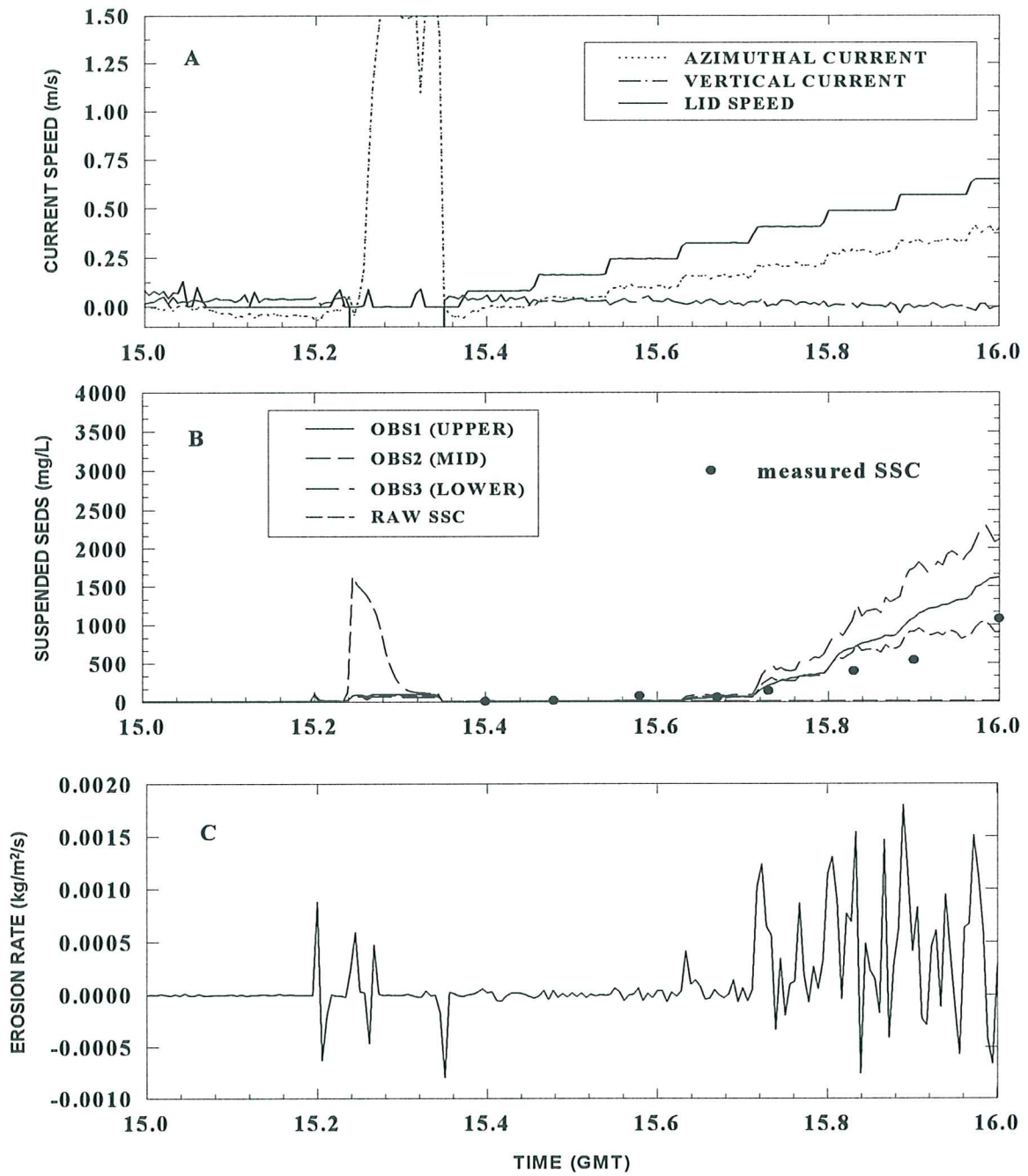
SITE R4 - 17 July, 1997

Figure 4.1.4. Time-series plots of results from Sea Carousel at station R4

SEA CAROUSEL - Rustico Bay, PEI

SITE R5 - 17 July, 1997
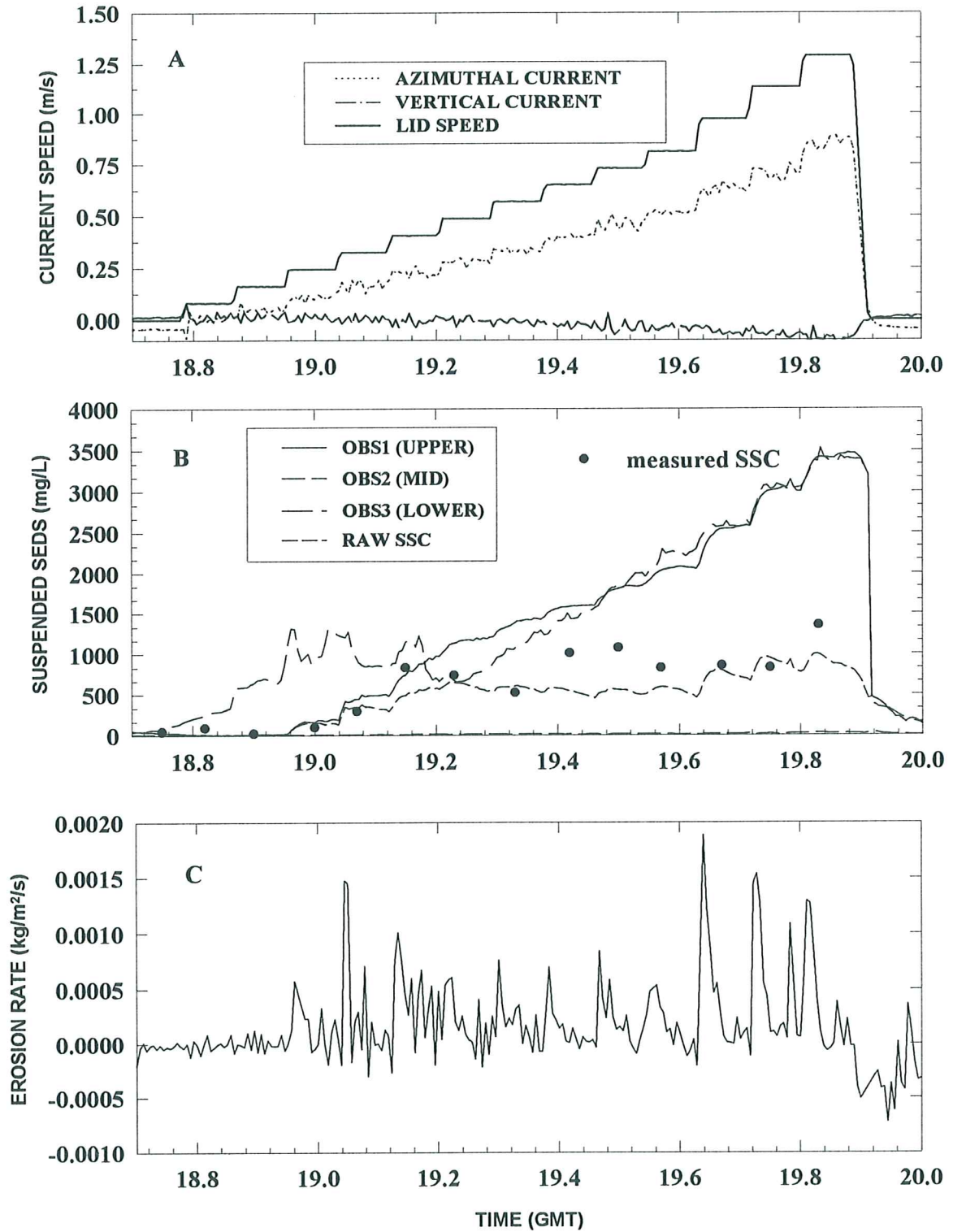
Figure 4.1.5. Time-series plots of results from Sea Carousel at station R5

SEA CAROUSEL - Rustico Bay, PEI

SITE R6 - 18 July, 1997
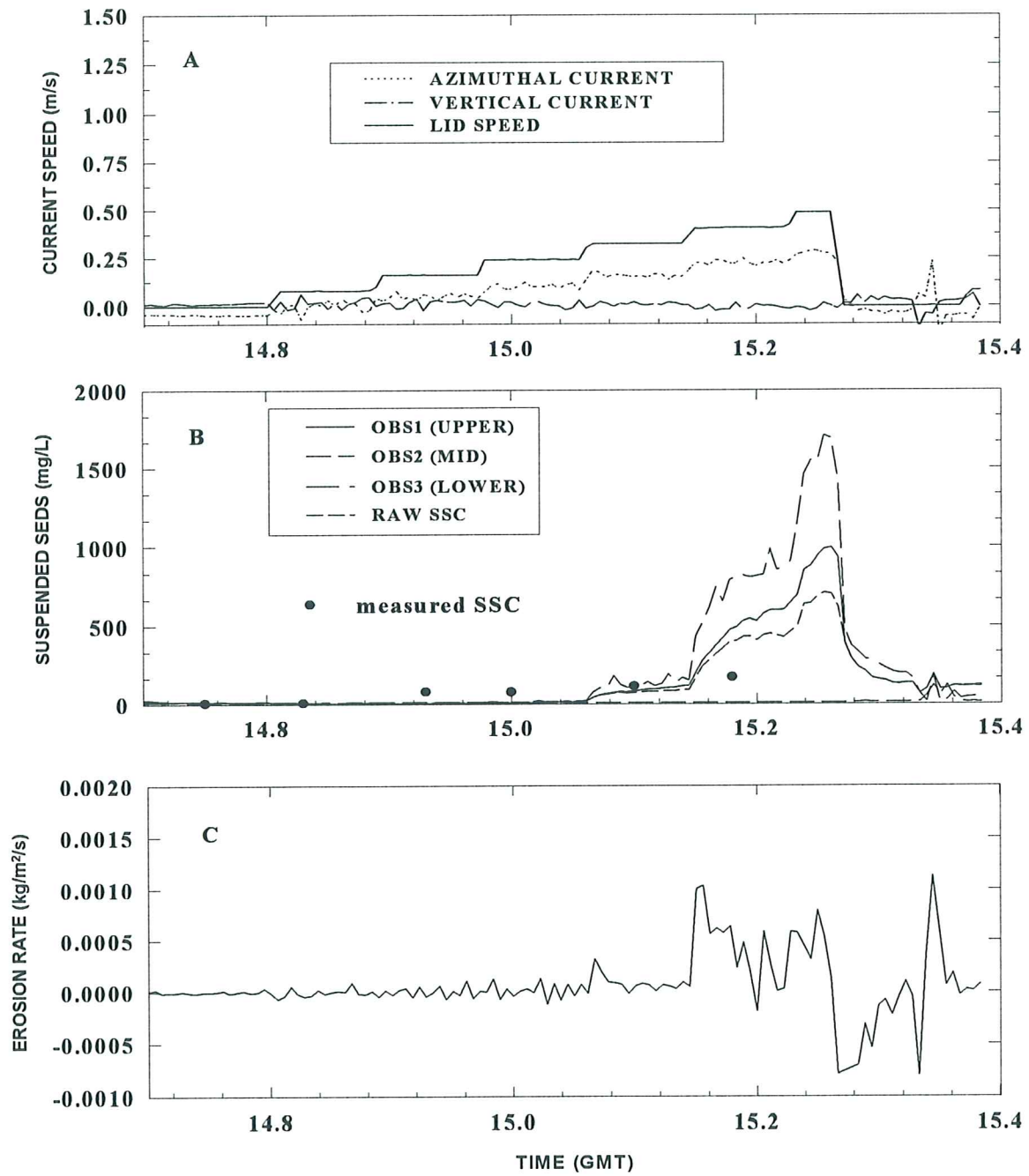
Figure 4.1.6. Time-series plots of results from Sea Carousel at station R6

41

SEA CAROUSEL - Rustico Bay, PEI

SITE R7 - 18 July, 1997
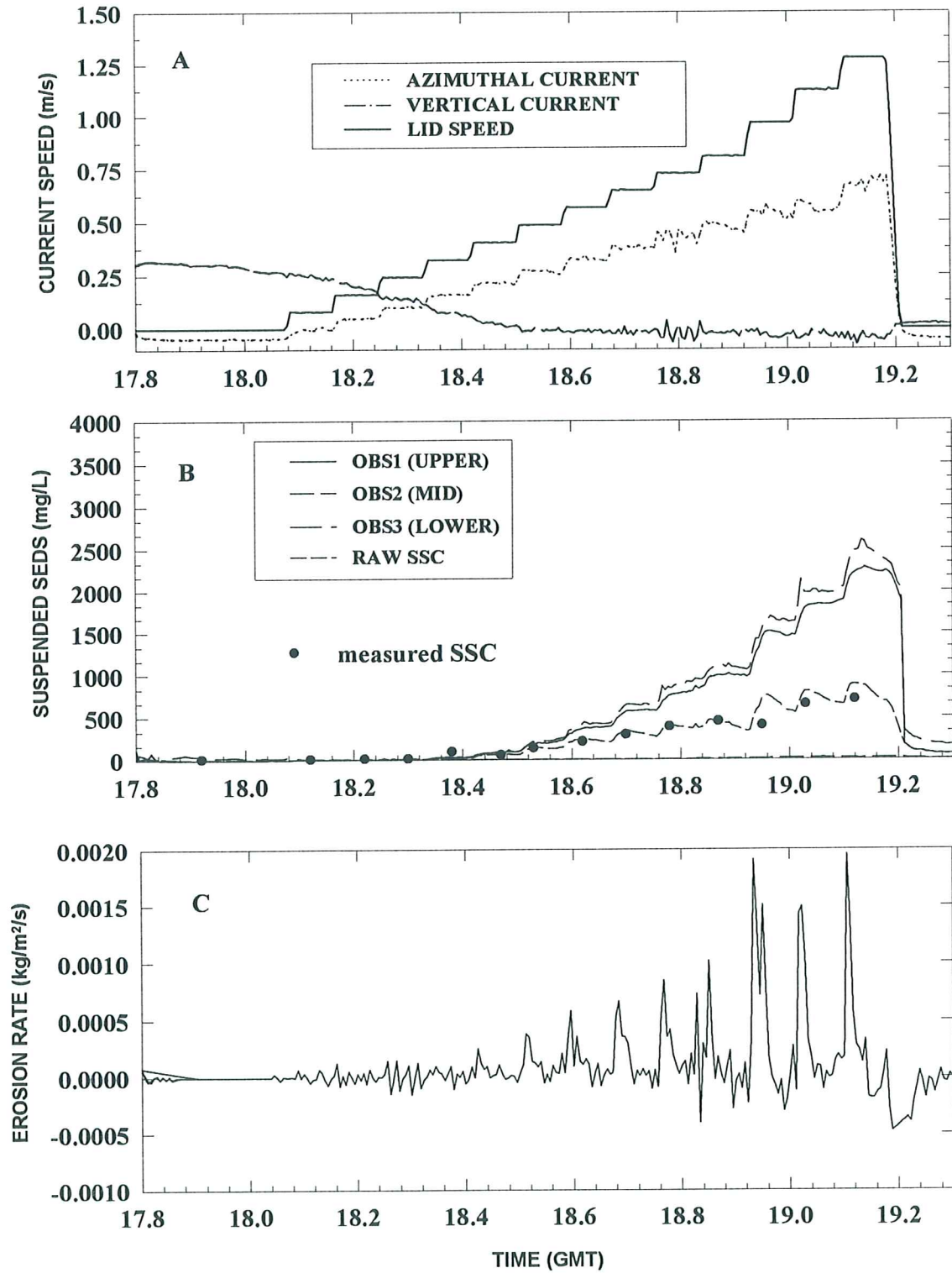
Figure 4.1.7. Time-series plots of results from Sea Carousel at station R7

SEA CAROUSEL - Rustico Bay, PEI

SITE R8 - 19 July, 1997
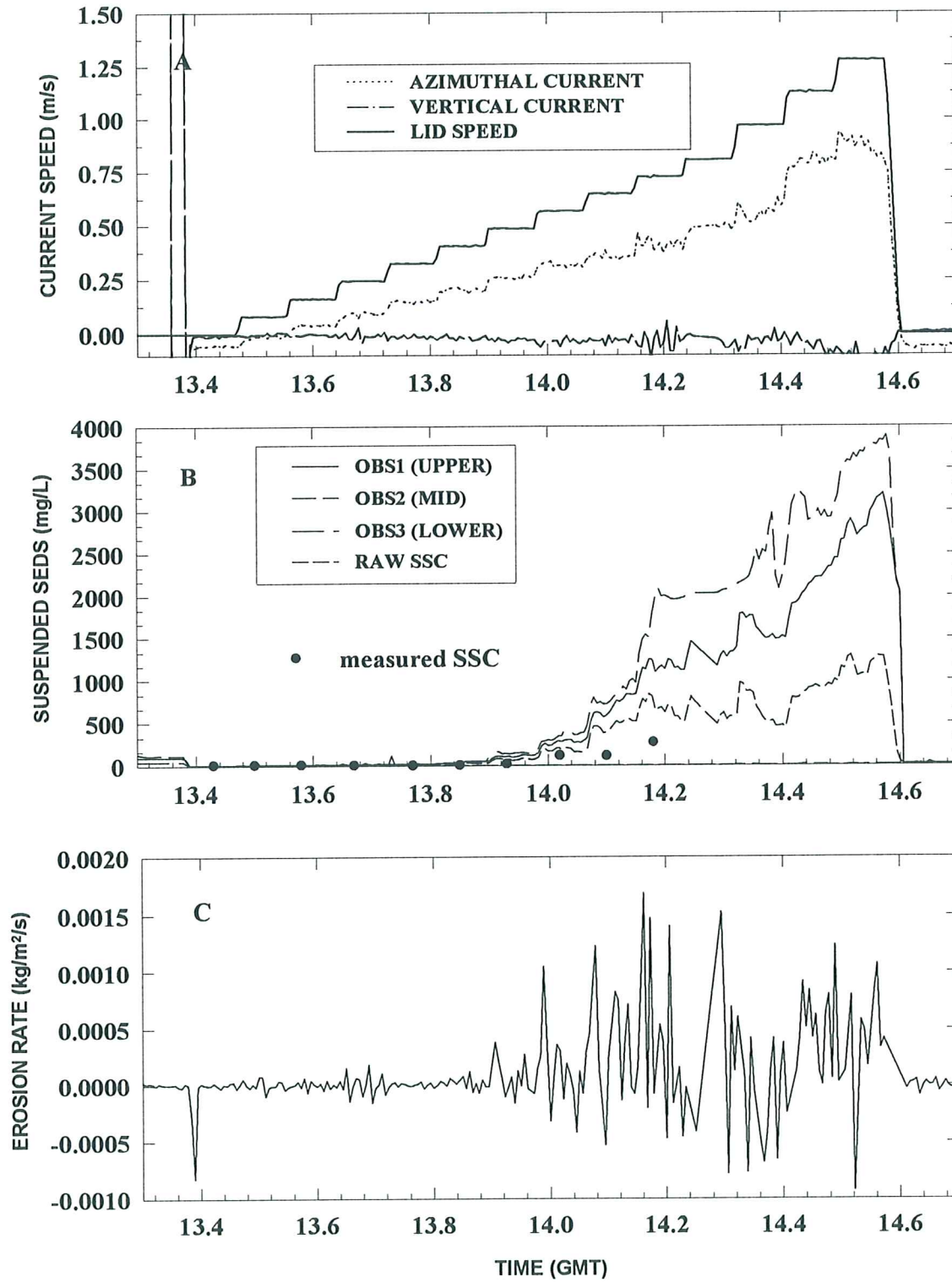
Figure 4.1.8. Time-series plots of results from Sea Carousel at station R8.

SEA CAROUSEL - Rustico Bay, PEI
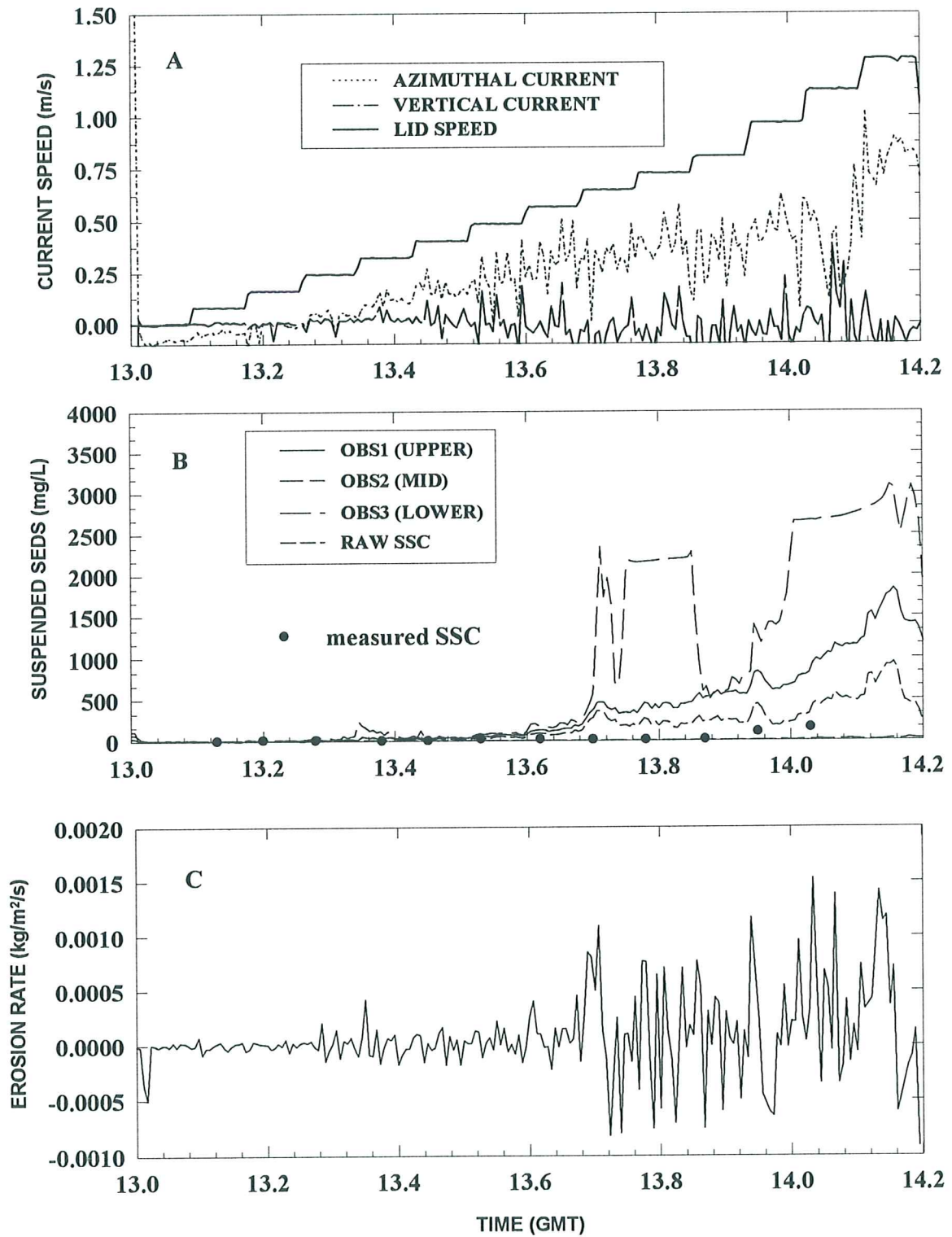
SITE R9 - 20 July, 1997

Figure 4.1.9. Time-series plots of results from Sea Carousel at station R9

44

SEA CAROUSEL - Rustico Bay, PEI

SITE R10 - 20 July, 1997
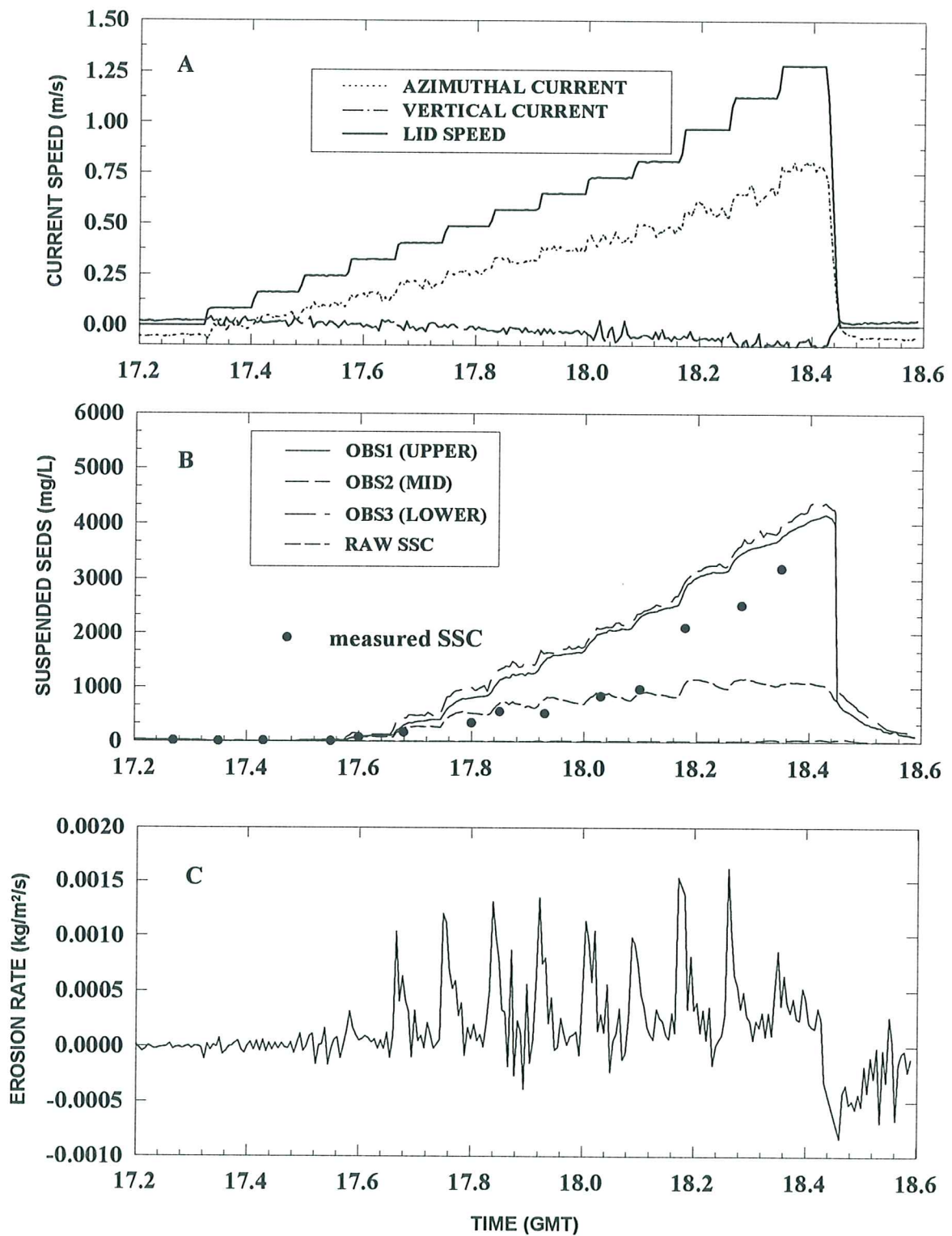
Figure 4.1.10. Time-series plots of results from Sea Carousel at station R10.

SEA CAROUSEL - Rustico Bay, PEI

SITE R11 - 21 July, 1997
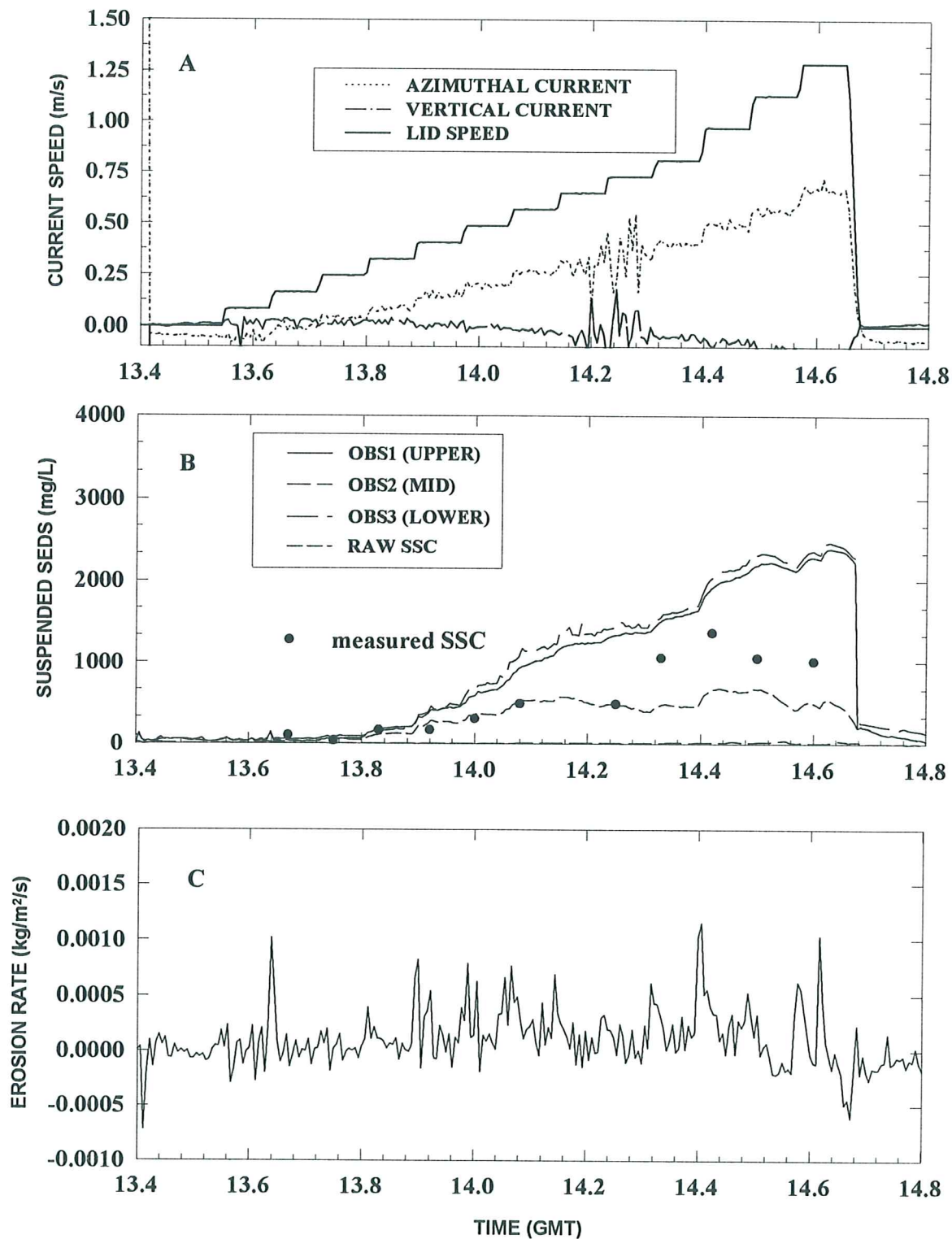
Figure 4.1.11. Time-series plots of results from Sea Carousel at station R11.

SEA CAROUSEL - Rustico Bay, PEI

SITE R12 - 21 July, 1997
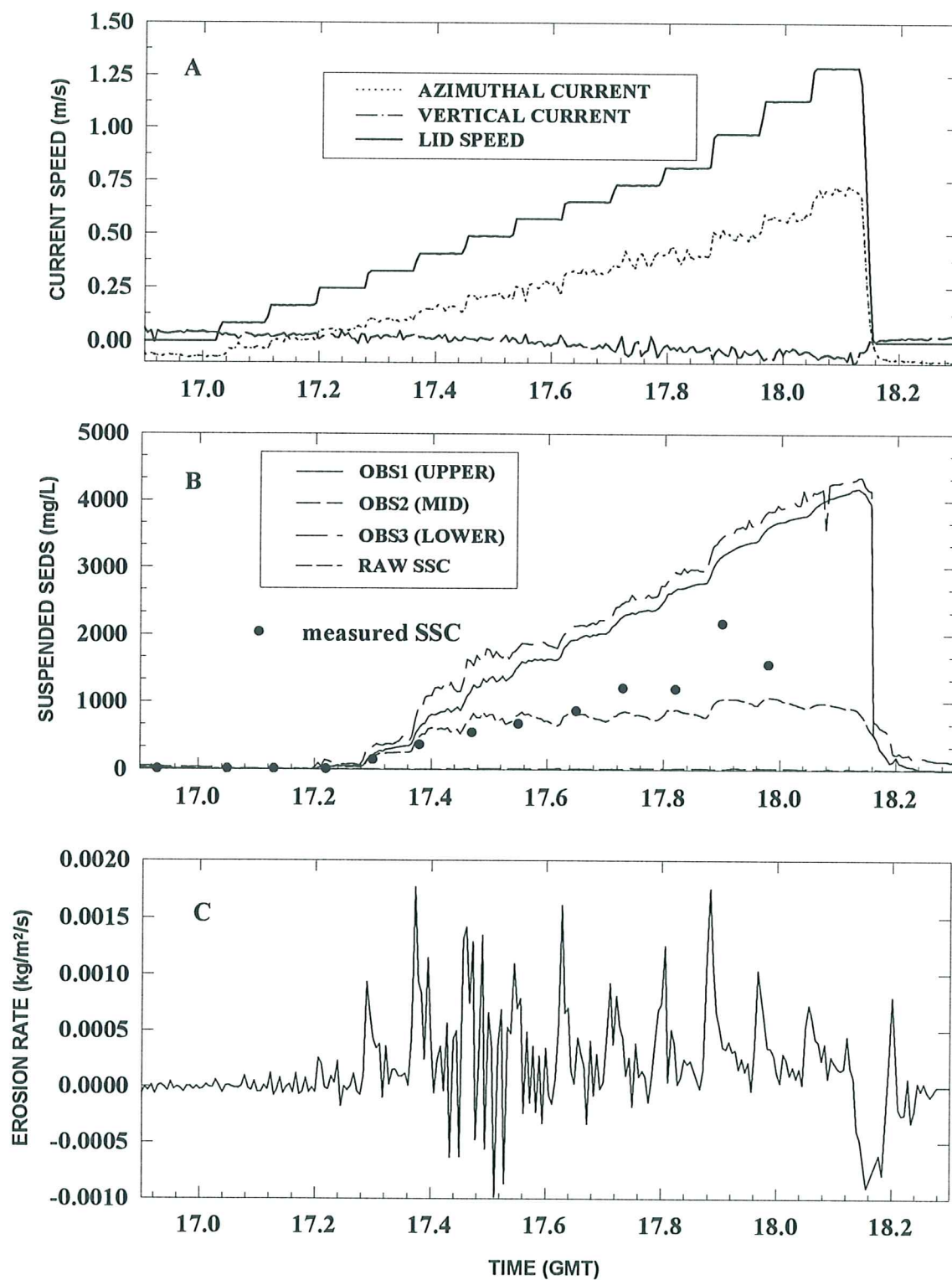
Figure 4.1.12. Time-series plots of results from Sea Carousel at station R12.

SEA CAROUSEL - Rustico Bay, PEI

SITE R13 - 22 July, 1997
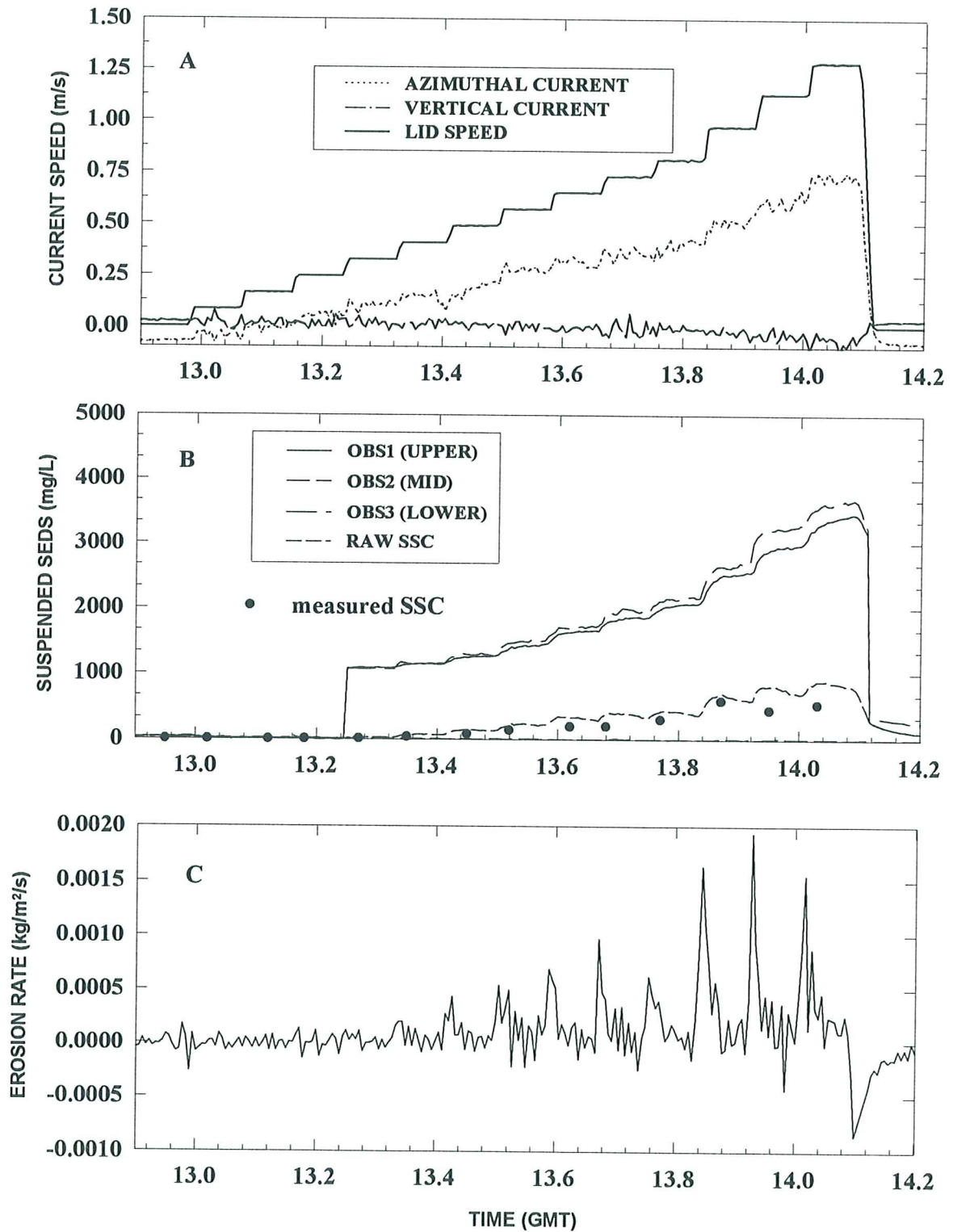
Figure 4.1.13. Time-series plots of results from Sea Carousel at station R13.

SEA CAROUSEL - Rustico Bay, PEI

SITE R14 - 22 July, 1997

Figure 4.1.14. Time-series plots of results from Sea Carousel at station R14.

SEA CAROUSEL - Rustico Bay, PEI

SITE R15 - 23 July, 1997
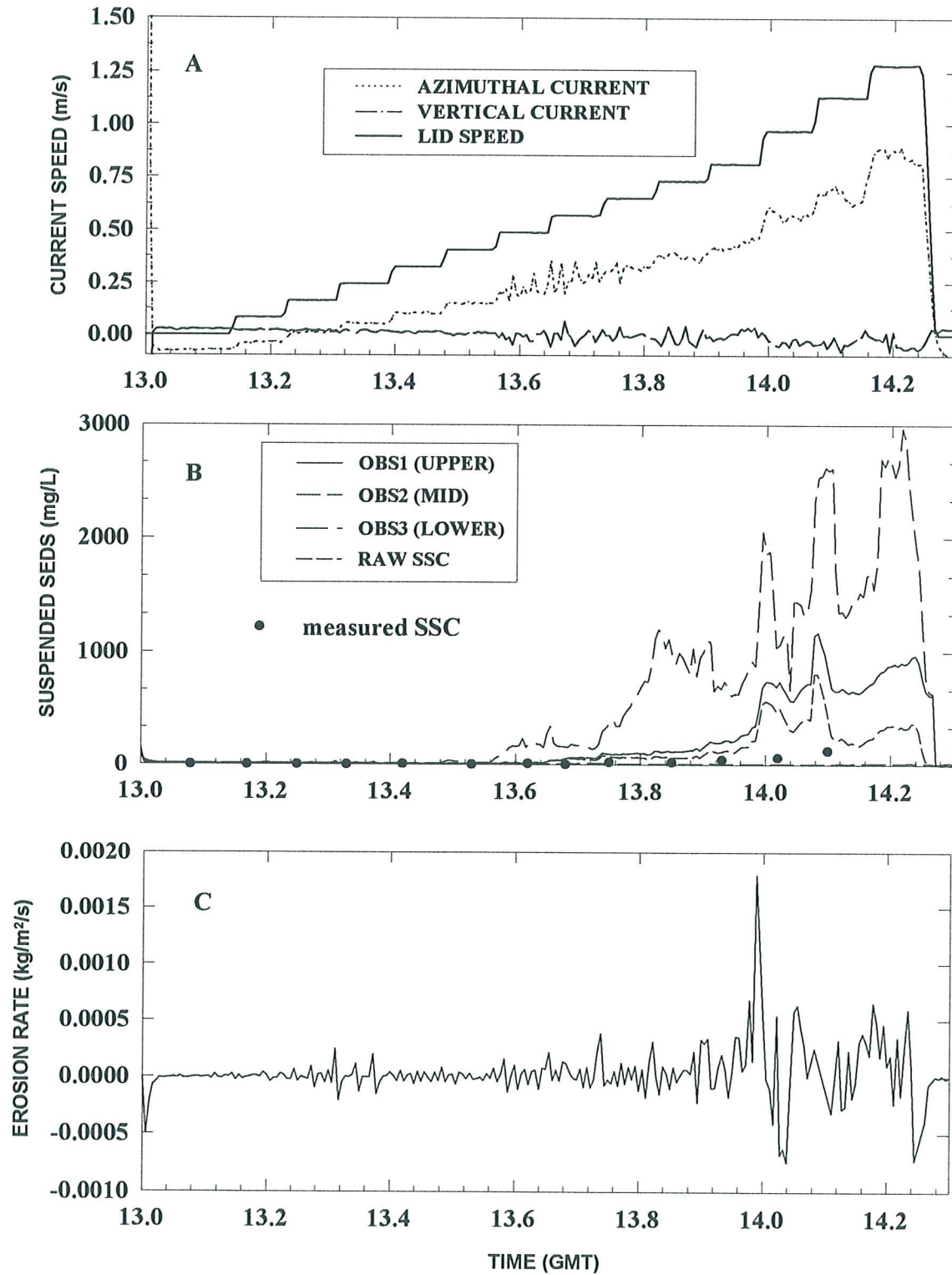
Figure 4.1.15. Time-series plots of results from Sea Carousel at station R15.
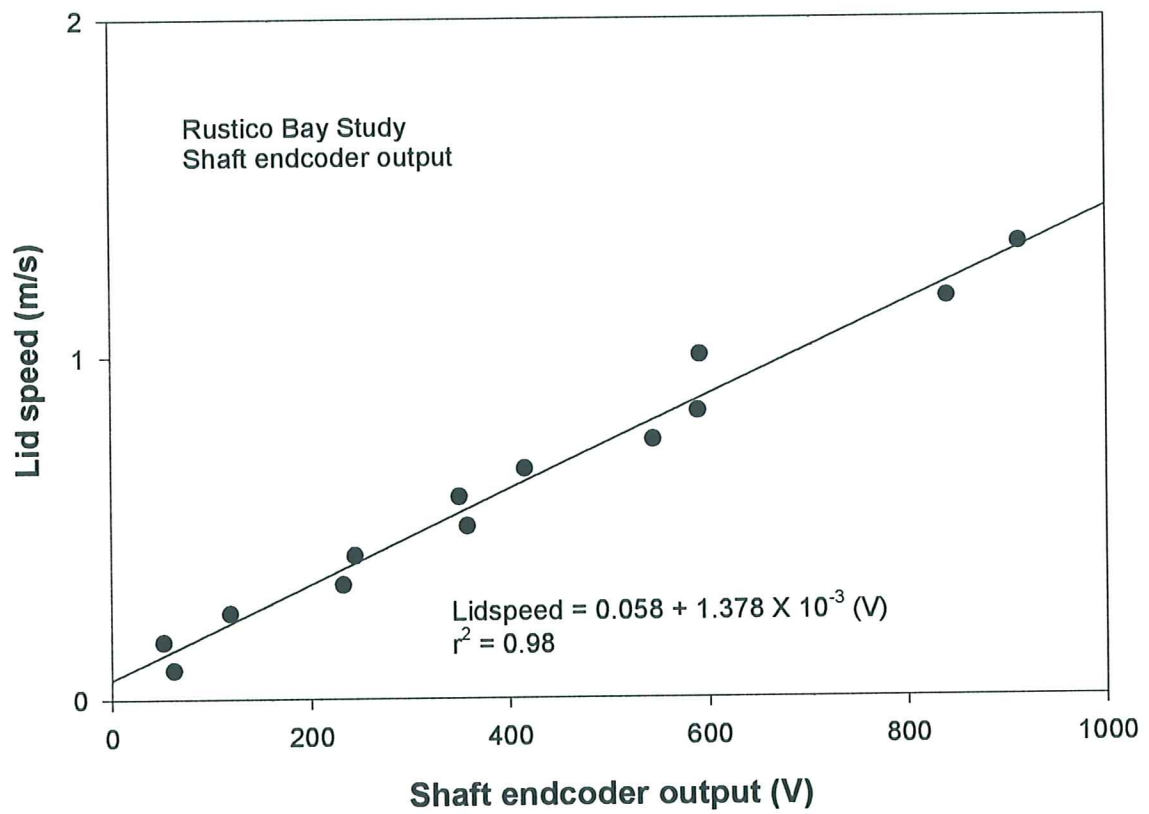
Figure 4.1.16. The relationship between shaft endcoder output (mV) and lid speed (m/s) . A good linear fit was found between the two variables.
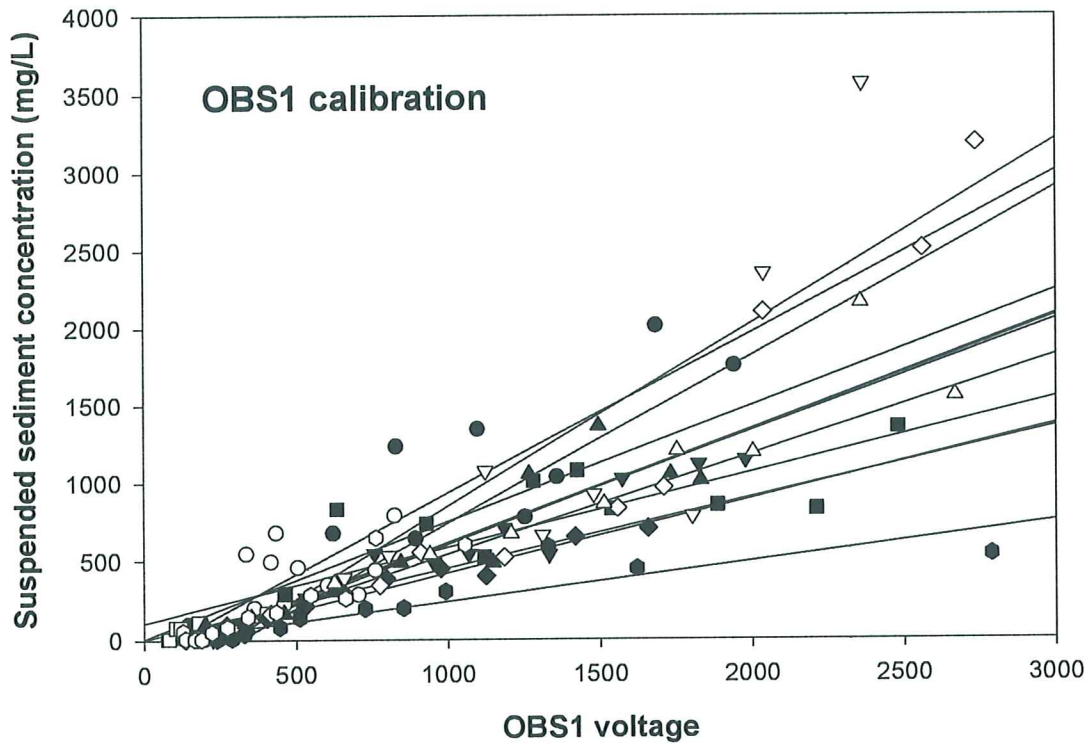
Figure 4.1.17. The calibration of the OBS1 (upper) sensor to suspended sediment concentration measured in samples pumped from the Sea Carousel.
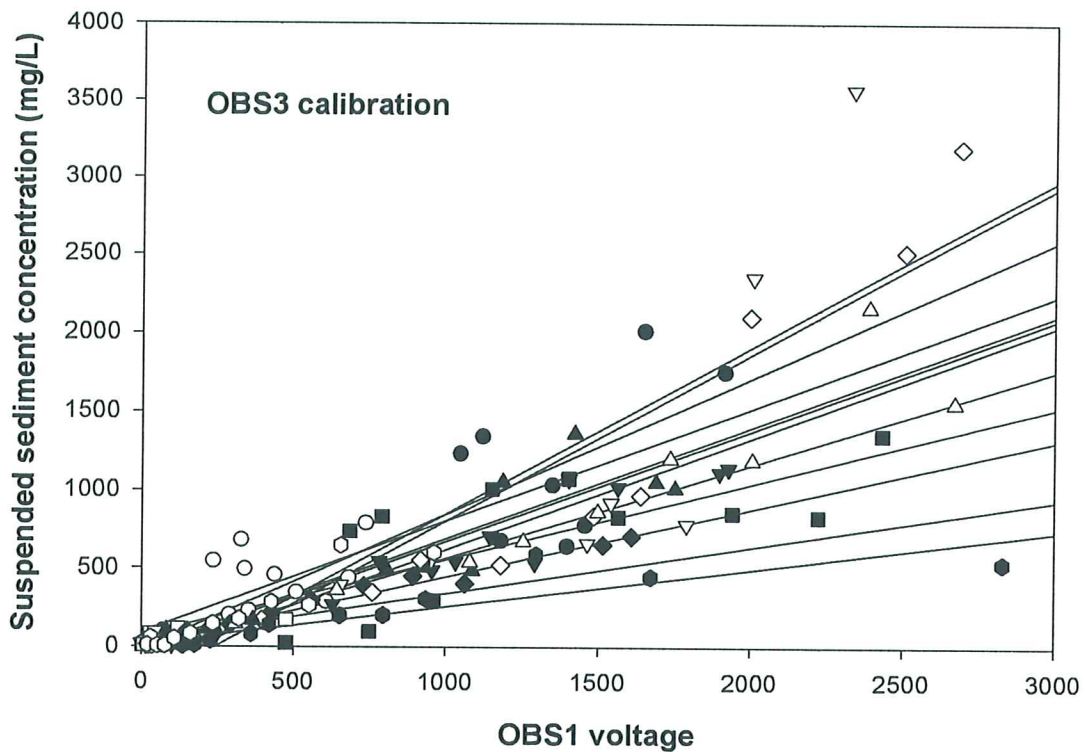
Figure 4.1.18. The calibration of the OBS3 (lower) sensor against suspended sediment concentration measured in samples pumped from the Sea Carousel.

SEA CAROUSEL - Rustico Bay, PEI

SITE R1 - 15 July, 1997

A

Suspended sediment concentration (mg/L)

$Tau_{crit} = 0.11$ Pa

Bed shear stress (Pa)

B

Erosion rate ($kg/m^2/s$)

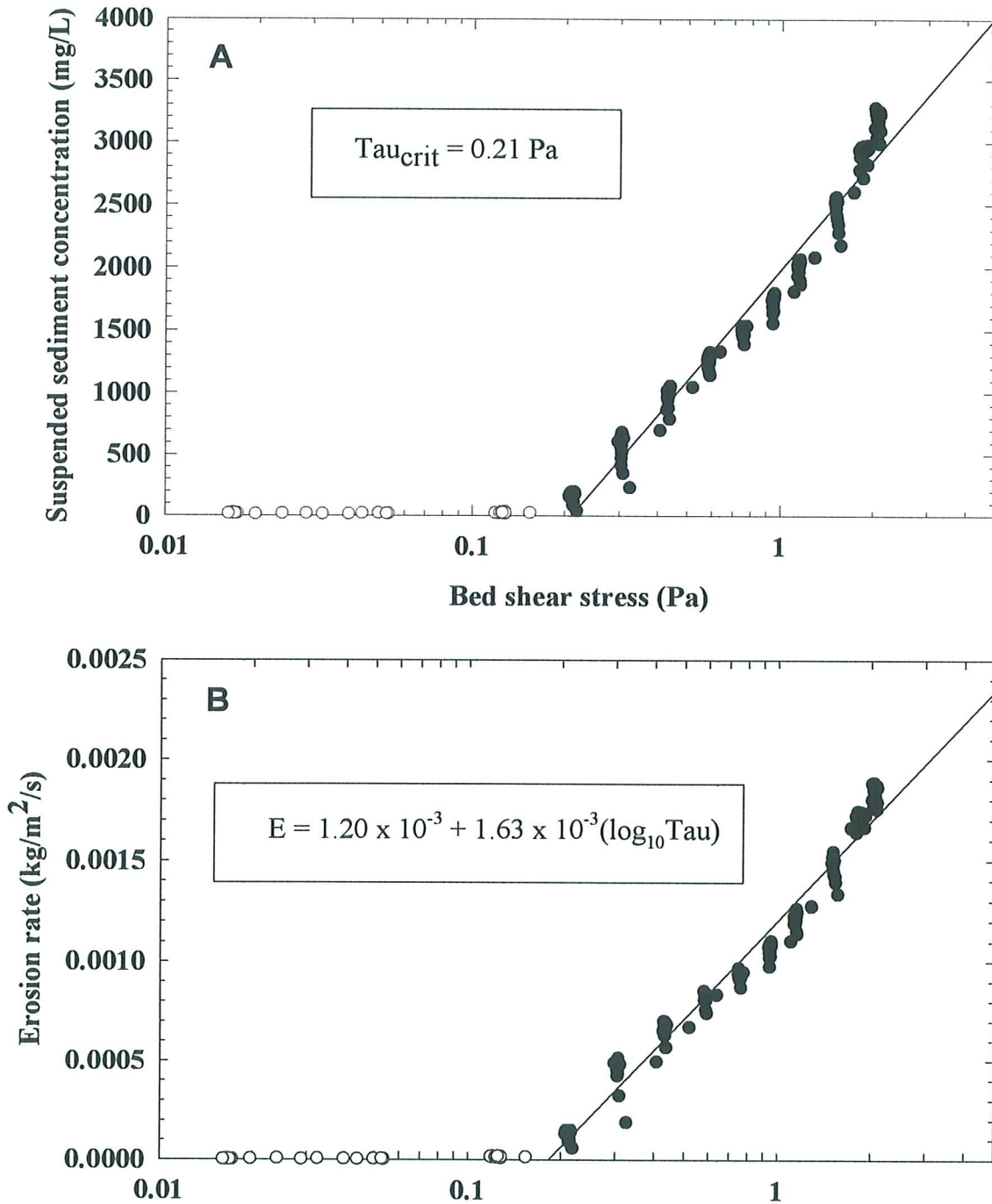$E = 3.44 \times 10^{-3} + 3.80 \times 10^{-3}(\log_{10} Tau)$
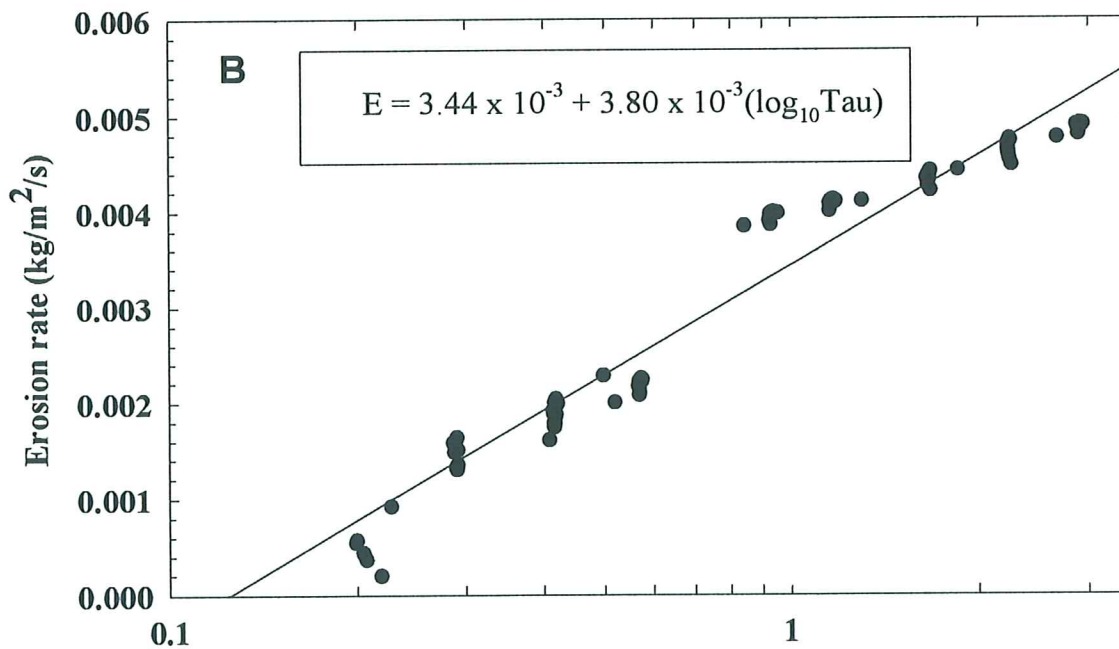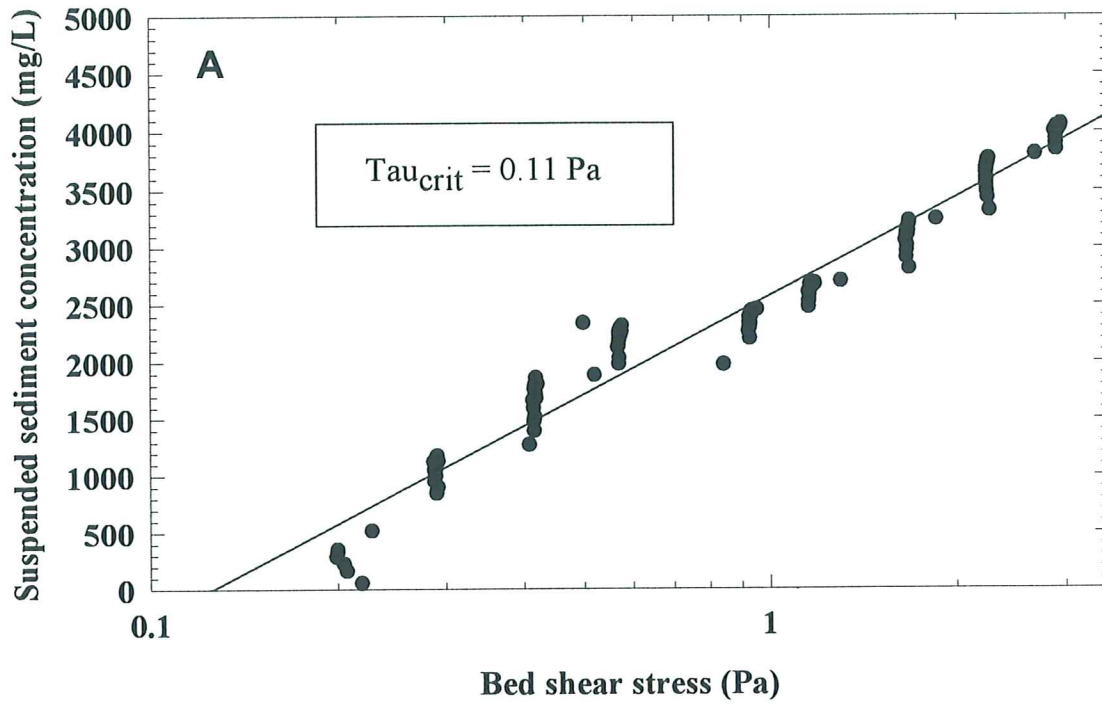
Figure 4.1.19. Estimations of the erosion threshold and erodibility for station R1 from (A) the relationship between bed shear stress and suspended sediment concentration, and (B) the relationship between bed shear stress and erosion rate

SEA CAROUSEL - Rustico Bay, PEI

SITE R2 - 16 July, 1997

A

$Tau_{crit} = 0.18$ Pa

B

$E = 1.26 \times 10^{-3} + 1.86 \times 10^{-3}(\log_{10} Tau)$
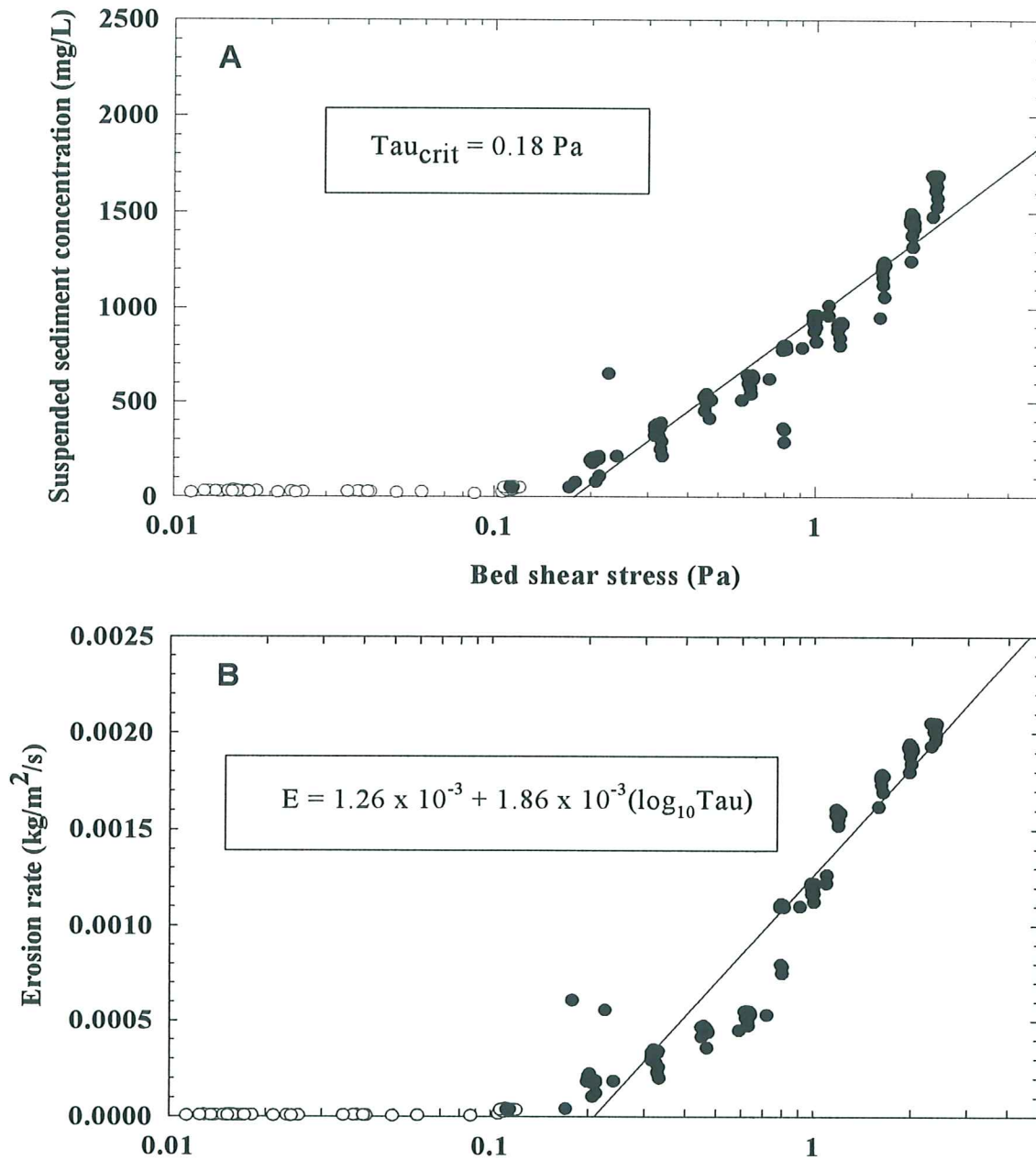
Figure 4.1.20. Estimations of the erosion threshold and erodibility for station R2 from (A) the relationship between bed shear stress and suspended sediment concentration, and (B) the relationship between bed shear stress and erosion rate

SEA CAROUSEL - Rustico Bay, PEI

SITE R3 - 16 July, 1997

A

$Tau_{crit} = 0.21$ Pa

B

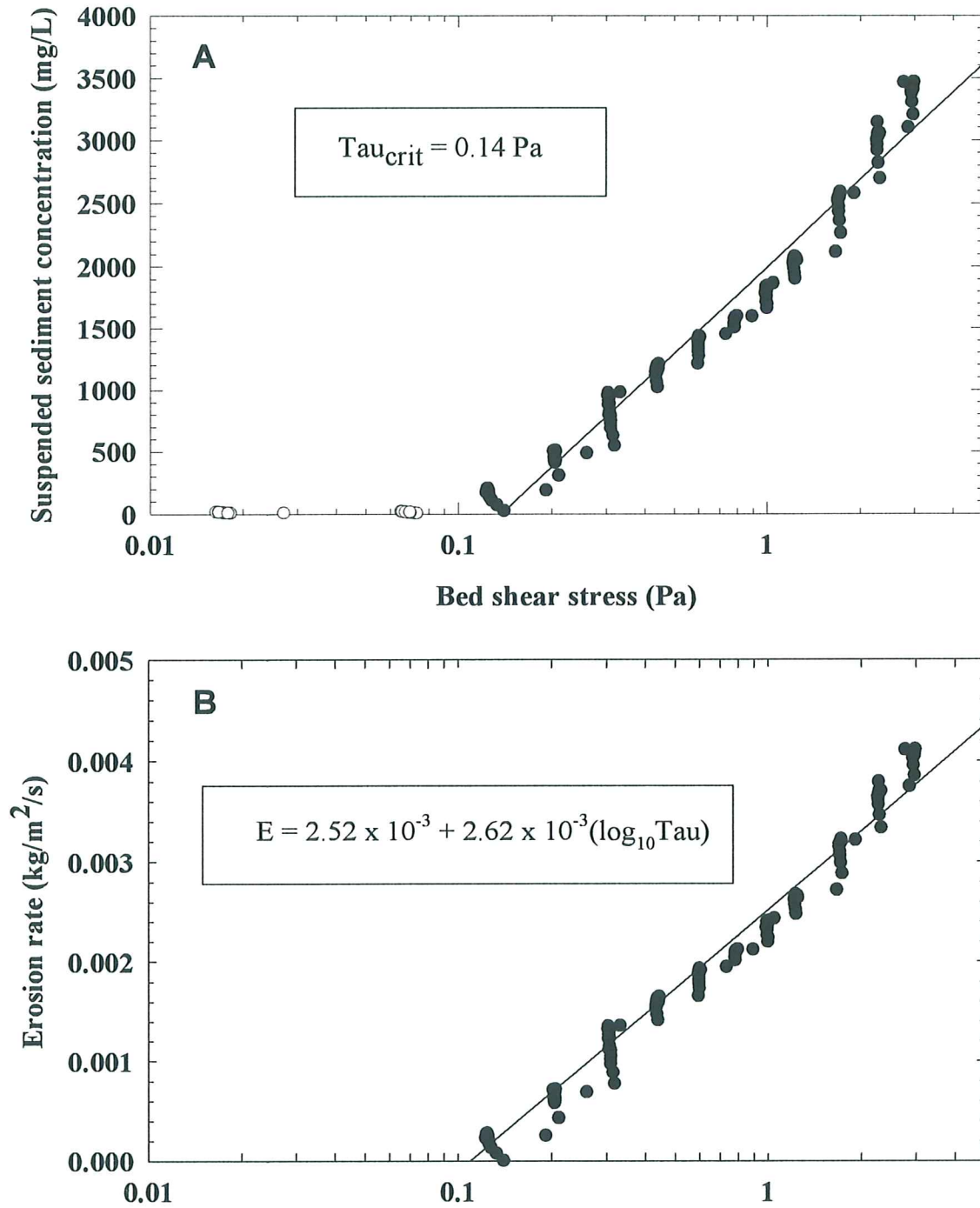$E = 1.20 \times 10^{-3} + 1.63 \times 10^{-3}(\log_{10} Tau)$

Figure 4.1.21. Estimations of the erosion threshold and erodibility for station R3 from (A) the relationship between bed shear stress and suspended sediment concentration, and (B) the relationship between bed shear stress and erosion rate

56

SEA CAROUSEL - Rustico Bay, PEI

SITE R4 - 17 July, 1997

A

$Tau_{crit} = 0.26$ Pa

B

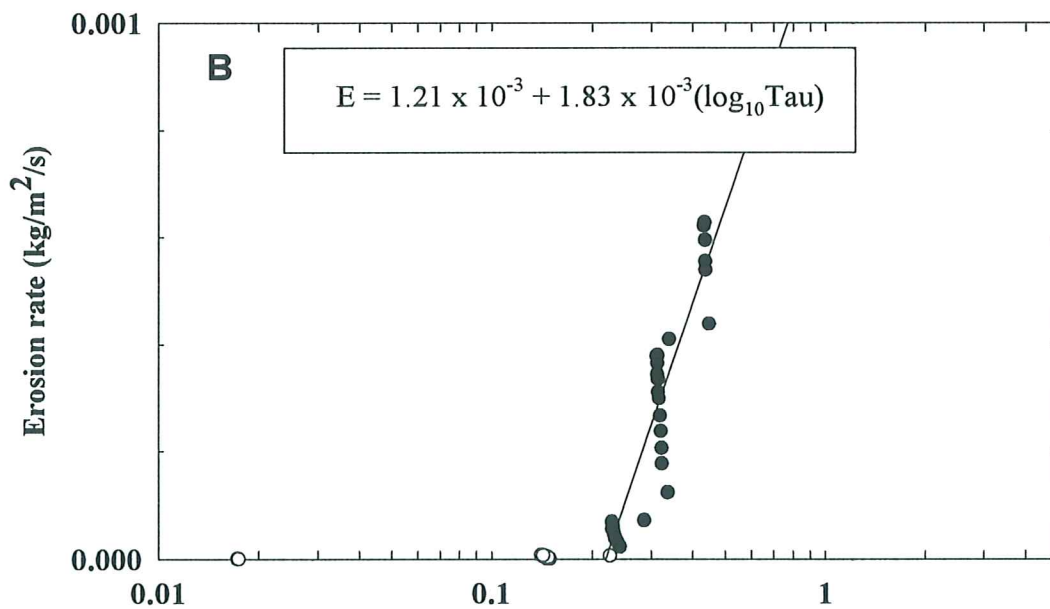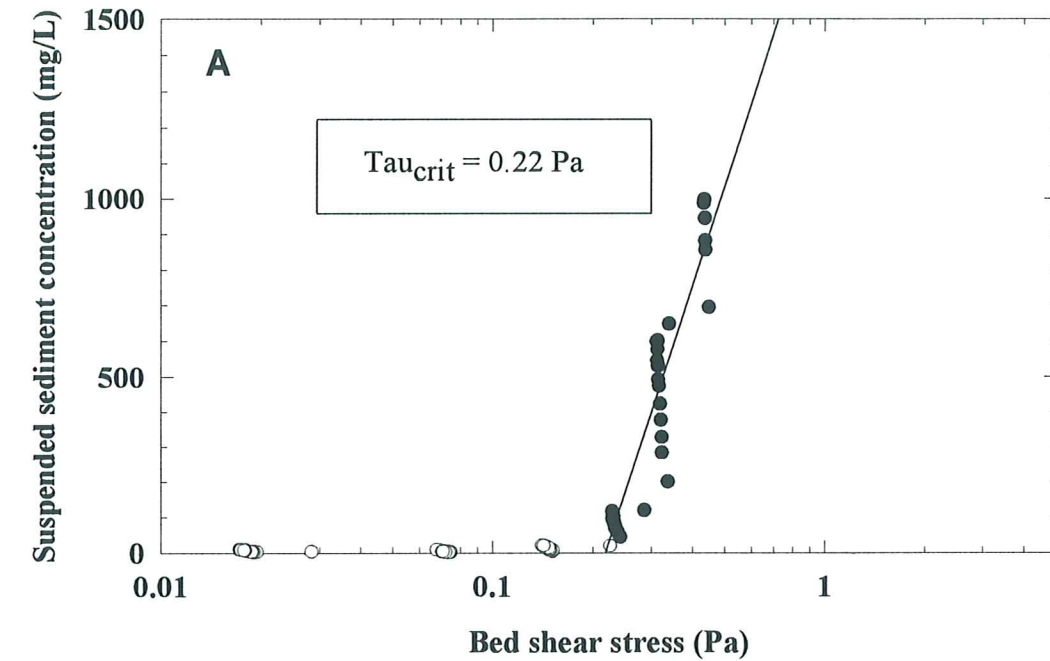$E = 1.26 \times 10^{-3} + 2.02 \times 10^{-3}(\log_{10} Tau)$
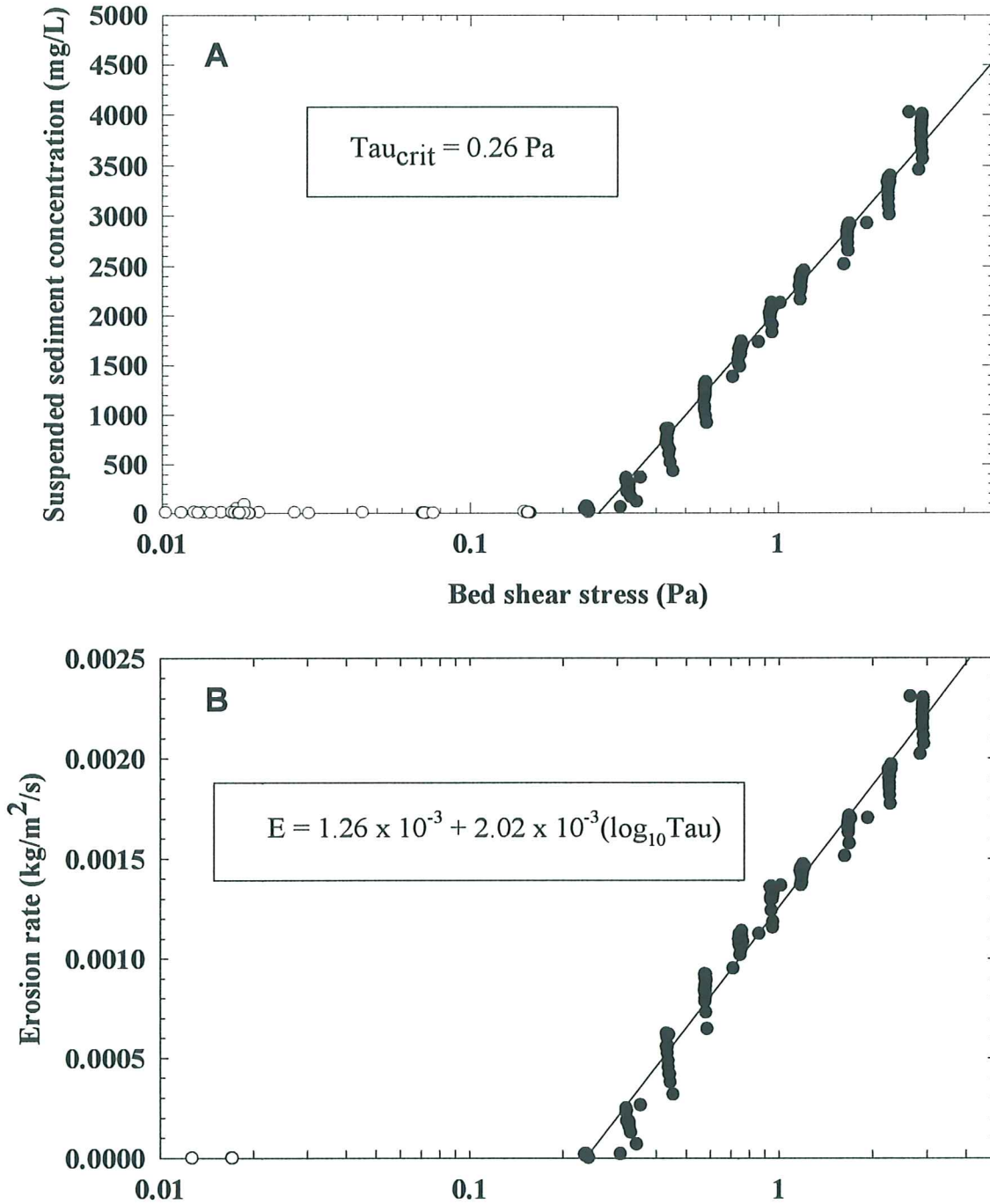
Figure 4.1.22. Estimations of the erosion threshold and erodibility for station R4 from (A) the relationship between bed shear stress and suspended sediment concentration, and (B) the relationship between bed shear stress and erosion rate

SEA CAROUSEL - Rustico Bay, PEI

SITE R5 - 17 July, 1997

A

$Tau_{crit} = 0.14$ Pa

B

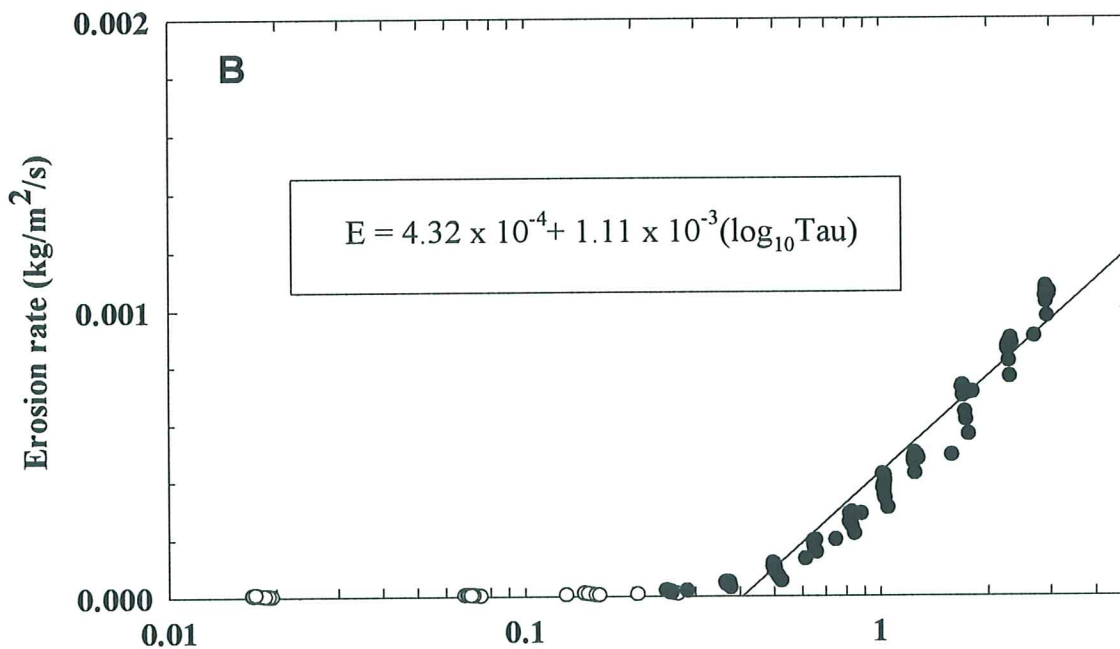$$E = 2.52 \times 10^{-3} + 2.62 \times 10^{-3}(\log_{10} Tau)$$

Figure 4.1.23. Estimations of the erosion threshold and erodibility for station R5 from (A) the relationship between bed shear stress and suspended sediment concentration, and (B) the relationship between bed shear stress and erosion rate
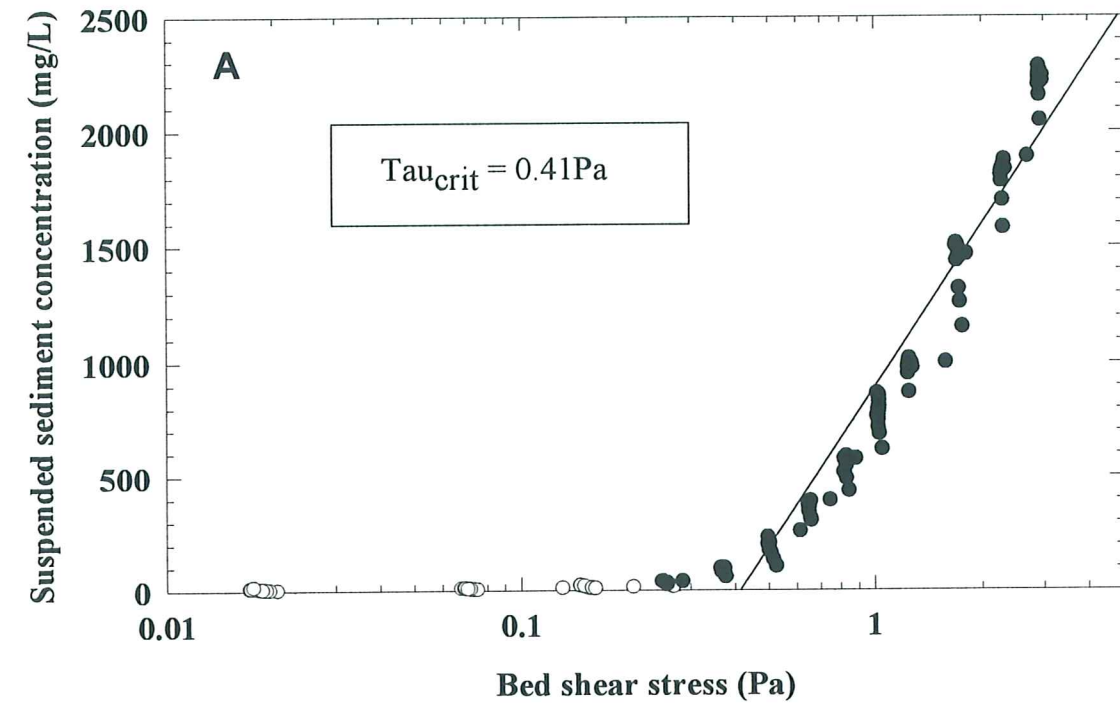
Figure 4.1.24. Estimations of the erosion threshold and erodibility for station R6 from (A) the relationship between bed shear stress and suspended sediment concentration, and (B) the relationship between bed shear stress and erosion rate

Figure 4.1.25. Estimations of the erosion threshold and erodibility for station R7 from (A) the relationship between bed shear stress and suspended sediment concentration, and (B) the relationship between bed shear stress and erosion rate

SEA CAROUSEL - Rustico Bay, PEI
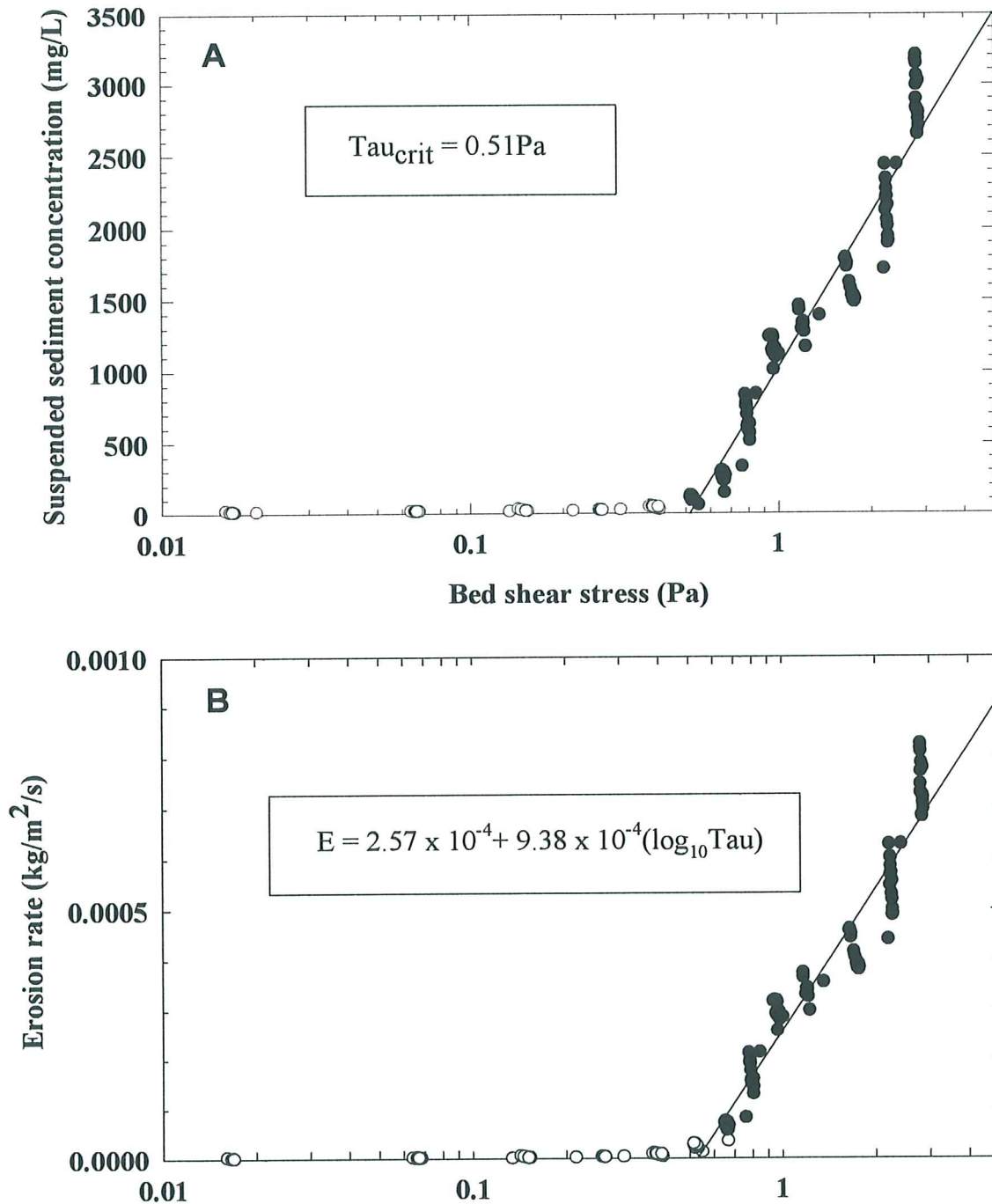
SITE R8 - 19 July, 1997

Figure 4.1.26. Estimations of the erosion threshold and erodibility for station R8 from (A) the relationship between bed shear stress and suspended sediment concentration, and (B) the relationship between bed shear stress and erosion rate

SEA CAROUSEL - Rustico Bay, PEI

SITE R9 - 20 July, 1997

A

Tau$_{crit}$ = 0.62 Pa

B

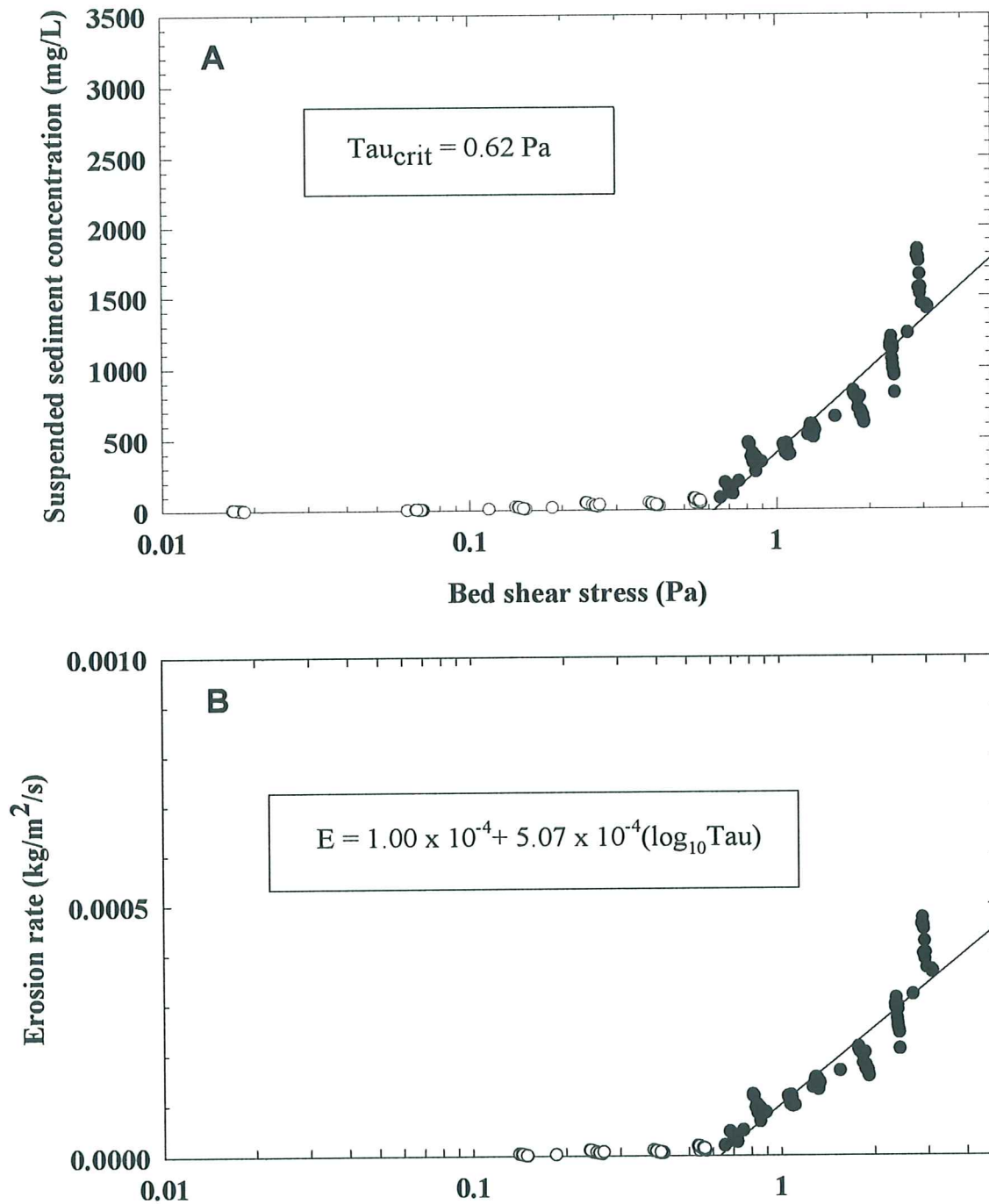$$E = 1.00 \times 10^{-4} + 5.07 \times 10^{-4}(\log_{10} Tau)$$

Figure 4.1.27. Estimations of the erosion threshold and erodibility for station R9 from (A) the relationship between bed shear stress and suspended sediment concentration, and (B) the relationship between bed shear stress and erosion rate

SEA CAROUSEL - Rustico Bay, PEI

SITE R10 - 20 July, 1997

A

$Tau_{crit} = 0.26$ Pa

Suspended sediment concentration (mg/L) vs *Bed shear stress (Pa)*

B

$E = 1.99 \times 10^{-3} + 3.24 \times 10^{-3} (\log_{10} Tau)$
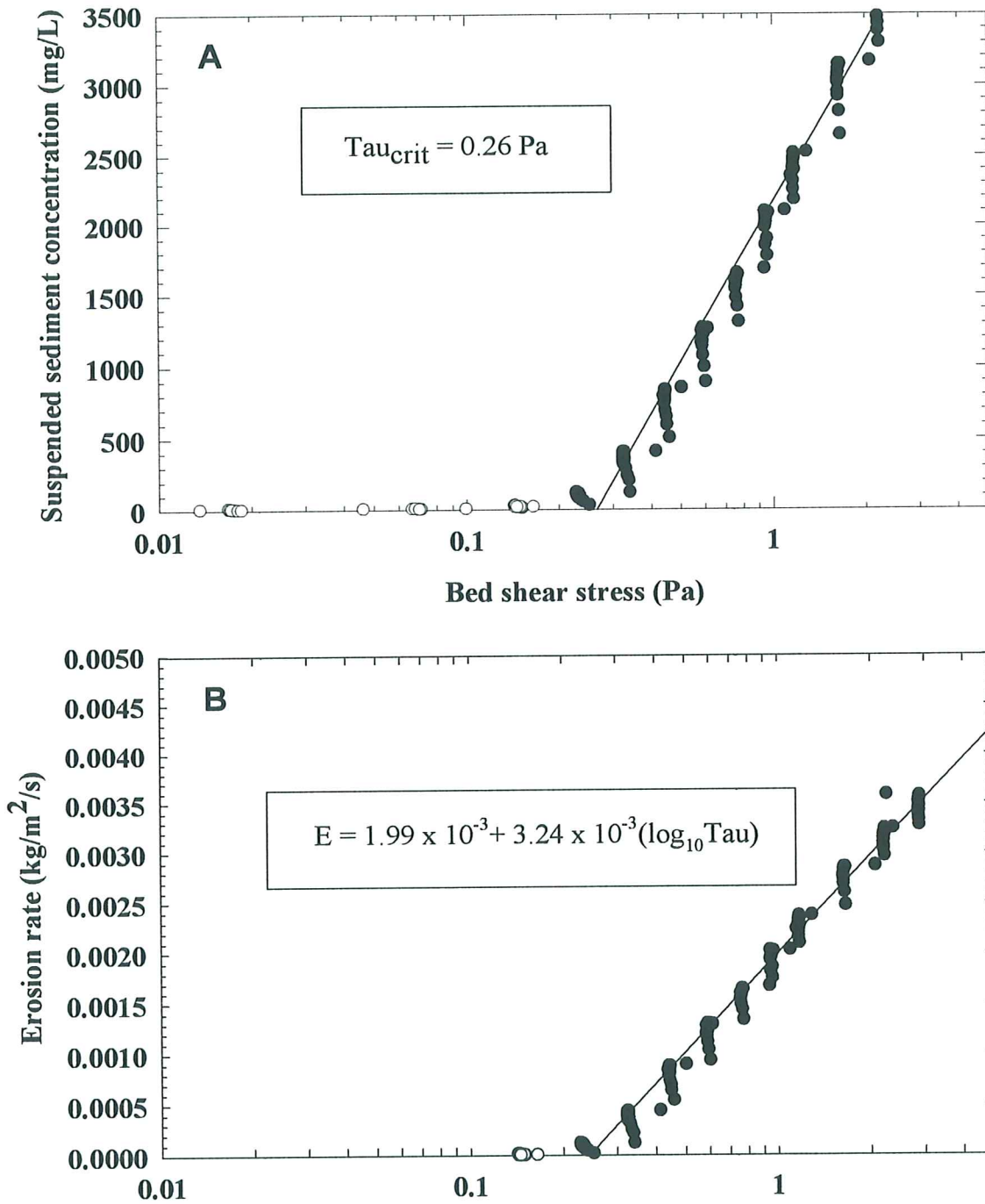
Erosion rate (kg/m²/s)

Figure 4.1.28. Estimations of the erosion threshold and erodibility for station R10 from (A) the relationship between bed shear stress and suspended sediment concentration, and (B) the relationship between bed shear stress and erosion rate

63

SEA CAROUSEL - Rustico Bay, PEI

SITE R11 - 21 July, 1997

A — Suspended sediment concentration (mg/L) vs Bed shear stress (Pa)

$$Tau_{crit} = 0.17 \ Pa$$

B — Erosion rate (kg/m^2/s) vs Bed shear stress (Pa)

$$E = 2.48 \times 10^{-3} + 3.10 \times 10^{-3}(\log_{10} Tau)$$
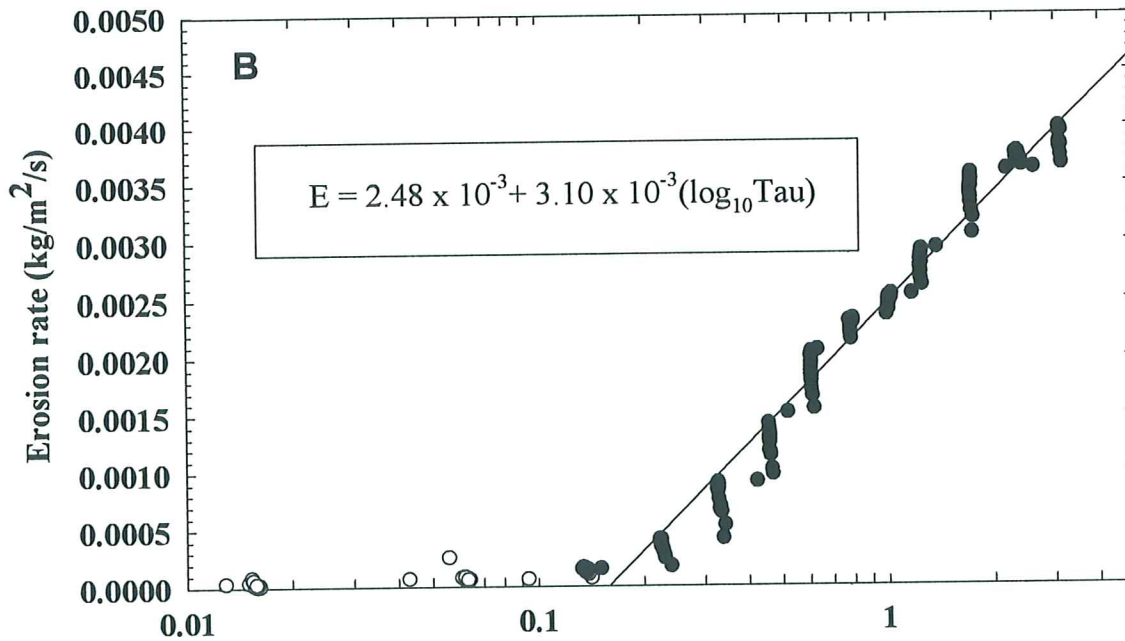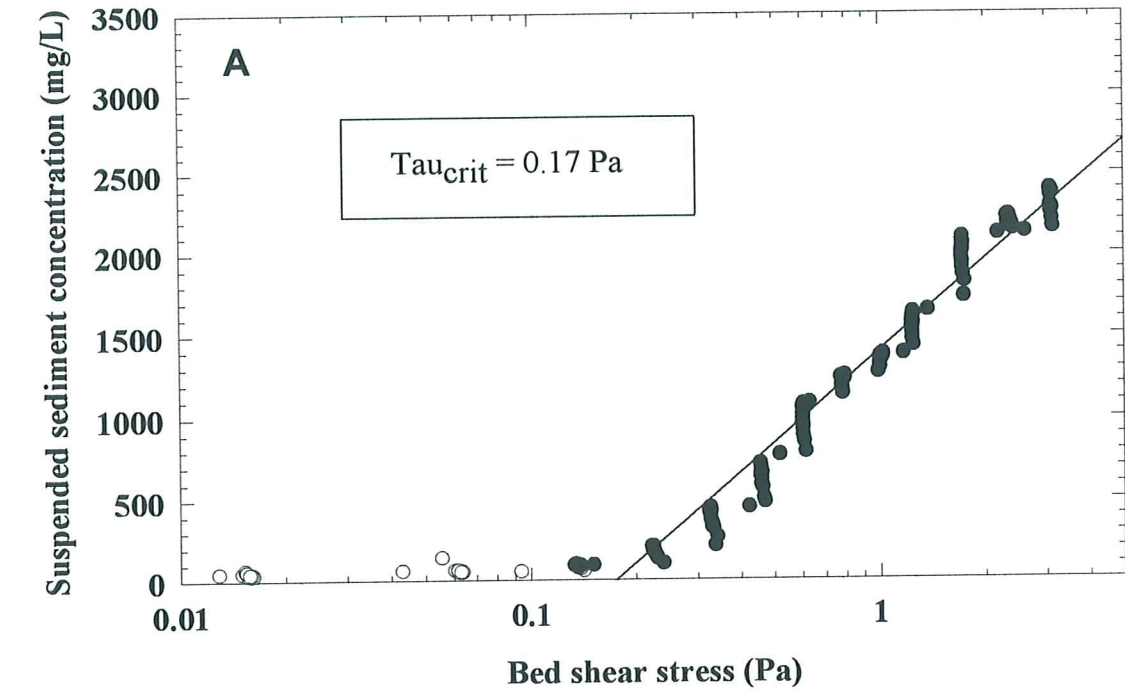
Figure 4.1.29. Estimations of the erosion threshold and erodibility for station R11 from (A) the relationship between bed shear stress and suspended sediment concentration, and (B) the relationship between bed shear stress and erosion rate

64

SEA CAROUSEL - Rustico Bay, PEI

SITE R12 - 21 July, 1997

A Tau$_{crit}$ = 0.17 Pa

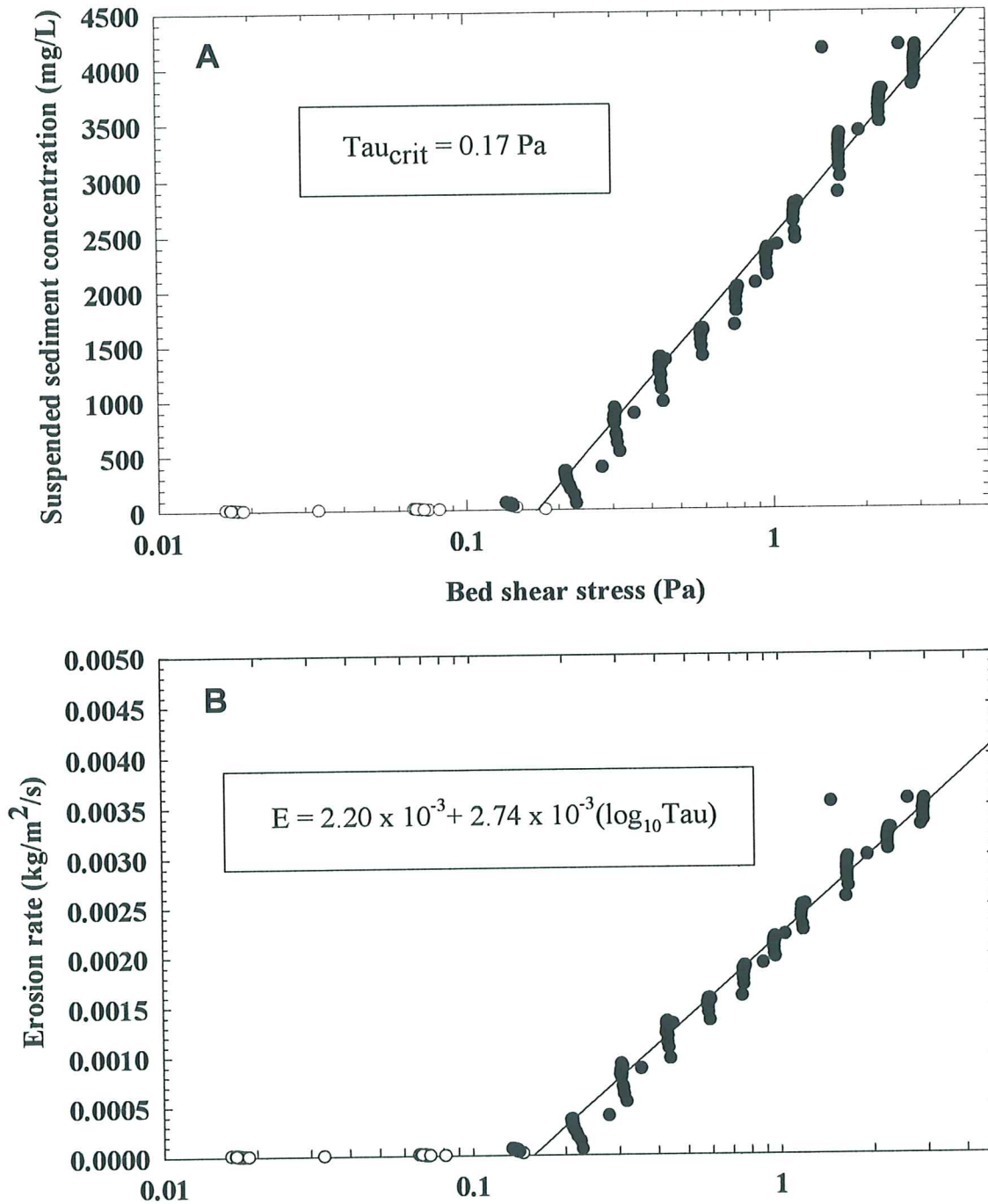**B** $E = 2.20 \times 10^{-3} + 2.74 \times 10^{-3}(\log_{10}Tau)$

Figure 4.1.30. Estimations of the erosion threshold and erodibility for station R12 from (A) the relationship between bed shear stress and suspended sediment concentration, and (B) the relationship between bed shear stress and erosion rate

65

SEA CAROUSEL - Rustico Bay, PEI

SITE R13 - 22 July, 1997

A

$Tau_{crit} = 0.40$ Pa

B

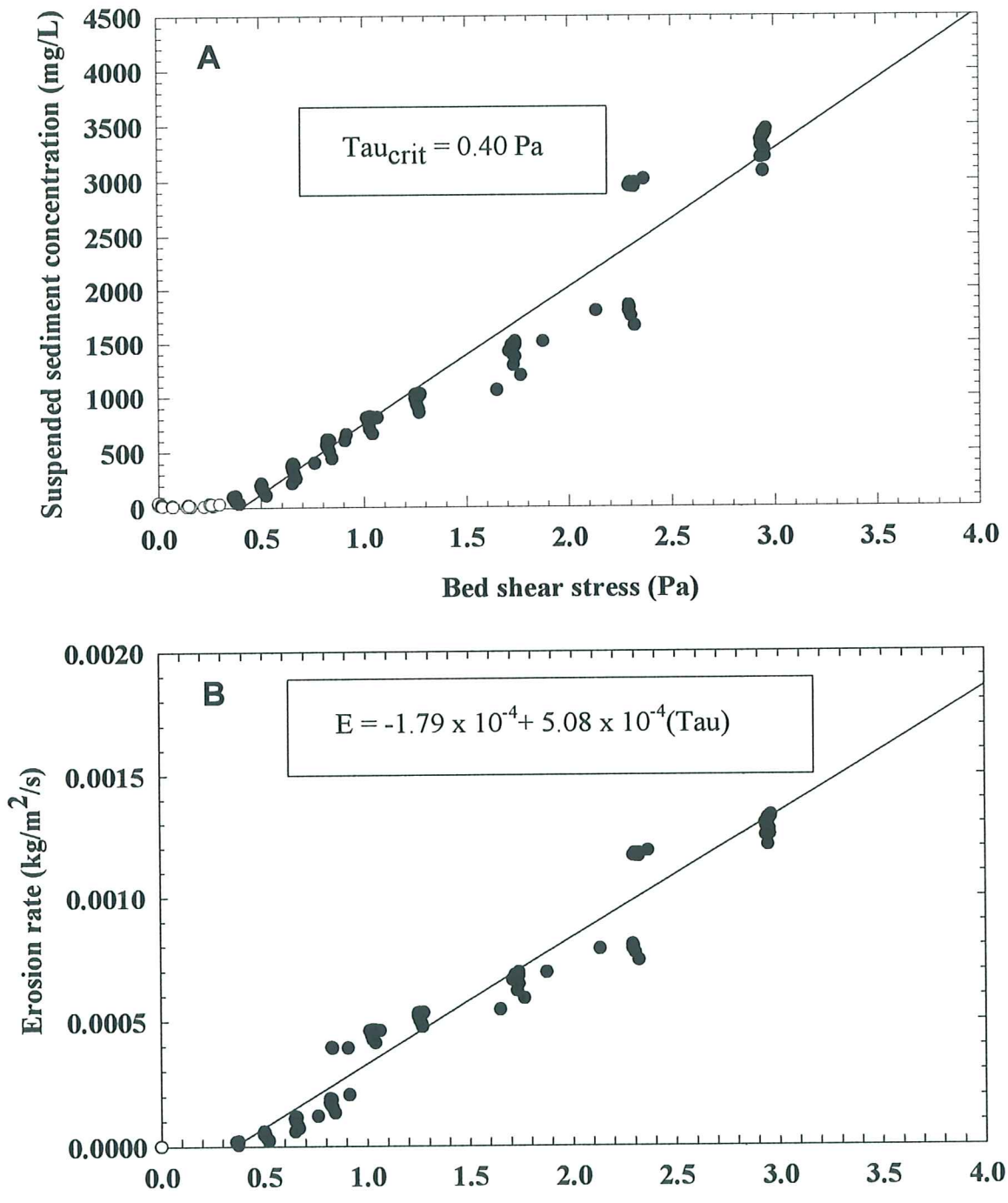$E = -1.79 \times 10^{-4} + 5.08 \times 10^{-4} (Tau)$

Figure 4.1.31. Estimations of the erosion threshold and erodibility for station R13 from (A) the relationship between bed shear stress and suspended sediment concentration, and (B) the relationship between bed shear stress and erosion rate

SEA CAROUSEL - Rustico Bay, PEI
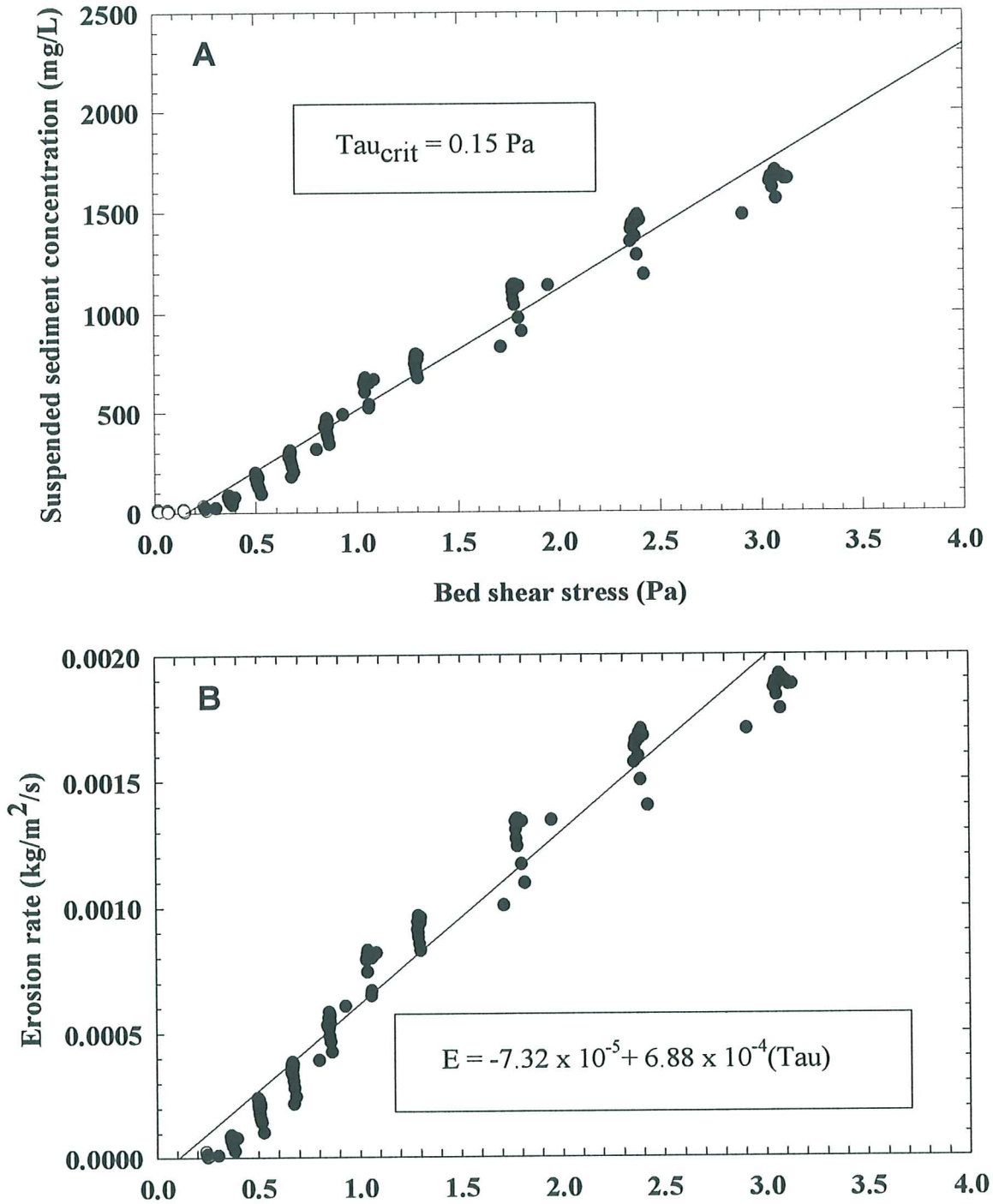
SITE R14 - 22 July, 1997

Figure 4.1.32. Estimations of the erosion threshold and erodibility for station R14 from (A) the relationship between bed shear stress and suspended sediment concentration, and (B) the relationship between bed shear stress and erosion rate

SEA CAROUSEL - Rustico Bay, PEI

SITE R15 - 23 July, 1997

A — $Tau_{crit} = 0.79$ Pa

Suspended sediment concentration (mg/L) vs Bed shear stress (Pa)

B — $E = 1.93 \times 10^{-4} + 1.82 \times 10^{-3}(Tau)$

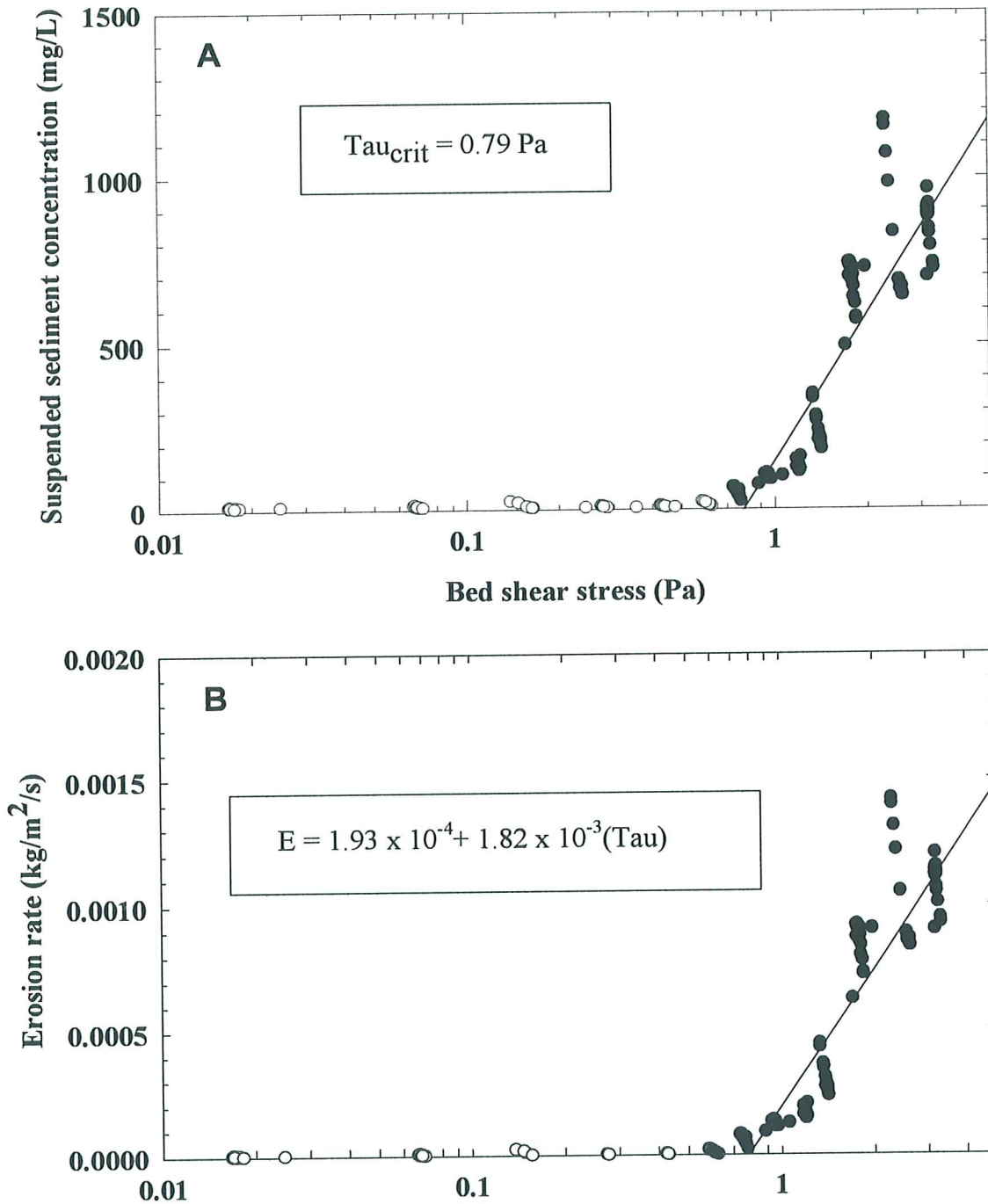Erosion rate (kg/m^2/s) vs Bed shear stress (Pa)

Figure 4.1.33. Estimations of the erosion threshold and erodibility for station R15 from (A) the relationship between bed shear stress and suspended sediment concentration, and (B) the relationship between bed shear stress and erosion rate
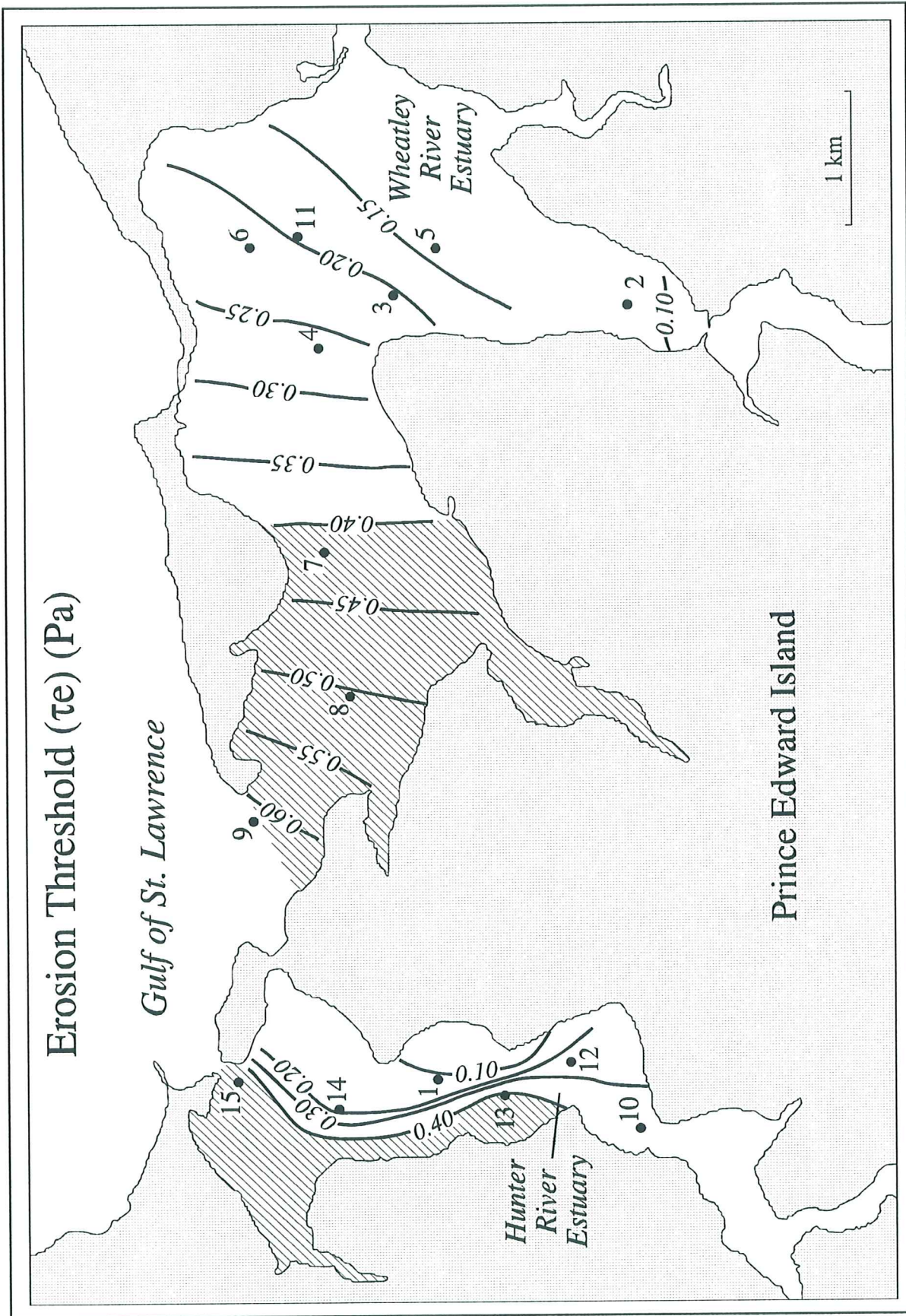
Erosion Threshold (τe) (Pa)

Figure 4.1.34. The distribution of erosion thresholds of bottom sediment in Rustico Bay. The highest thresholds are found in the eastern parts of the Hunter and Wheatley river estuaries in regions of high mud content. The thresholds appear to decrease systematically landwards in the Wheatley estuary, but appears to be influenced by other factors in the Hunter estuary.

Erosion Rate (E) (kg/m^2/s x 10^{3}log$_{10}$ (τ_0))

Figure 4.1.35. The distribution of erosion rate of bottom sediment in Rustico Bay. The highest rates are found in the eastern parts of the Hunter and Wheatley river estuaries in regions of high mud content.
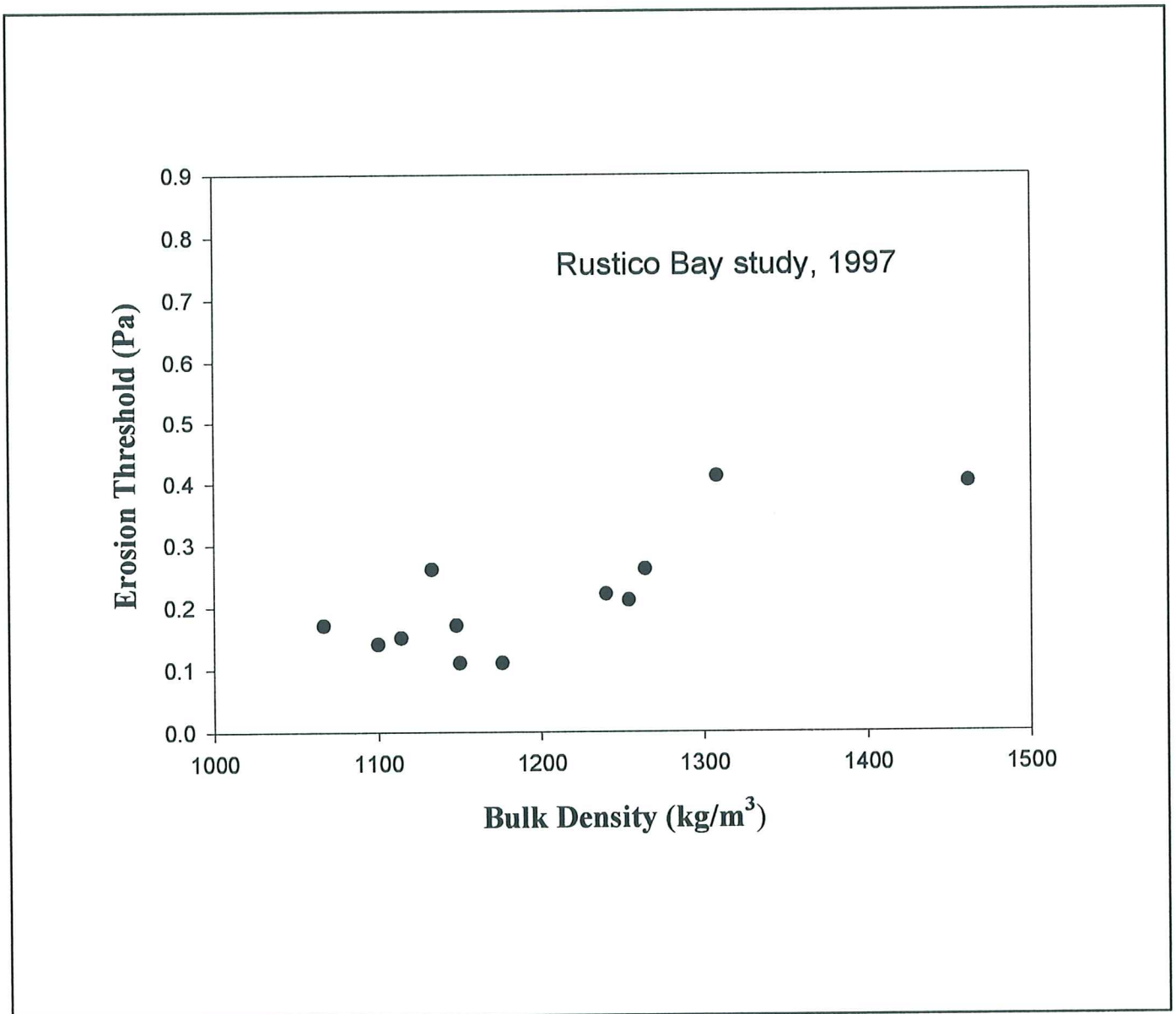
Prince Edward Island

Figure 4.1.36. A scattergram of the measured erosion thresholds of bottom sediments in Rustico Bay plotted against sediment bulk density determined from Catscan analyses of syringe cores. No clear trend emerges, though a weak positive relationship may be inferred.
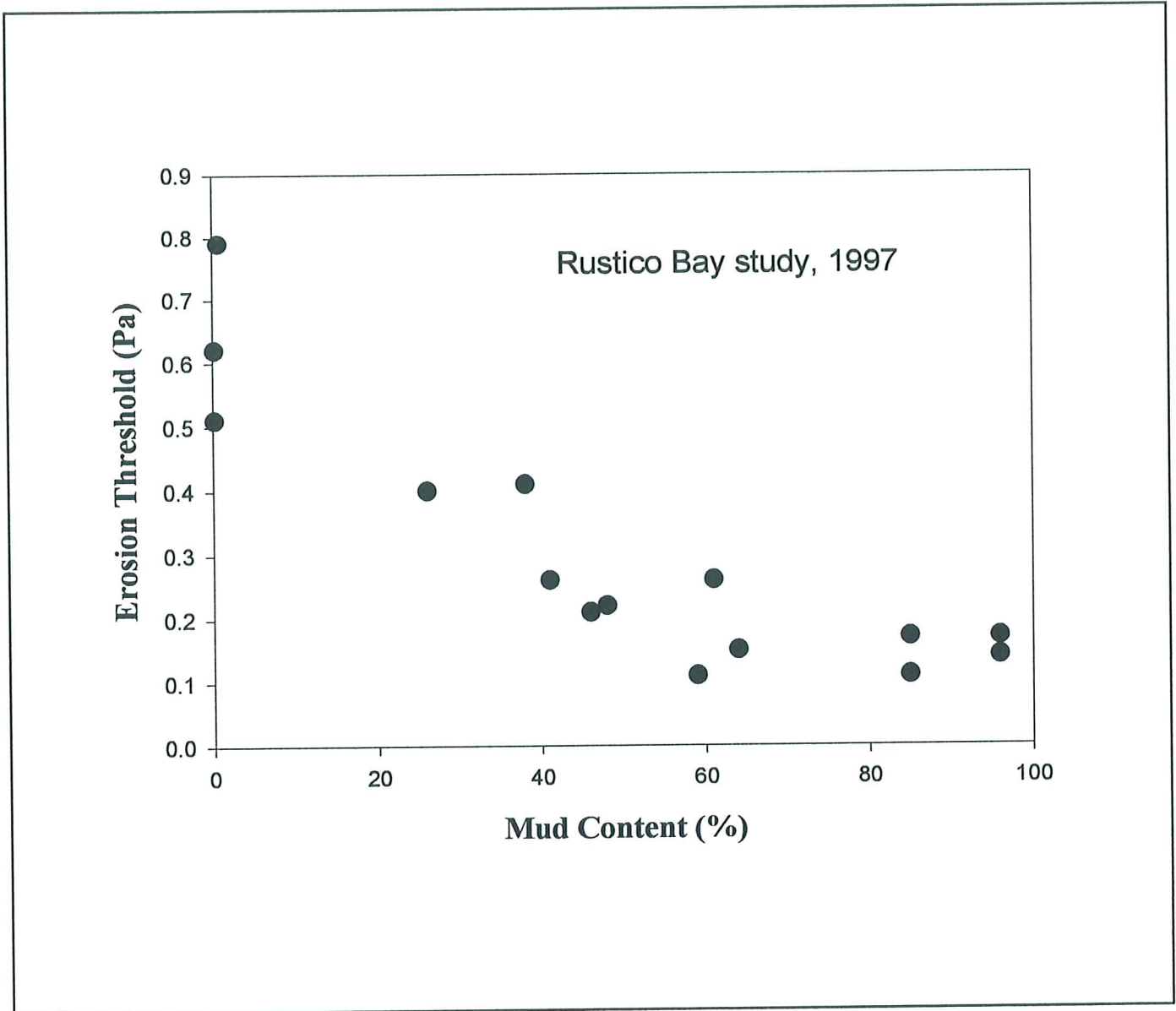
Figure 4.1.36. A scattergram of the measured erosion thresholds of bottom sediments in Rustico Bay plotted against sediment mud content. A clear inverse relationship is apparent: the higher the erosion threshold, the lower the mud content.
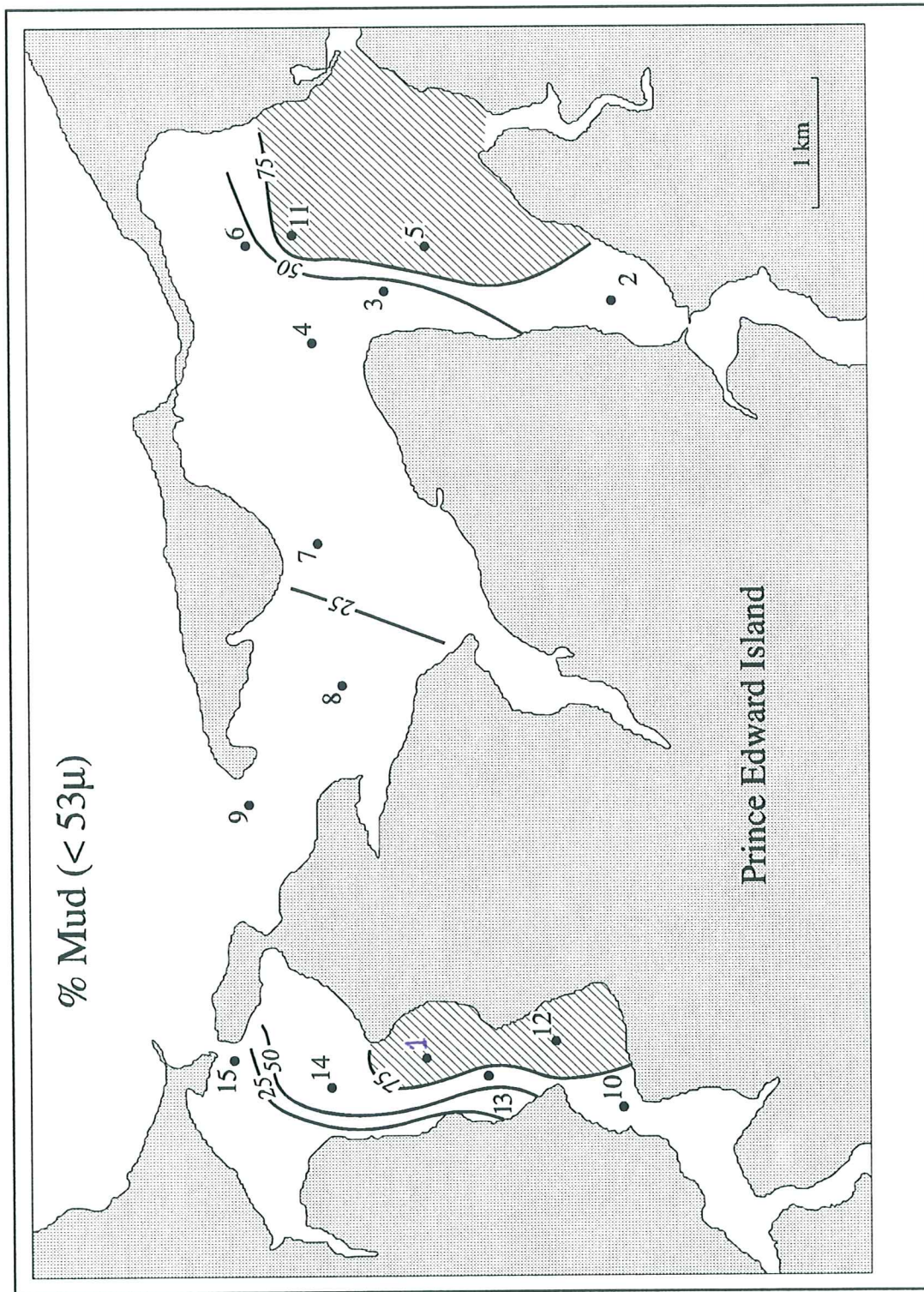
Figure 3.1.37. The mud content of bottom sediments in Rustico Bay determined from analyses of the samples collected at each of the Sea Carousel stations. In general the estuaries are largely muddy in the inner and central parts and sandy in the outer parts. The regions of highest mud content are found along the eastermost flanks of the Hunter and Wheatley river estuaries. The inner parts of the estuaries are intermediate in mud content reflecting the effects of the bridge/causeways.

73

Figure 4.2.1. The still-water settling of material eroded from the bed during the Sea Carousel deployment at station R1 (A) the time-series of suspended sediment concentration and incremental deposited mass; and (B) the estimated mass settling rate and equivalent sedimentation diameter.

74

Figure 4.2.2. The still-water settling of material eroded from the bed during the Sea Carousel deployment at station R2 (A) the time-series of suspended sediment concentration and incremental deposited mass; and (B) the estimated mass settling rate and equivalent sedimentation diameter.

Figure 4.2.3. The still-water settling of material eroded from the bed during the Sea Carousel deployment at station R3 (A) the time-series of suspended sediment concentration and incremental deposited mass; and (B) the estimated mass settling rate and equivalent sedimentation diameter.
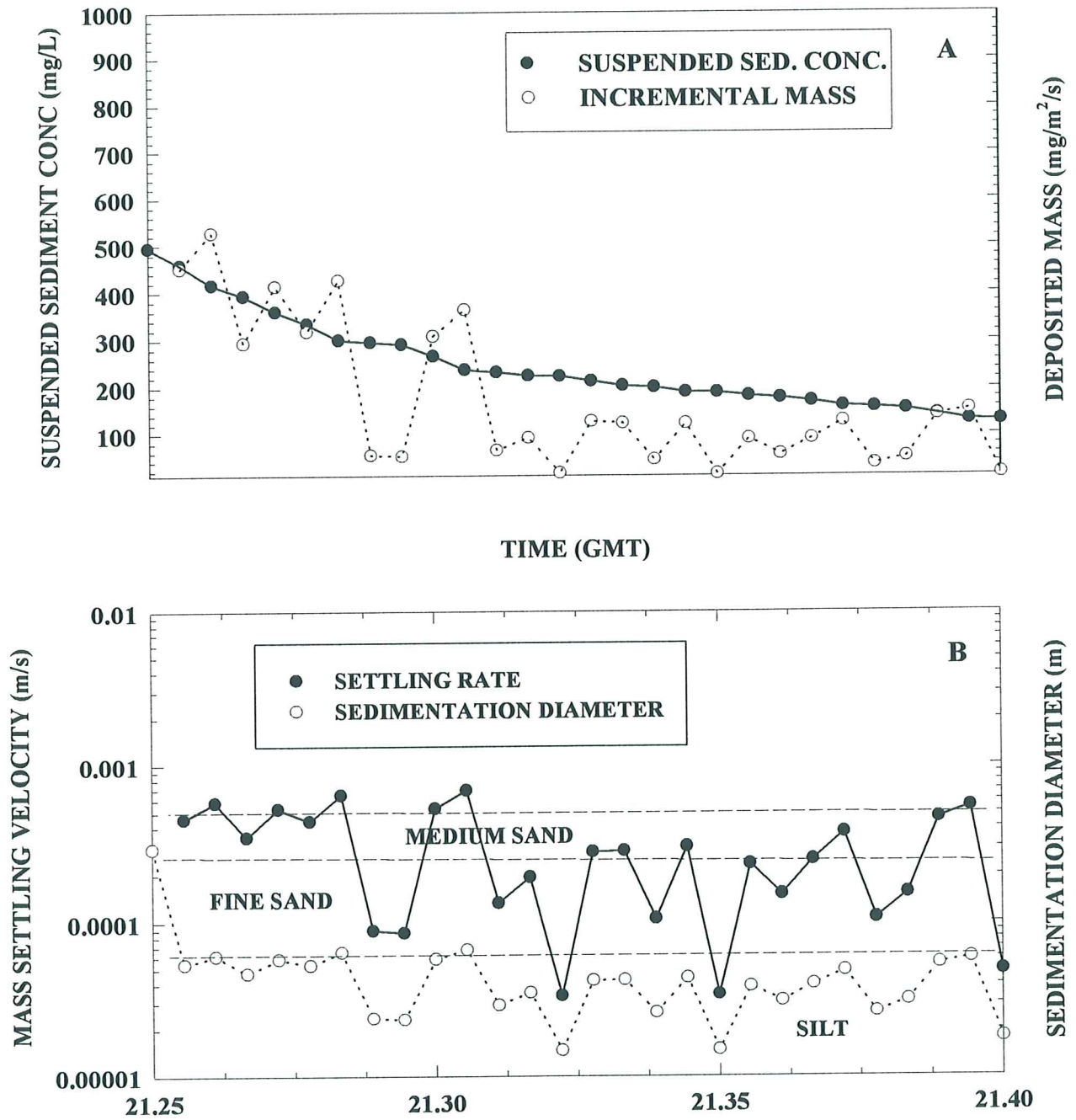
Figure 4.2.4. The still-water settling of material eroded from the bed during the Sea Carousel deployment at station R4 (A) the time-series of suspended sediment concentration and incremental deposited mass; and (B) the estimated mass settling rate and equivalent sedimentation diameter.
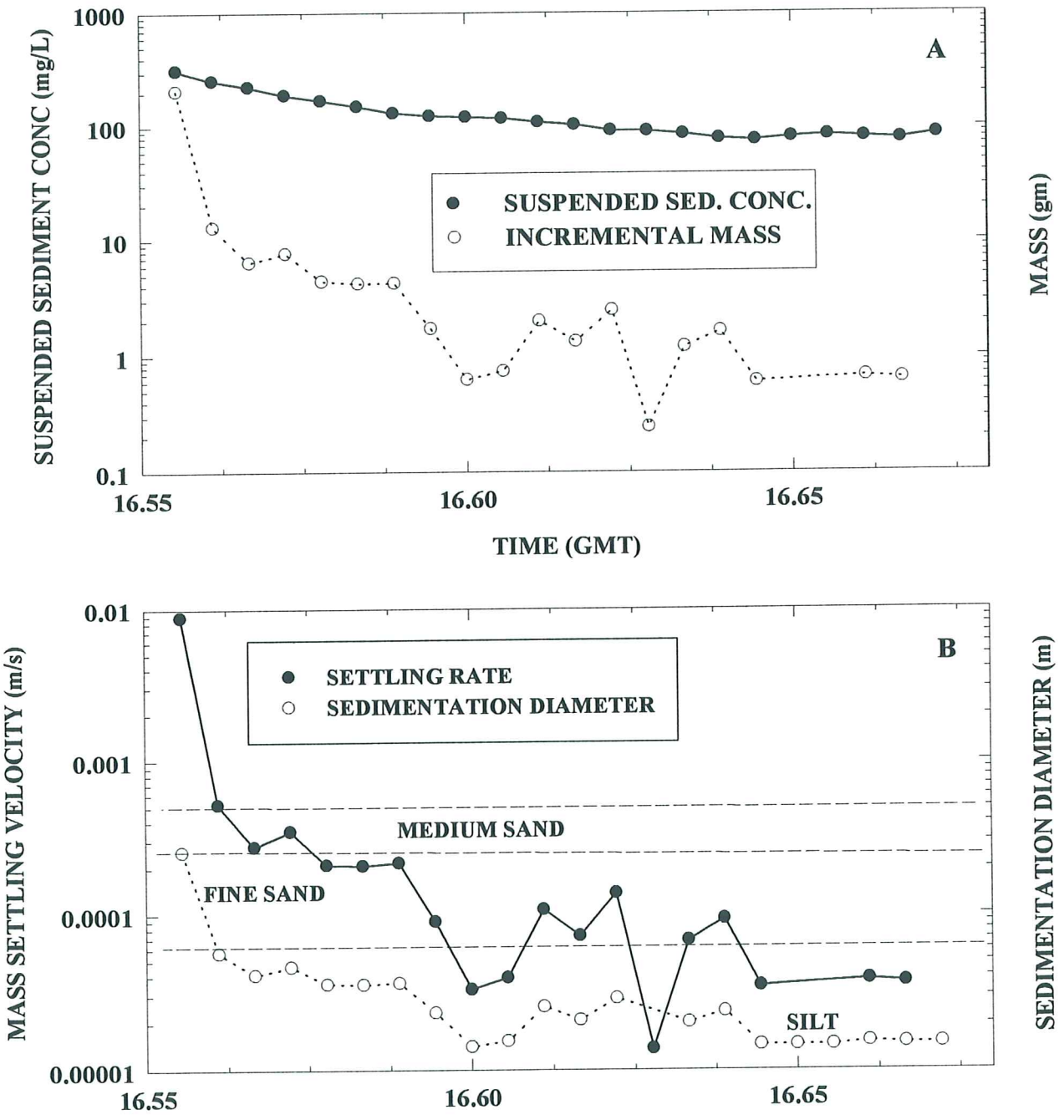
Figure 4.2.5. The still-water settling of material eroded from the bed during the Sea Carousel deployment at station R5 (A) the time-series of suspended sediment concentration and incremental deposited mass; and (B) the estimated mass settling rate and equivalent sedimentation diameter.

Figure 4.2.6. The still-water settling of material eroded from the bed during the Sea Carousel deployment at station R6 (A) the time-series of suspended sediment concentration and incremental deposited mass; and (B) the estimated mass settling rate and equivalent sedimentation diameter.
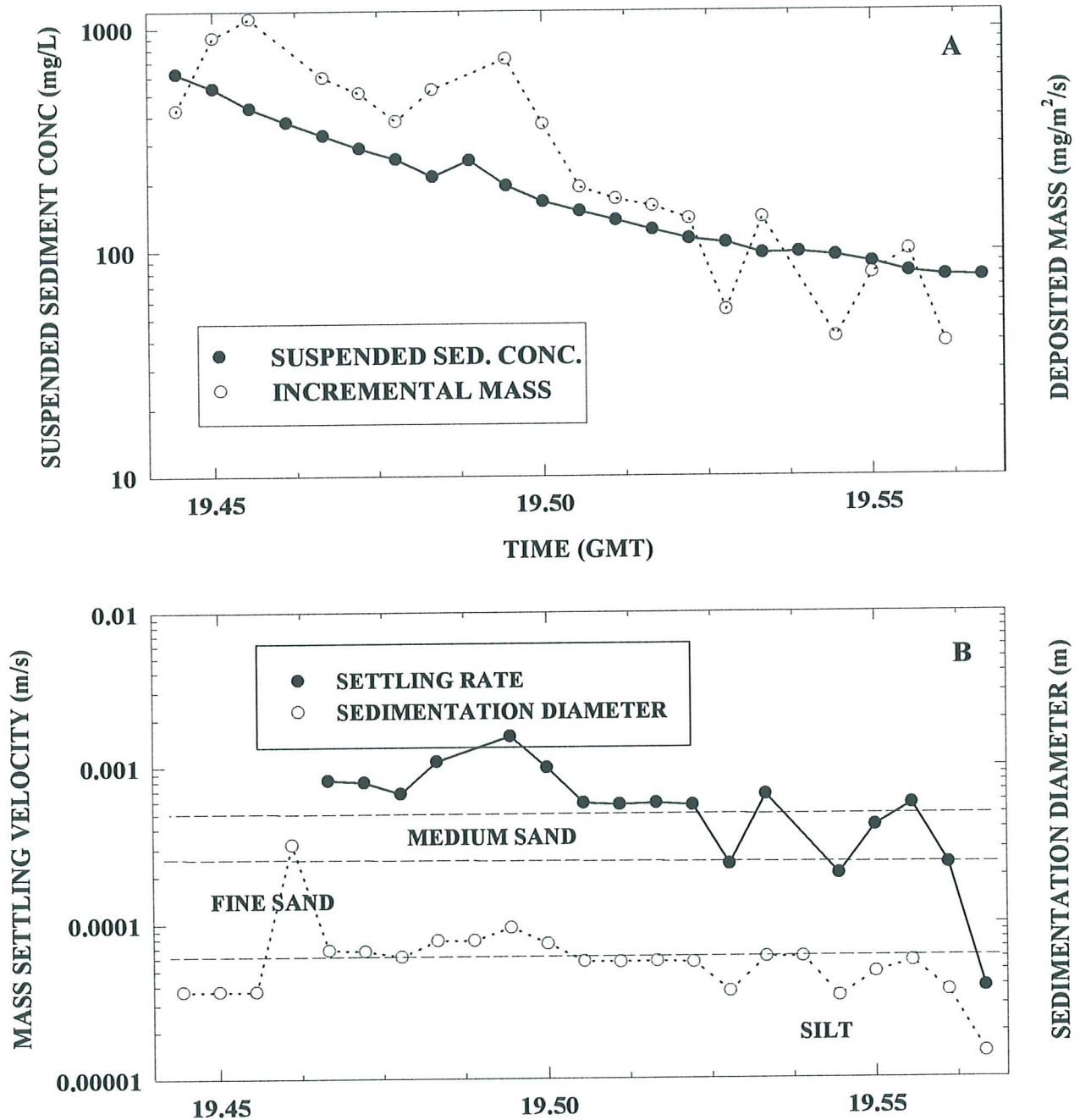
Figure 4.2.7. The still-water settling of material eroded from the bed during the Sea Carousel deployment at station R7 (A) the time-series of suspended sediment concentration and incremental deposited mass; and (B) the estimated mass settling rate and equivalent sedimentation diameter.
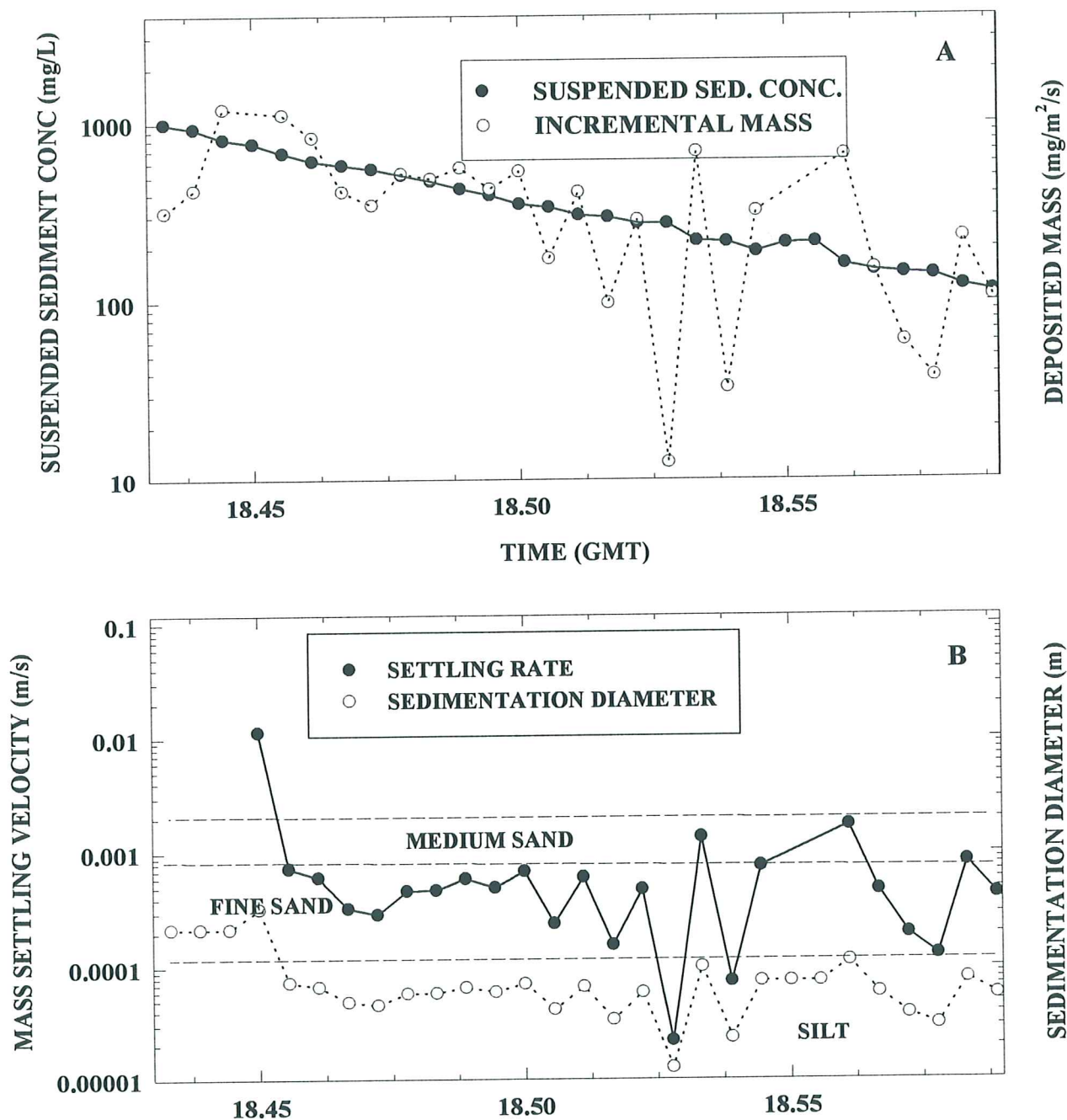
Figure 4.2.8. The still-water settling of material eroded from the bed during the Sea Carousel deployment at station R10 (A) the time-series of suspended sediment concentration and incremental deposited mass; and (B) the estimated mass settling rate and equivalent sedimentation diameter.
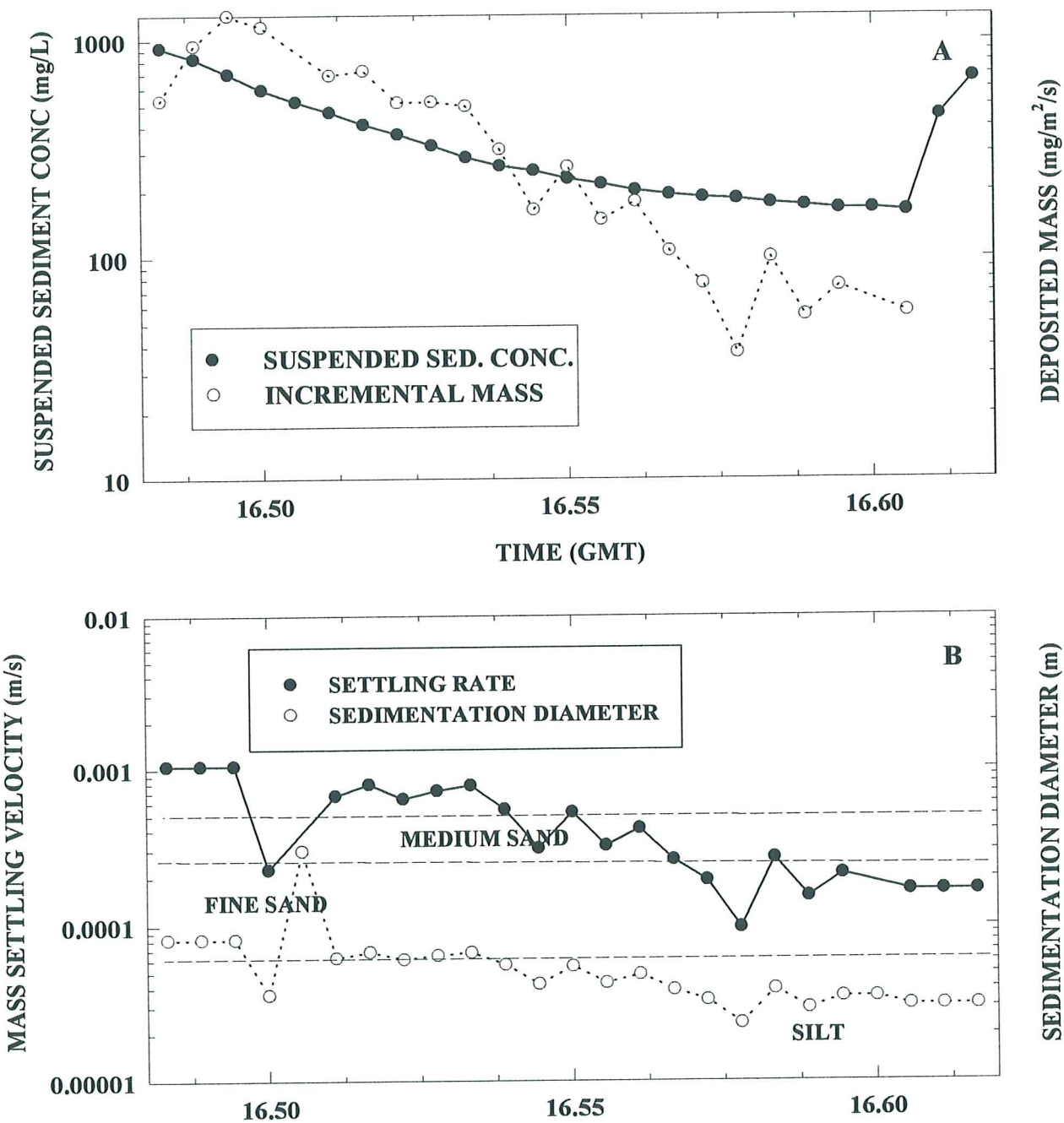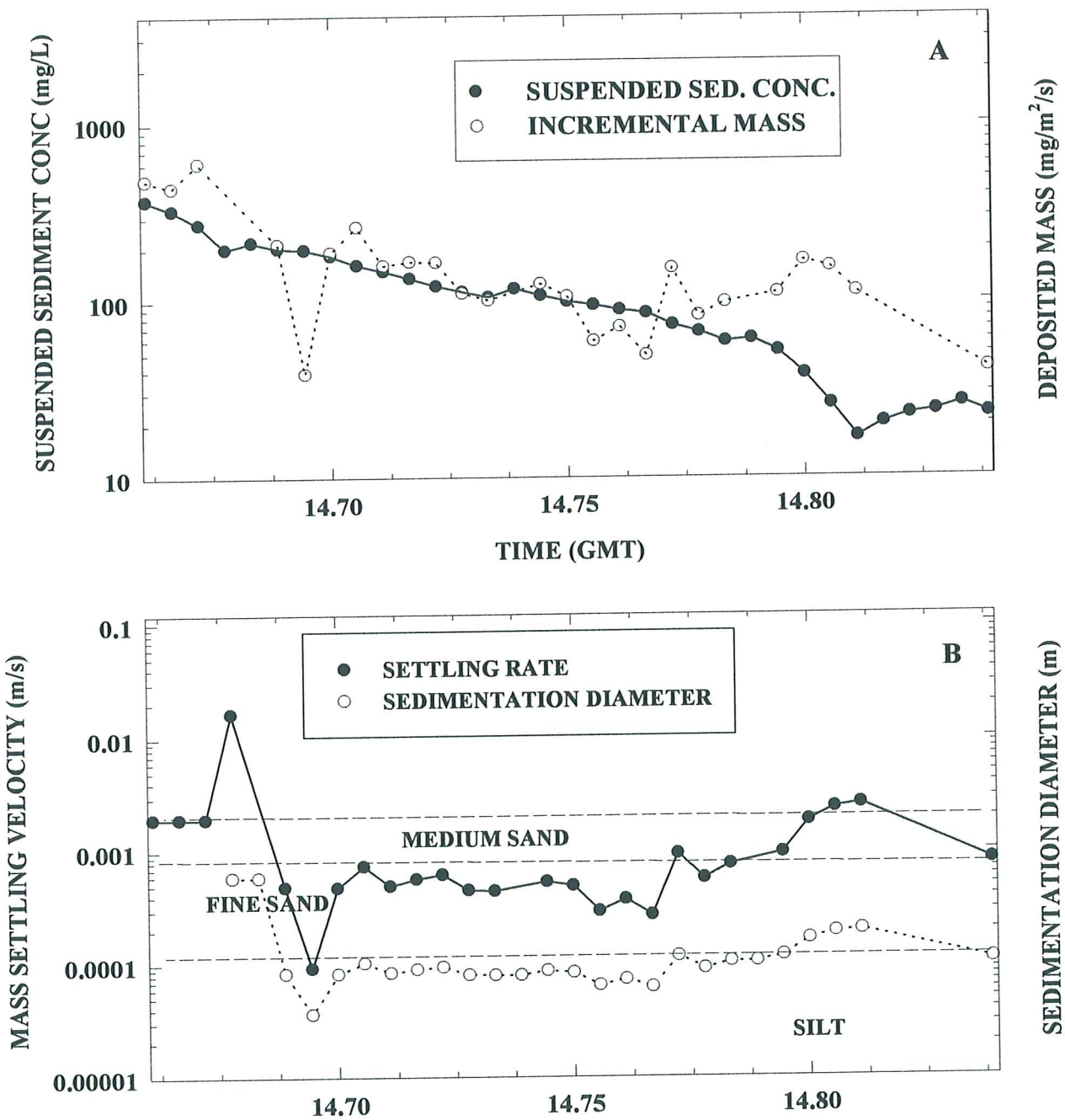
Figure 4.2.9. The still-water settling of material eroded from the bed during the Sea Carousel deployment at station R11 (A) the time-series of suspended sediment concentration and incremental deposited mass; and (B) the estimated mass settling rate and equivalent sedimentation diameter.
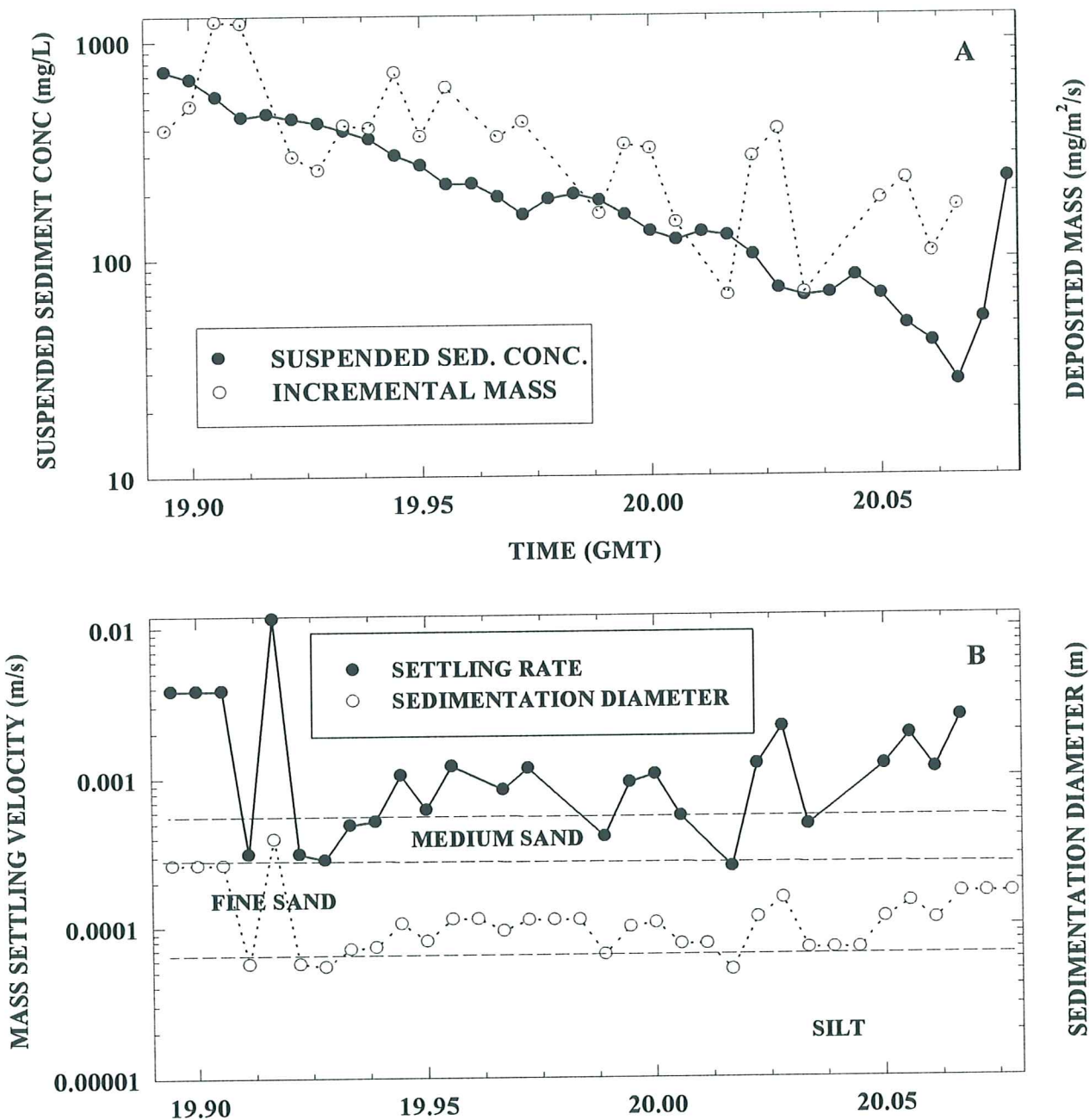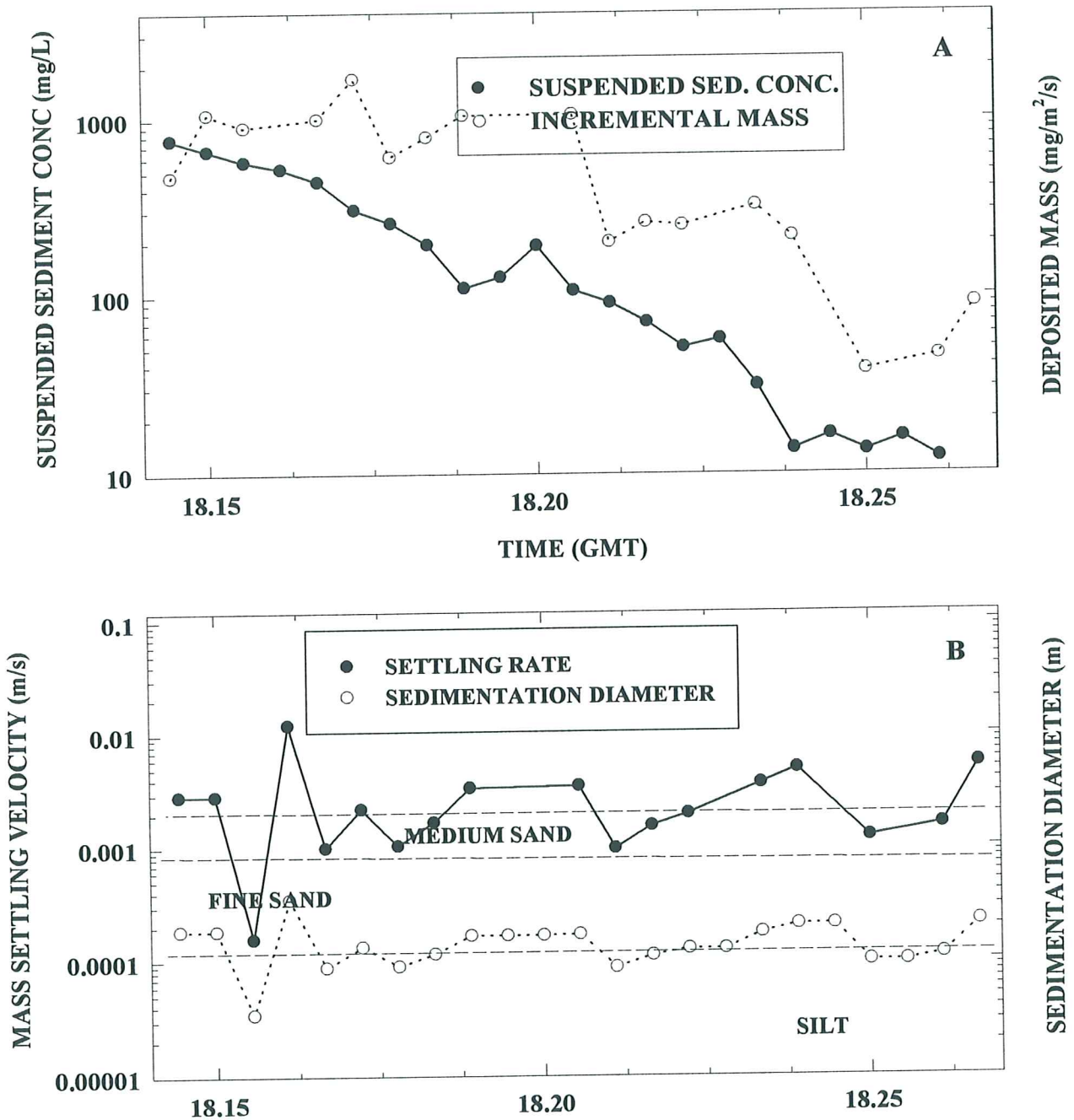
Figure 4.2.10. The still-water settling of material eroded from the bed during the Sea Carousel deployment at station R12 (A) the time-series of suspended sediment concentration and incremental deposited mass; and (B) the estimated mass settling rate and equivalent sedimentation diameter.
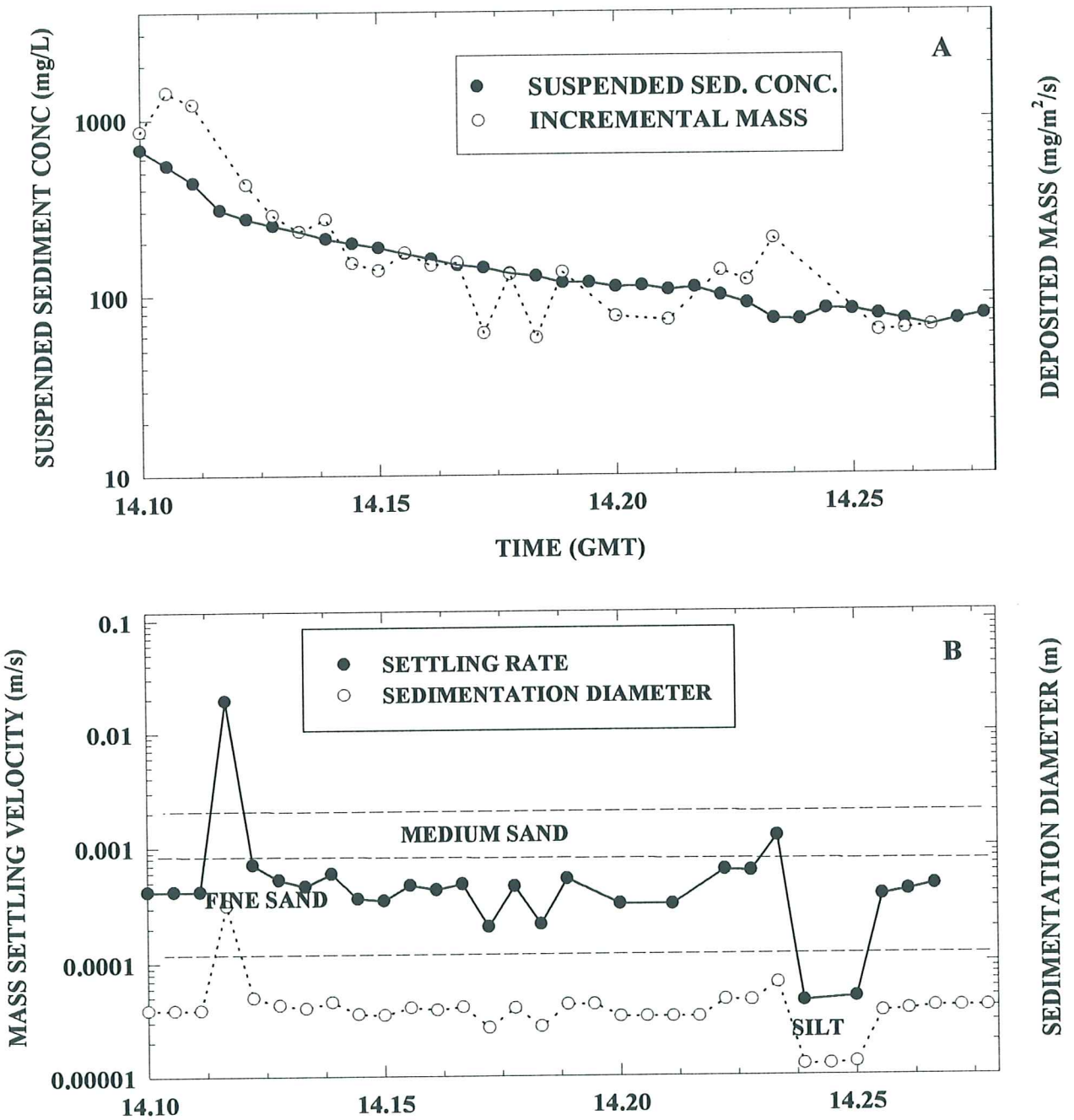
Figure 4.2.11. The still-water settling of material eroded from the bed during the Sea Carousel deployment at station R13 (A) the time-series of suspended sediment concentration and incremental deposited mass; and (B) the estimated mass settling rate and equivalent sedimentation diameter.
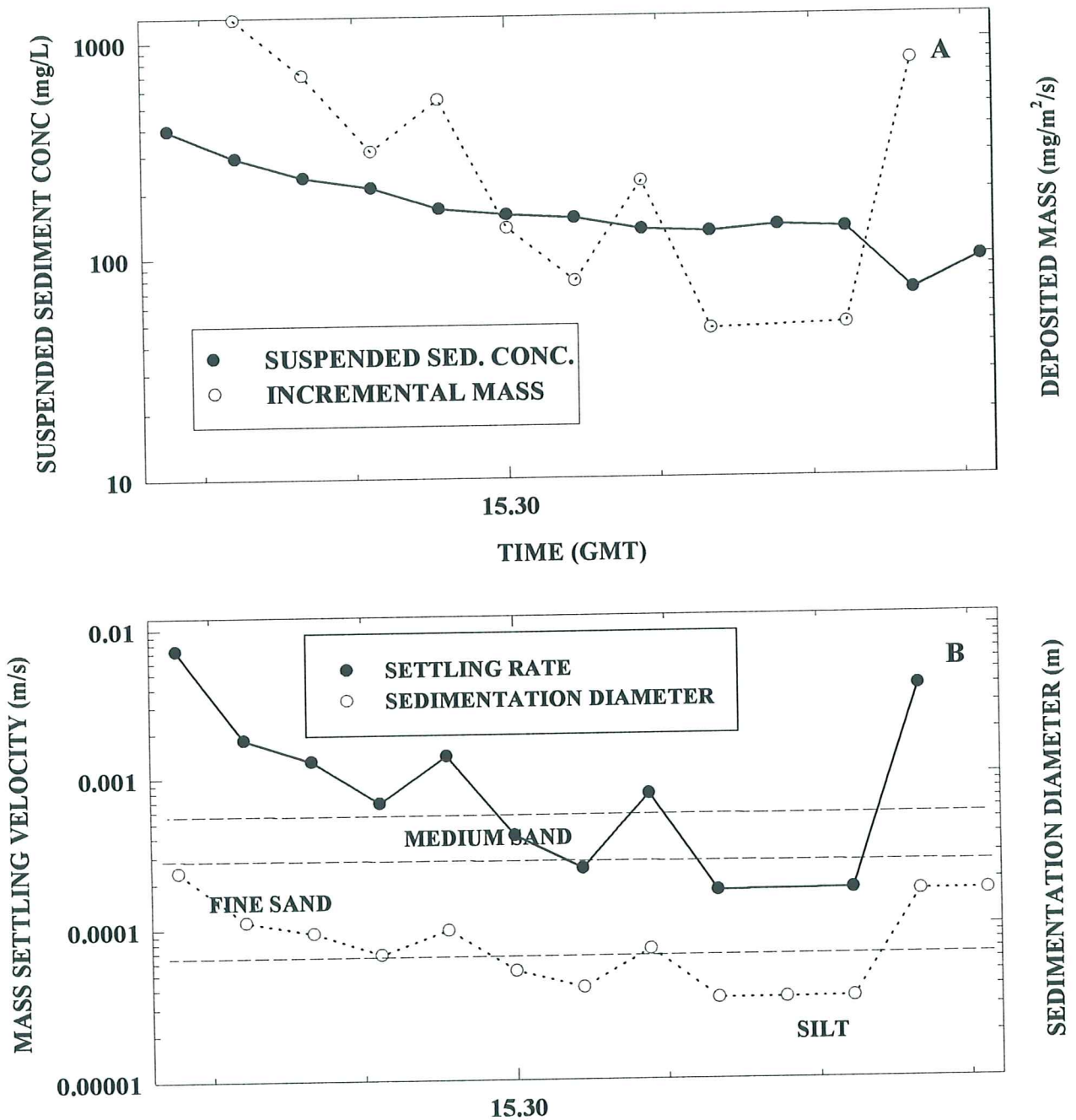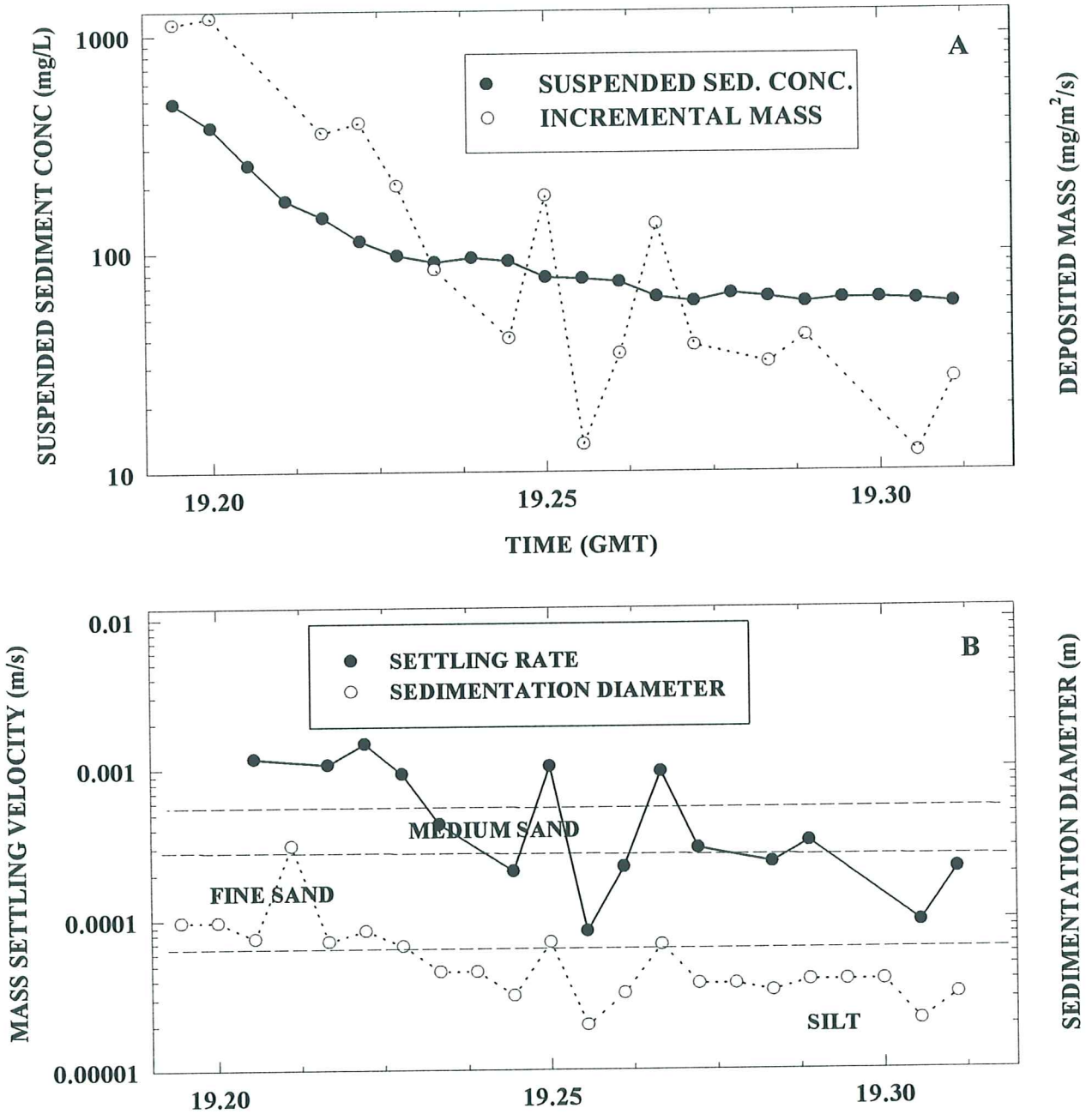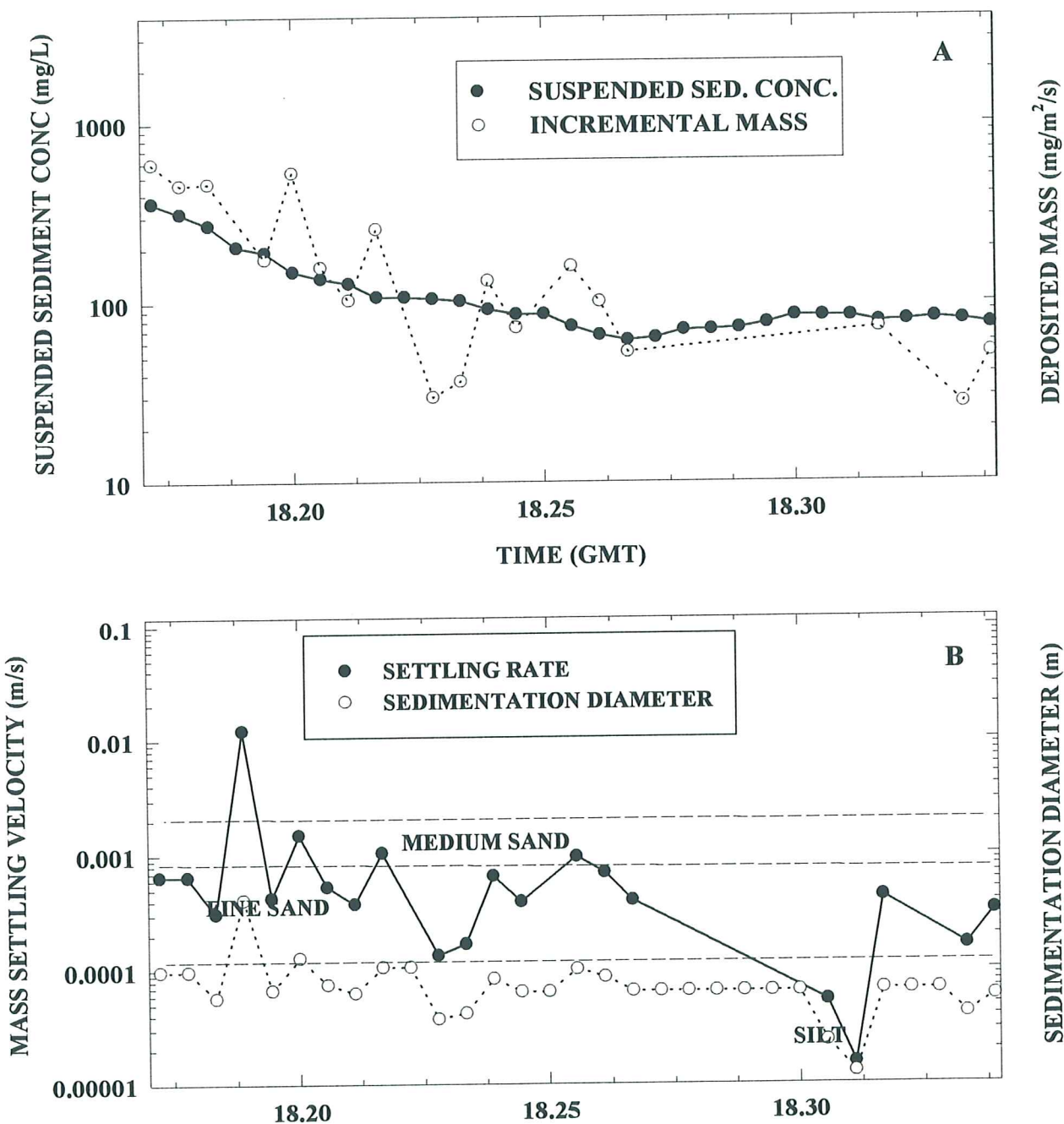
Figure 4.2.12. The still-water settling of material eroded from the bed during the Sea Carousel deployment at station R14 (A) the time-series of suspended sediment concentration and incremental deposited mass; and (B) the estimated mass settling rate and equivalent sedimentation diameter.
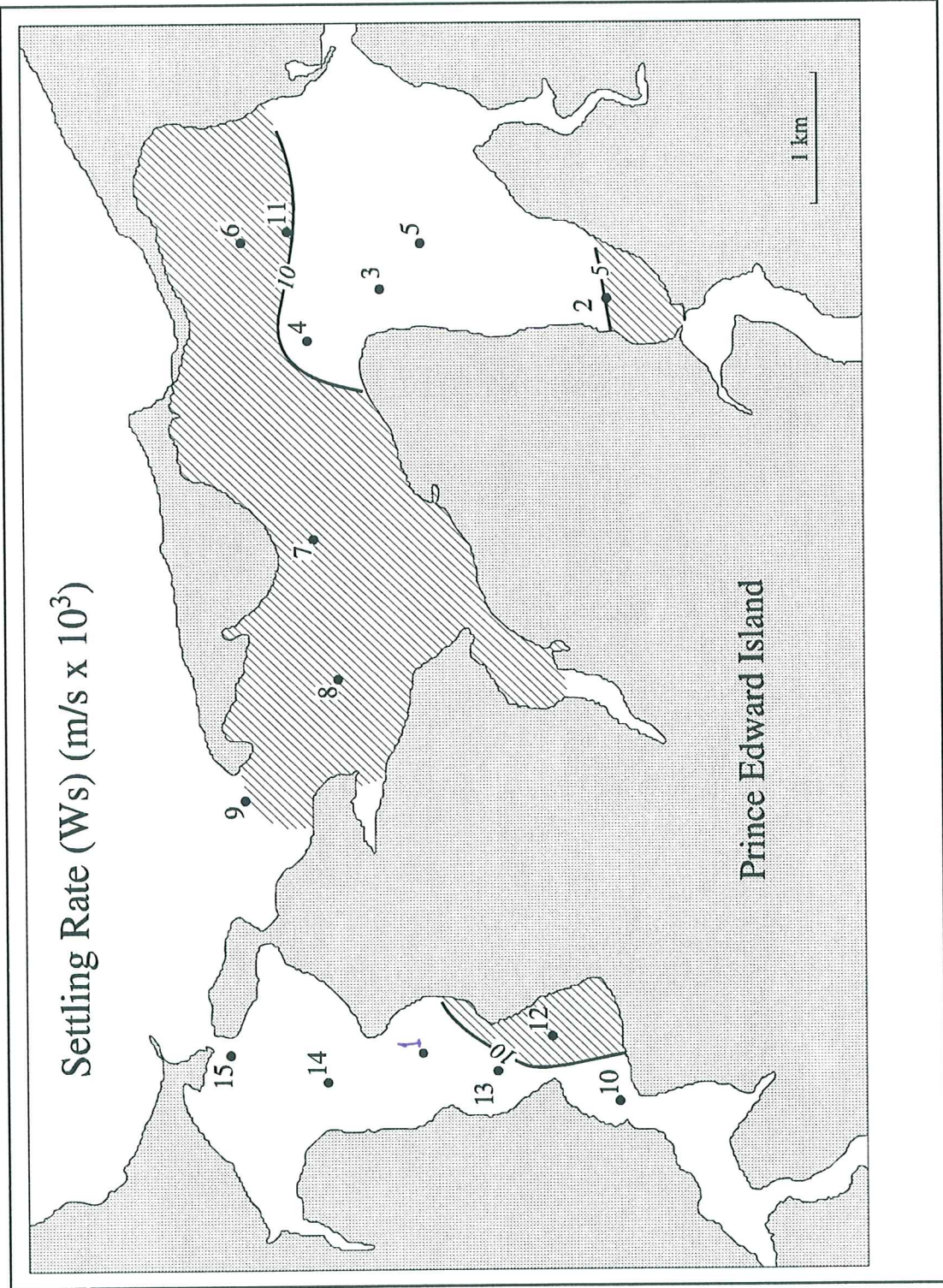
Figure 4.2.13. The distribution of still water settling velocities determined from Sea Carousel in Rustico Bay. The shaded regions denote highest settling rates.
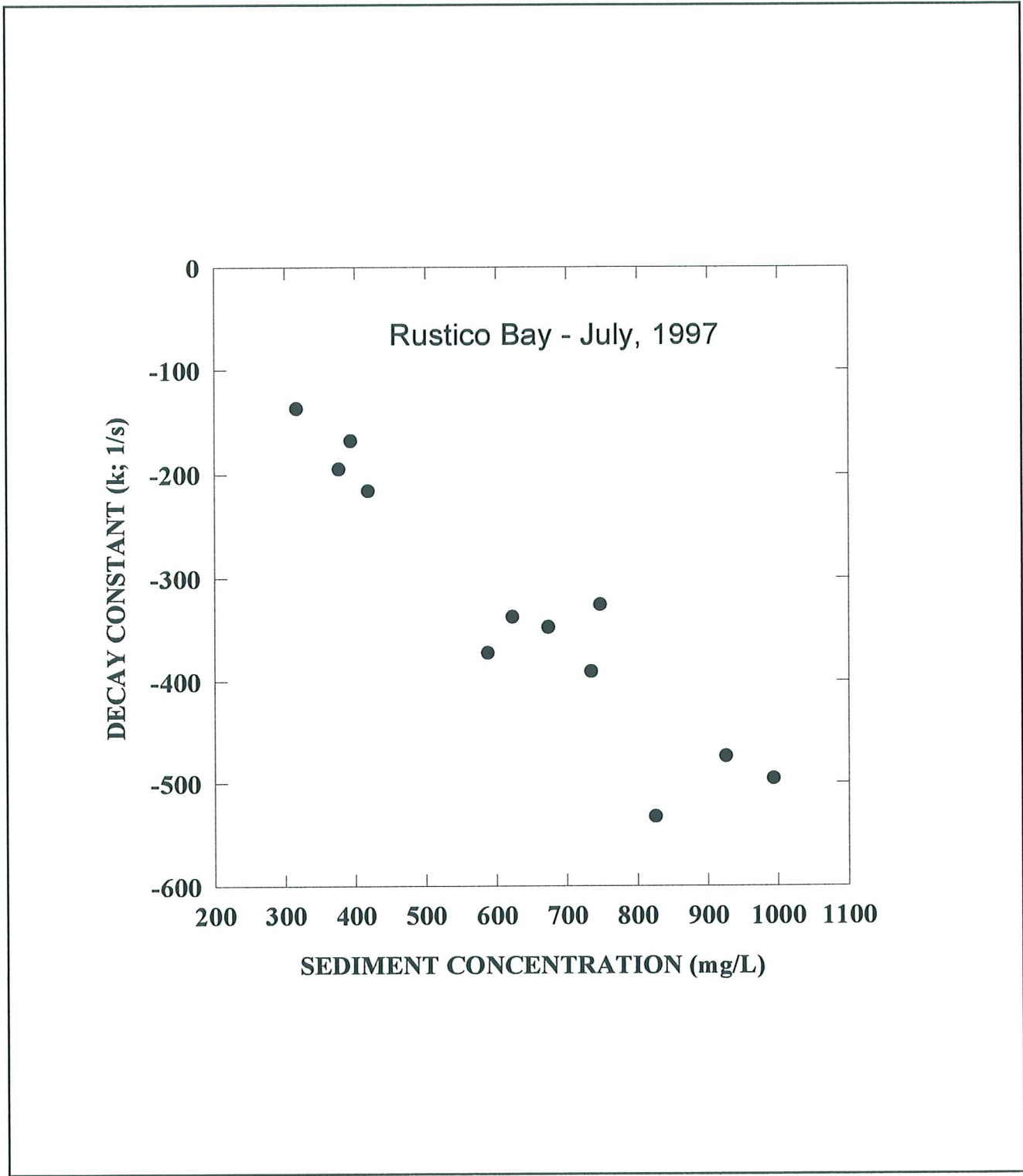
Figure 4.2.14. A scattergram of the sedimentation decay constant k plotted against initial sediment concentration for all stations. Notice the linear trend between the two variables, that is consistent for both the Wheatley and Hunter River estuaries.
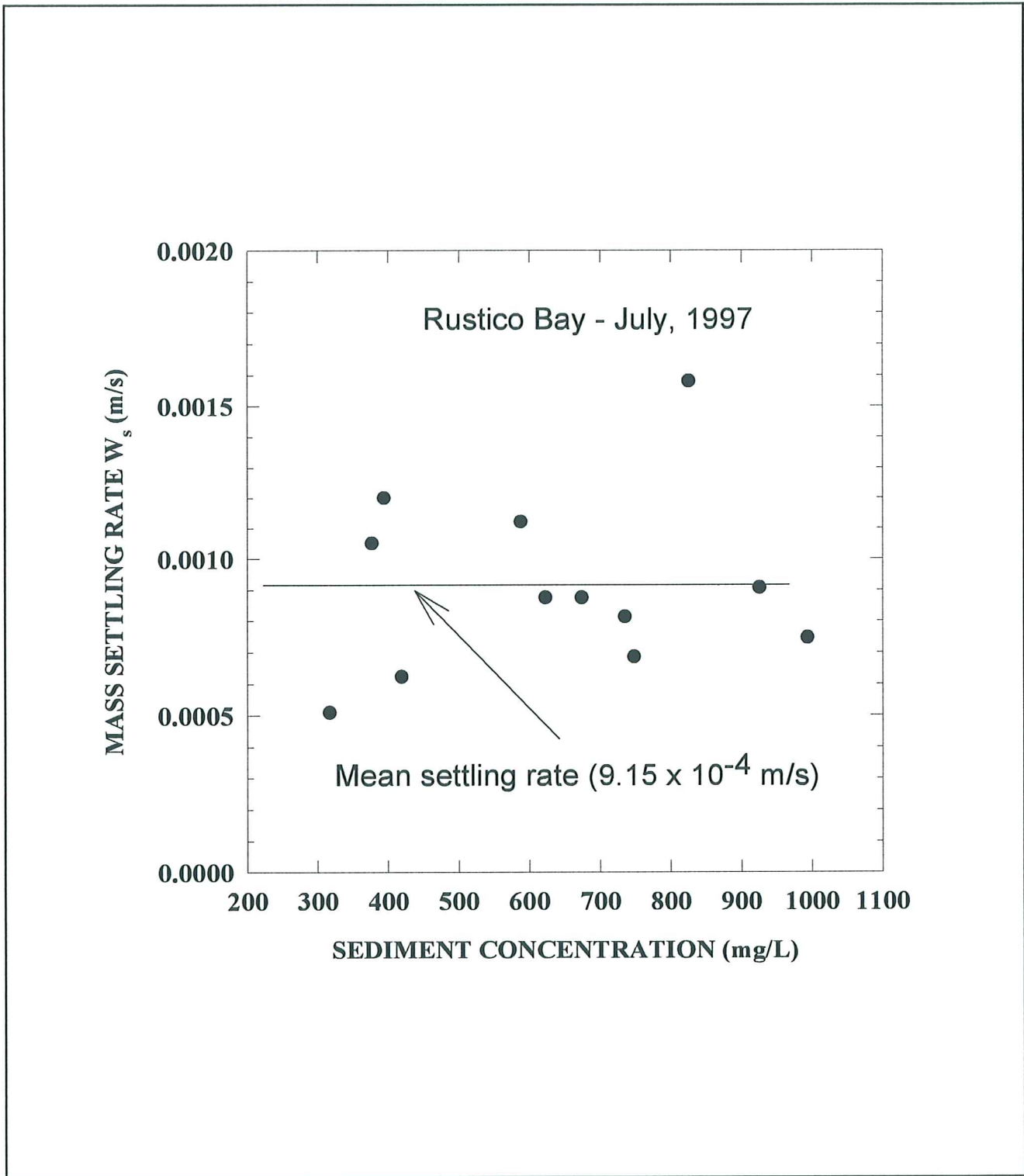
Figure 4.2.15 A scattergram of the still water settling rate W_s plotted against initial sediment concentration for all stations. A mean estuary-wide value of settling rate is 9.15×10^{-4} m/s.
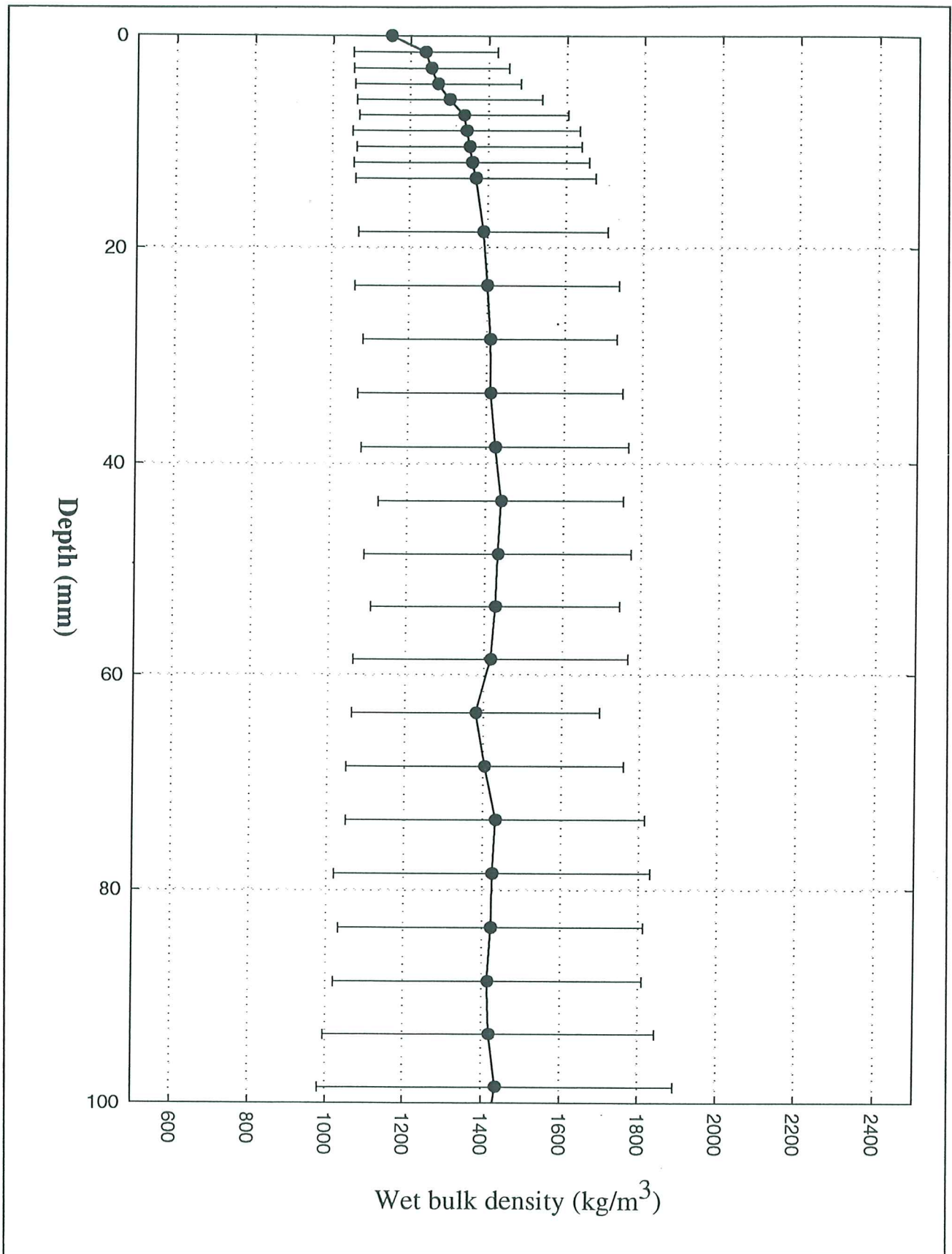
Figure 4.3.1. Sediment bulk density and the variance of density plotted against sediment depth. The values are derived from Catscan analyses of a syringe core collected at station R1.
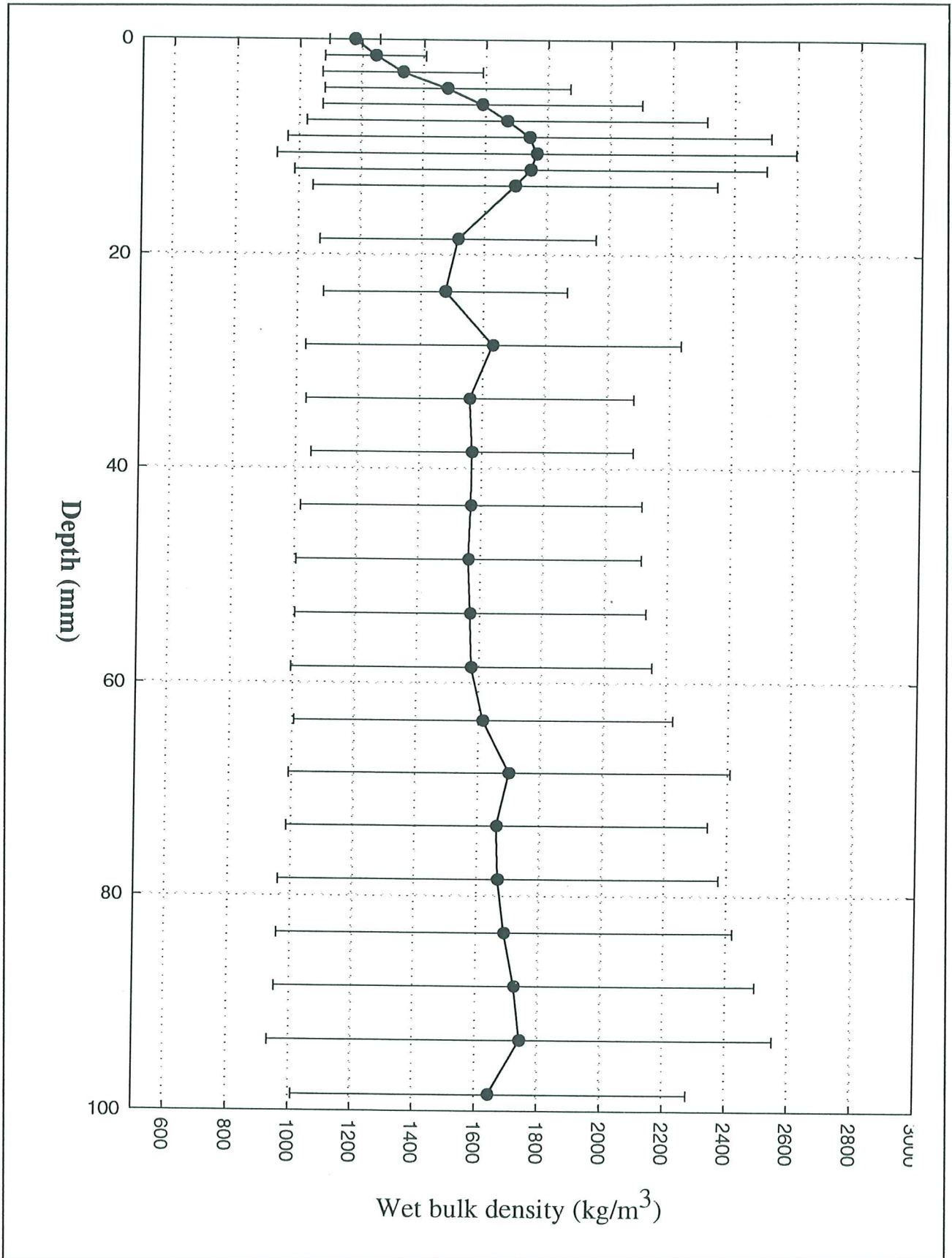
Figure 4.3.2. Sediment bulk density and the variance of density plotted against sediment depth. The values are derived from Catscan analyses of a syringe core collected at station R2.
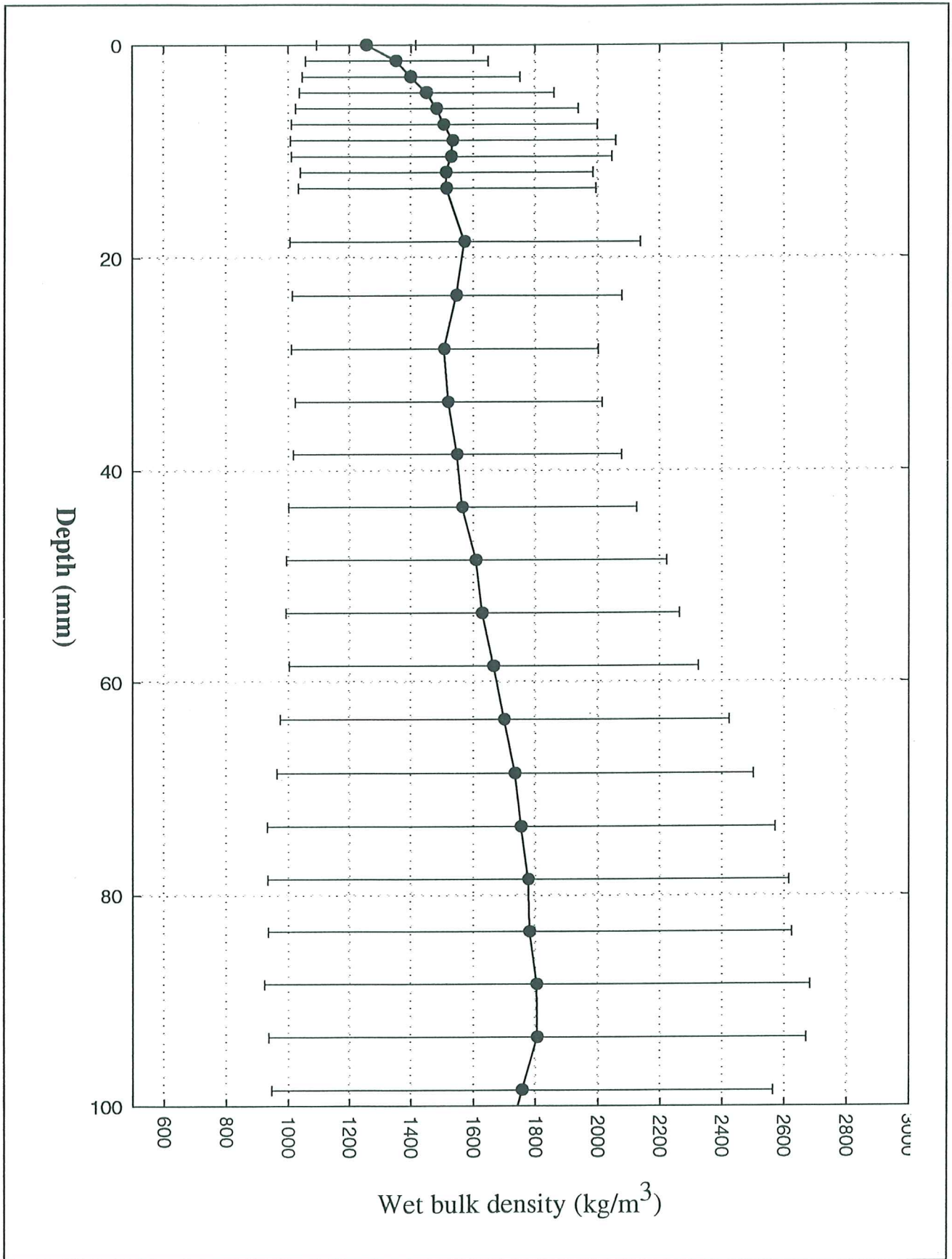
Figure 4.3.3. Sediment bulk density and the variance of density plotted against sediment depth. The values are derived from Catscan analyses of a syringe core collected at station R3.
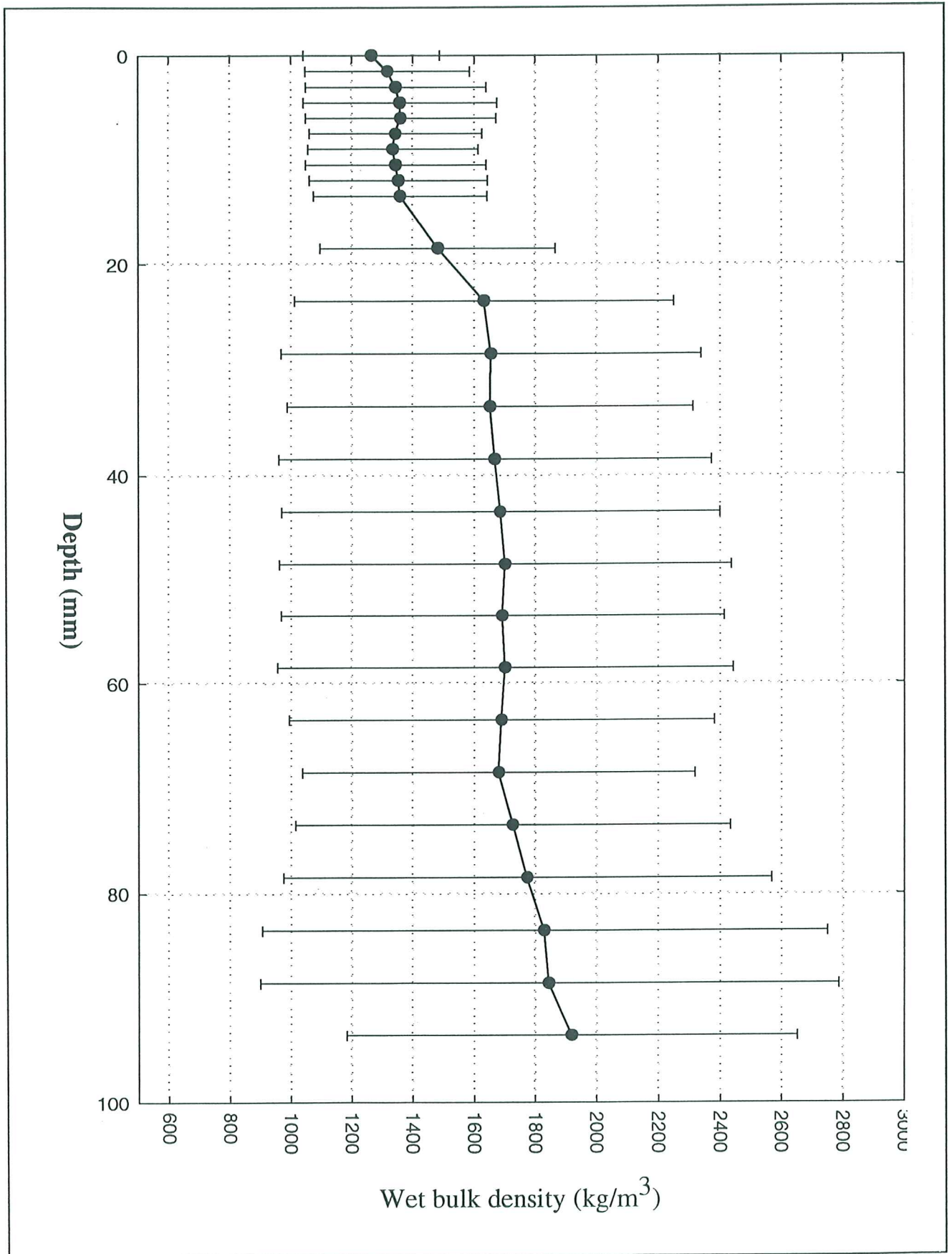
Figure 4.3.4. Sediment bulk density and the variance of density plotted against sediment depth. The values are derived from Catscan analyses of a syringe core collected at station R4.
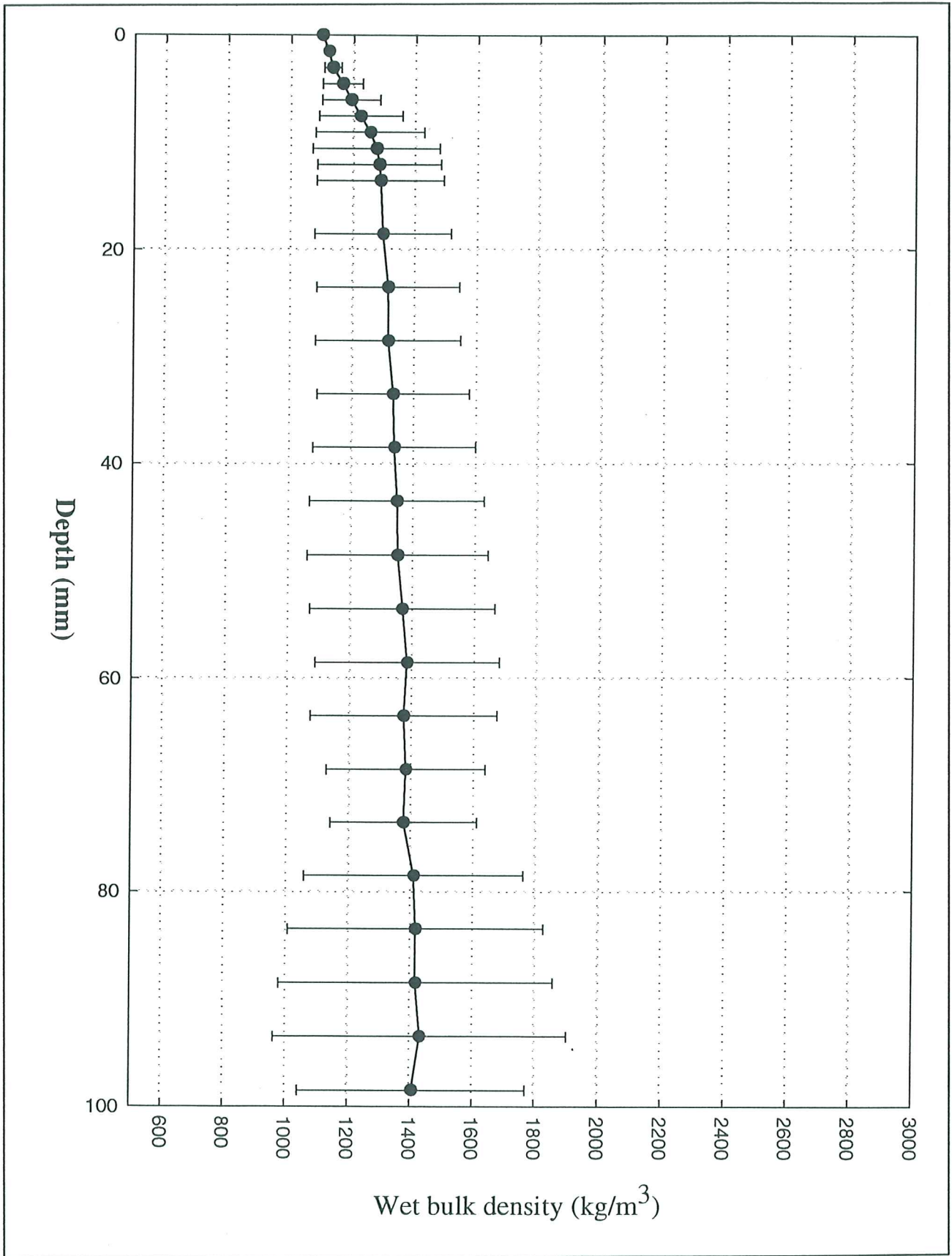
Figure 4.3.5. Sediment bulk density and the variance of density plotted against sediment depth. The values are derived from Catscan analyses of a syringe core collected at station R5.
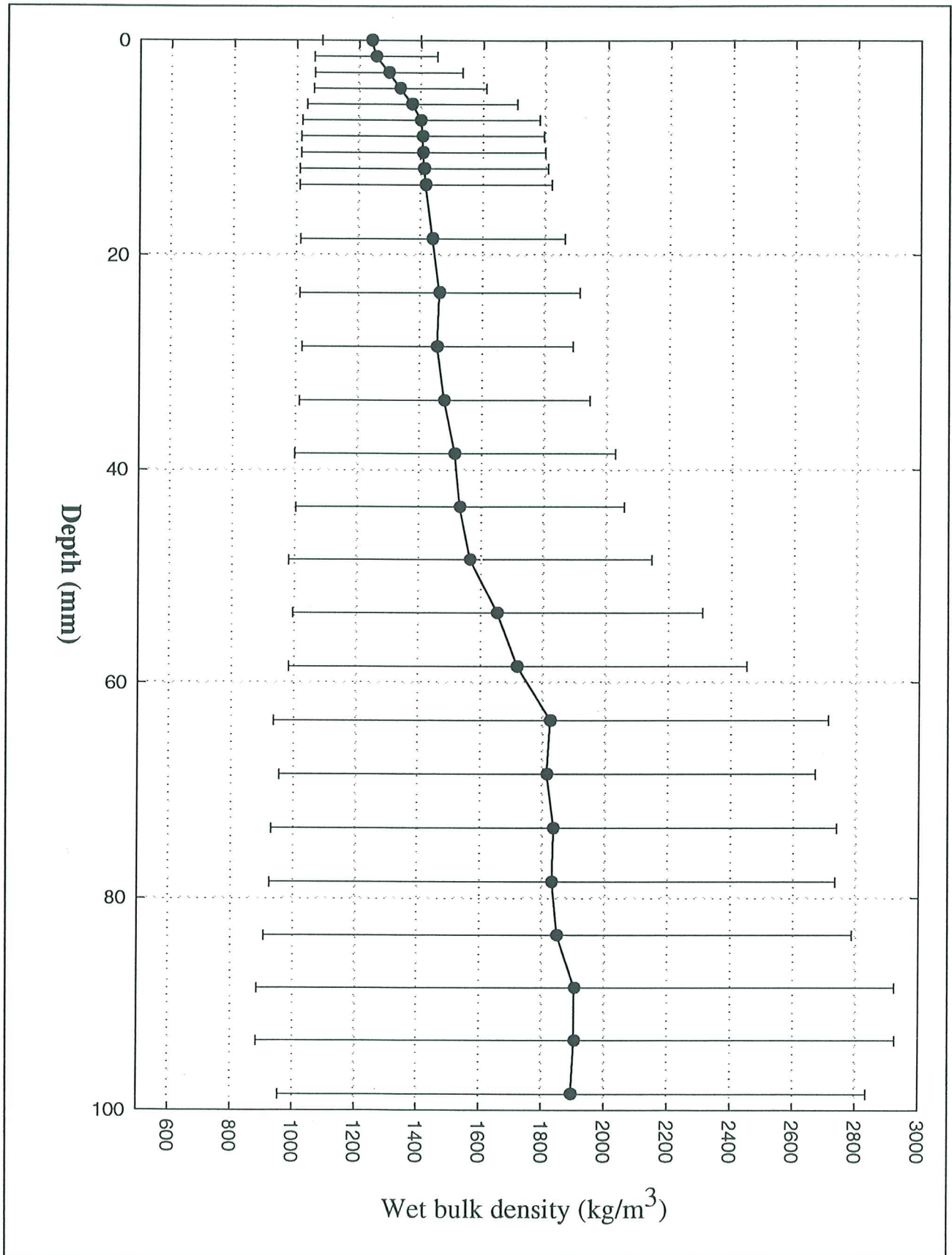
Figure 4.3.6. Sediment bulk density and the variance of density plotted against sediment depth. The values are derived from Catscan analyses of a syringe core collected at station R6.
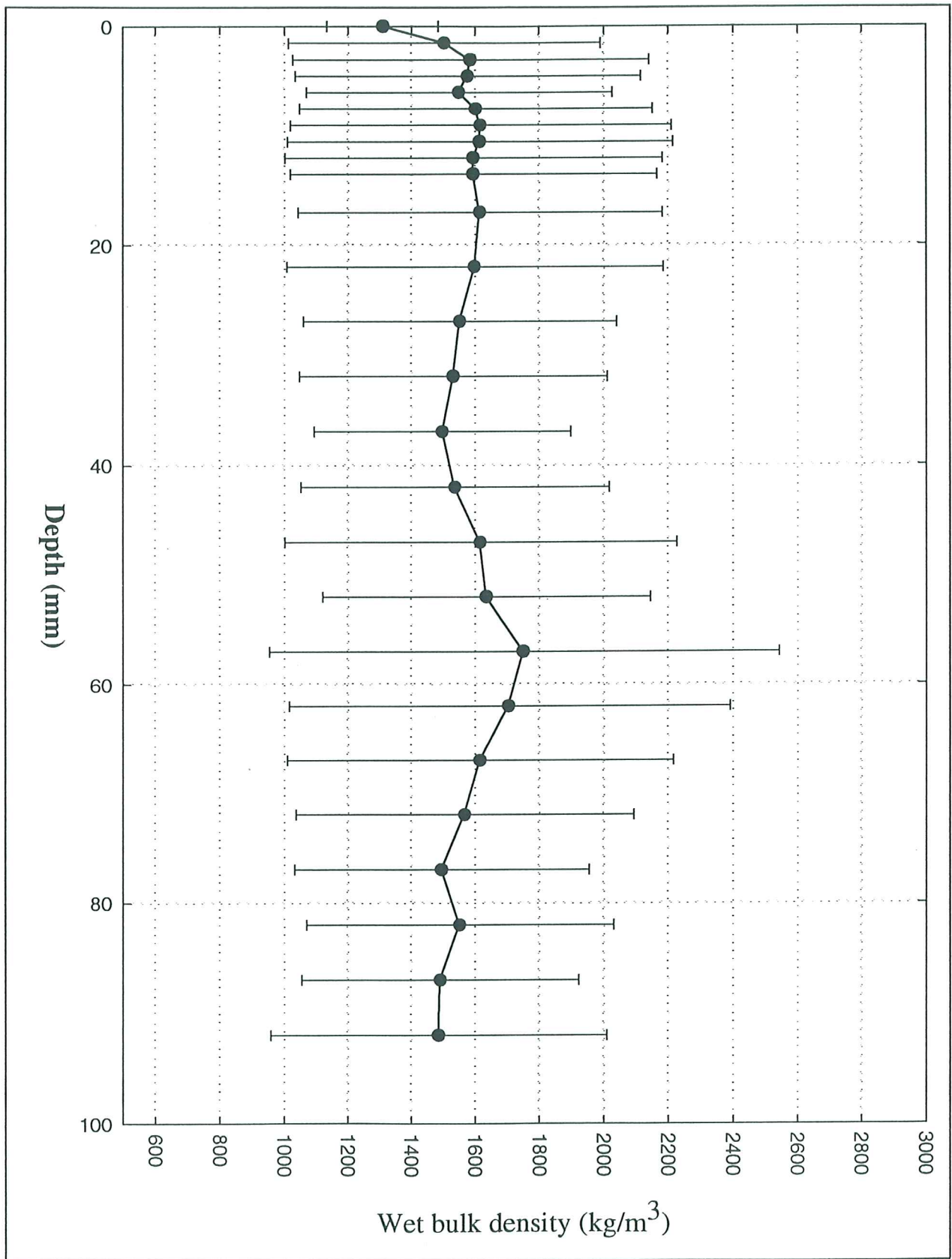
Figure 4.3.7. Sediment bulk density and the variance of density plotted against sediment depth. The values are derived from Catscan analyses of a syringe core collected at station R7.
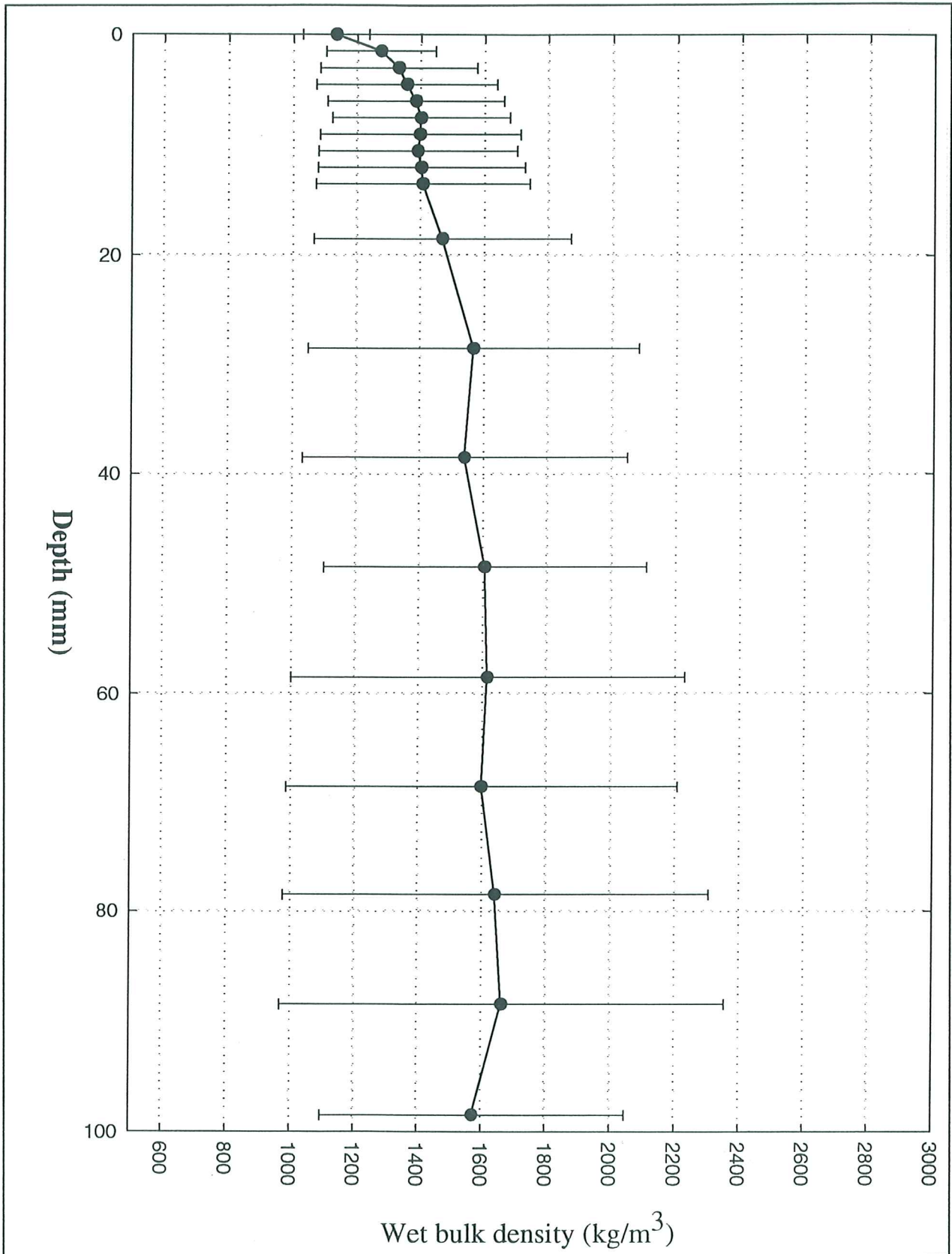
Figure 4.3.8. Sediment bulk density and the variance of density plotted against sediment depth. The values are derived from Catscan analyses of a syringe core collected at station R10.
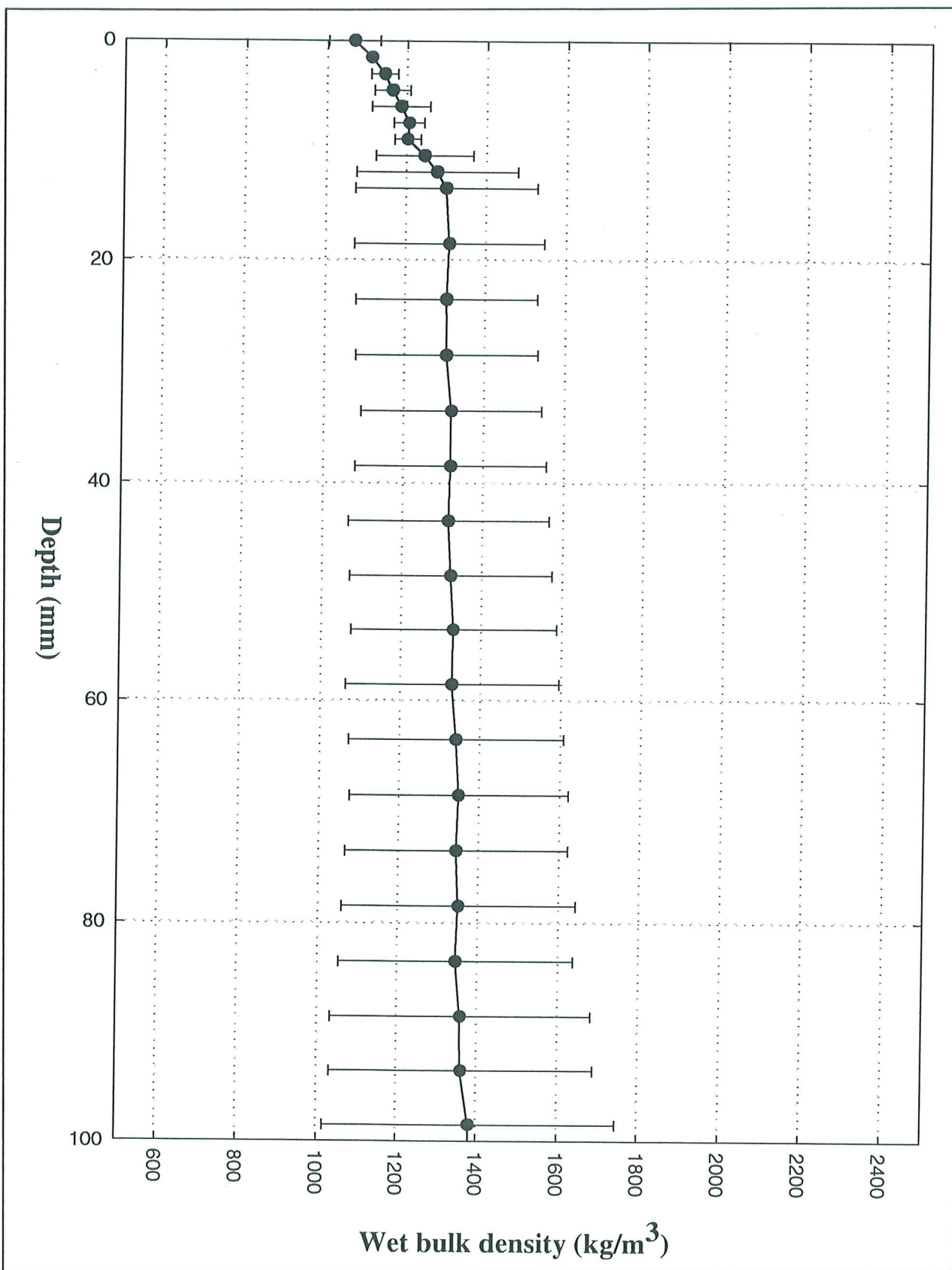
Figure 4.3.9. Sediment bulk density and the variance of density plotted against sediment depth. The values are derived from Catscan analyses of a syringe core collected at station R11.
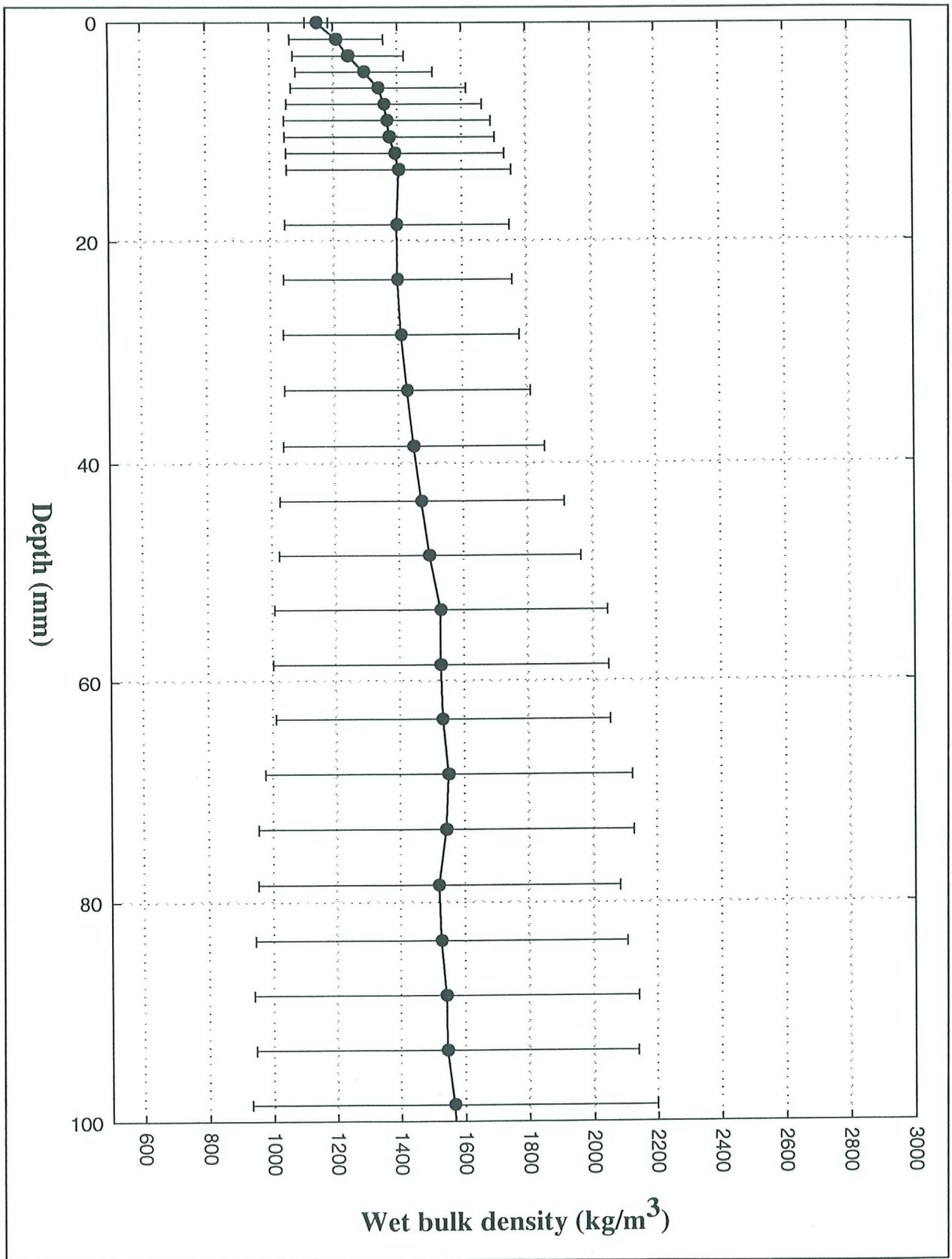
Figure 4.3.10. Sediment bulk density and the variance of density plotted against sediment depth. The values are derived from Catscan analyses of a syringe core collected at station R12.
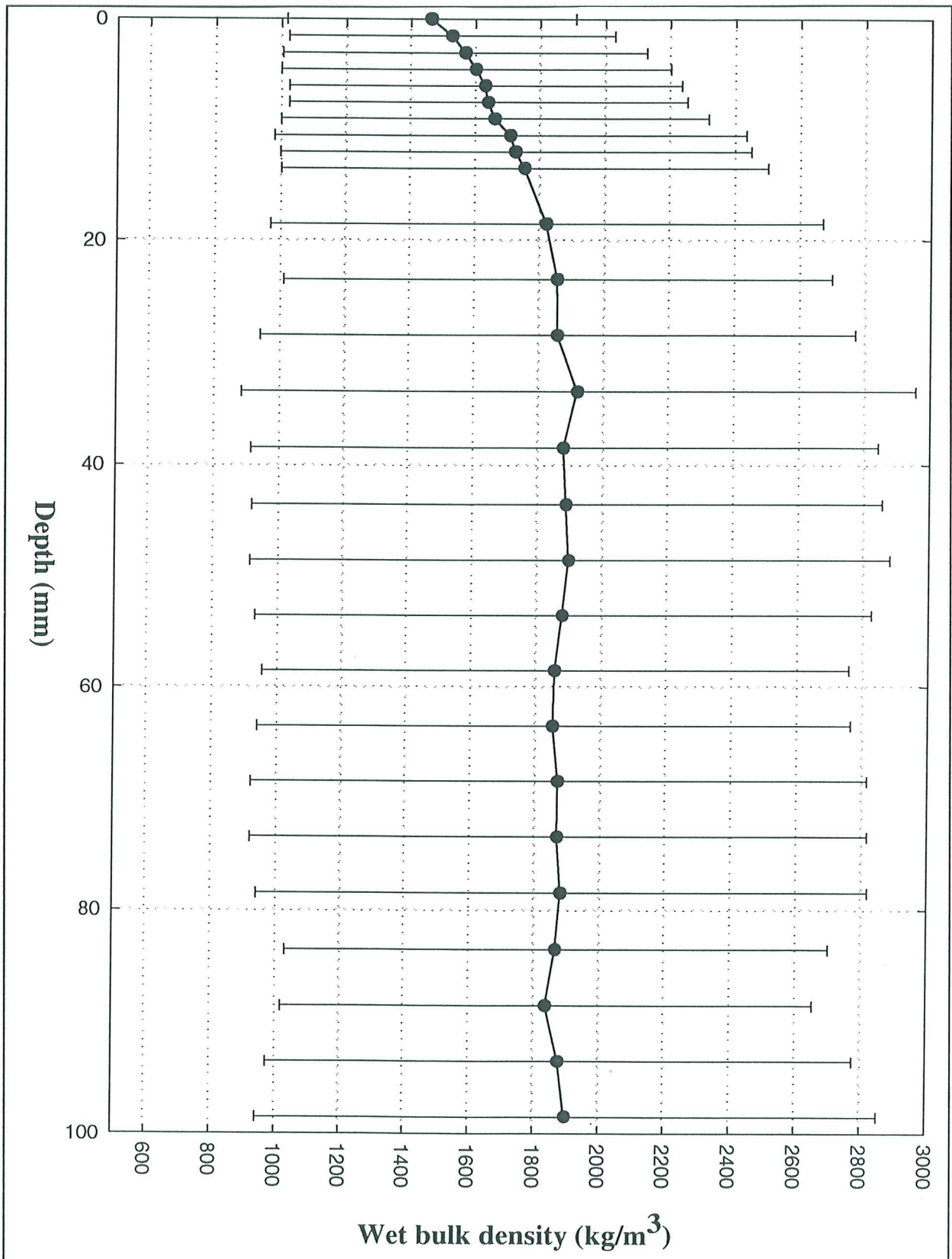
Figure 4.3.11. Sediment bulk density and the variance of density plotted against sediment depth. The values are derived from Catscan analyses of a syringe core collected at station R13.
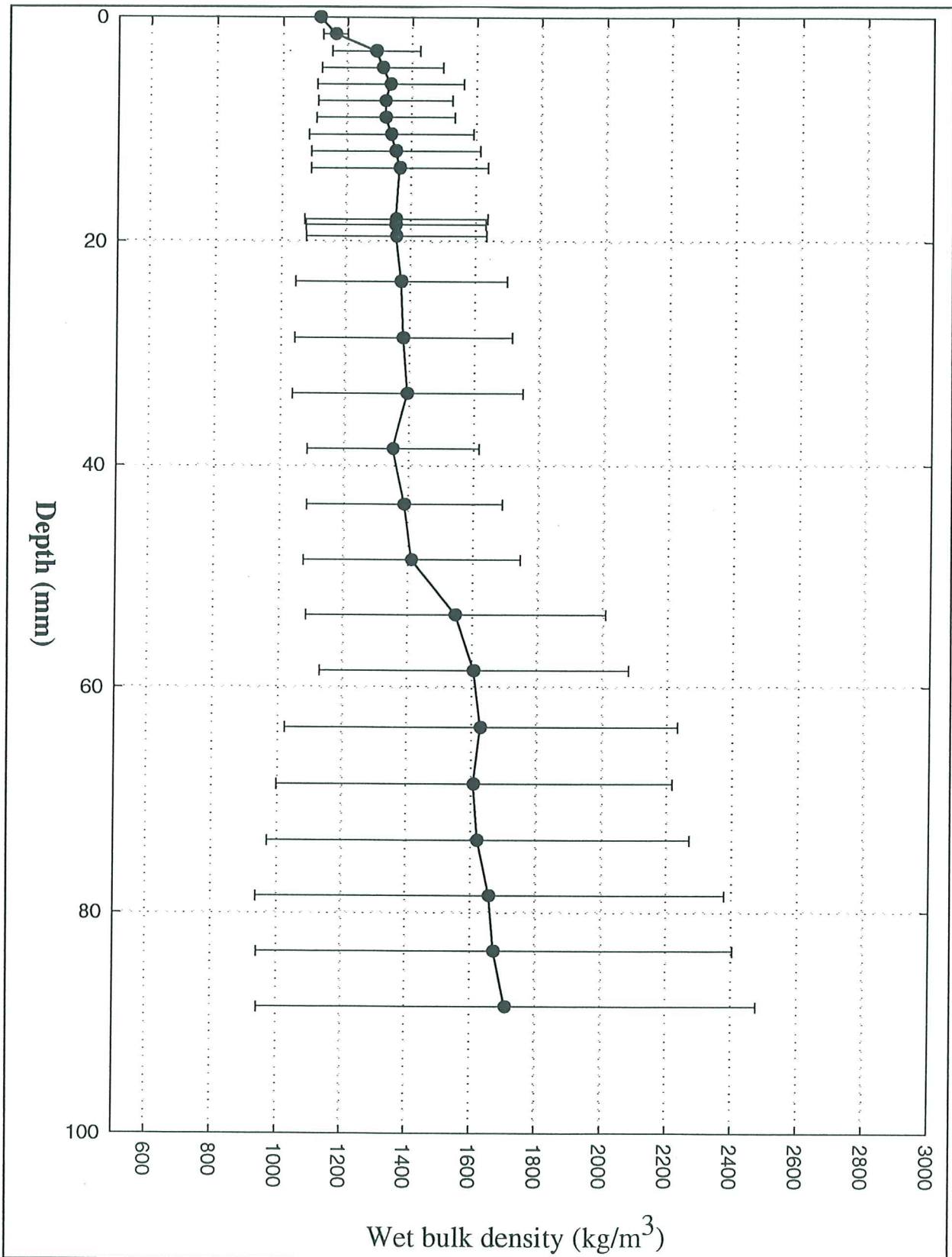
Figure 4.3.12. Sediment bulk density and the variance of density plotted against sediment depth. The values are derived from Catscan analyses of a syringe core collected at station R14.

Catscan Bulk Density (kg/m³)

Prince Edward Island
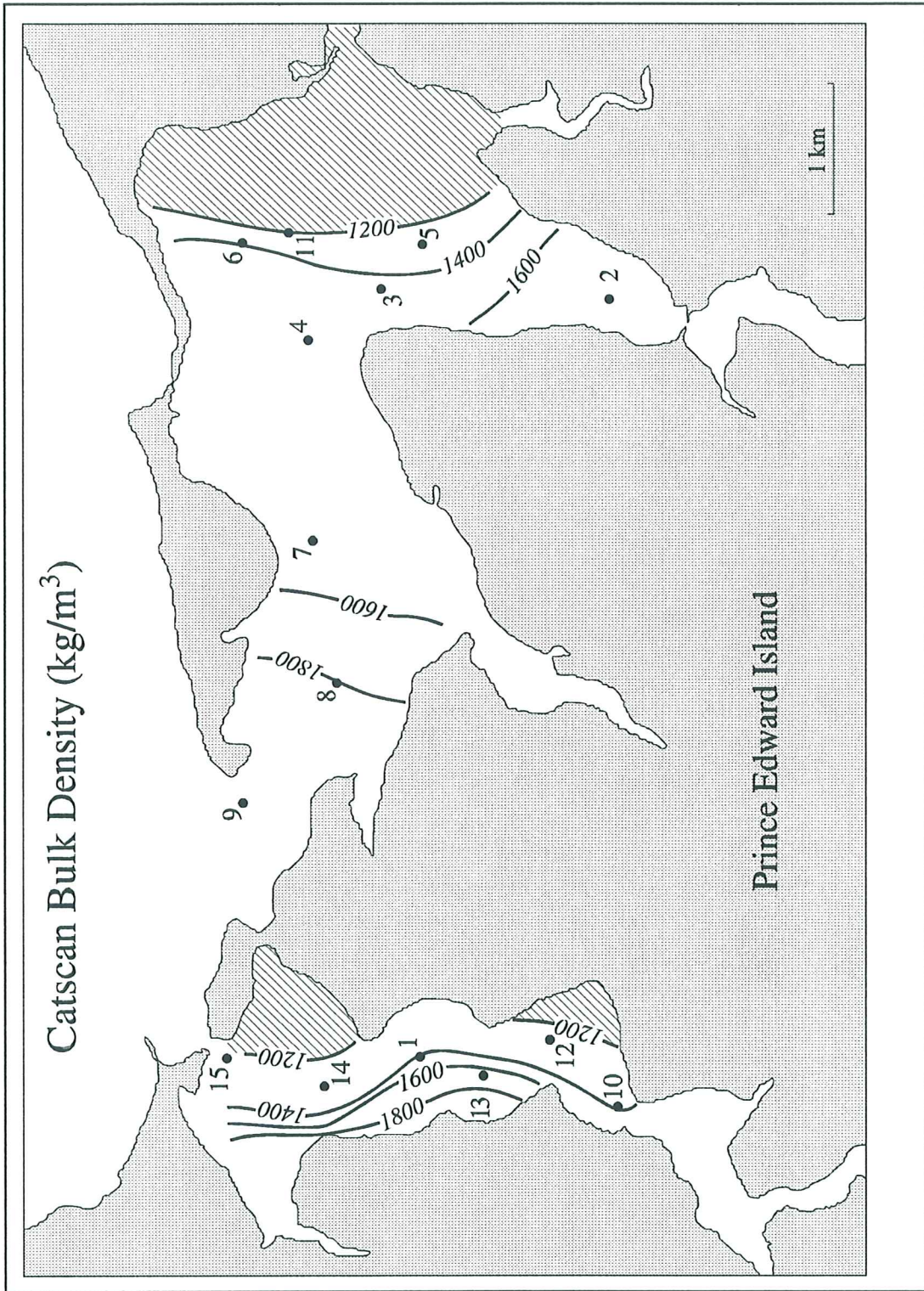
Figure 4.3.13. The distribution of sediment bulk density within Rustico Bay. Notice that the regions of lowest bulk density correspond to the regions of high mud content. In general there is an increase in density from east to west across the two estuaries.
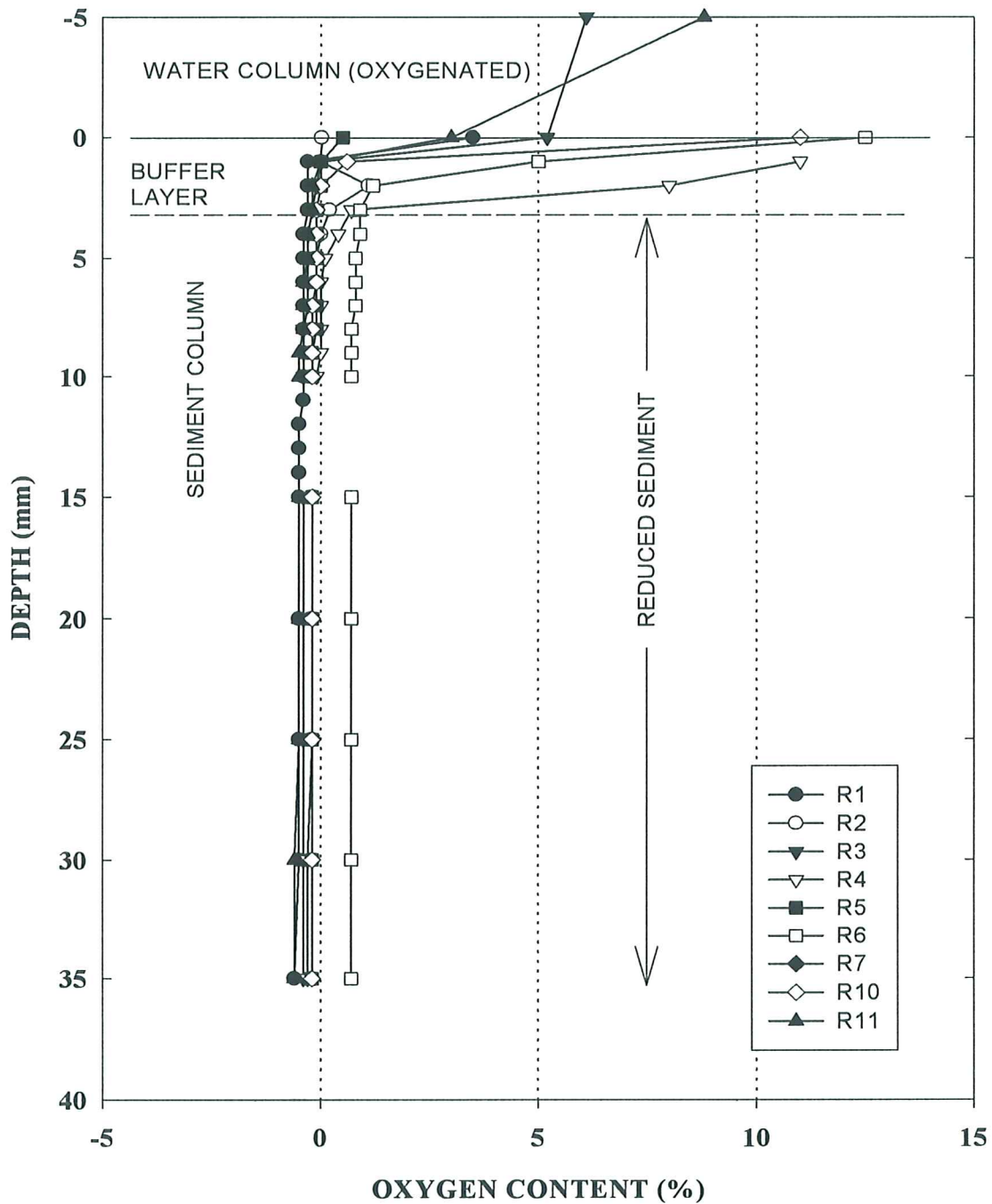
Figure 4.3.14. Oxygen content profiles through the topmost 4 cm of seabed sediment measured at the muddy Sea Carousel stations. Notice that the water column has low but measureble free oxygen and that most of the sediments are reduced (oxygen defficient), and a buffer zone about 4 mm thick is present at the sediment water interface.
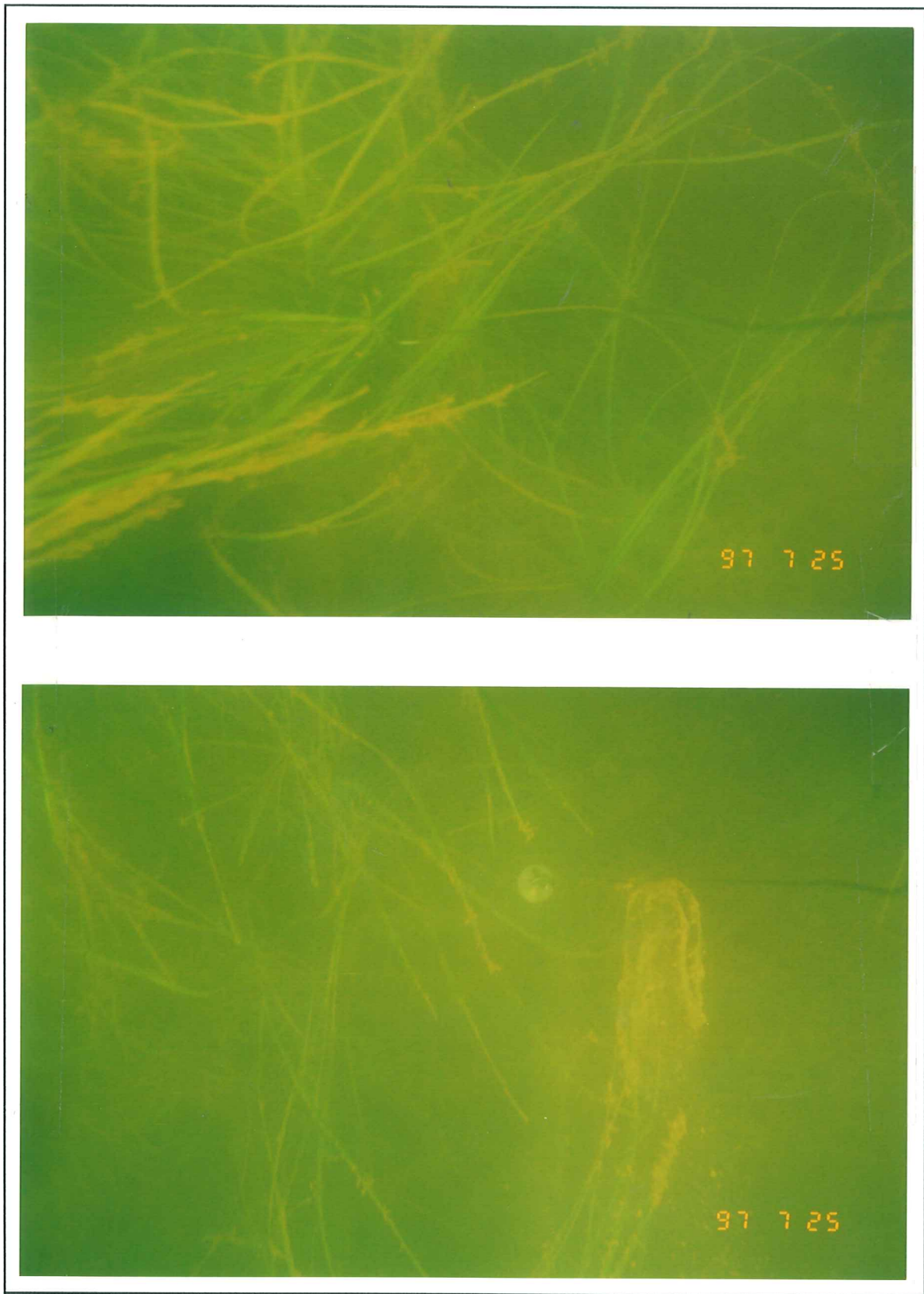
Figure 4.4.1. Bottom photographs taken at station R1. Notice the presence of sea grasses and the green colour of the water column. This we attribute to high levels of organic matter.
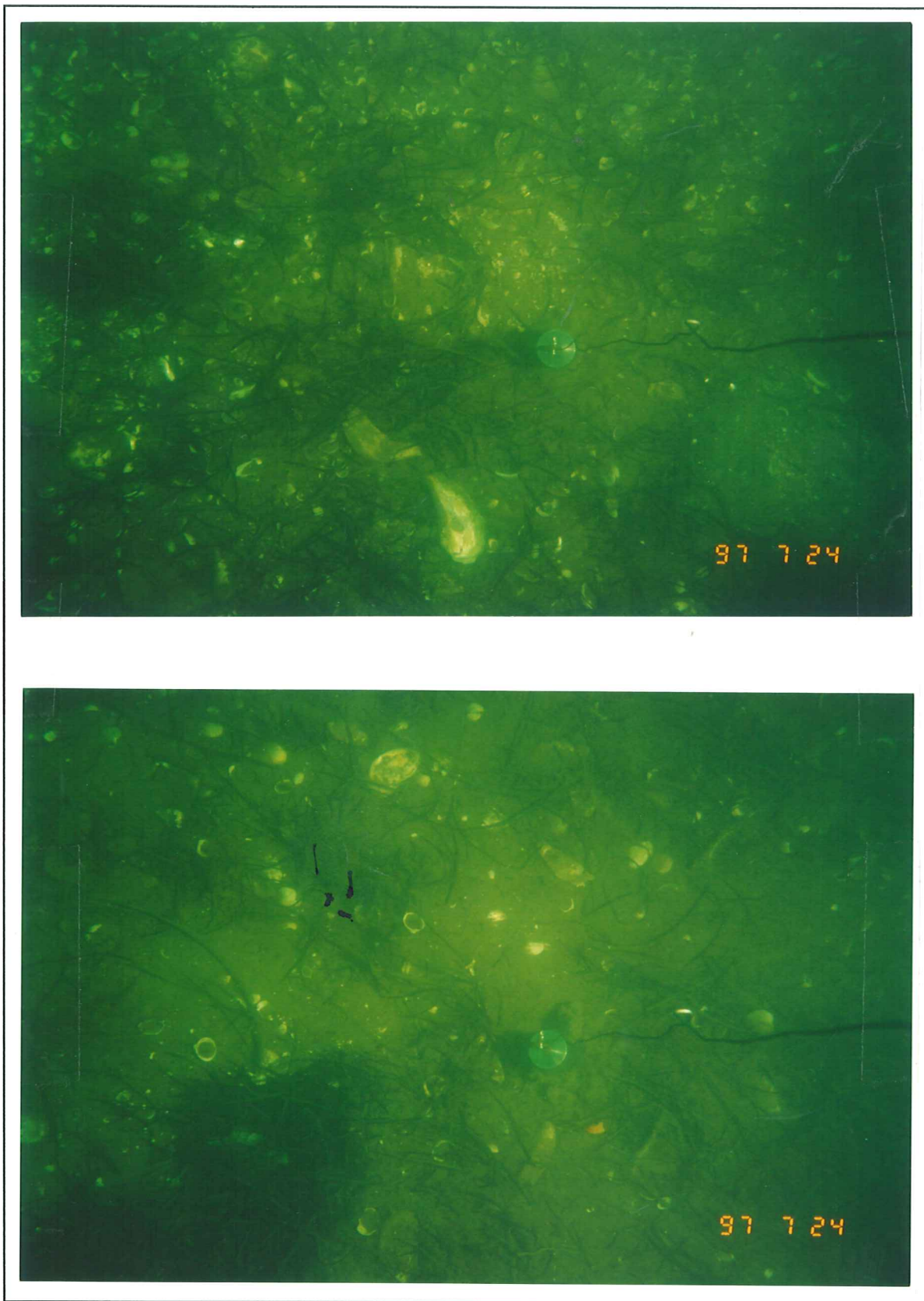
Figure 4.4.2. Bottom photographs taken at station R7. This site is largely sandy with abundant shell fragments. Sea grasses are also evident but in lesser amounts than at landward stations.
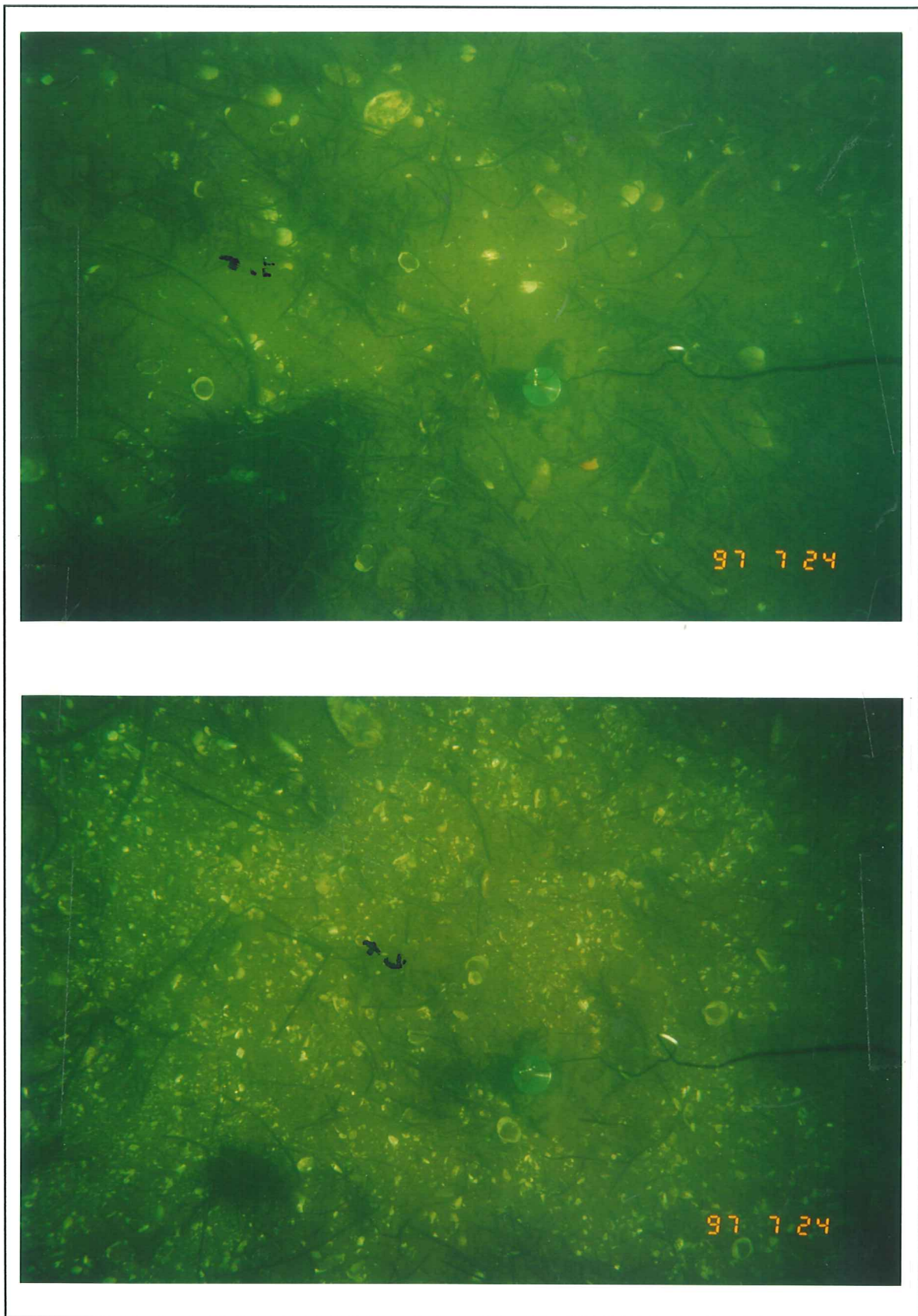
Figure 4.4.3. Bottom photographs taken at station R7. Notice the variation in the size of the shell debris which appears to be sorted by the tidal flows in the region.
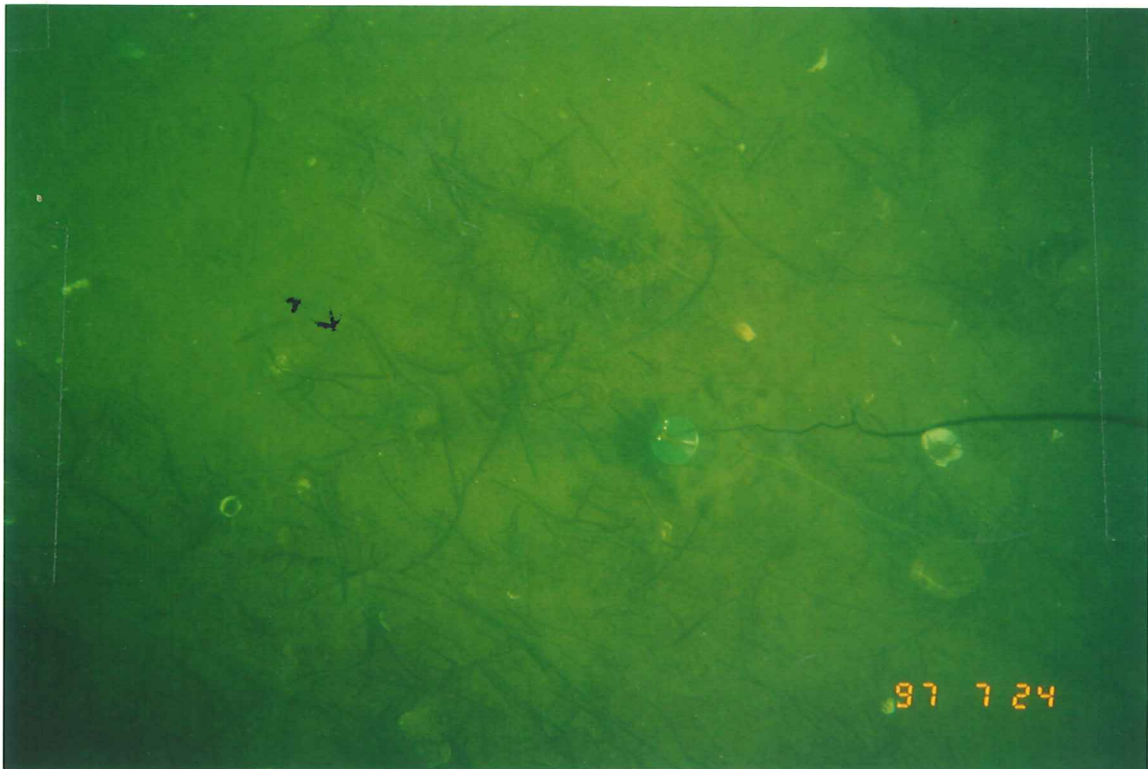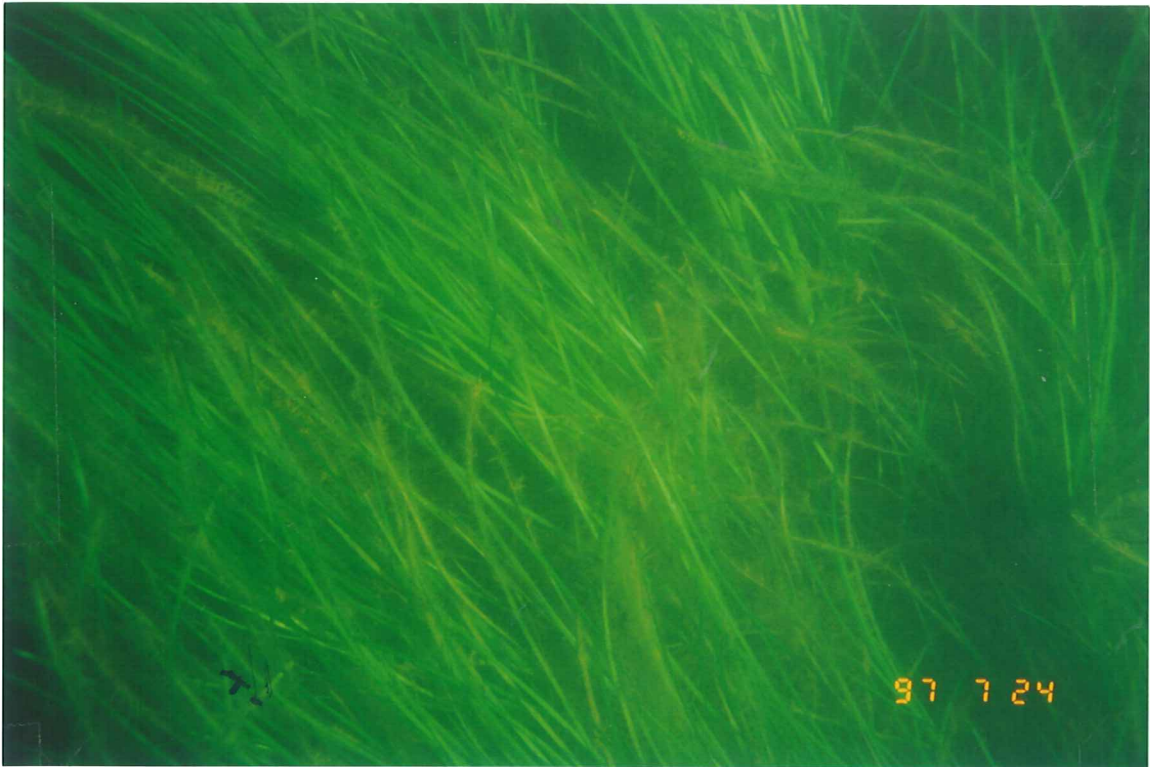
Figure 4.4.4. Bottom photographs taken at station R1. Notice the presence of thick sea grasses in one photo and the absence in the adjacent one indicating strong patchiness.
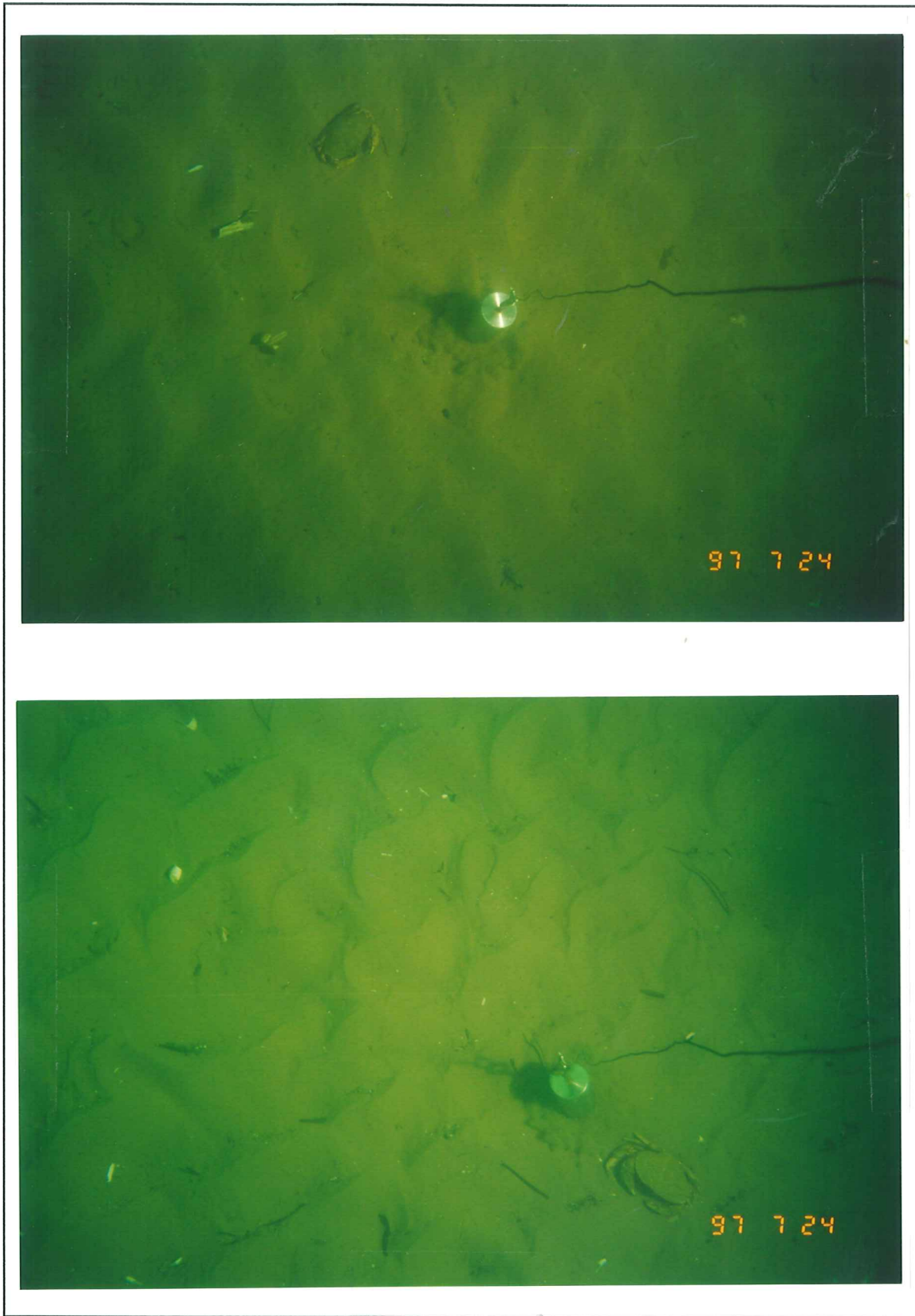
Figure 4.4.6. Bottom photographs taken at station R8. Current ripple sand is evident indicating sand transport as bedload.
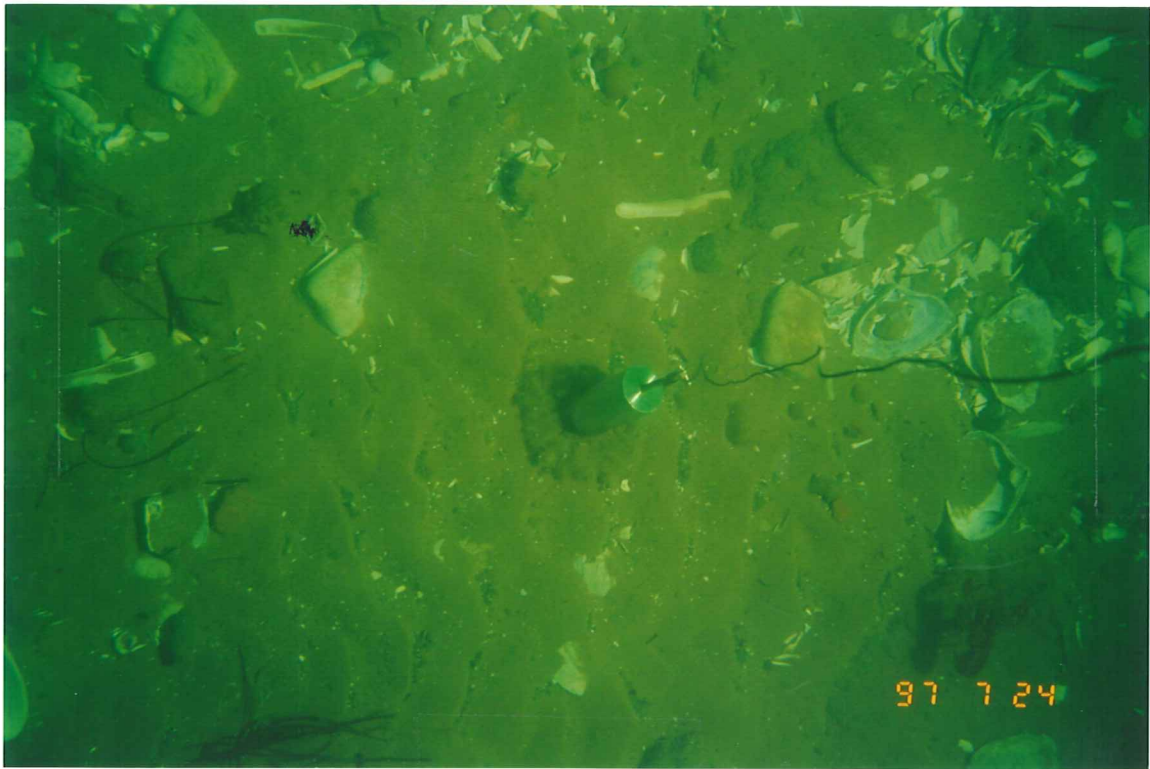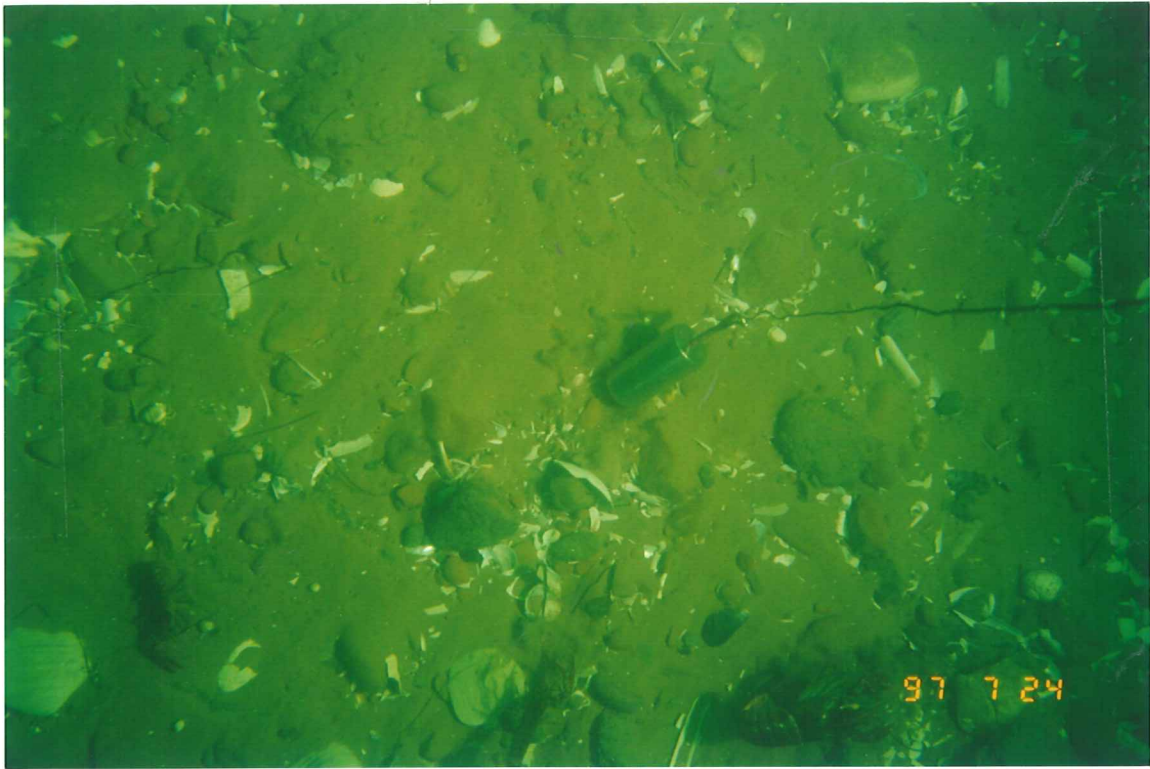
Figure 4.4.7. Bottom photographs taken at station R9. Notice the presence of sand over rounded gravel suggesting strong tidal flows. Disarticulated shells are also abundant suggesting bed winnowing and transport.
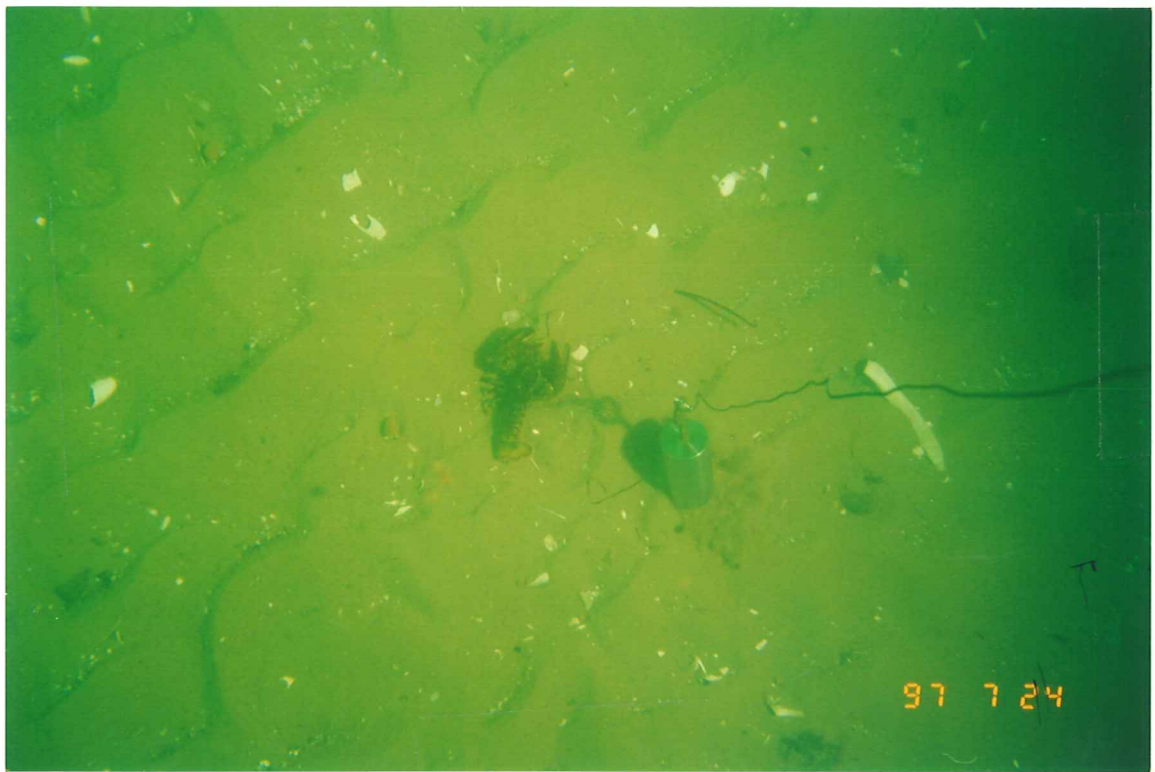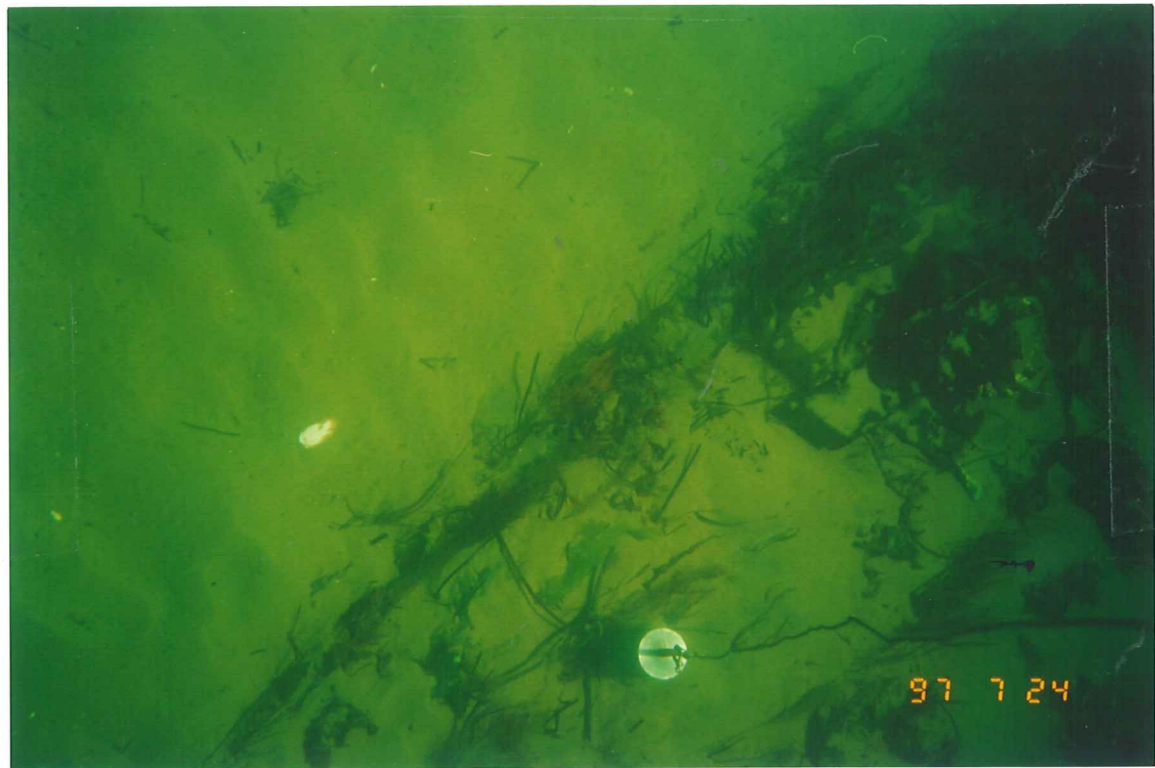
Figure 4.4.8. Bottom photographs taken at station R9. Current ripple sand is evident together with current aligned eel grasses.
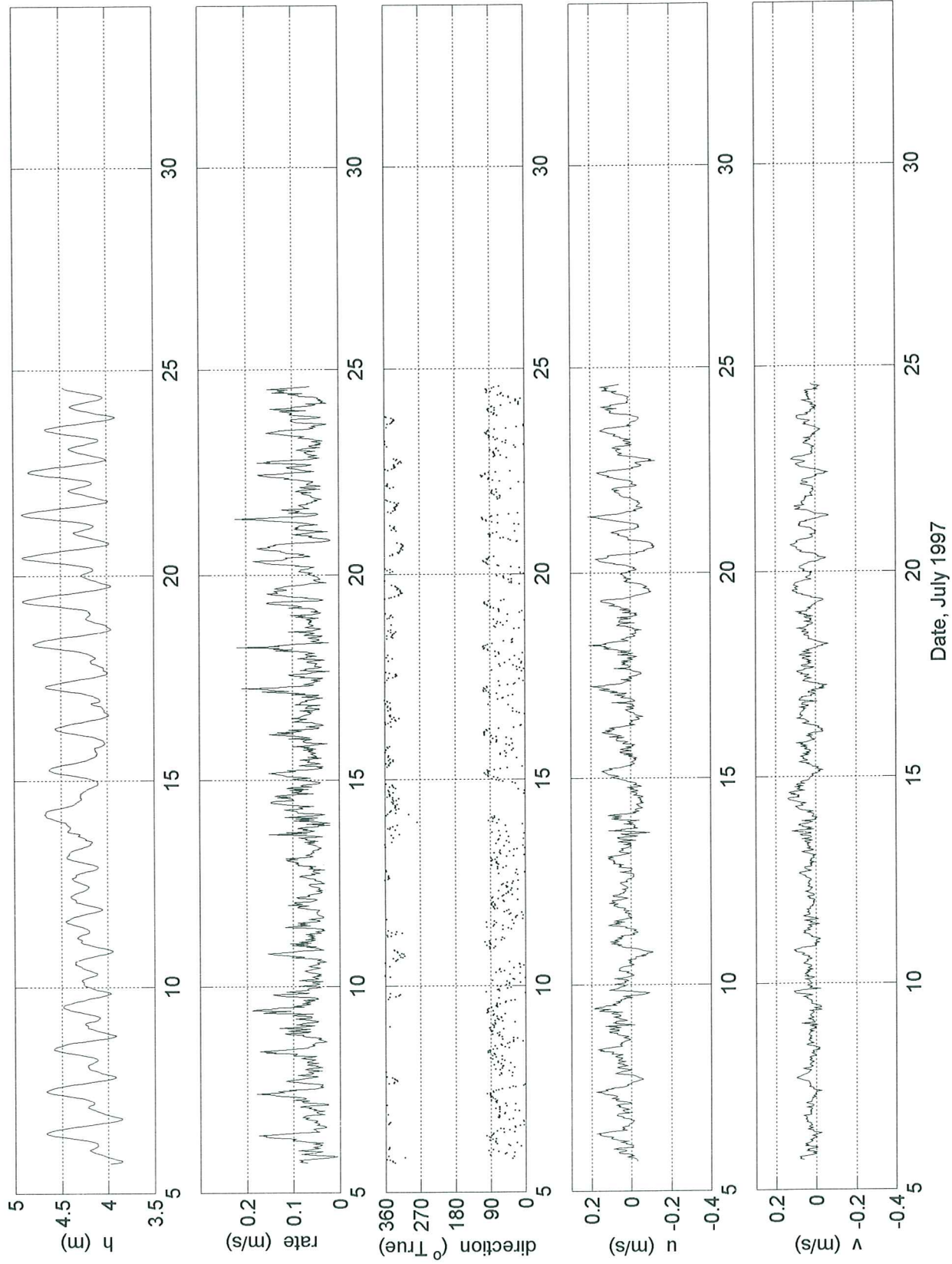
Fig. 4.5.1. Sea level and current time series. Current meter deployment rus1.
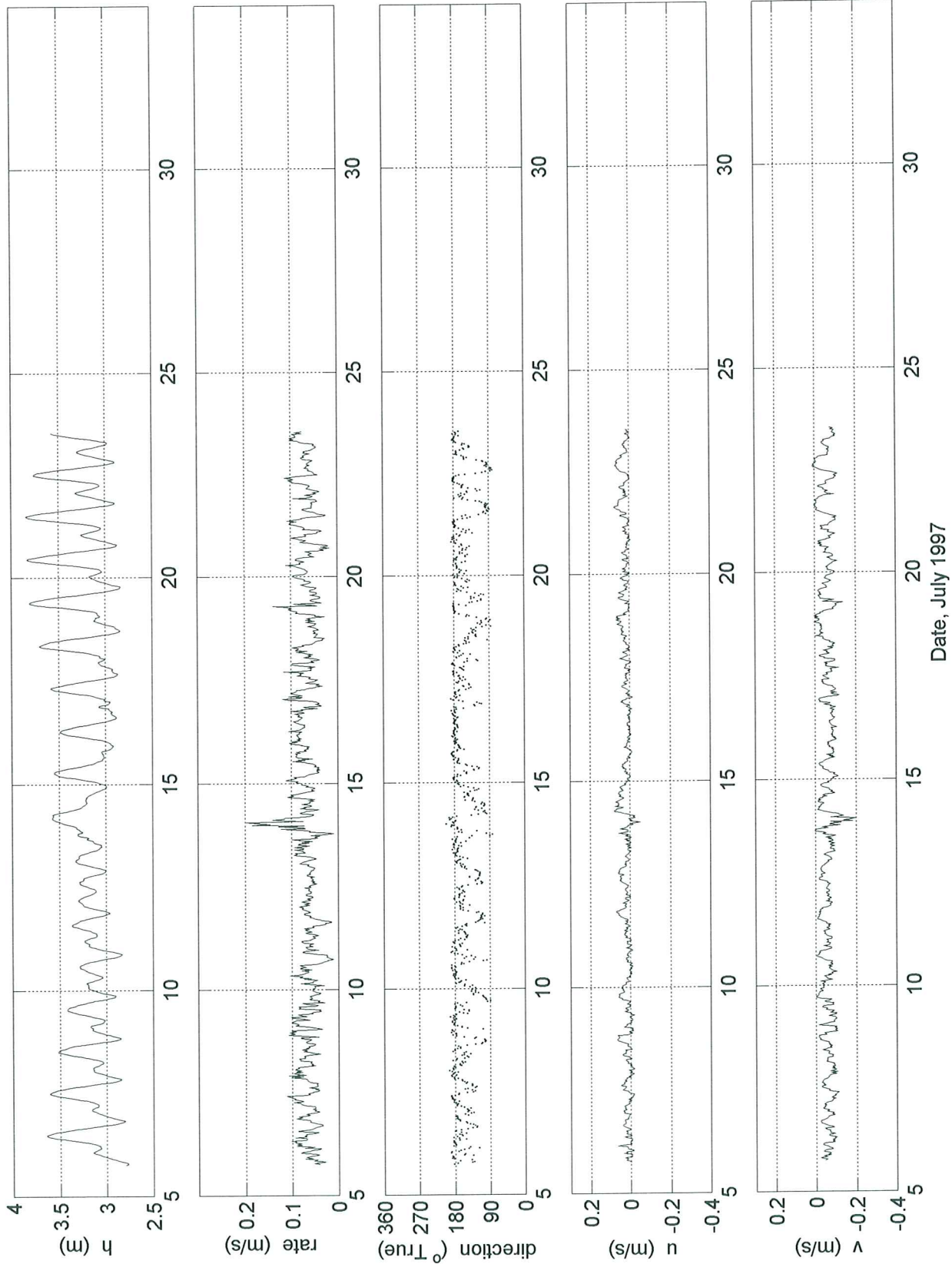
Fig. 4.5.2. Sea level and current time series. Current meter deployment rus2.
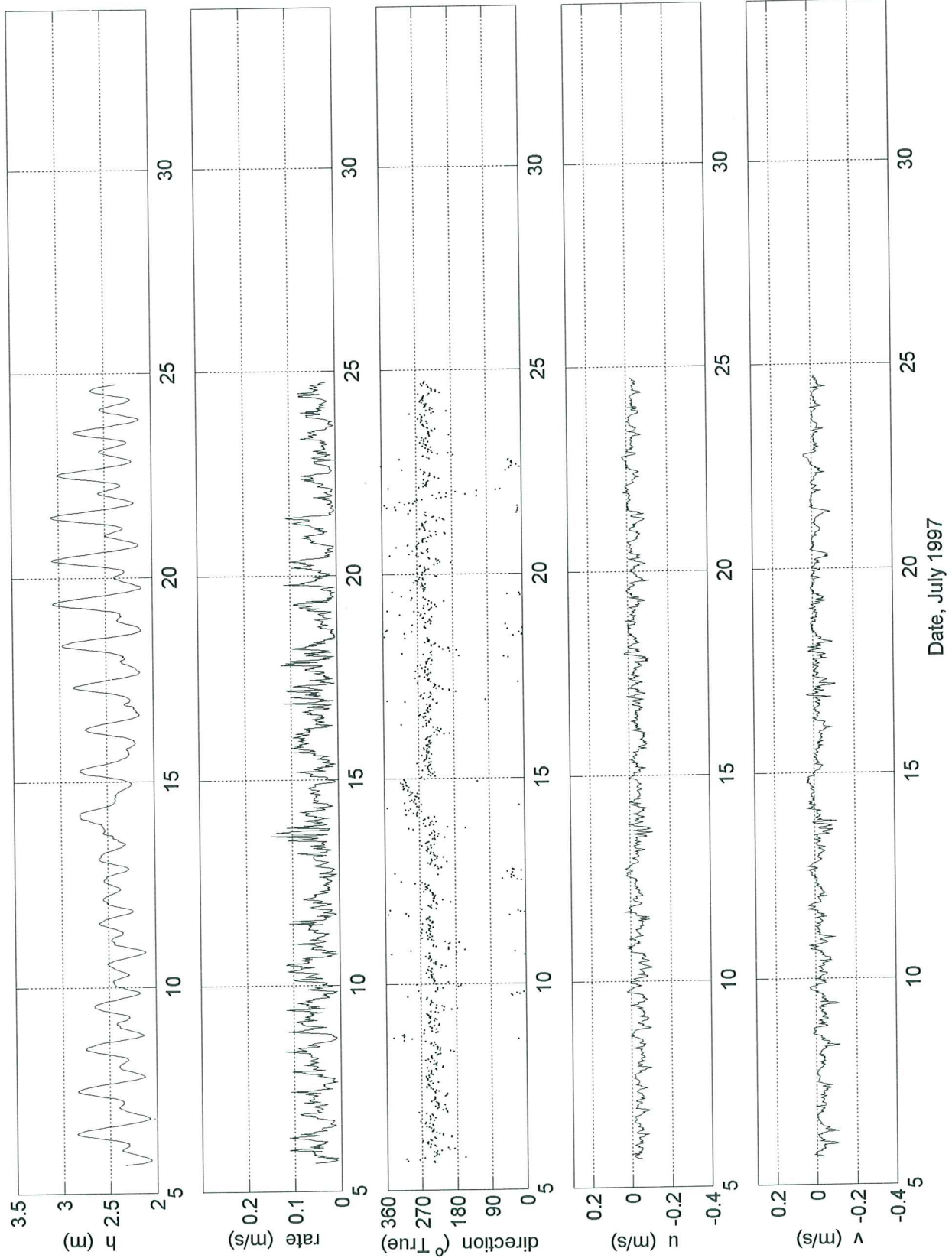
Fig. 4.5.3. Sea level and current time series. Current meter deployment rus3.
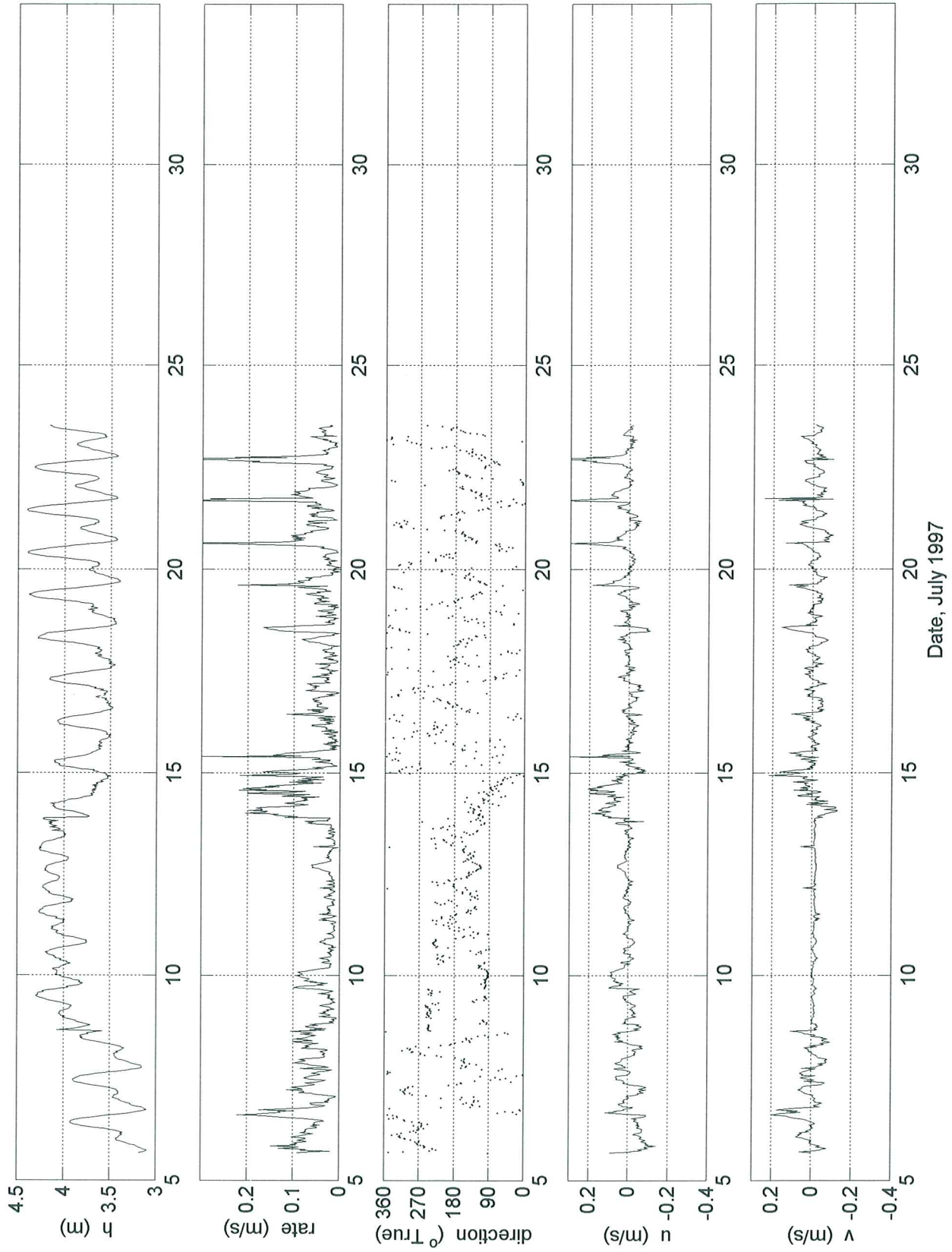
Fig. 4.5.4. Sea level and current time series. Current meter deployment rus4.
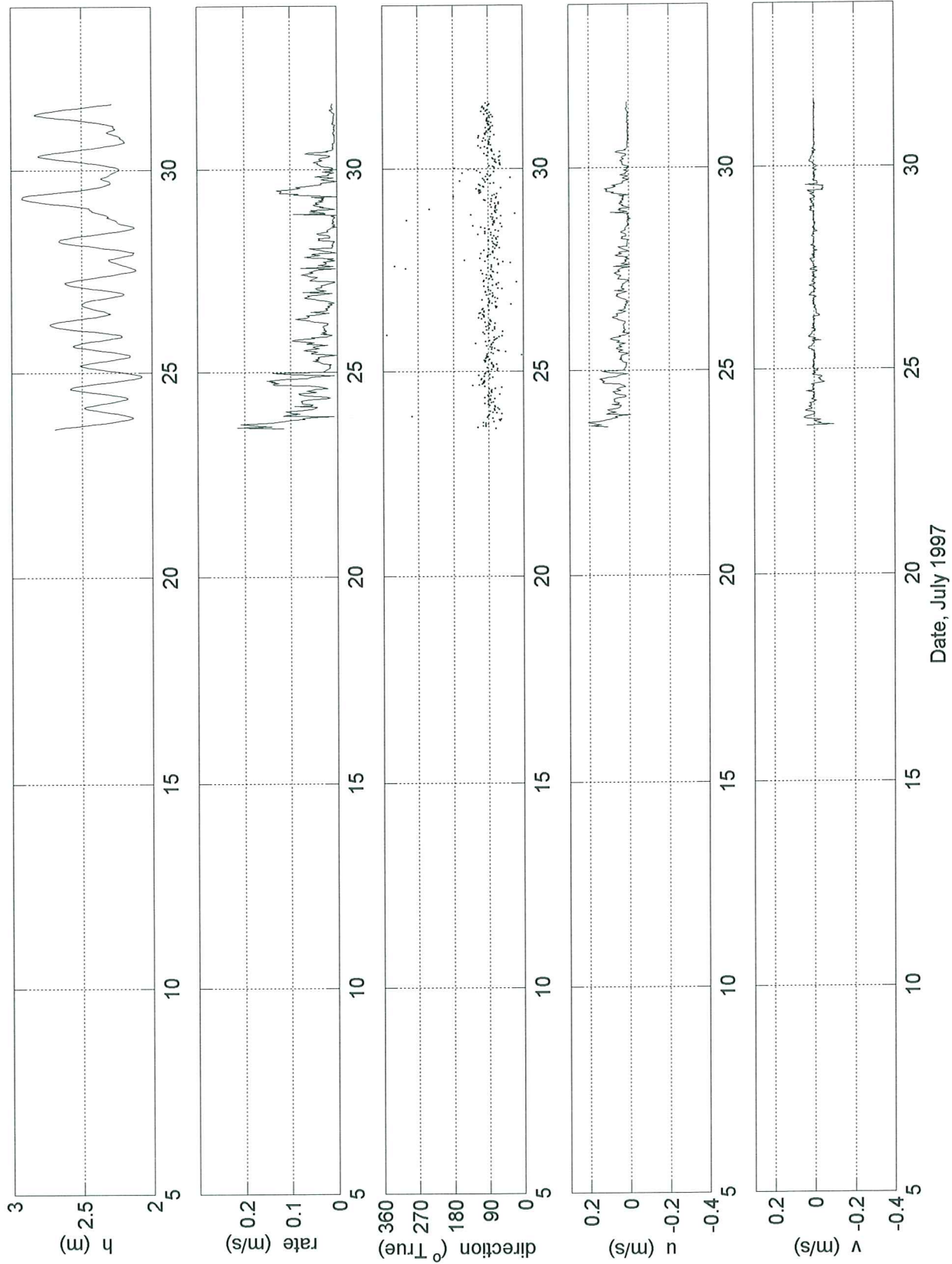
Fig. 4.5.5. Sea level and current time series. Current meter deployment rus6.
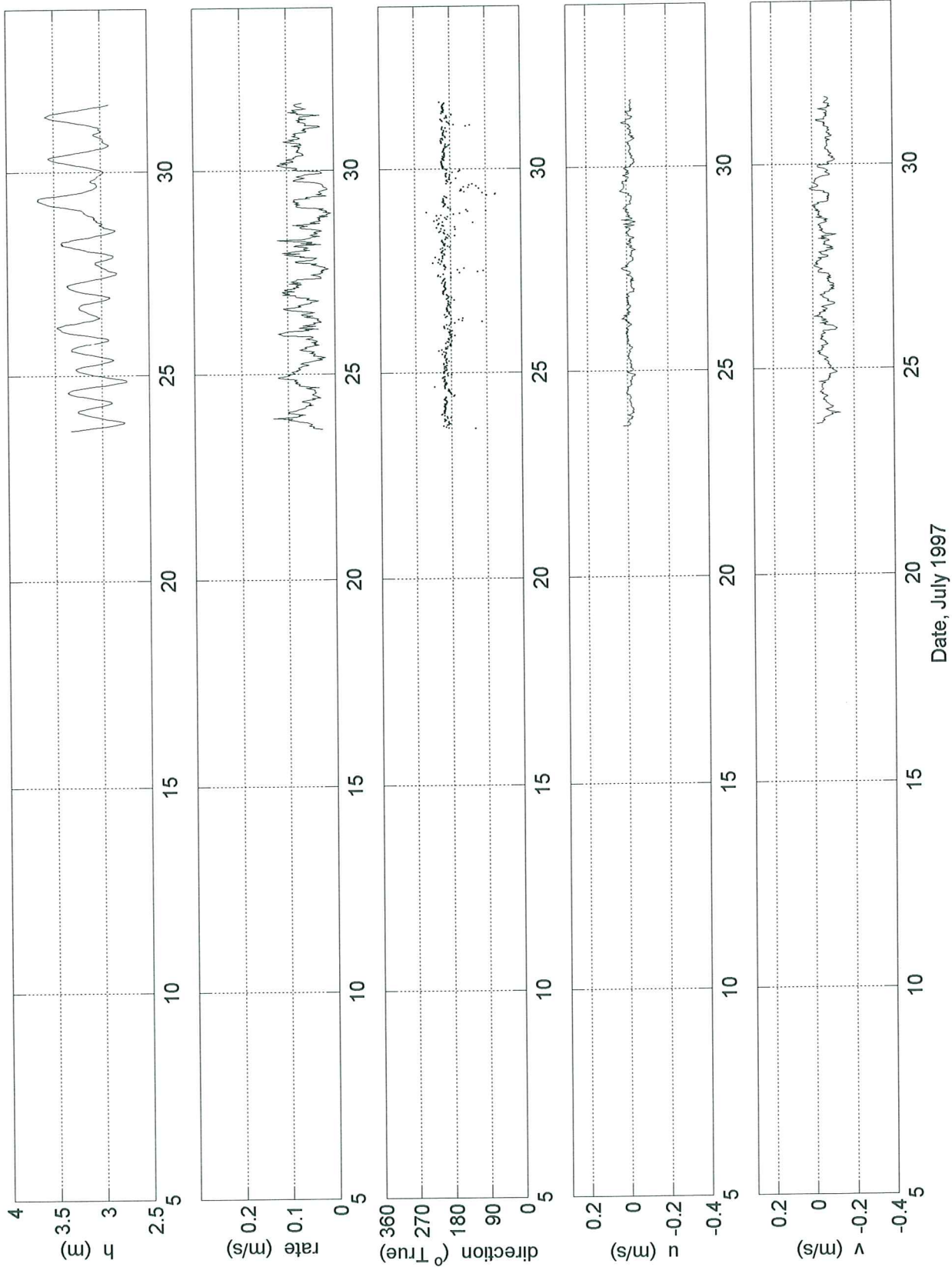
Fig. 4.5.6. Sea level and current time series. Current meter deployment rus7.
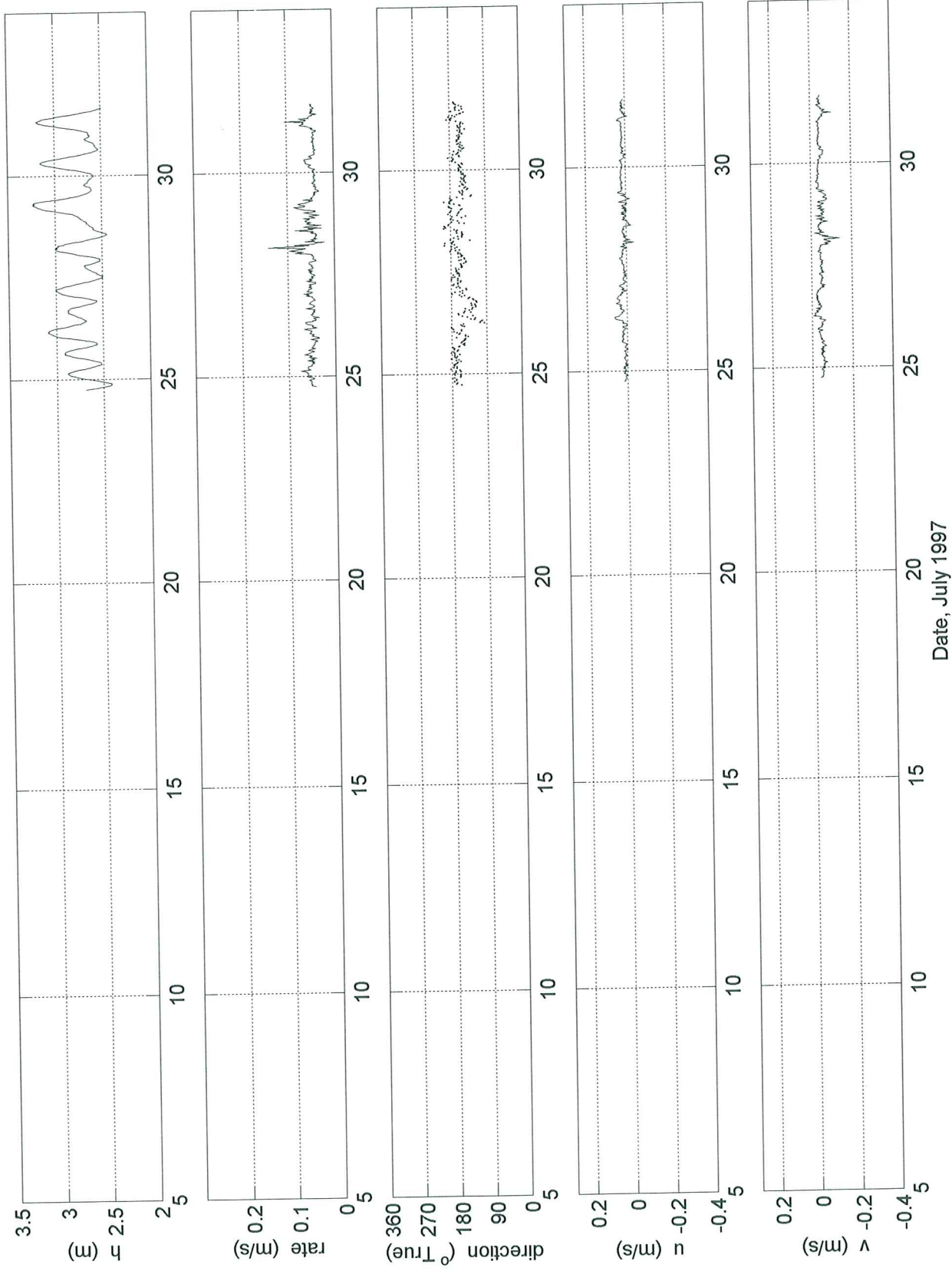
Fig. 4.5.7. Sea level and current time series. Current meter deployment rus8.

117
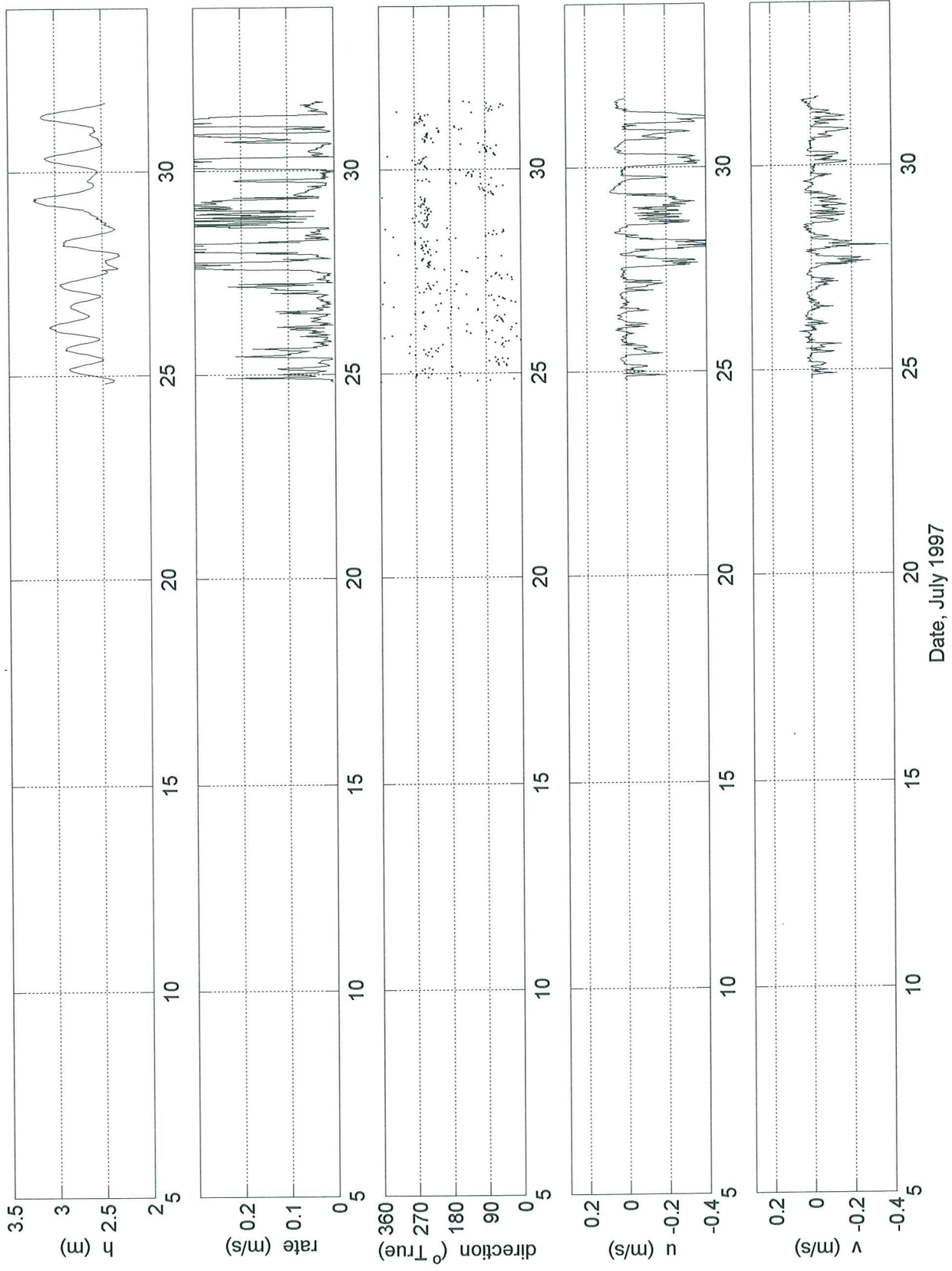
Fig. 4.5.8. Sea level and current time series. Current meter deployment rus9.
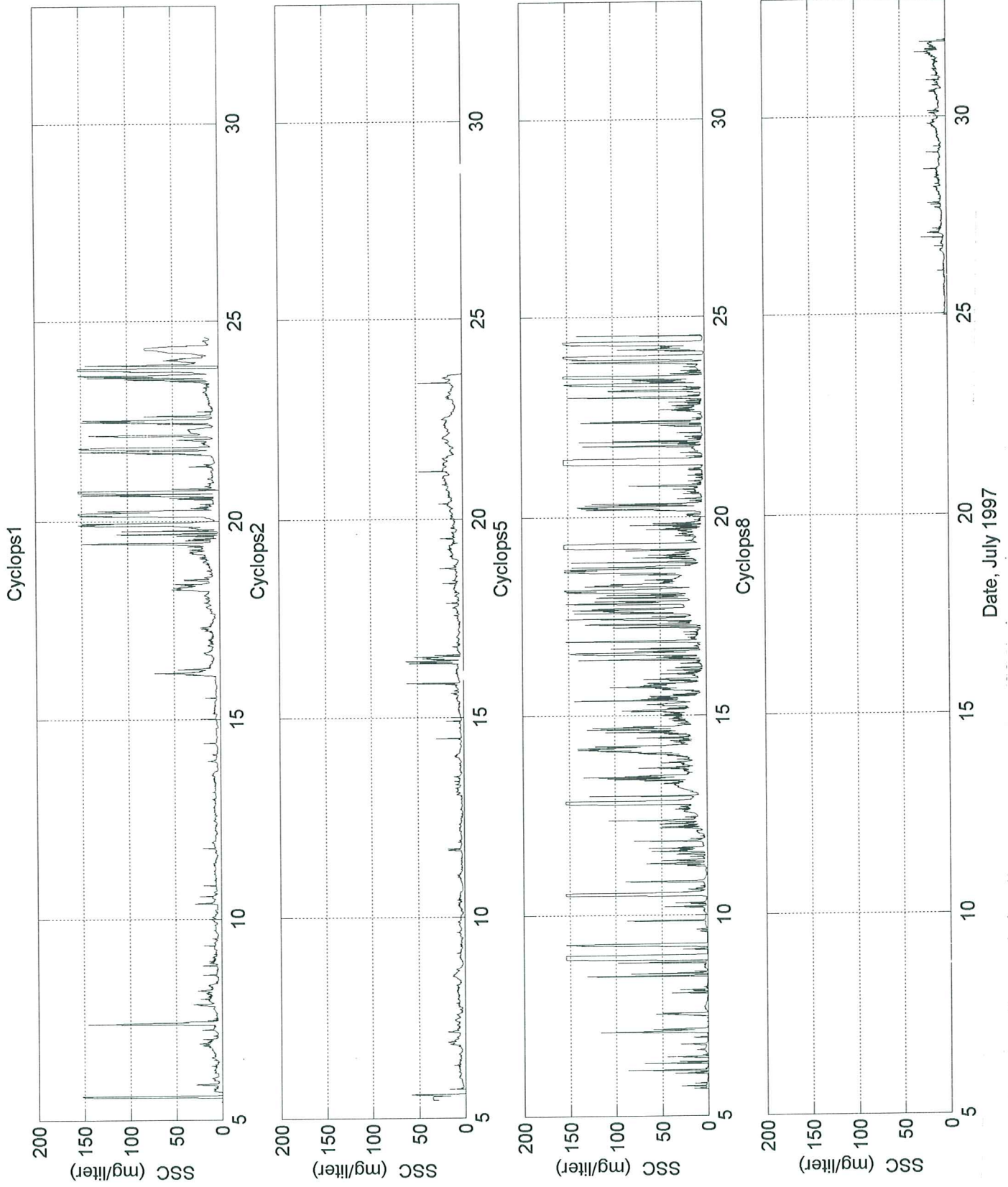
Figure 4.6.1 Suspended sediment concentration measured by Cyclops at four sites in Rustico Bay.

LAB CAROUSEL - Rustico Bay, PEI

Sample R11-1 22 November, 1997
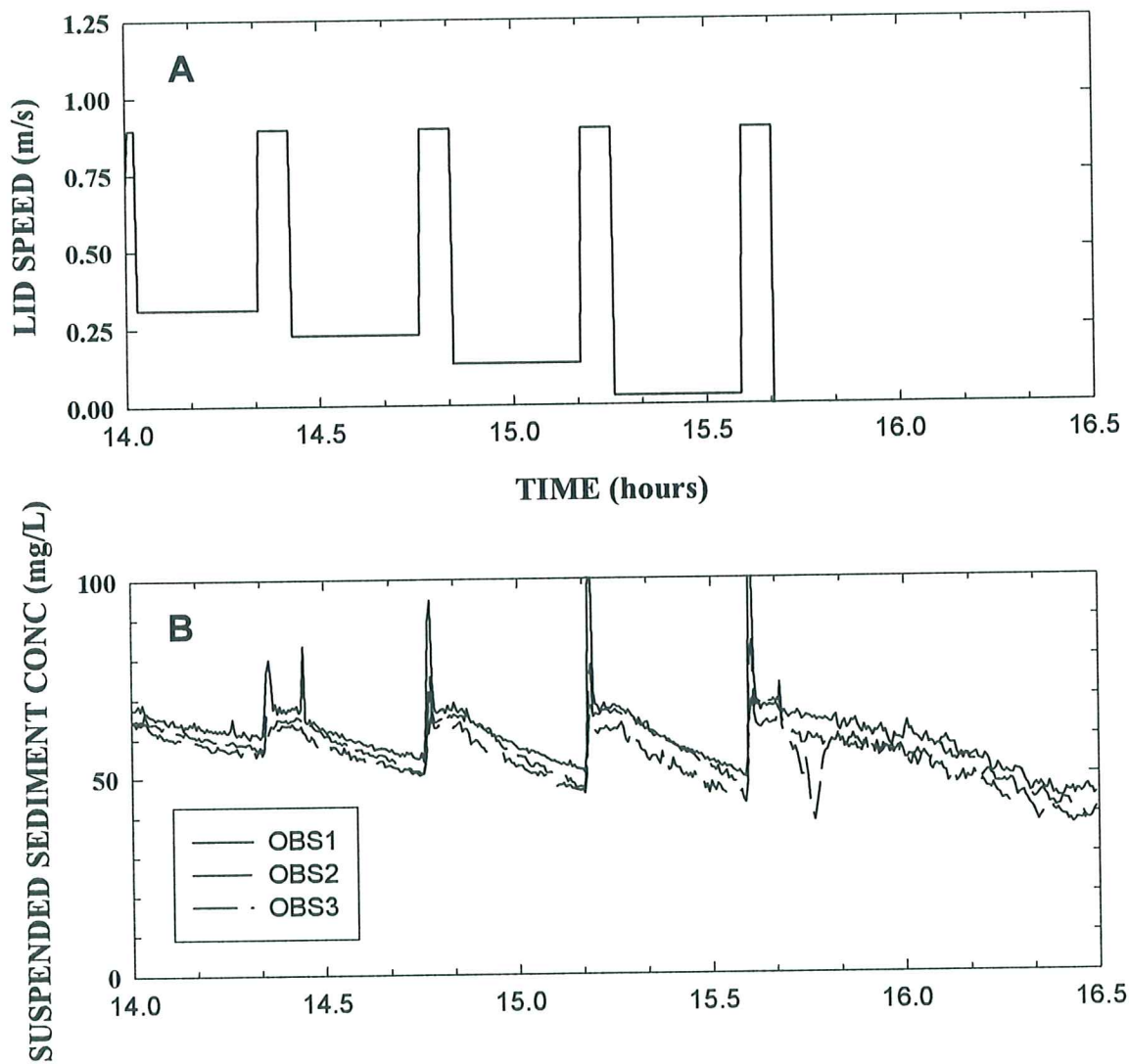
Figure 4.8.1. The time-series of suspended sediment concentration recorded in Lab Carousel during the settling experiments of sample R11 at 65 mg/L

LAB CAROUSEL - Rustico Bay, PEI

Sample R11-2 22 November, 1997
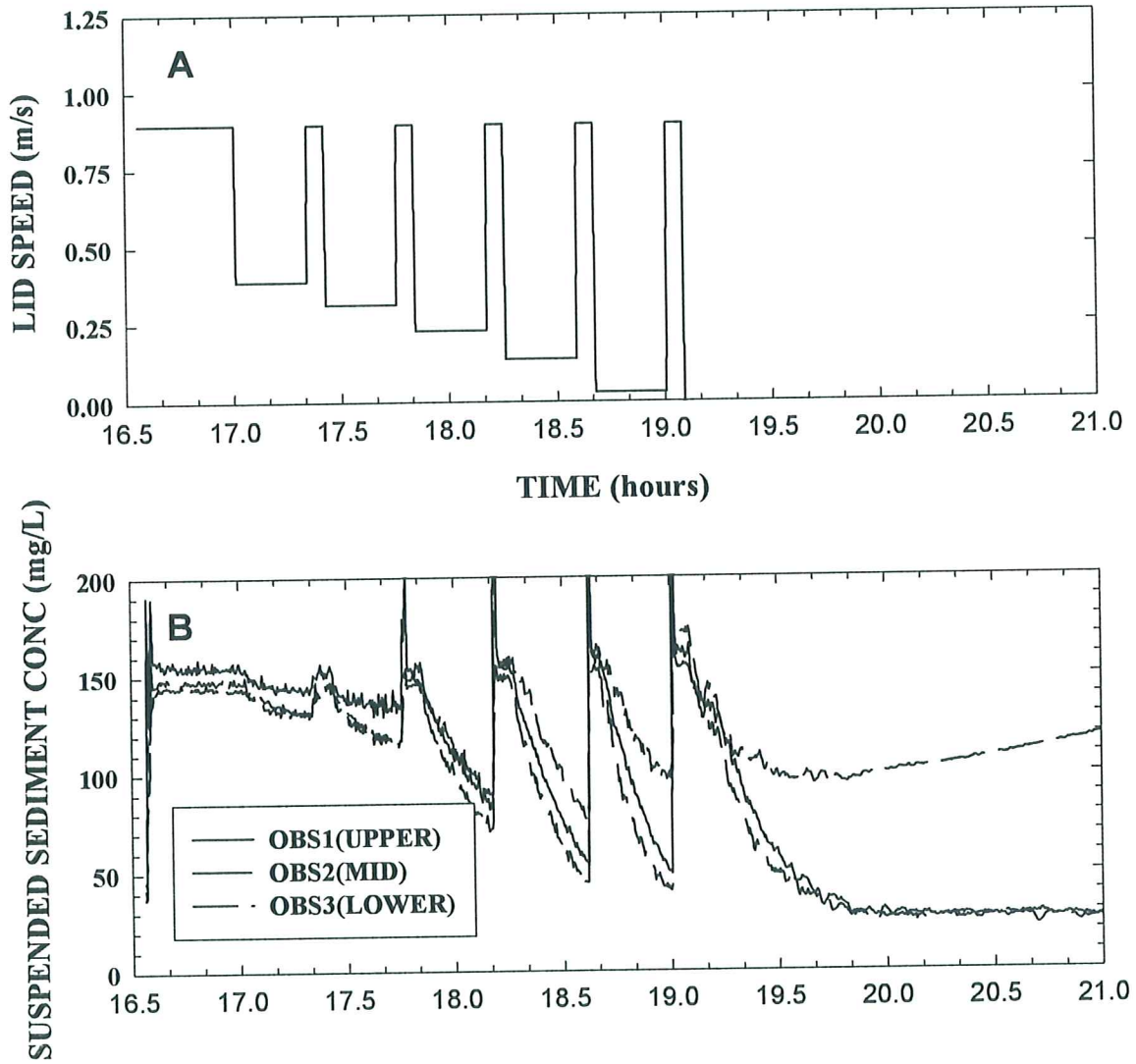
Figure 4.8.2. The time-series of suspended sediment concentration recorded in Lab Carousel during the settling experiments of sample R11 at 150 mg/L

LAB CAROUSEL - Rustico Bay, PEI

Sample R11-3 23 November, 1997
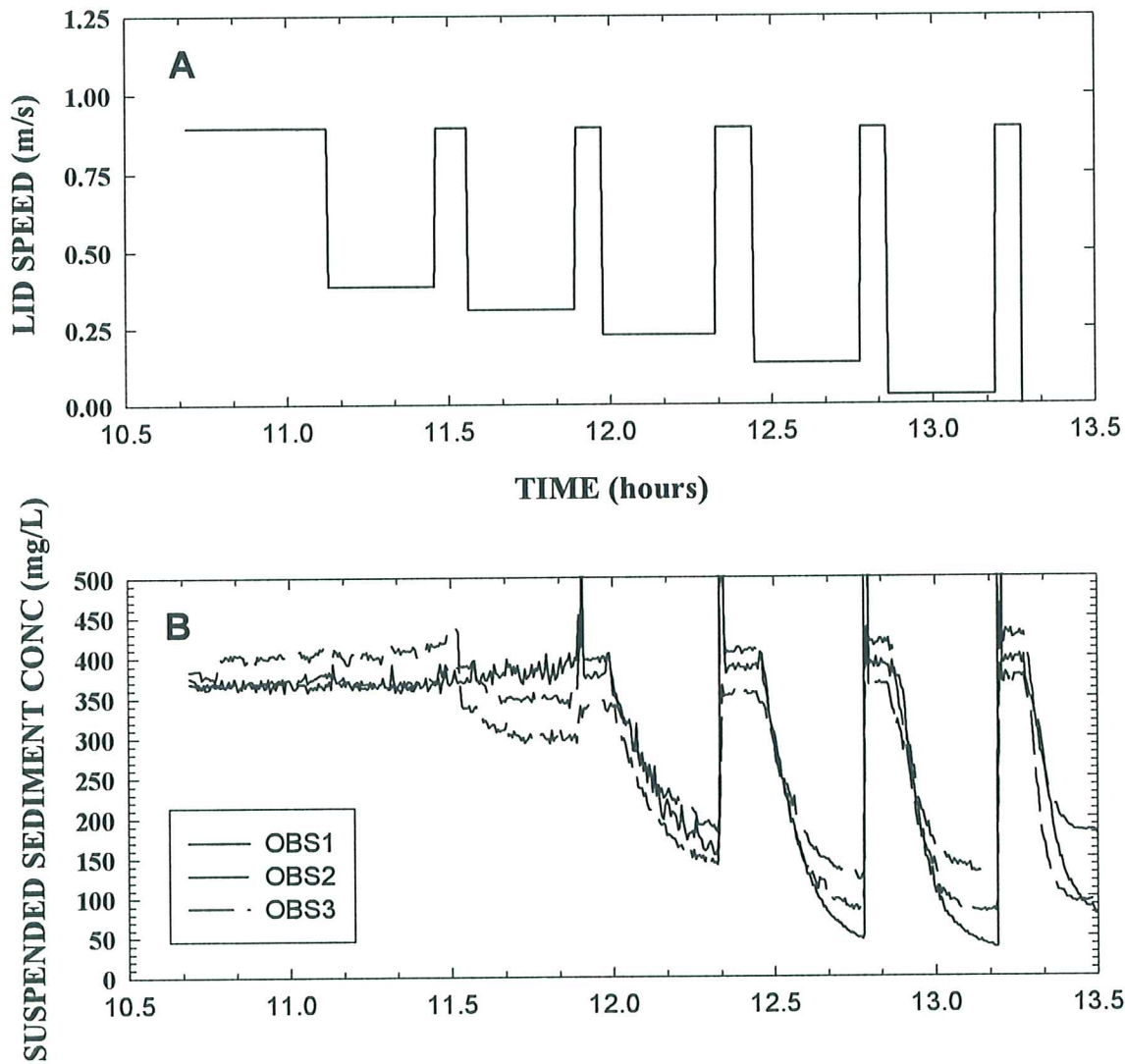
Figure 4.8.3. The time-series of suspended sediment concentration recorded in Lab Carousel during the settling experiments of sample R11 at 375 mg/L

LAB CAROUSEL - Rustico Bay, PEI

Sample R11-4 23 November, 1997

A

LID SPEED (m/s)

TIME (hours)

B

SUSPENDED SEDIMENT CONC (mg/L)

— OBS1
— OBS2
-- · OBS3
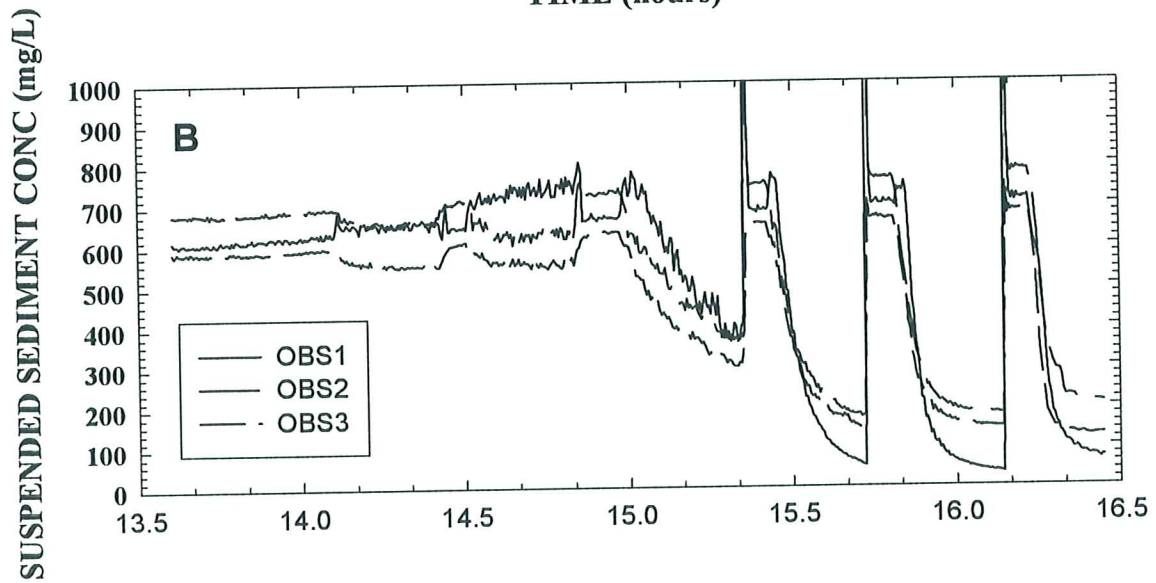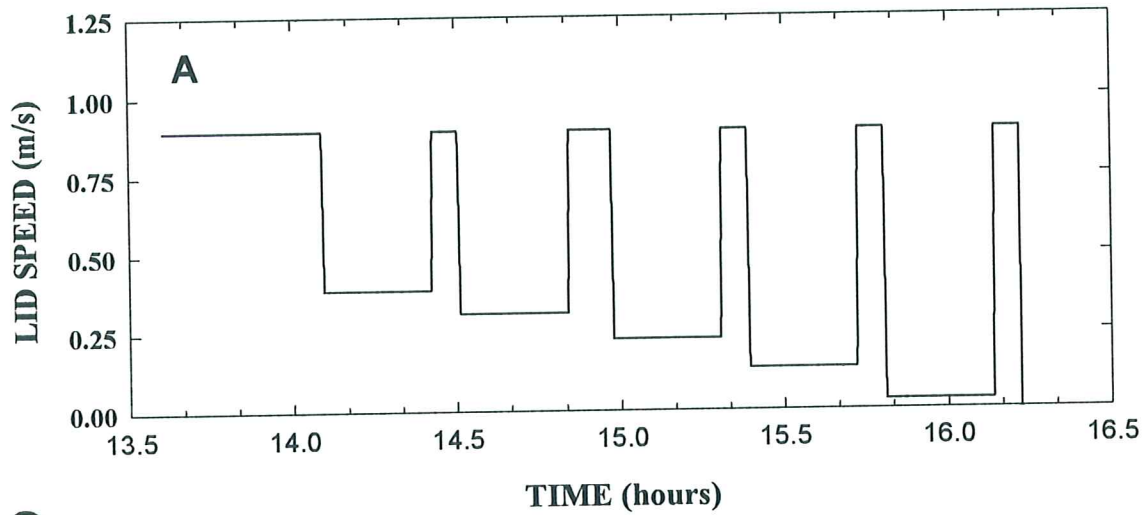
Figure 4.8.4. The time-series of suspended sediment concentration recorded in Lab Carousel during the settling experiments of sample R11 at 700 mg/L

123

LAB CAROUSEL - Rustico Bay, PEI

Sample R12-1 24 November, 1997
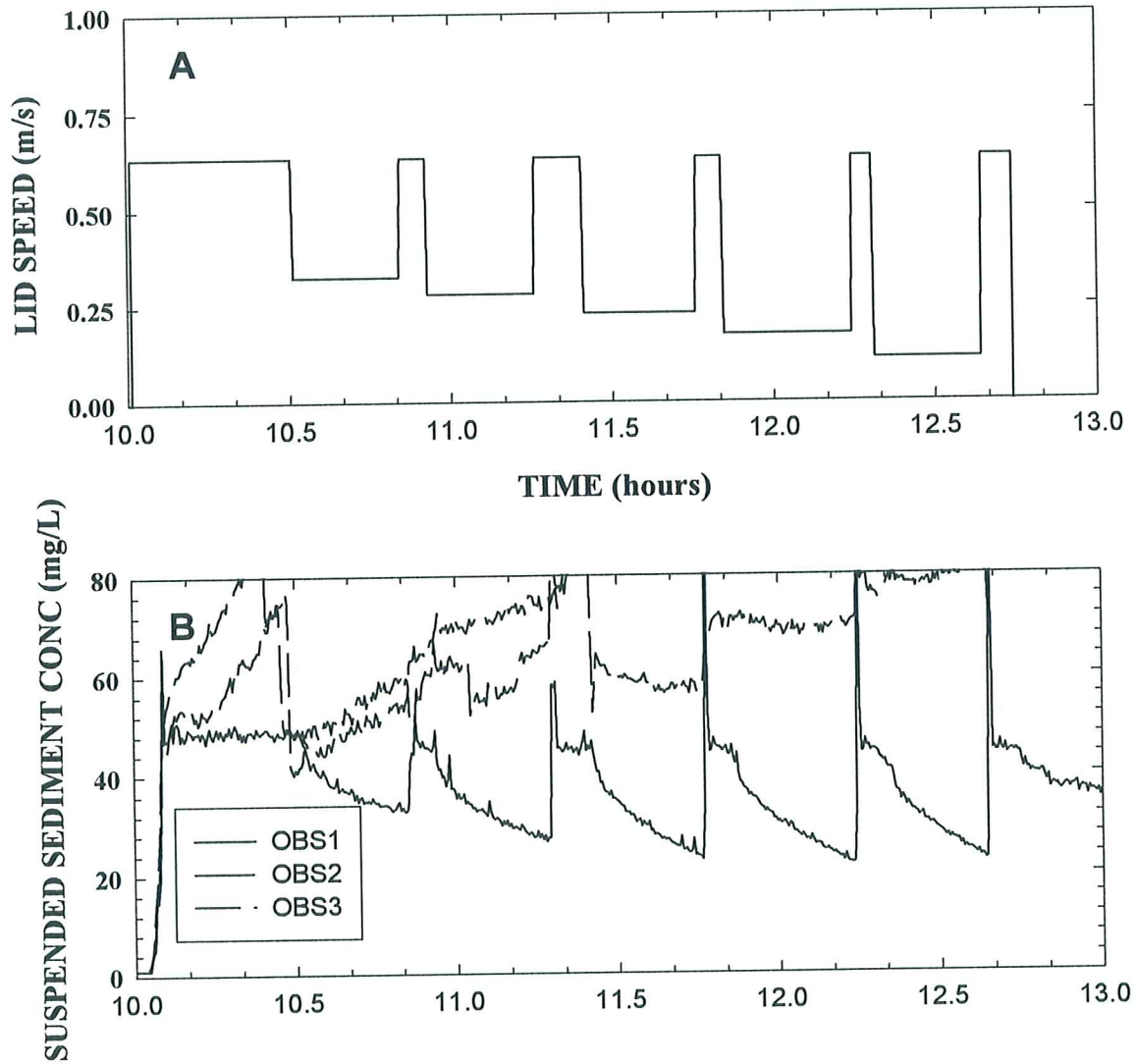
Figure 4.8.5. The time-series of suspended sediment concentration recorded in Lab Carousel during the settling experiments of sample R12 at 40 mg/L

LAB CAROUSEL - Rustico Bay, PEI

Sample R12-2 24 November, 1997

A

LID SPEED (m/s) vs TIME (hours)

B

SUSPENDED SEDIMENT CONC (mg/L)

- OBS1
- OBS2
- · OBS3
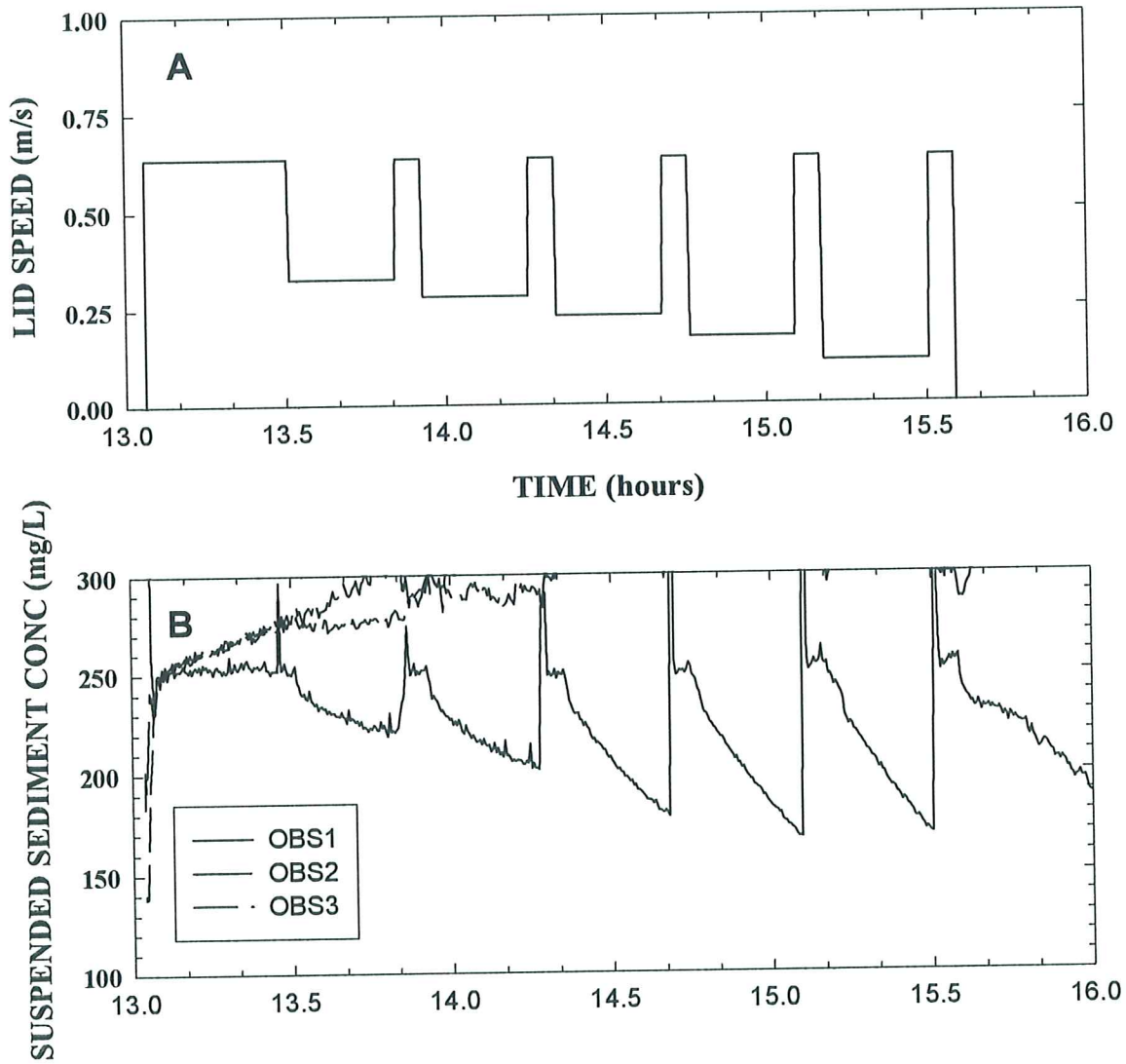
Figure 4.8.6. The time-series of suspended sediment concentration recorded in Lab Carousel during the settling experiments of sample R12 at 240 mg/L

LAB CAROUSEL - Rustico Bay, PEI

Sample R12-3 25 November, 1997
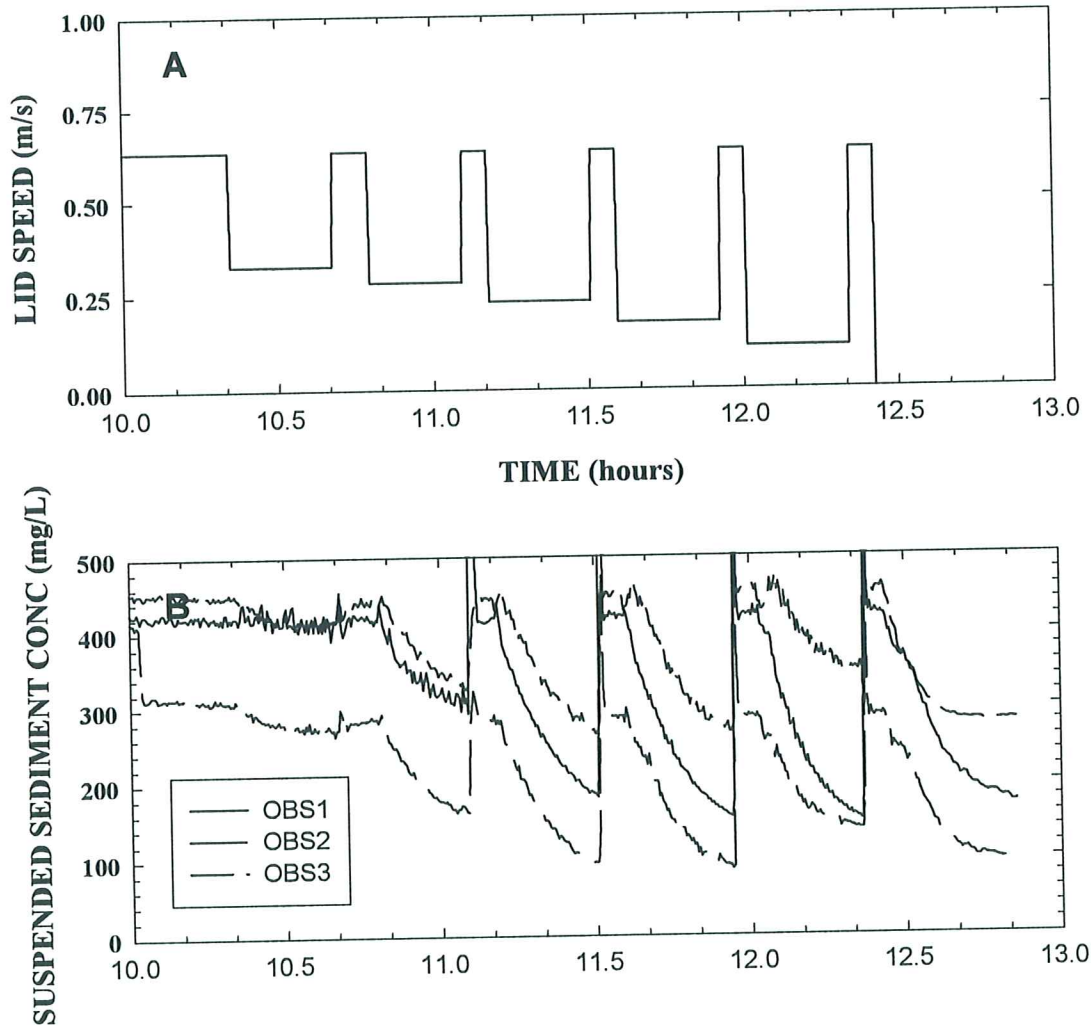
Figure 4.8.7. The time-series of suspended sediment concentration recorded in Lab Carousel during the settling experiments of sample R12 at 400 mg/L

LAB CAROUSEL - Rustico Bay, PEI

Sample R12-4 25 November, 1997
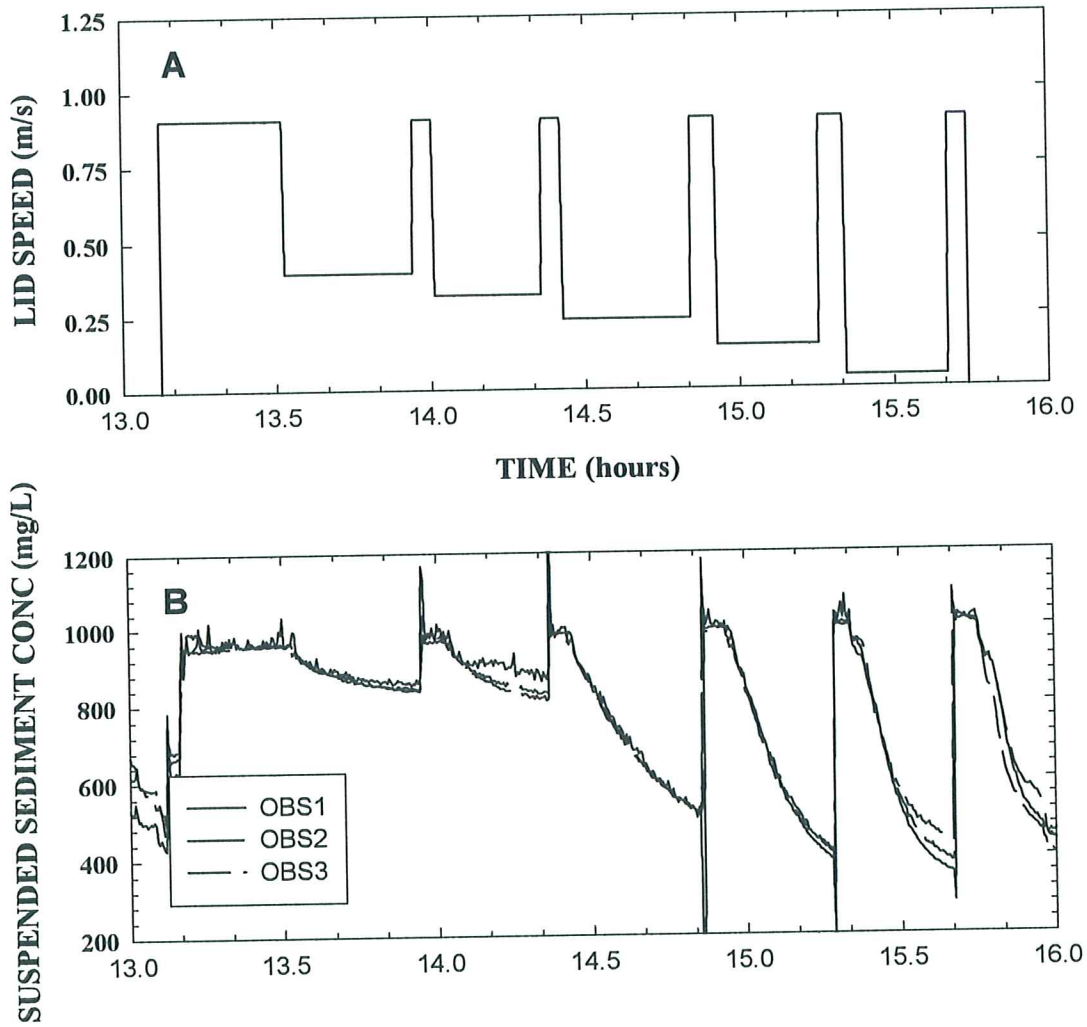
Figure 4.8.8. A time-series of suspended sediment concentration within the Lab Carousel during settling of sample R12 at a concentration of 950 mg/L.

LAB CAROUSEL - Rustico Bay, PEI

Sample R11-1 22 November, 1997

$$SSC(t) = S_o \exp^{kt}$$

Legend:
- —— 0.31 Pa
- —— 0.23 Pa
- — · 0.14 Pa
- — — 0.03 Pa
- ······ still water

Y-axis: SUSPENDED SEDIMENT CONC (mg/L)

X-axis: TIME (secs)
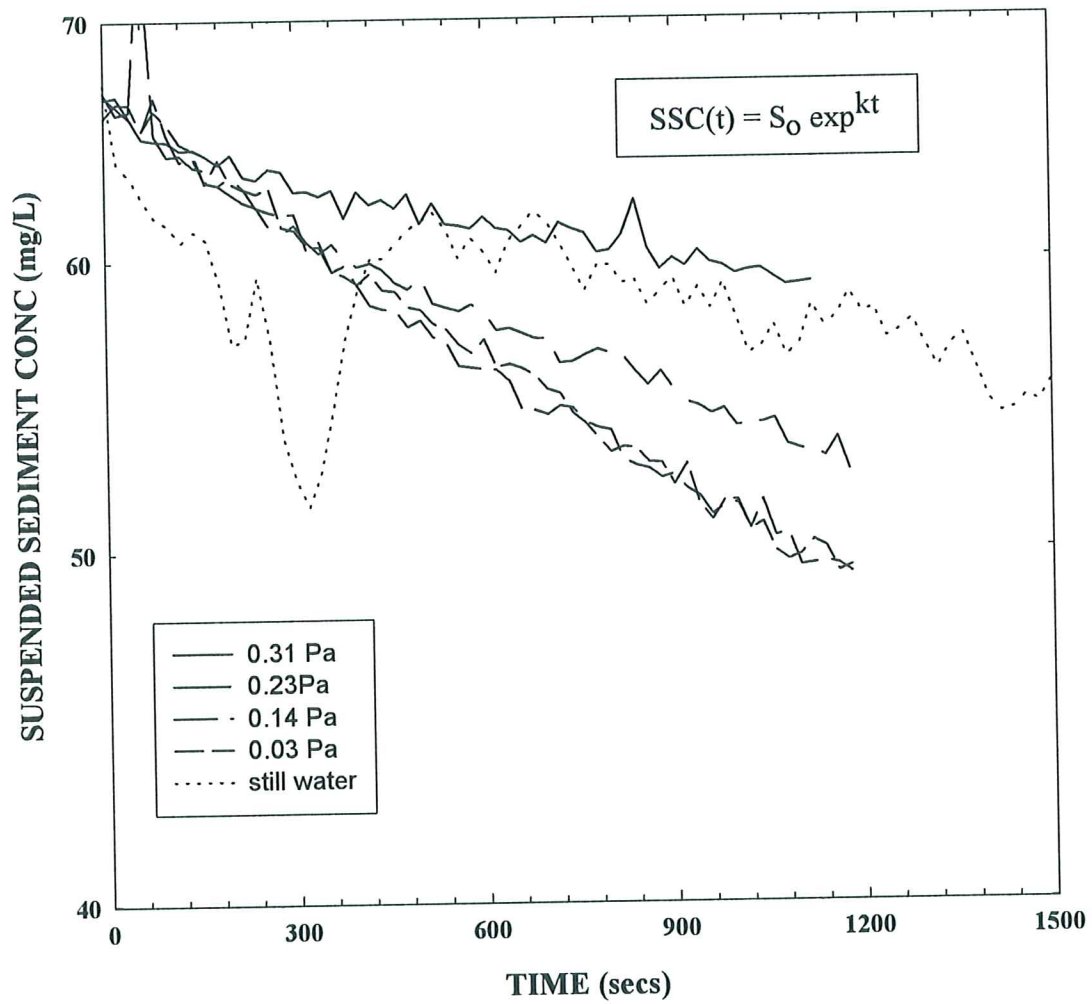
Figure 4.8.9. A time-series of settling in Lab Carousel for sample R11 for all current speeds at a concentration of 65 mg/L.

LAB CAROUSEL - Rustico Bay, PEI

Sample R11-2 22 November, 1997

$$SSC(t) = S_O \exp^{kt}$$

Legend:
- 0.39 Pa
- 0.31 Pa
- 0.23 Pa
- 0.14 Pa
- 0.03 Pa
- still water

Axis labels: SUSPENDED SEDIMENT CONC (mg/L) vs TIME (secs)
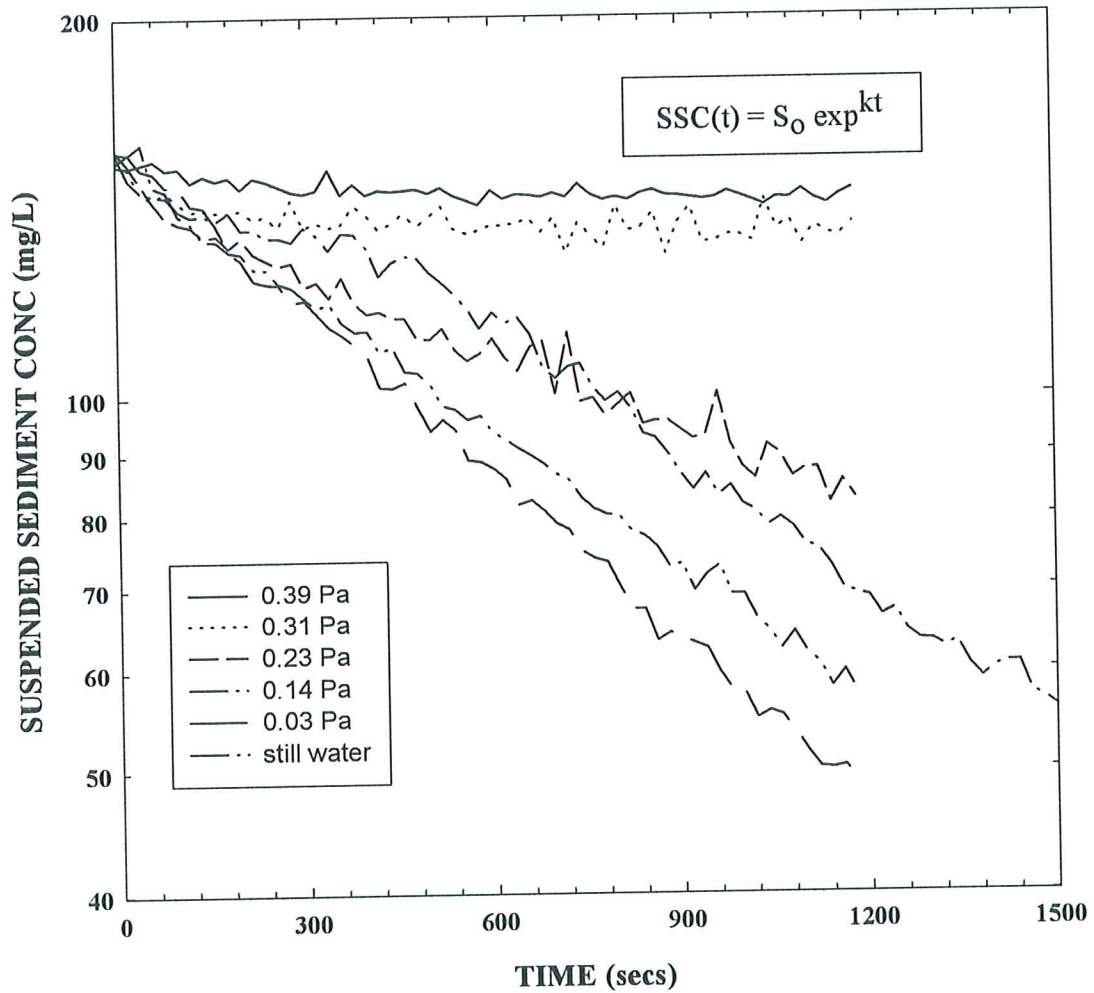
Figure 4.8.10. A time-series of settling in Lab Carousel for sample R11 for all current speeds at a concentration of 150 mg/L.

LAB CAROUSEL - Rustico Bay, PEI

Sample R11-3 22 November, 1997

$$SSC(t) = S_O \exp^{kt}$$

Legend:
- 0.39 Pa
- 0.31 Pa
- 0.23 Pa
- 0.14 Pa
- 0.03 Pa
- still water

X-axis: TIME (secs)
Y-axis: SUSPENDED SEDIMENT CONC (mg/L)
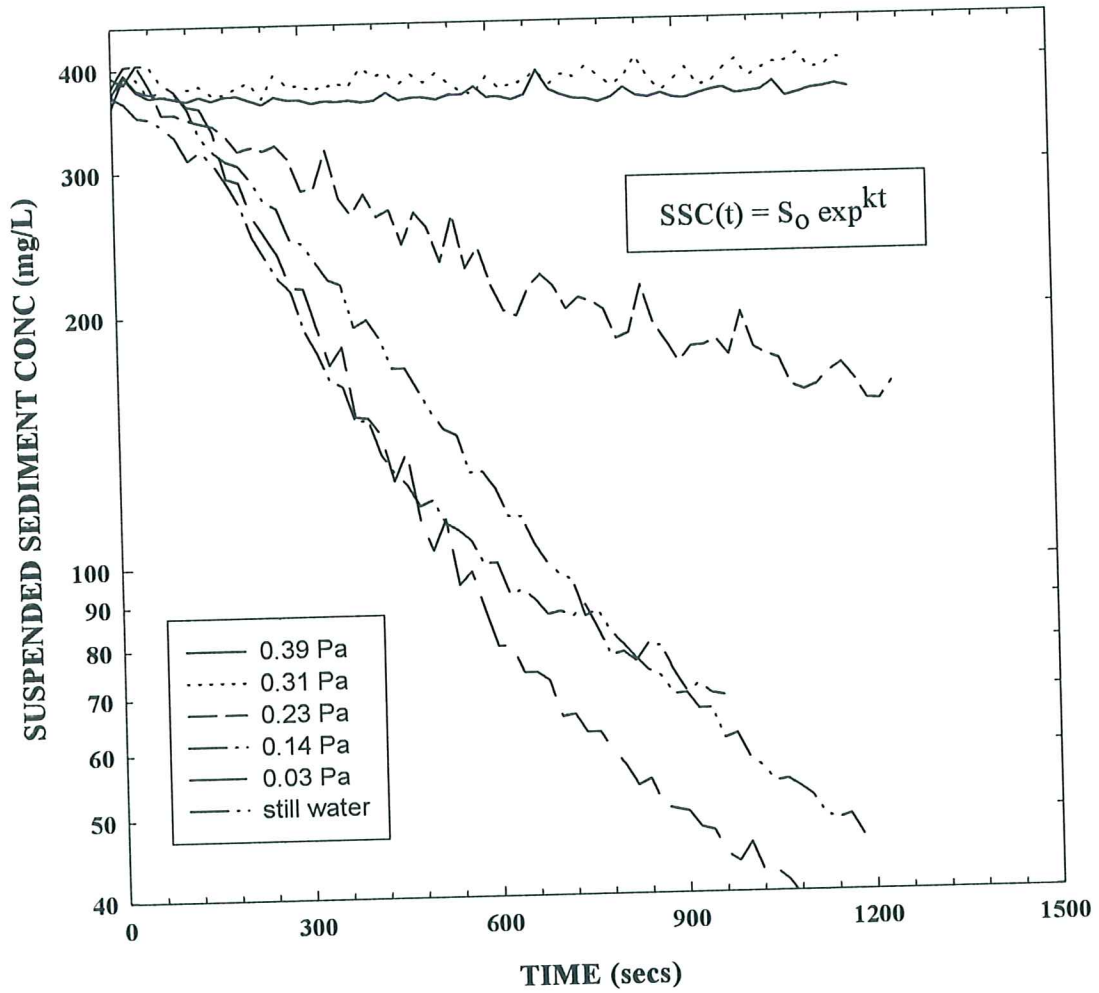
Figure 4.8.11. A time-series of settling in Lab Carousel for sample R11 for all current speeds at a concentration of 375 mg/L.

LAB CAROUSEL - Rustico Bay, PEI

Sample R11-4 22 November, 1997

SUSPENDED SEDIMENT CONC (mg/L) vs TIME (secs)

Legend:
- 0.39 Pa
- 0.31 Pa
- 0.23 Pa
- 0.14 Pa
- 0.03 Pa
- still water

$$SSC(t) = S_o \exp^{kt}$$
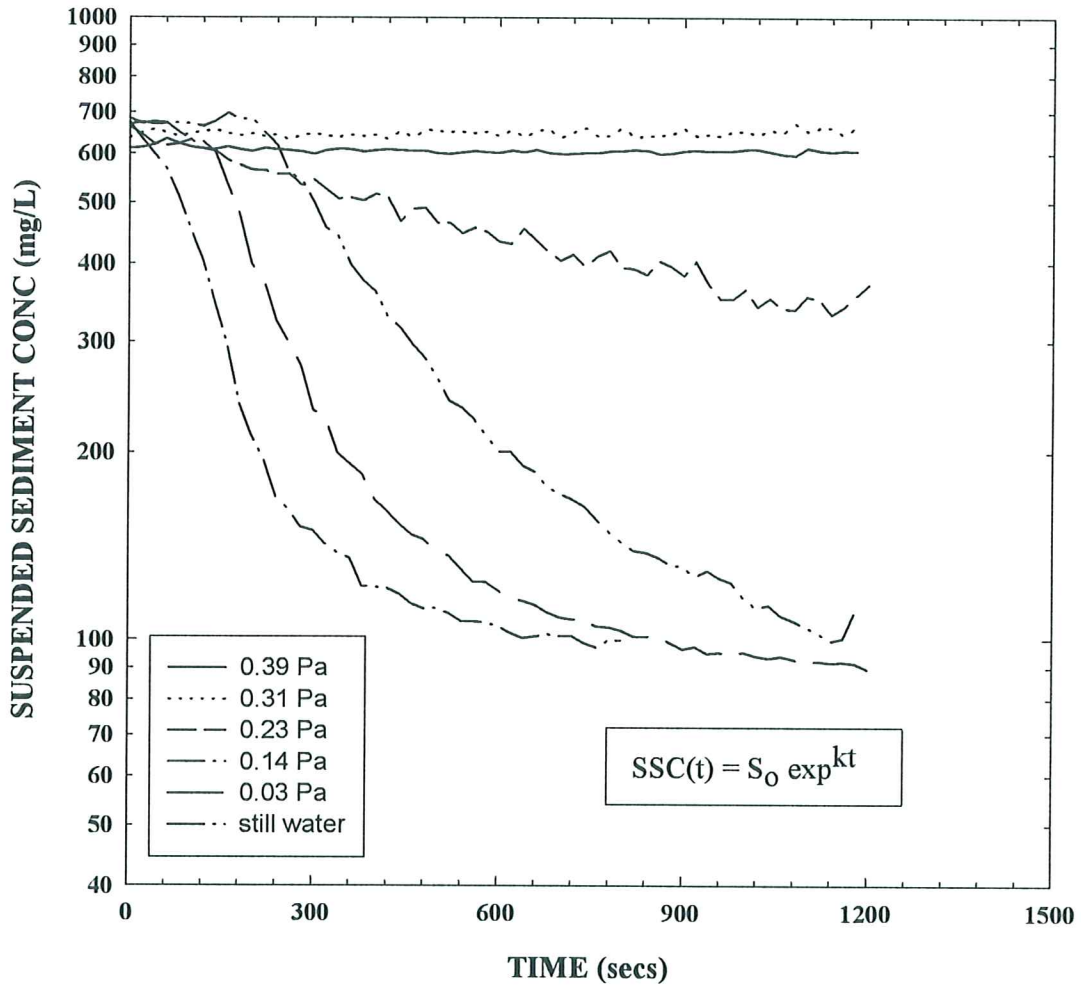
Figure 4.8.12 A time-series of settling in Lab Carousel for sample R11 for all current speeds at a concentration of 700mg/L.
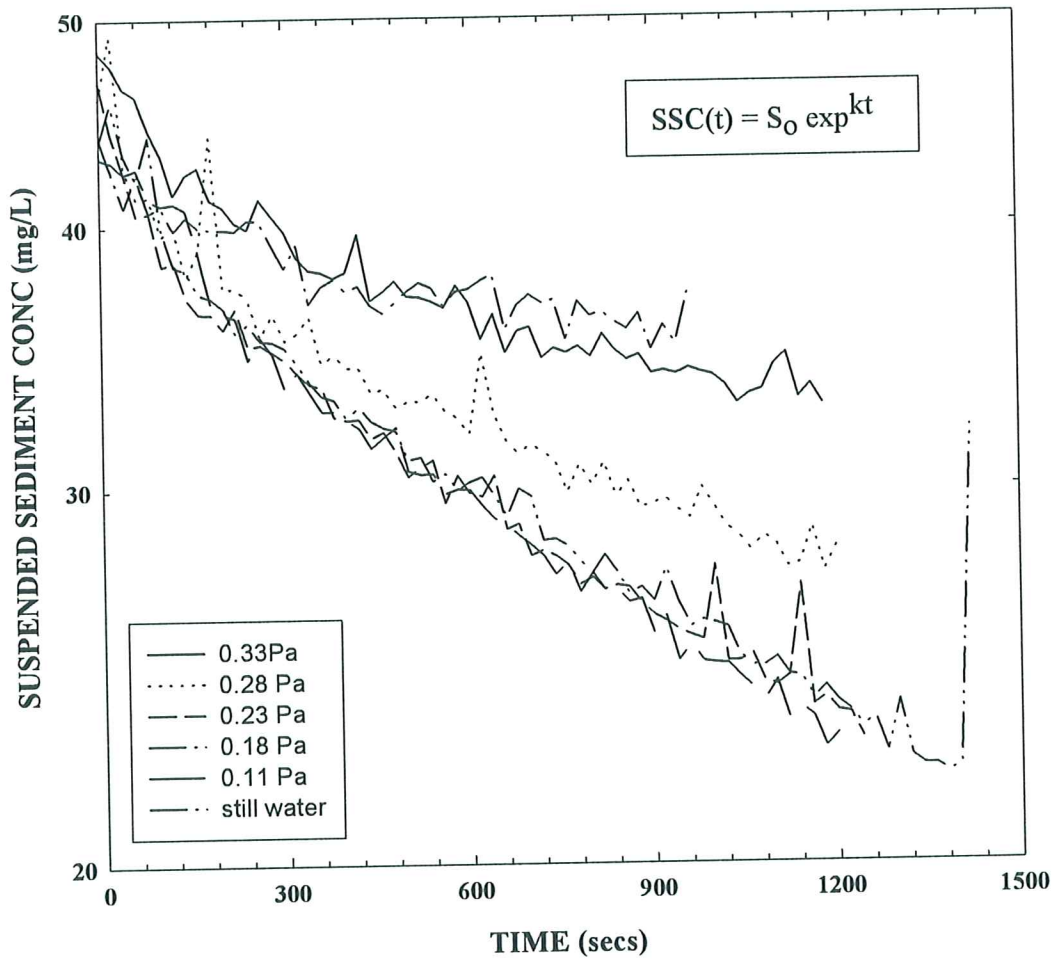
Figure 4.8.13 A time-series of settling in Lab Carousel for sample R12 for all current speeds at a concentration of 40 mg/L.

LAB CAROUSEL - Rustico Bay, PEI

Sample R12-2 24 November, 1997

$$SSC(t) = S_O \exp^{kt}$$

Legend:
— 0.33Pa
····· 0.28 Pa
— — 0.23 Pa
—·· 0.18 Pa
— 0.11 Pa
—·· still water

Axis labels: SUSPENDED SEDIMENT CONC (mg/L), TIME (secs)
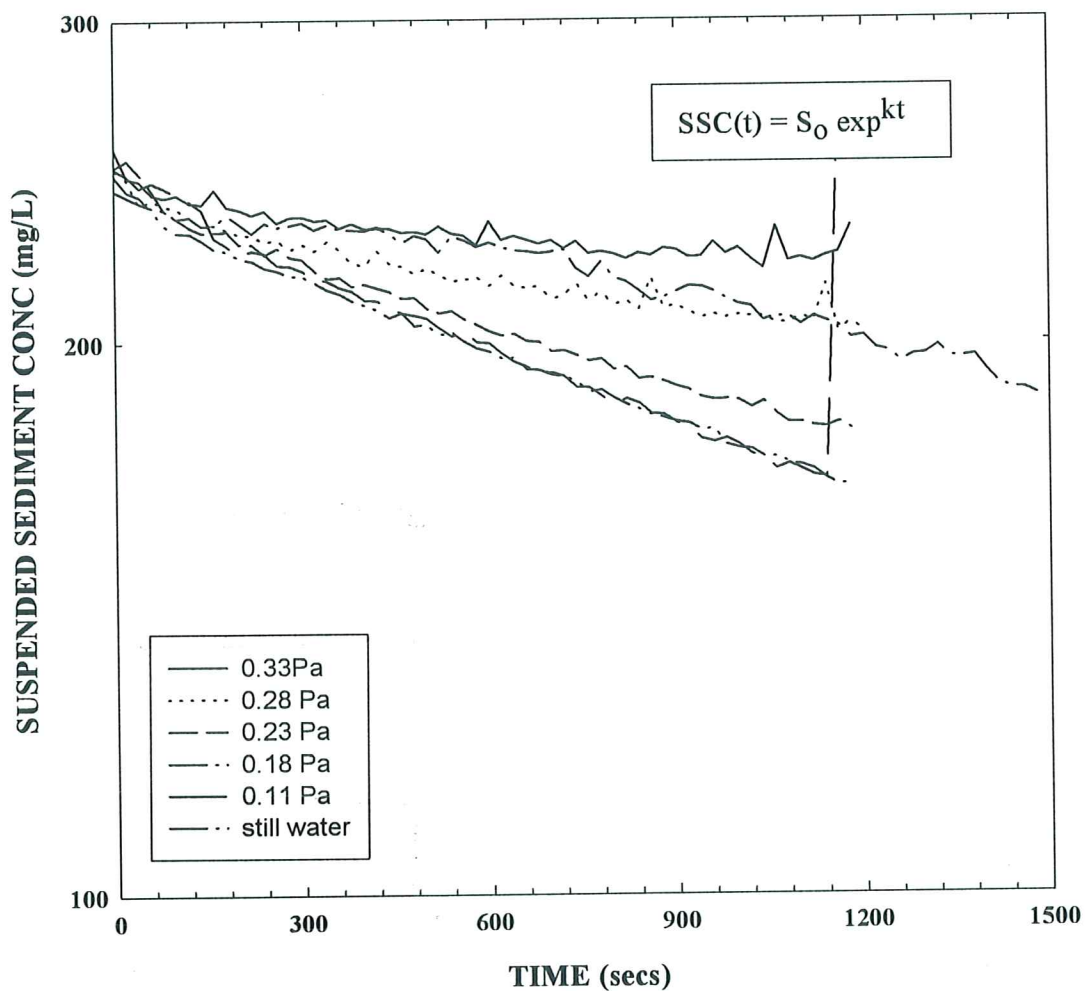
Figure 4.8.14 A time-series of settling in Lab Carousel for sample R12 for all current speeds at a concentration of 240 mg/L.

LAB CAROUSEL - Rustico Bay, PEI

Sample R12-3 25 November, 1997
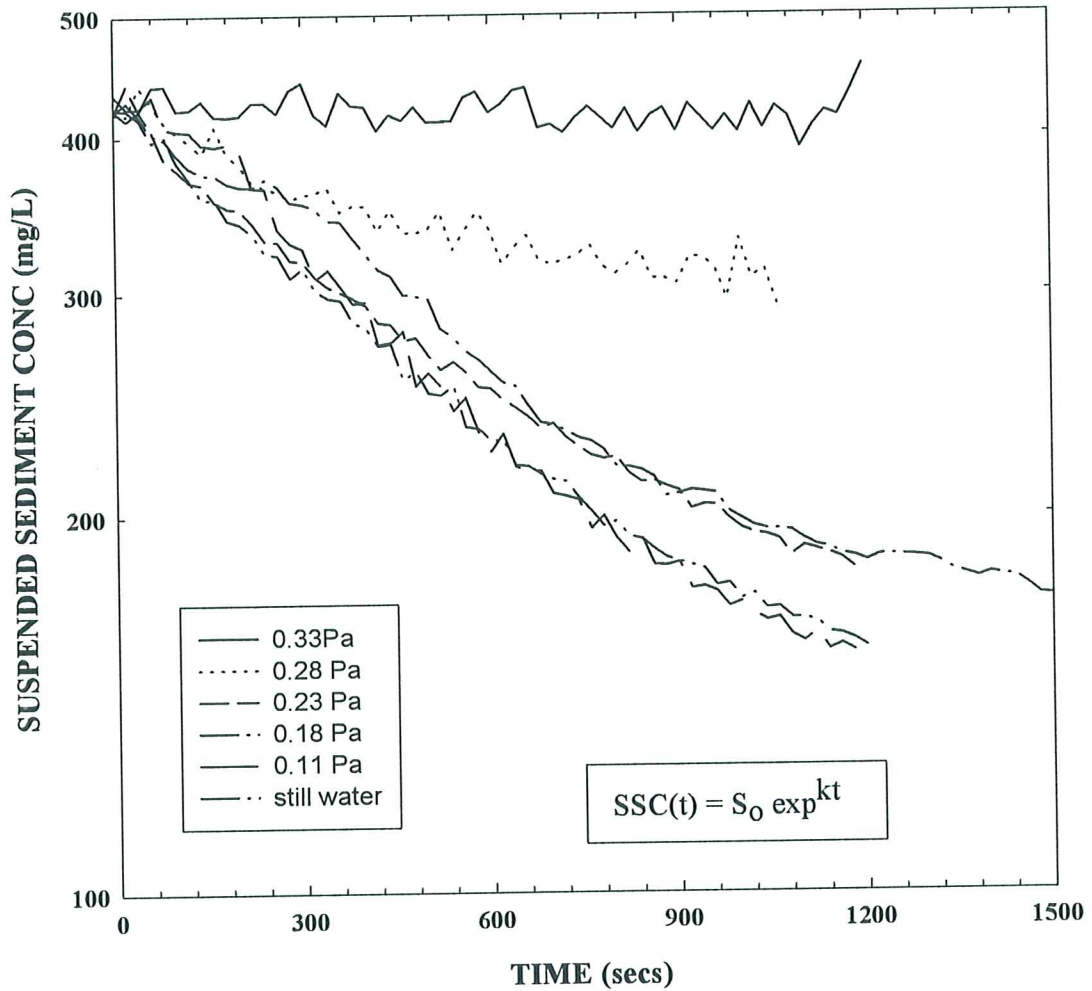
Figure 4.8.15. A time-series of settling in Lab Carousel for sample R12 for all current speeds at a concentration of 400 mg/L.

LAB CAROUSEL - Rustico Bay, PEI

Sample R12-4 25 November, 1997

Legend:
- 0.33Pa
- 0.28 Pa
- 0.23 Pa
- 0.18 Pa
- 0.11 Pa
- still water

$$SSC(t) = S_o \exp^{kt}$$
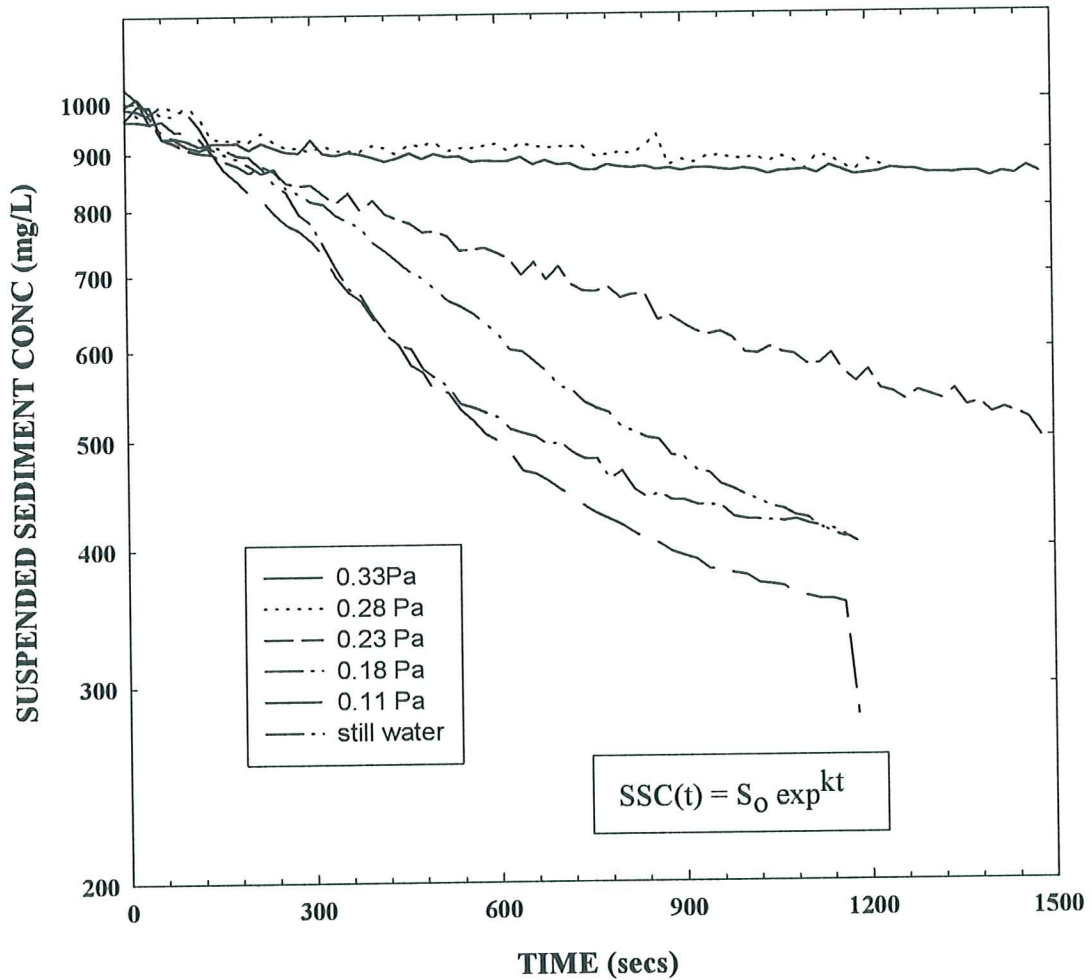
Figure 4.8.16. A time-series of settling in Lab Carousel for sample R12 for all current speeds at a concentration of 950 mg/L.
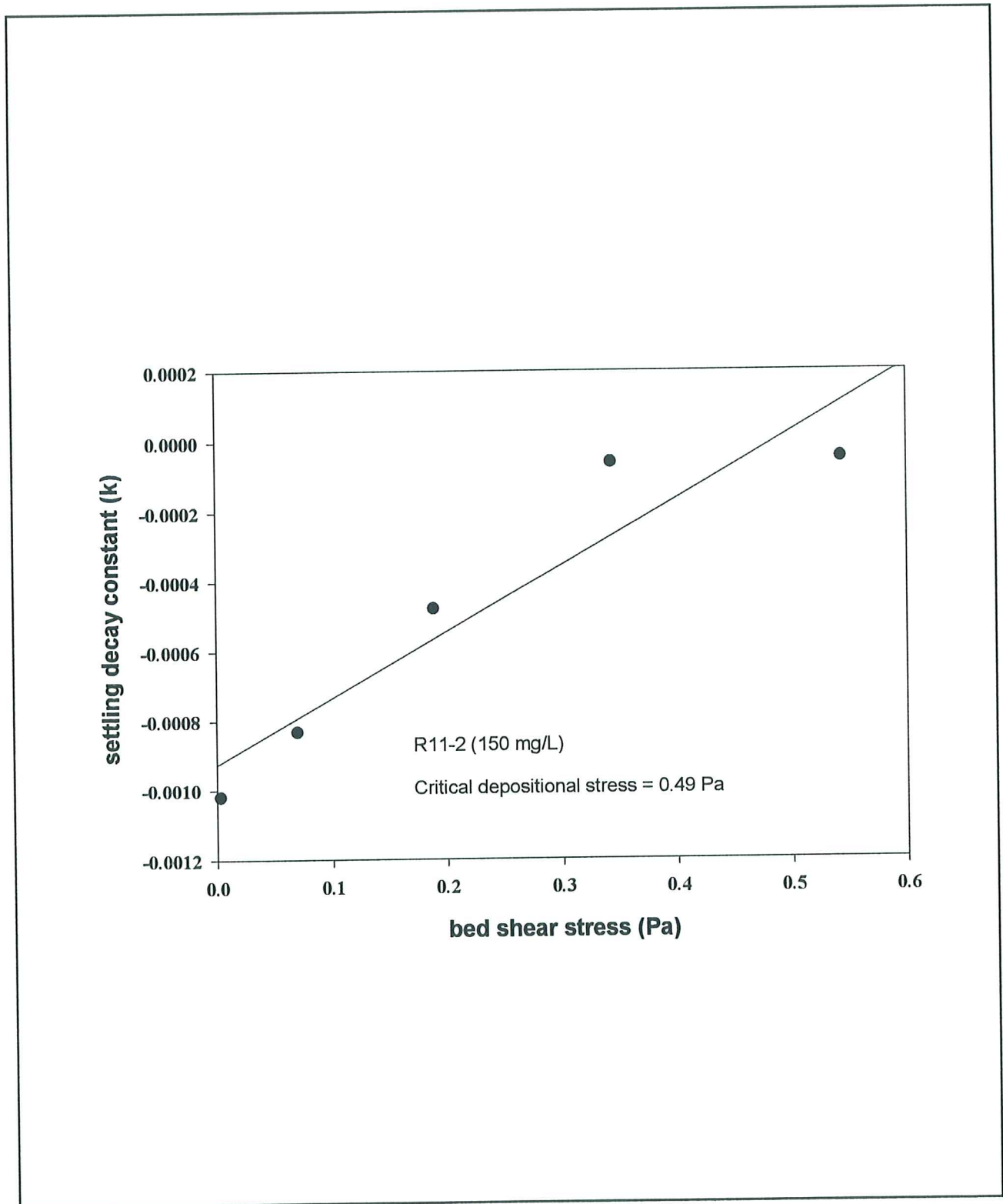
Figure 4.8.17. An example of the decay constant k plotted against applied bed shear stress for sample R11. The deposition threshold of 0.49 Pa was determined by solving the stress value for k = 0 using best-fit linear regression.

136
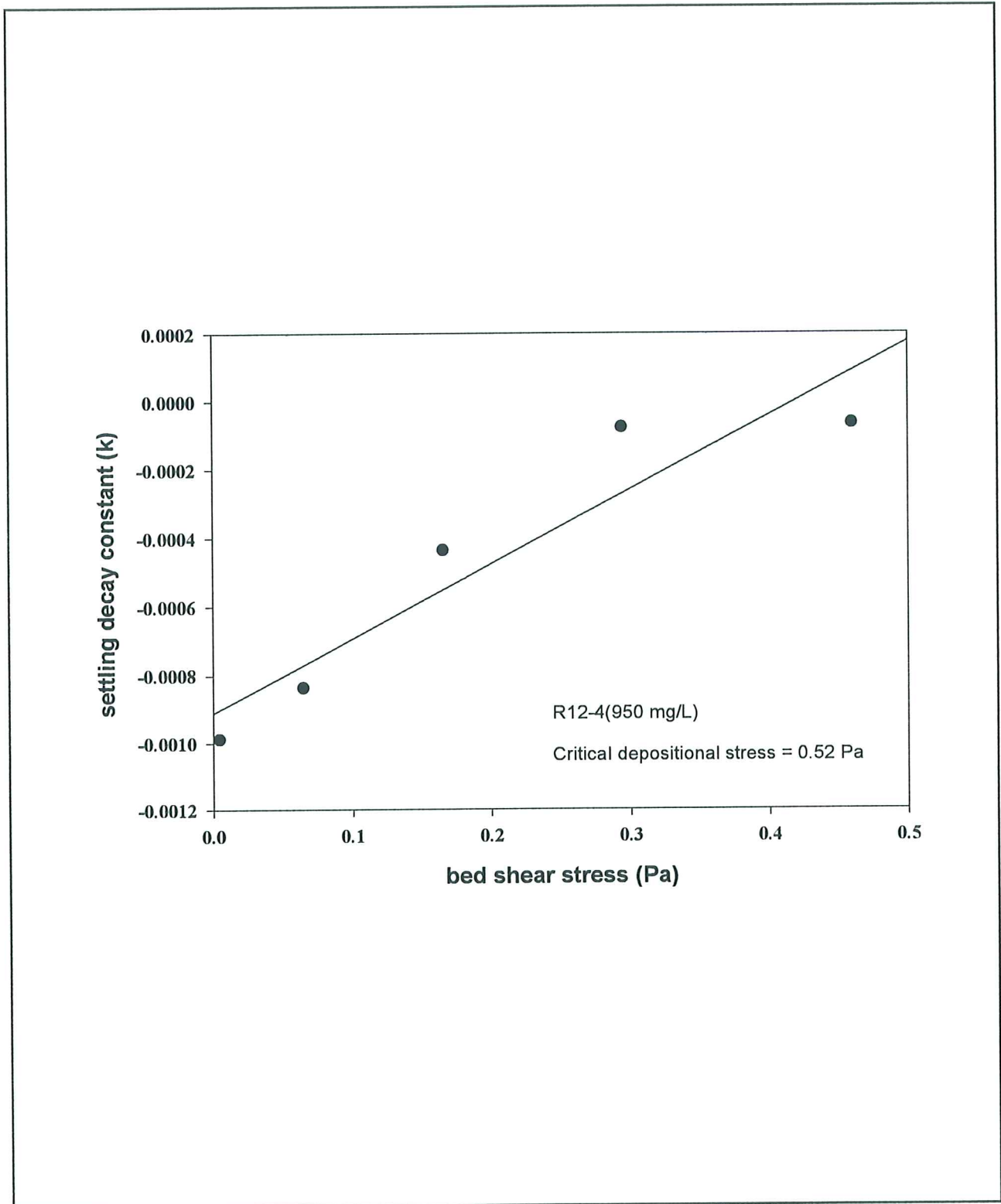
Figure 4.8.18. An example of the decay constant k plotted against applied bed shear stress for sample R12. The deposition threshold of 0.52 Pa was determined by solving the stress value for k = 0 using best-fit linear regression.

137
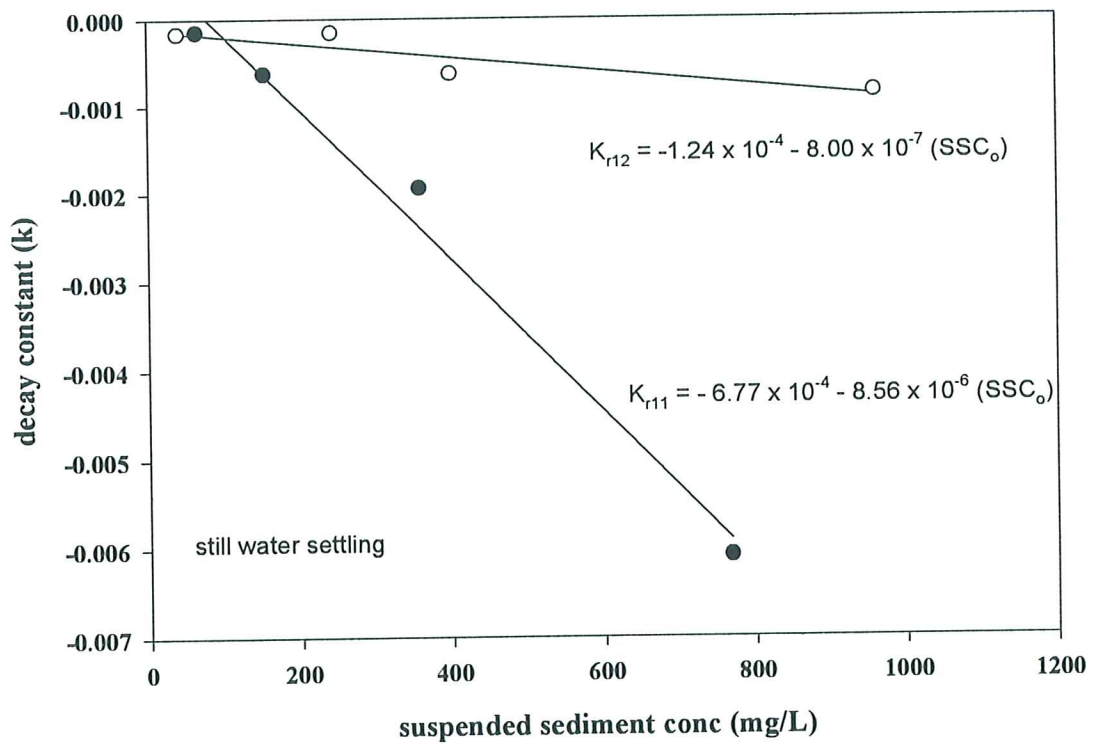
Figure 4.8.19. An example of the still water decay constant k plotted against suspended sediment concentration for samples R11 and R12. In both cases the magnitude of k increases with SSC, though the rates of increase are very different for the two samples.

138
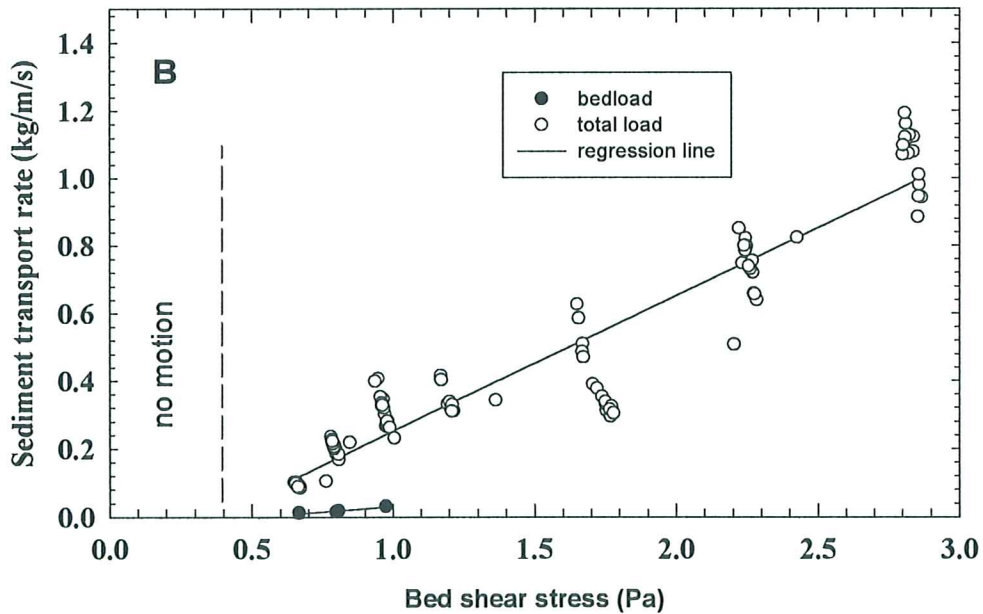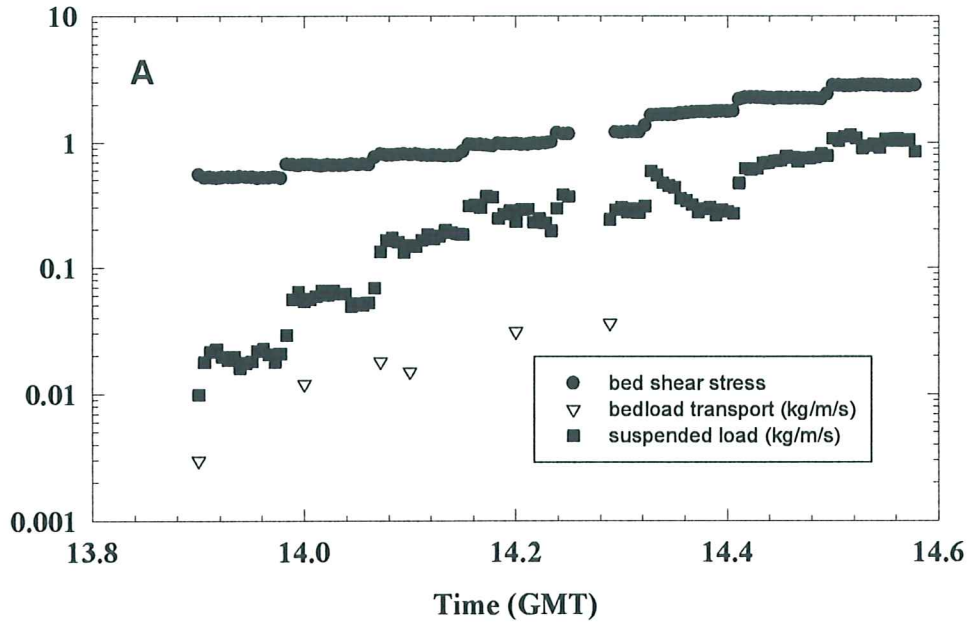
Figure 4.9.1. Sediment transport results from the sand site R8. (A) bedload and suspended load transport plotted with bed shear stress, and (B) bedload and total (bedload and suspended) load transport plotted against shear stress. A linear relationship is evident.
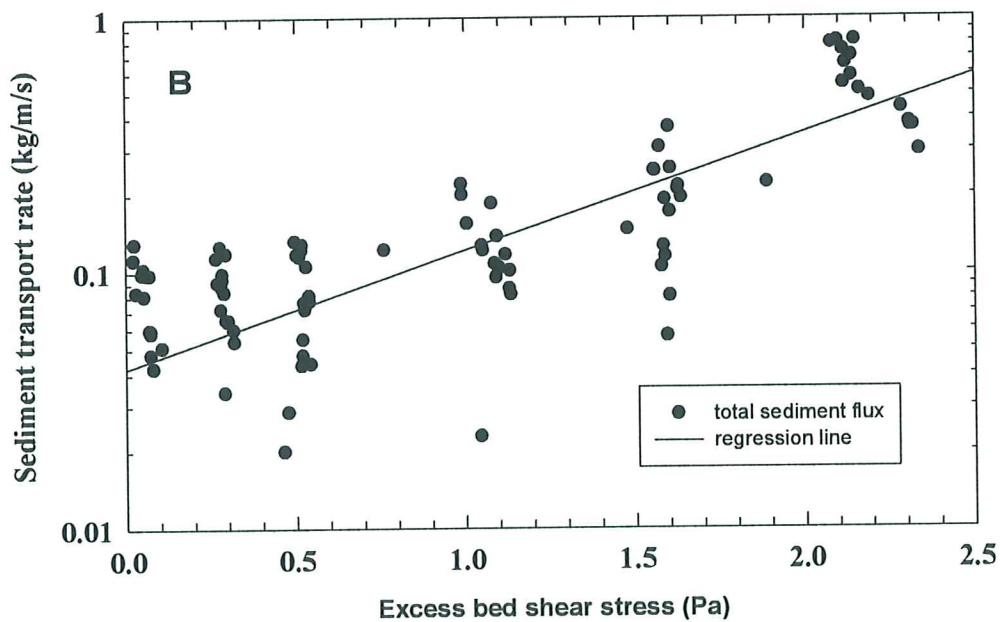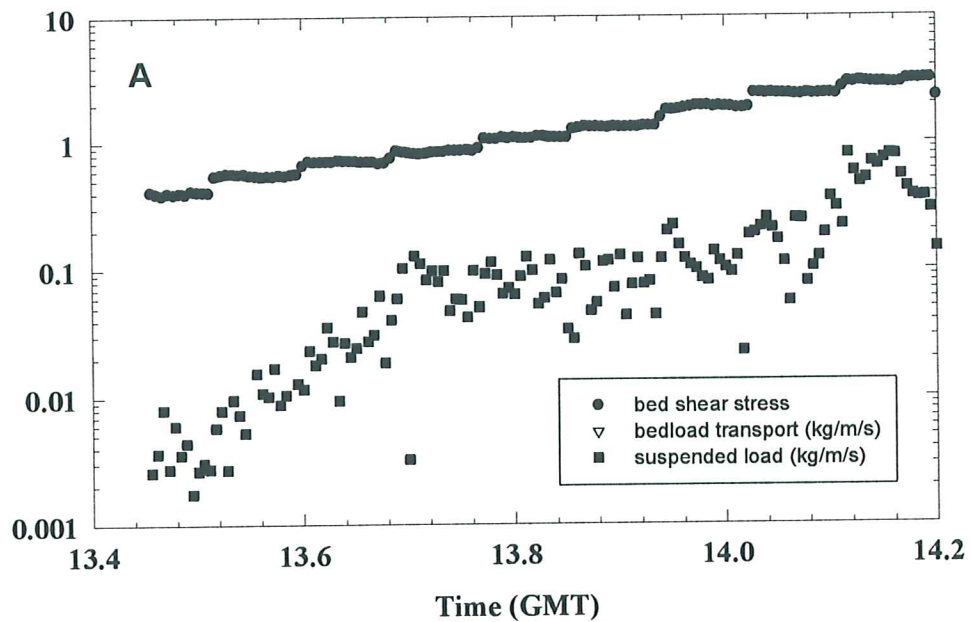
Figure 4.9.2. Sediment transport results from the sand site R9. (A) bedload and suspended load transport plotted with bed shear stress, and (B) bedload and total (bedload and suspended) load transport plotted against shear stress. A linear relationship is evident.
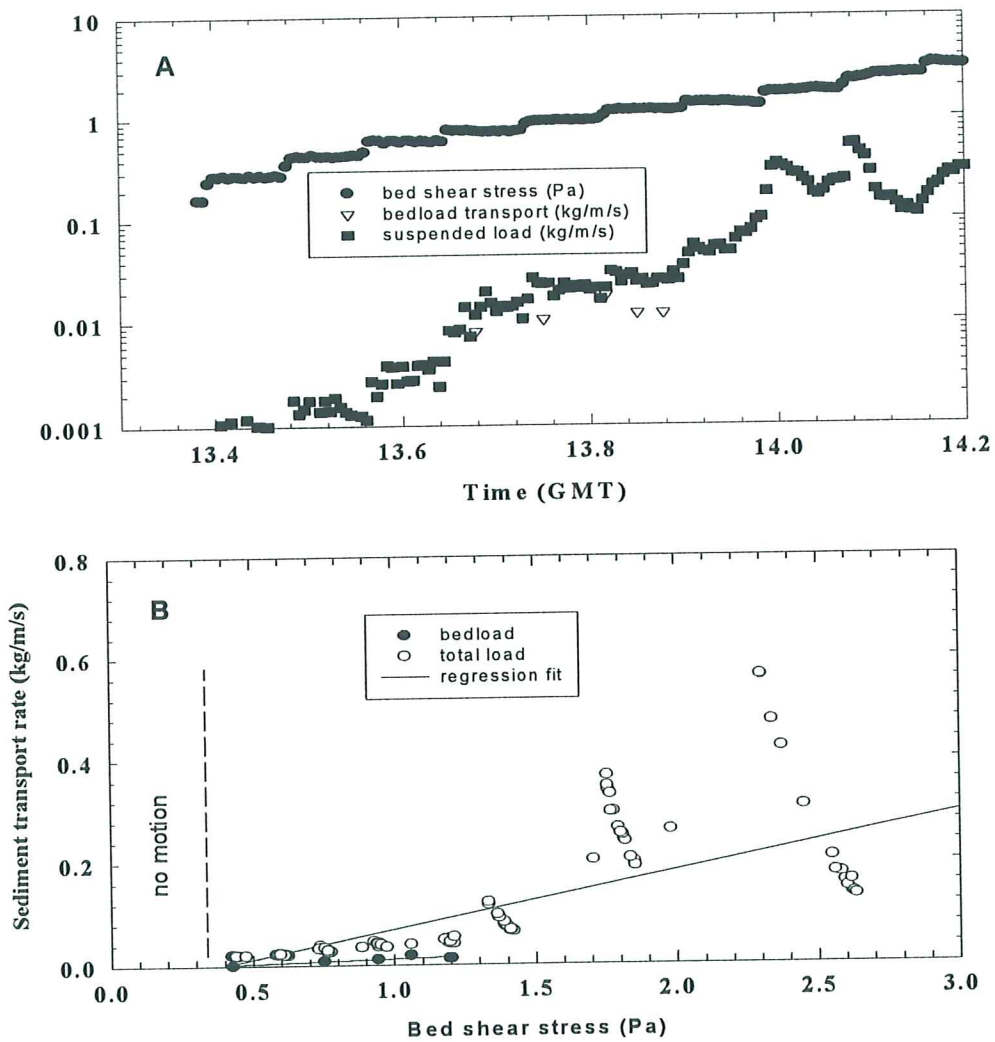
Figure 4.9.3. Sediment transport results from the sand site R15. (A) bedload and suspended load transport plotted with bed shear stress, and (B) bedload and total (bedload and suspended) load transport plotted against shear stress.

APPENDIX 1 - Grain size analyses of bottom sediment samples

97RUSTICO-001-R1,RDO11283,   DR. CARL AMOS
,00409,   SYRINGE CORE, RUSTICO BAY, PEI
                             MILLIMETER EQUIVALENTS
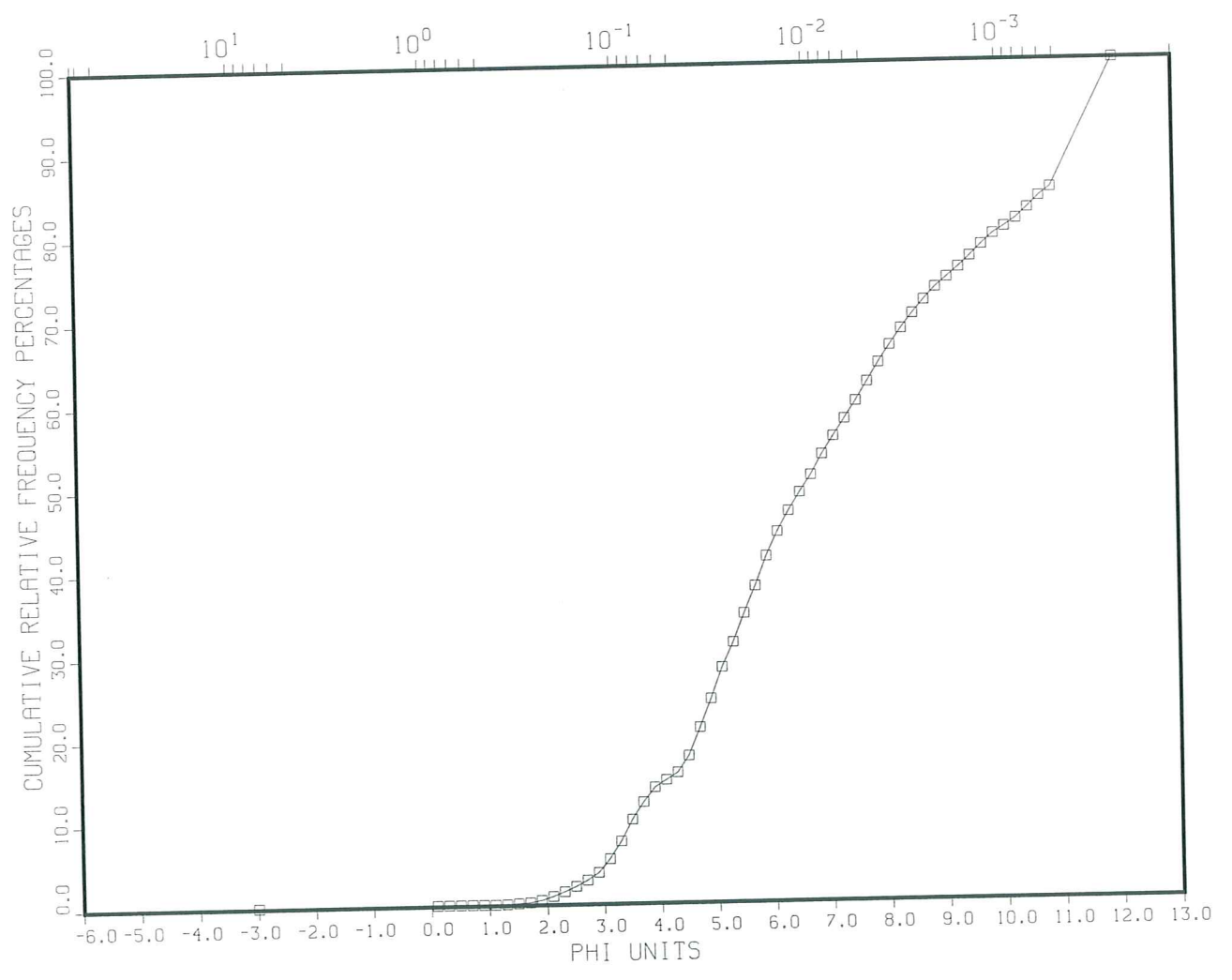
Calculation Results for
The Sample with the Identifier:

V4.0
23:10:1997
11283
57
97RUSTIC0-001-R1
97RUSTICO
960030
DR. CARL AMOS
SYRINGE CORE, RUSTICO BAY, PEI
RD011283
SWF00409
0.00000000000000E+0000
0.00000000000000E+0000
0
0
0
0
0
0
0
0
53103
001-R1
001-R1
SYRINGE
CORE
46:26.50
-63:18.22
3.00
n lines for future expansion
#

Results

Midpoints		Relative Frequency	Cumulative Frequency
MM	PHI	Percentages	Percentages
8.00e+00	-3.00	0.12	0.12
9.33e-01	0.10	0.00	0.12
8.12e-01	0.30	0.00	0.12
7.07e-01	0.50	0.00	0.12

6.16e-01	0.70	0.00	0.12
5.36e-01	0.90	0.00	0.12
4.67e-01	1.10	0.00	0.12
4.06e-01	1.30	0.03	0.15
3.54e-01	1.50	0.09	0.24
3.08e-01	1.70	0.08	0.32
2.68e-01	1.90	0.26	0.58
2.33e-01	2.10	0.44	1.02
2.03e-01	2.30	0.53	1.55
1.77e-01	2.50	0.61	2.16
1.54e-01	2.70	0.72	2.88
1.34e-01	2.90	0.89	3.77
1.17e-01	3.10	1.60	5.37
1.02e-01	3.30	2.09	7.46
8.84e-02	3.50	2.57	10.03
7.69e-02	3.70	2.07	12.10
6.70e-02	3.90	1.75	13.85
5.83e-02	4.10	0.88	14.73
5.08e-02	4.30	0.88	15.60
4.42e-02	4.50	2.01	17.62
3.85e-02	4.70	3.38	20.99
3.35e-02	4.90	3.41	24.41
2.92e-02	5.10	3.73	28.13
2.54e-02	5.30	2.97	31.10
2.21e-02	5.50	3.45	34.55
1.92e-02	5.70	3.22	37.77
1.67e-02	5.90	3.54	41.31
1.46e-02	6.10	2.90	44.21
1.27e-02	6.30	2.47	46.68
1.10e-02	6.50	2.20	48.88
9.62e-03	6.70	2.06	50.93
8.37e-03	6.90	2.47	53.40
7.29e-03	7.10	2.14	55.54
6.35e-03	7.30	2.08	57.62
5.52e-03	7.50	2.12	59.74
4.81e-03	7.70	2.26	62.00
4.19e-03	7.90	2.24	64.24
3.64e-03	8.10	2.05	66.29
3.17e-03	8.30	1.93	68.23
2.76e-03	8.50	1.77	70.00
2.40e-03	8.70	1.59	71.59
2.09e-03	8.90	1.49	73.08
1.82e-03	9.10	1.15	74.23
1.59e-03	9.30	1.17	75.40
1.38e-03	9.50	1.28	76.68

1.20e-03	9.70	1.37	78.05
1.05e-03	9.90	1.24	79.29
9.11e-04	10.10	0.83	80.12
7.93e-04	10.30	0.94	81.05
6.91e-04	10.50	1.26	82.31
6.01e-04	10.70	1.37	83.68
5.23e-04	10.90	1.03	84.72
2.44e-04	12.00	15.28	100.00

Grain Size Breakdown

% Gravel	% Sand	% Silt	% Clay	% Mud
0.12	13.73	50.39	35.76	86.15

Statistical Measures

Mean (PHI)	Standard Deviation (PHI)	Kurtosis (No Dim.)	Skewness (No Dim.)
7.20	2.87	2.18	0.29

97RUSTICO-002-R2,RD011284,   DR. CARL AMOS
,00409,   SYRINGE CORE, RUSTICO BAY, PEI
                    MILLIMETER EQUIVALENTS
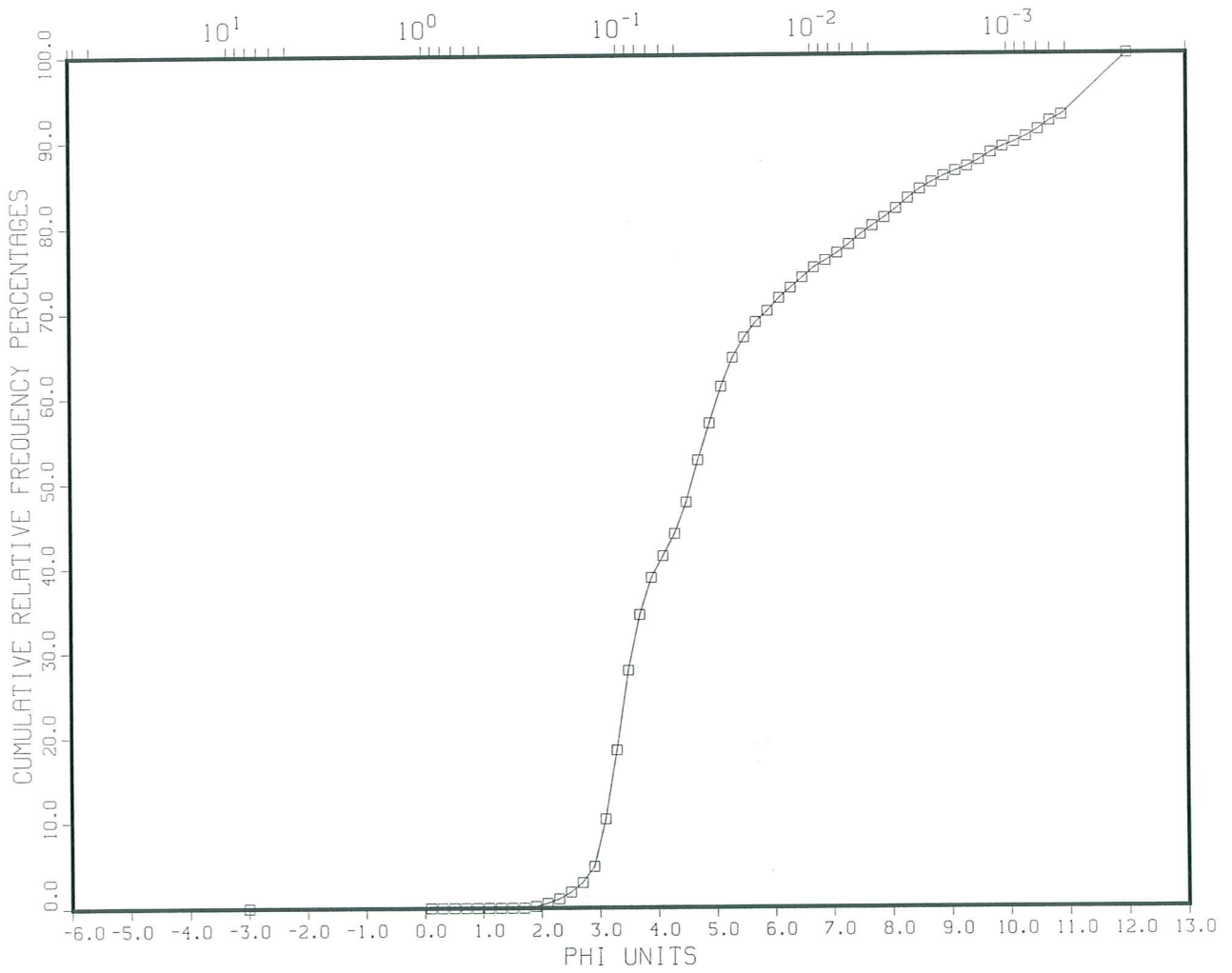
Calculation Results for
The Sample with the Identifier:

V4.0
23:10:1997
11284
57
97RUSTICO-002-R2
97RUSTICO
960030
DR. CARL AMOS
SYRINGE CORE, RUSTICO BAY, PEI
RD011284
SWF00409
0.00000000000000E+0000
0.00000000000000E+0000
0
0
0
0
0
0
0
0
53104
002-R2
002-R2
SYRINGE
CORE
46:24.40
-63:14.83
2.00
n lines for future expansion
#

Results

Midpoints		Relative Frequency	Cumulative Frequency
MM	PHI	Percentages	Percentages
8.00e+00	-3.00	0.00	0.00
9.33e-01	0.10	0.00	0.00
8.12e-01	0.30	0.00	0.00

7.07e-01	0.50	0.00	0.00
6.16e-01	0.70	0.00	0.00
5.36e-01	0.90	0.00	0.00
4.67e-01	1.10	0.00	0.00
4.06e-01	1.30	0.00	0.00
3.54e-01	1.50	0.00	0.00
3.08e-01	1.70	0.00	0.00
2.68e-01	1.90	0.18	0.18
2.33e-01	2.10	0.36	0.54
2.03e-01	2.30	0.51	1.05
1.77e-01	2.50	0.79	1.84
1.54e-01	2.70	1.10	2.94
1.34e-01	2.90	1.88	4.82
1.17e-01	3.10	5.51	10.32
1.02e-01	3.30	8.12	18.44
8.84e-02	3.50	9.35	27.80
7.69e-02	3.70	6.57	34.37
6.70e-02	3.90	4.36	38.73
5.83e-02	4.10	2.55	41.28
5.08e-02	4.30	2.63	43.91
4.42e-02	4.50	3.70	47.62
3.85e-02	4.70	4.99	52.61
3.35e-02	4.90	4.33	56.94
2.92e-02	5.10	4.28	61.23
2.54e-02	5.30	3.40	64.62
2.21e-02	5.50	2.39	67.01
1.92e-02	5.70	1.81	68.83
1.67e-02	5.90	1.29	70.12
1.46e-02	6.10	1.53	71.65
1.27e-02	6.30	1.18	72.83
1.10e-02	6.50	1.19	74.02
9.62e-03	6.70	1.17	75.19
8.37e-03	6.90	0.81	76.00
7.29e-03	7.10	0.89	76.89
6.35e-03	7.30	1.00	77.89
5.52e-03	7.50	1.18	79.07
4.81e-03	7.70	0.99	80.05
4.19e-03	7.90	0.93	80.98
3.64e-03	8.10	1.03	82.01
3.17e-03	8.30	1.18	83.19
2.76e-03	8.50	1.06	84.25
2.40e-03	8.70	0.80	85.06
2.09e-03	8.90	0.69	85.75
1.82e-03	9.10	0.59	86.34
1.59e-03	9.30	0.53	86.87

1.38e-03	9.50	0.74	87.61
1.20e-03	9.70	0.87	88.48
1.05e-03	9.90	0.69	89.17
9.11e-04	10.10	0.52	89.69
7.93e-04	10.30	0.66	90.35
6.91e-04	10.50	0.80	91.15
6.01e-04	10.70	0.99	92.14
5.23e-04	10.90	0.67	92.81
2.44e-04	12.00	7.19	100.00

Grain Size Breakdown

% Gravel	% Sand	% Silt	% Clay	% Mud
0.00	38.73	42.25	19.02	61.27

Statistical Measures

Mean (PHI)	Standard Deviation (PHI)	Kurtosis (No Dim.)	Skewness (No Dim.)
5.58	2.68	3.27	1.17

97RUSTICO-003-R3,RD011285,   DR. CARL AMOS
,00409,   SYRINGE CORE, RUSTICO BAY, PEI
                    MILLIMETER EQUIVALENTS
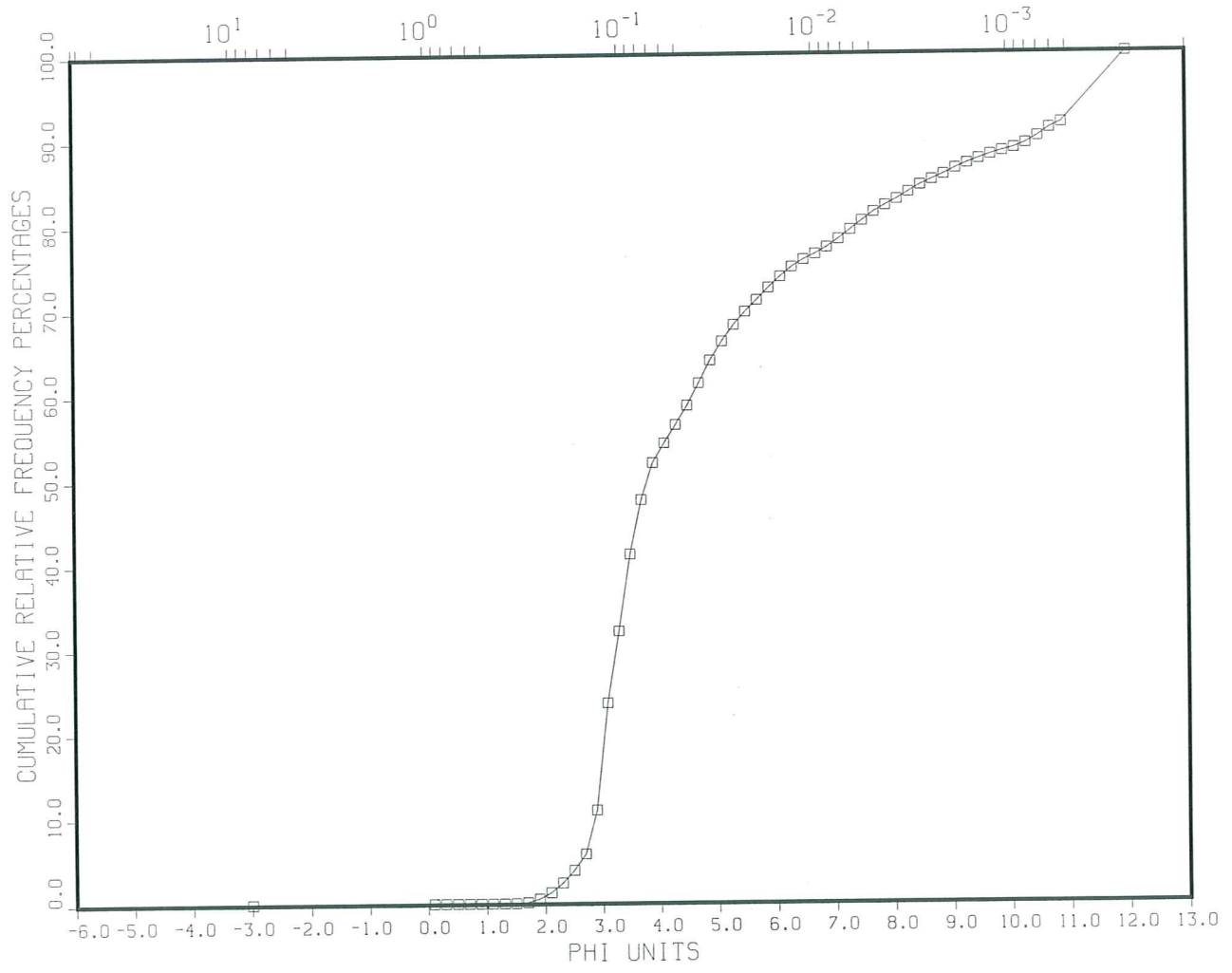
Calculation Results for
The Sample with the Identifier:

V4.0
24:10:1997
11285
57
97RUSTICO-003-R3
97RUSTICO
960030
DR. CARL AMOS
SYRINGE CORE, RUSTICO BAY, PEI
RD011285
SWF00409
0.00000000000000E+0000
0.00000000000000E+0000
0
0
0
0
0
0
0
0
53105
003-R3
003-R3
SYRINGE
CORE
46:25.17
-63:14.19
2.50
n lines for future expansion
#

Results

Midpoints		Relative	Cumulative
		Frequency	Frequency
MM	PHI	Percentages	Percentages
8.00e+00	-3.00	0.09	0.09
9.33e-01	0.10	0.00	0.09
8.12e-01	0.30	0.00	0.09

7.07e-01	0.50	0.00	0.09
6.16e-01	0.70	0.00	0.09
5.36e-01	0.90	0.00	0.09
4.67e-01	1.10	0.00	0.09
4.06e-01	1.30	0.00	0.09
3.54e-01	1.50	0.02	0.11
3.08e-01	1.70	0.11	0.22
2.68e-01	1.90	0.40	0.62
2.33e-01	2.10	0.72	1.34
2.03e-01	2.30	1.12	2.47
1.77e-01	2.50	1.45	3.92
1.54e-01	2.70	1.90	5.82
1.34e-01	2.90	5.14	10.96
1.17e-01	3.10	12.69	23.65
1.02e-01	3.30	8.53	32.18
8.84e-02	3.50	9.10	41.28
7.69e-02	3.70	6.43	47.71
6.70e-02	3.90	4.34	52.05
5.83e-02	4.10	2.32	54.36
5.08e-02	4.30	2.14	56.50
4.42e-02	4.50	2.25	58.75
3.85e-02	4.70	2.62	61.38
3.35e-02	4.90	2.65	64.03
2.92e-02	5.10	2.23	66.26
2.54e-02	5.30	1.93	68.19
2.21e-02	5.50	1.56	69.75
1.92e-02	5.70	1.39	71.13
1.67e-02	5.90	1.43	72.57
1.46e-02	6.10	1.29	73.86
1.27e-02	6.30	1.14	75.00
1.10e-02	6.50	0.85	75.85
9.62e-03	6.70	0.65	76.50
8.37e-03	6.90	0.78	77.28
7.29e-03	7.10	0.94	78.22
6.35e-03	7.30	1.07	79.28
5.52e-03	7.50	1.04	80.33
4.81e-03	7.70	1.02	81.35
4.19e-03	7.90	0.76	82.11
3.64e-03	8.10	0.71	82.82
3.17e-03	8.30	0.84	83.66
2.76e-03	8.50	0.82	84.48
2.40e-03	8.70	0.63	85.11
2.09e-03	8.90	0.61	85.72
1.82e-03	9.10	0.71	86.42
1.59e-03	9.30	0.58	87.00

1.38e-03	9.50	0.52	87.52
1.20e-03	9.70	0.47	88.00
1.05e-03	9.90	0.41	88.41
9.11e-04	10.10	0.35	88.76
7.93e-04	10.30	0.54	89.30
6.91e-04	10.50	0.80	90.10
6.01e-04	10.70	0.96	91.06
5.23e-04	10.90	0.63	91.69
2.44e-04	12.00	8.31	100.00

Grain Size Breakdown

% Gravel	% Sand	% Silt	% Clay	% Mud
0.09	51.96	30.06	17.89	47.95

Statistical Measures

Mean (PHI)	Standard Deviation (PHI)	Kurtosis (No Dim.)	Skewness (No Dim.)
5.26	2.86	3.37	1.23

97RUSTICO-004-R4,RD011286,   DR. CARL AMOS
,00409,   SYRINGE CORE, RUSTICO BAY, PEI
                         MILLIMETER EQUIVALENTS
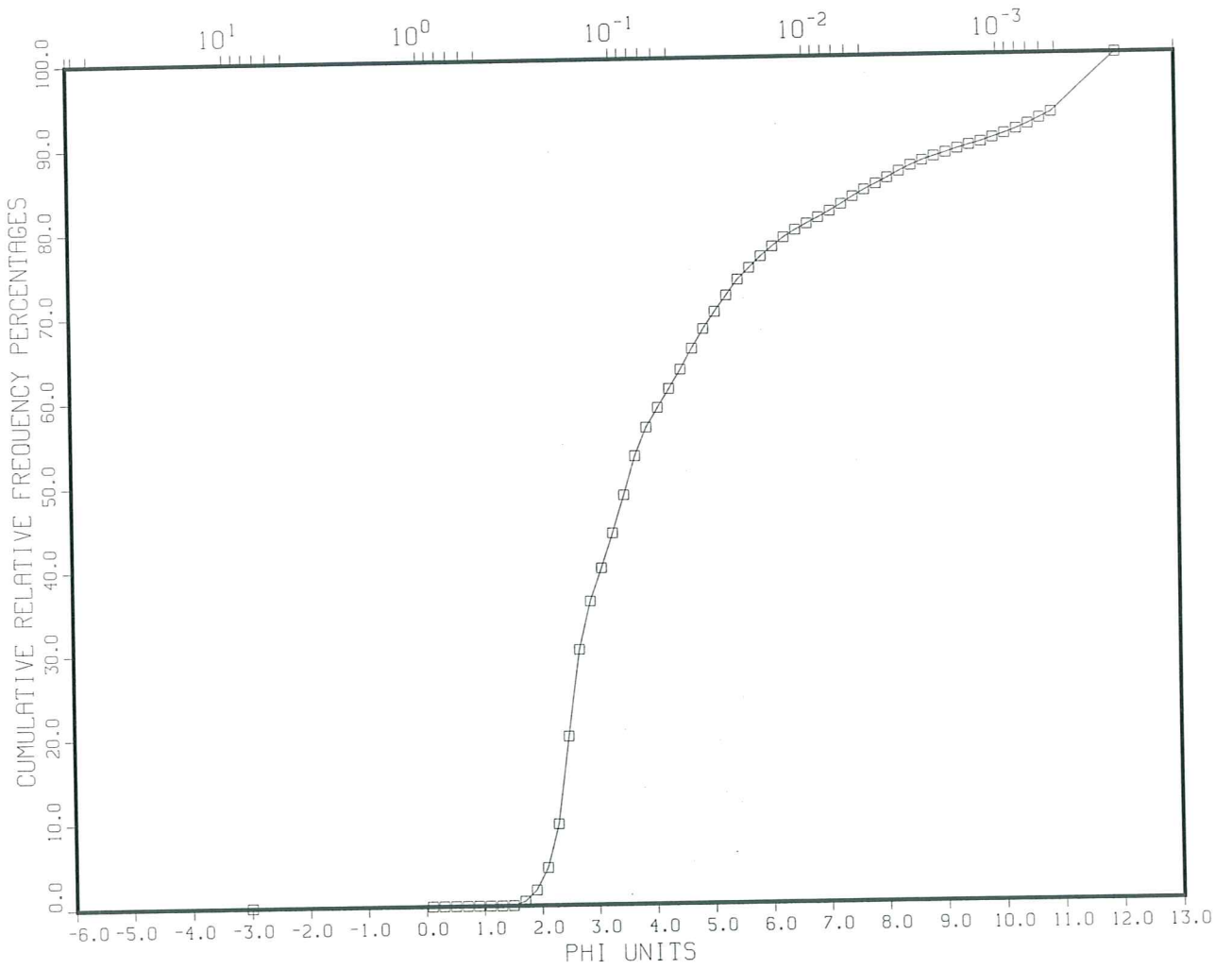
Calculation Results for
The Sample with the Identifier:

V4.0
24:10:1997
11286
57
97RUSTICO-004-R4
97RUSTICO
960030
DR. CARL AMOS
SYRINGE CORE, RUSTICO BAY, PEI
RD011286
SWF00409
0.00000000000000E+0000
0.00000000000000E+0000
0
0
0
0
0
0
0
0
53106
004-R4
004-R4
SYRINGE
CORE
46:23.34
-63:14.13
2.50
n lines for future expansion
#

Results

| Midpoints | | Relative Frequency | Cumulative Frequency |
MM	PHI	Percentages	Percentages
8.00e+00	-3.00	0.00	0.00
9.33e-01	0.10	0.00	0.00
8.12e-01	0.30	0.00	0.00

7.07e-01	0.50	0.00	0.00
6.16e-01	0.70	0.00	0.00
5.36e-01	0.90	0.00	0.00
4.67e-01	1.10	0.00	0.00
4.06e-01	1.30	0.00	0.00
3.54e-01	1.50	0.02	0.02
3.08e-01	1.70	0.49	0.52
2.68e-01	1.90	1.29	1.81
2.33e-01	2.10	2.63	4.44
2.03e-01	2.30	5.11	9.55
1.77e-01	2.50	10.35	19.90
1.54e-01	2.70	10.28	30.19
1.34e-01	2.90	5.74	35.93
1.17e-01	3.10	3.94	39.87
1.02e-01	3.30	4.12	43.99
8.84e-02	3.50	4.53	48.52
7.69e-02	3.70	4.63	53.15
6.70e-02	3.90	3.35	56.50
5.83e-02	4.10	2.31	58.80
5.08e-02	4.30	2.20	61.00
4.42e-02	4.50	2.27	63.27
3.85e-02	4.70	2.48	65.75
3.35e-02	4.90	2.29	68.05
2.92e-02	5.10	1.98	70.03
2.54e-02	5.30	1.92	71.95
2.21e-02	5.50	1.86	73.81
1.92e-02	5.70	1.37	75.18
1.67e-02	5.90	1.35	76.53
1.46e-02	6.10	1.15	77.68
1.27e-02	6.30	1.04	78.72
1.10e-02	6.50	0.87	79.58
9.62e-03	6.70	0.73	80.31
8.37e-03	6.90	0.72	81.03
7.29e-03	7.10	0.75	81.79
6.35e-03	7.30	0.79	82.58
5.52e-03	7.50	0.87	83.46
4.81e-03	7.70	0.79	84.25
4.19e-03	7.90	0.70	84.94
3.64e-03	8.10	0.69	85.63
3.17e-03	8.30	0.74	86.37
2.76e-03	8.50	0.68	87.05
2.40e-03	8.70	0.57	87.63
2.09e-03	8.90	0.47	88.10
1.82e-03	9.10	0.42	88.52
1.59e-03	9.30	0.45	88.96

1.38e-03	9.50	0.41	89.37
1.20e-03	9.70	0.37	89.74
1.05e-03	9.90	0.48	90.22
9.11e-04	10.10	0.46	90.68
7.93e-04	10.30	0.52	91.20
6.91e-04	10.50	0.58	91.78
6.01e-04	10.70	0.67	92.45
5.23e-04	10.90	0.65	93.09
2.44e-04	12.00	6.91	100.00

Grain Size Breakdown

%	%	%	%	%
Gravel	Sand	Silt	Clay	Mud
0.00	56.50	28.45	15.06	43.50

Statistical Measures

Mean (PHI)	Standard Deviation (PHI)	Kurtosis (No Dim.)	Skewness (No Dim.)
4.79	2.85	3.74	1.35

97RUSTICO-OO5-R5,RDO11287,   DR. CARL AMOS
  # ,OO409,   SYRINGE CORE, RUSTICO BAY, PEI
                              MILLIMETER EQUIVALENTS
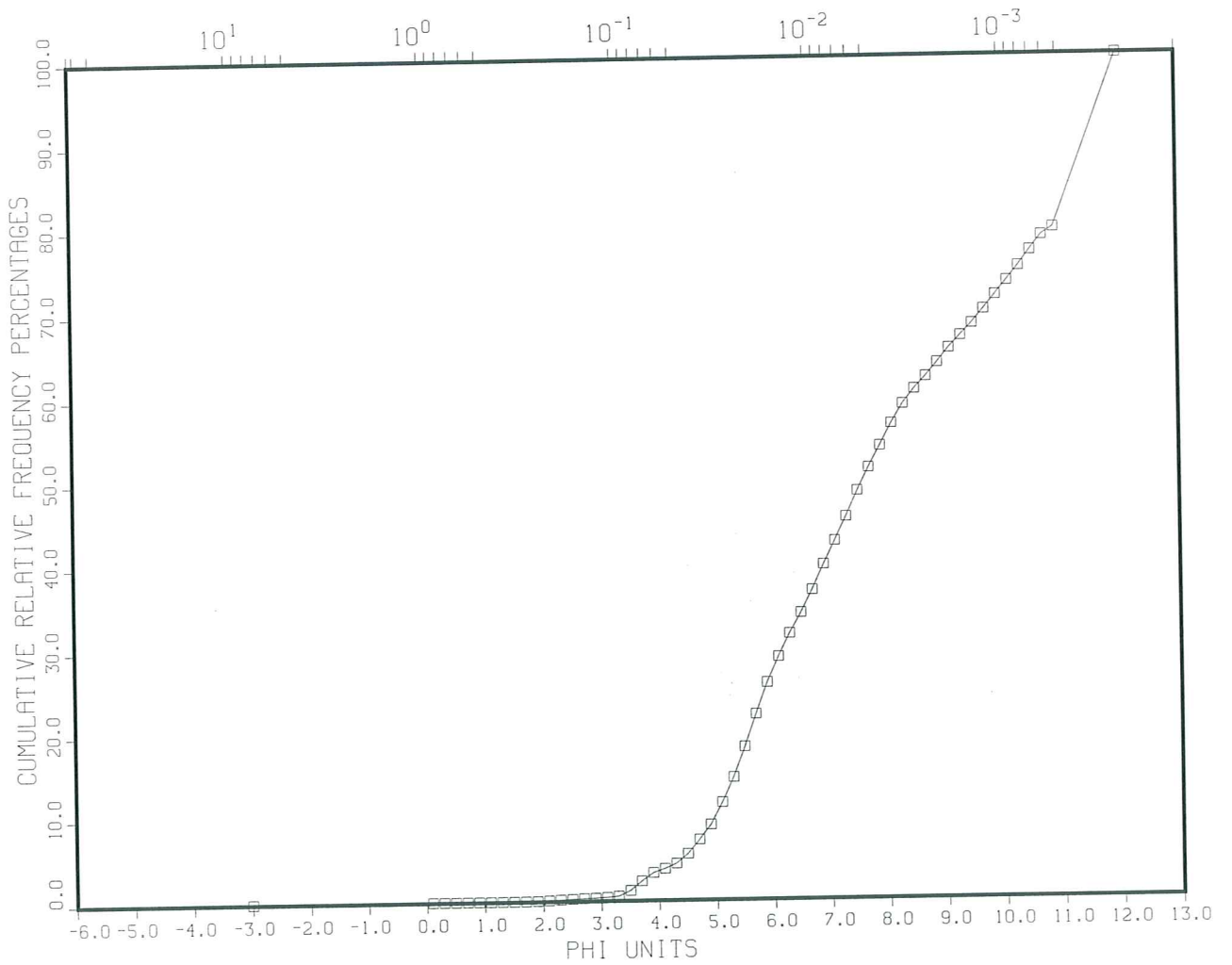
Calculation Results for
The Sample with the Identifier:

V4.0
24:10:1997
11287
57
97RUSTICO-005-R5
97RUSTICO
960030
DR. CARL AMOS
SYRINGE CORE, RUSTICO BAY, PEI
RD011287
SWF00409
0.00000000000000E+0000
0.00000000000000E+0000
0
0
0
0
0
0
0
0
53107
005-R5
005-R5
SYRINGE
CORE
46:24.90
-63:14.11
3.00
n lines for future expansion
#

Results

Midpoints		Relative Frequency	Cumulative Frequency
MM	PHI	Percentages	Percentages
8.00e+00	-3.00	0.05	0.05
9.33e-01	0.10	0.00	0.05
8.12e-01	0.30	0.00	0.05

7.07e-01	0.50	0.00	0.05
6.16e-01	0.70	0.00	0.05
5.36e-01	0.90	0.00	0.05
4.67e-01	1.10	0.00	0.05
4.06e-01	1.30	0.00	0.05
3.54e-01	1.50	0.00	0.05
3.08e-01	1.70	0.01	0.07
2.68e-01	1.90	0.03	0.09
2.33e-01	2.10	0.05	0.14
2.03e-01	2.30	0.07	0.21
1.77e-01	2.50	0.07	0.28
1.54e-01	2.70	0.06	0.33
1.34e-01	2.90	0.05	0.39
1.17e-01	3.10	0.07	0.45
1.02e-01	3.30	0.12	0.58
8.84e-02	3.50	0.65	1.22
7.69e-02	3.70	1.10	2.32
6.70e-02	3.90	0.97	3.29
5.83e-02	4.10	0.49	3.77
5.08e-02	4.30	0.59	4.37
4.42e-02	4.50	1.14	5.51
3.85e-02	4.70	1.66	7.17
3.35e-02	4.90	1.77	8.94
2.92e-02	5.10	2.69	11.63
2.54e-02	5.30	2.99	14.62
2.21e-02	5.50	3.64	18.26
1.92e-02	5.70	3.85	22.11
1.67e-02	5.90	3.71	25.82
1.46e-02	6.10	3.05	28.87
1.27e-02	6.30	2.77	31.64
1.10e-02	6.50	2.45	34.08
9.62e-03	6.70	2.68	36.76
8.37e-03	6.90	3.02	39.78
7.29e-03	7.10	2.78	42.57
6.35e-03	7.30	2.87	45.43
5.52e-03	7.50	3.09	48.53
4.81e-03	7.70	2.76	51.29
4.19e-03	7.90	2.59	53.87
3.64e-03	8.10	2.65	56.53
3.17e-03	8.30	2.29	58.81
2.76e-03	8.50	1.75	60.57
2.40e-03	8.70	1.44	62.01
2.09e-03	8.90	1.62	63.63
1.82e-03	9.10	1.69	65.32
1.59e-03	9.30	1.46	66.78

1.38e-03	9.50	1.43	68.21
1.20e-03	9.70	1.67	69.88
1.05e-03	9.90	1.68	71.56
9.11e-04	10.10	1.66	73.22
7.93e-04	10.30	1.70	74.92
6.91e-04	10.50	1.84	76.76
6.01e-04	10.70	1.75	78.51
5.23e-04	10.90	0.90	79.40
2.44e-04	12.00	20.60	100.00

Grain Size Breakdown

% Gravel	% Sand	% Silt	% Clay	% Mud
0.05	3.24	50.59	46.13	96.71

Statistical Measures

Mean (PHI)	Standard Deviation (PHI)	Kurtosis (No Dim.)	Skewness (No Dim.)
8.14	2.60	1.99	0.16

97RUSTICO-006-R6,RDO11288,   DR. CARL AMOS
,00409,   SYRINGE CORE, RUSTICO BAY, PEI
                              MILLIMETER EQUIVALENTS
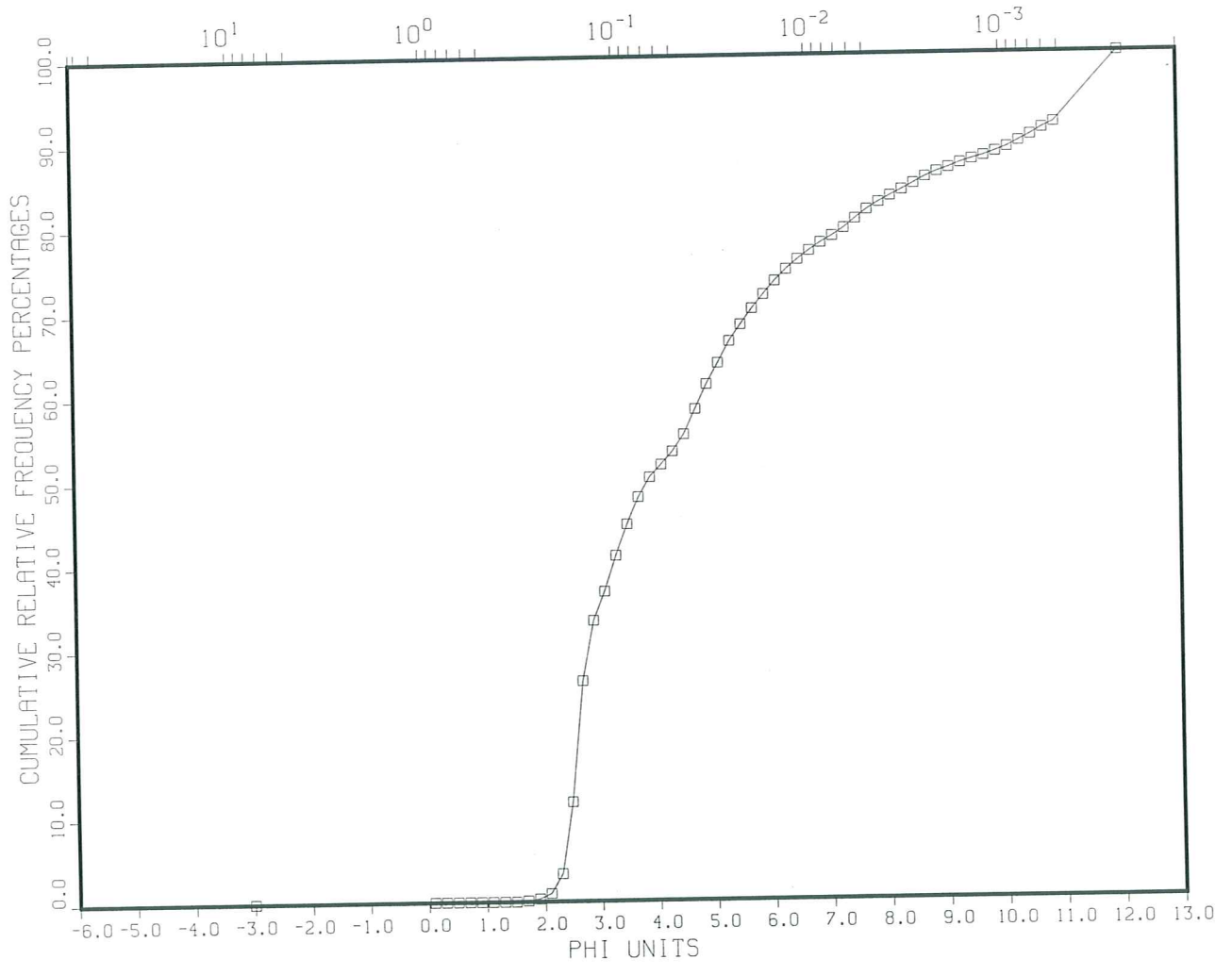
Calculation Results for
The Sample with the Identifier:

V4.0
24:10:1997
11288
57
97RUSTICO-006-R6
97RUSTICO
960030
DR. CARL AMOS
SYRINGE CORE, RUSTICO BAY, PEI
RD011288
SWF00409
0.00000000000000E+0000
0.00000000000000E+0000
0
0
0
0
0
0
0
0
53108
006-R6
006-R6
SYRINGE
CORE
46:25.51
-63:13.81
3.50
n lines for future expansion
#

Results

Midpoints		Relative Frequency	Cumulative Frequency
MM	PHI	Percentages	Percentages
8.00e+00	-3.00	0.00	0.00
9.33e-01	0.10	0.00	0.00
8.12e-01	0.30	0.00	0.00

7.07e-01	0.50	0.00	0.00
6.16e-01	0.70	0.00	0.00
5.36e-01	0.90	0.00	0.00
4.67e-01	1.10	0.00	0.00
4.06e-01	1.30	0.00	0.00
3.54e-01	1.50	0.00	0.00
3.08e-01	1.70	0.10	0.10
2.68e-01	1.90	0.22	0.33
2.33e-01	2.10	0.61	0.94
2.03e-01	2.30	2.32	3.26
1.77e-01	2.50	8.49	11.75
1.54e-01	2.70	14.34	26.09
1.34e-01	2.90	7.18	33.27
1.17e-01	3.10	3.46	36.73
1.02e-01	3.30	4.27	41.00
8.84e-02	3.50	3.72	44.72
7.69e-02	3.70	3.23	47.95
6.70e-02	3.90	2.35	50.30
5.83e-02	4.10	1.50	51.80
5.08e-02	4.30	1.54	53.35
4.42e-02	4.50	2.03	55.38
3.85e-02	4.70	2.95	58.33
3.35e-02	4.90	2.93	61.26
2.92e-02	5.10	2.50	63.76
2.54e-02	5.30	2.60	66.36
2.21e-02	5.50	1.94	68.30
1.92e-02	5.70	1.88	70.18
1.67e-02	5.90	1.64	71.82
1.46e-02	6.10	1.57	73.39
1.27e-02	6.30	1.33	74.72
1.10e-02	6.50	1.15	75.87
9.62e-03	6.70	1.02	76.89
8.37e-03	6.90	0.93	77.82
7.29e-03	7.10	0.78	78.60
6.35e-03	7.30	0.88	79.49
5.52e-03	7.50	1.10	80.58
4.81e-03	7.70	1.05	81.63
4.19e-03	7.90	0.86	82.49
3.64e-03	8.10	0.73	83.23
3.17e-03	8.30	0.68	83.91
2.76e-03	8.50	0.73	84.64
2.40e-03	8.70	0.75	85.39
2.09e-03	8.90	0.60	85.99
1.82e-03	9.10	0.47	86.46
1.59e-03	9.30	0.54	87.00

1.38e-03	9.50	0.43	87.43
1.20e-03	9.70	0.38	87.81
1.05e-03	9.90	0.48	88.29
9.11e-04	10.10	0.52	88.81
7.93e-04	10.30	0.72	89.53
6.91e-04	10.50	0.71	90.24
6.01e-04	10.70	0.79	91.03
5.23e-04	10.90	0.65	91.68
2.44e-04	12.00	8.32	100.00

Grain Size Breakdown

% Gravel	% Sand	% Silt	% Clay	% Mud
0.00	50.30	32.19	17.51	49.70

Statistical Measures

Mean (PHI)	Standard Deviation (PHI)	Kurtosis (No Dim.)	Skewness (No Dim.)
5.16	2.96	3.16	1.15

97RUSTICO-007-R7,RD011289,   DR. CARL AMOS
 # ,00409,   SYRINGE CORE, RUSTICO BAY, PEI
                    MILLIMETER EQUIVALENTS
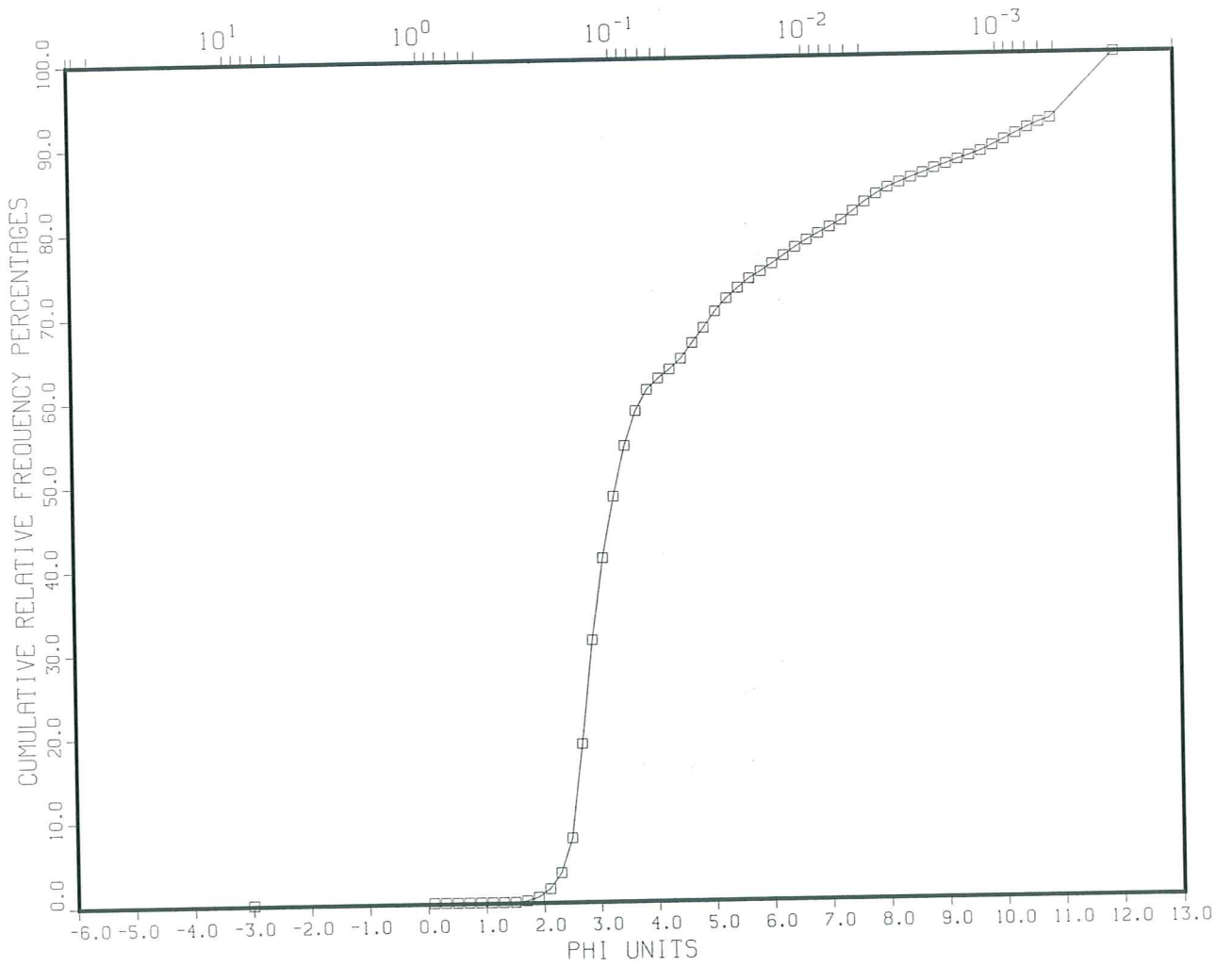
Calculation Results for
The Sample with the Identifier:

V4.0
24:10:1997
11289
57
97RUSTICO-007-R7
97RUSTICO
960030
DR. CARL AMOS
SYRINGE CORE, RUSTICO BAY, PEI
RD011289
SWF00409
0.00000000000000E+0000
0.00000000000000E+0000
0
0
0
0
0
0
0
0
53109
007-R7
007-R7
SYRINGE
CORE
46:25.75
-63:15.35
3.00
n lines for future expansion
#

Results

Midpoints		Relative Frequency	Cumulative Frequency
MM	PHI	Percentages	Percentages
8.00e+00	-3.00	0.13	0.13
9.33e-01	0.10	0.00	0.13
8.12e-01	0.30	0.00	0.13

7.07e-01	0.50	0.00	0.13
6.16e-01	0.70	0.00	0.13
5.36e-01	0.90	0.00	0.13
4.67e-01	1.10	0.00	0.13
4.06e-01	1.30	0.00	0.13
3.54e-01	1.50	0.00	0.13
3.08e-01	1.70	0.15	0.28
2.68e-01	1.90	0.41	0.69
2.33e-01	2.10	0.98	1.67
2.03e-01	2.30	1.85	3.52
1.77e-01	2.50	4.11	7.62
1.54e-01	2.70	11.18	18.80
1.34e-01	2.90	12.40	31.21
1.17e-01	3.10	9.72	40.93
1.02e-01	3.30	7.26	48.19
8.84e-02	3.50	6.04	54.23
7.69e-02	3.70	4.11	58.34
6.70e-02	3.90	2.51	60.85
5.83e-02	4.10	1.31	62.16
5.08e-02	4.30	1.05	63.21
4.42e-02	4.50	1.25	64.46
3.85e-02	4.70	1.84	66.30
3.35e-02	4.90	1.79	68.09
2.92e-02	5.10	1.92	70.01
2.54e-02	5.30	1.54	71.55
2.21e-02	5.50	1.21	72.76
1.92e-02	5.70	1.09	73.85
1.67e-02	5.90	0.81	74.65
1.46e-02	6.10	0.89	75.55
1.27e-02	6.30	0.92	76.47
1.10e-02	6.50	0.95	77.42
9.62e-03	6.70	0.85	78.26
8.37e-03	6.90	0.75	79.01
7.29e-03	7.10	0.73	79.75
6.35e-03	7.30	0.76	80.51
5.52e-03	7.50	1.04	81.54
4.81e-03	7.70	1.06	82.61
4.19e-03	7.90	0.92	83.53
3.64e-03	8.10	0.78	84.31
3.17e-03	8.30	0.59	84.90
2.76e-03	8.50	0.55	85.45
2.40e-03	8.70	0.51	85.96
2.09e-03	8.90	0.55	86.52
1.82e-03	9.10	0.49	87.01
1.59e-03	9.30	0.50	87.51

1.38e-03	9.50	0.46	87.97
1.20e-03	9.70	0.49	88.46
1.05e-03	9.90	0.66	89.11
9.11e-04	10.10	0.66	89.78
7.93e-04	10.30	0.70	90.48
6.91e-04	10.50	0.66	91.14
6.01e-04	10.70	0.61	91.75
5.23e-04	10.90	0.45	92.20
2.44e-04	12.00	7.80	100.00

Grain Size Breakdown

% Gravel	% Sand	% Silt	% Clay	% Mud
0.13	60.73	22.68	16.47	39.15

Statistical Measures

Mean (PHI)	Standard Deviation (PHI)	Kurtosis (No Dim.)	Skewness (No Dim.)
4.90	2.93	3.54	1.31

97RUSTICO-008-R8,RDO11290,   DR. CARL AMOS
,00409,   SYRINGE CORE, RUSTICO BAY, PEI
                        MILLIMETER EQUIVALENTS
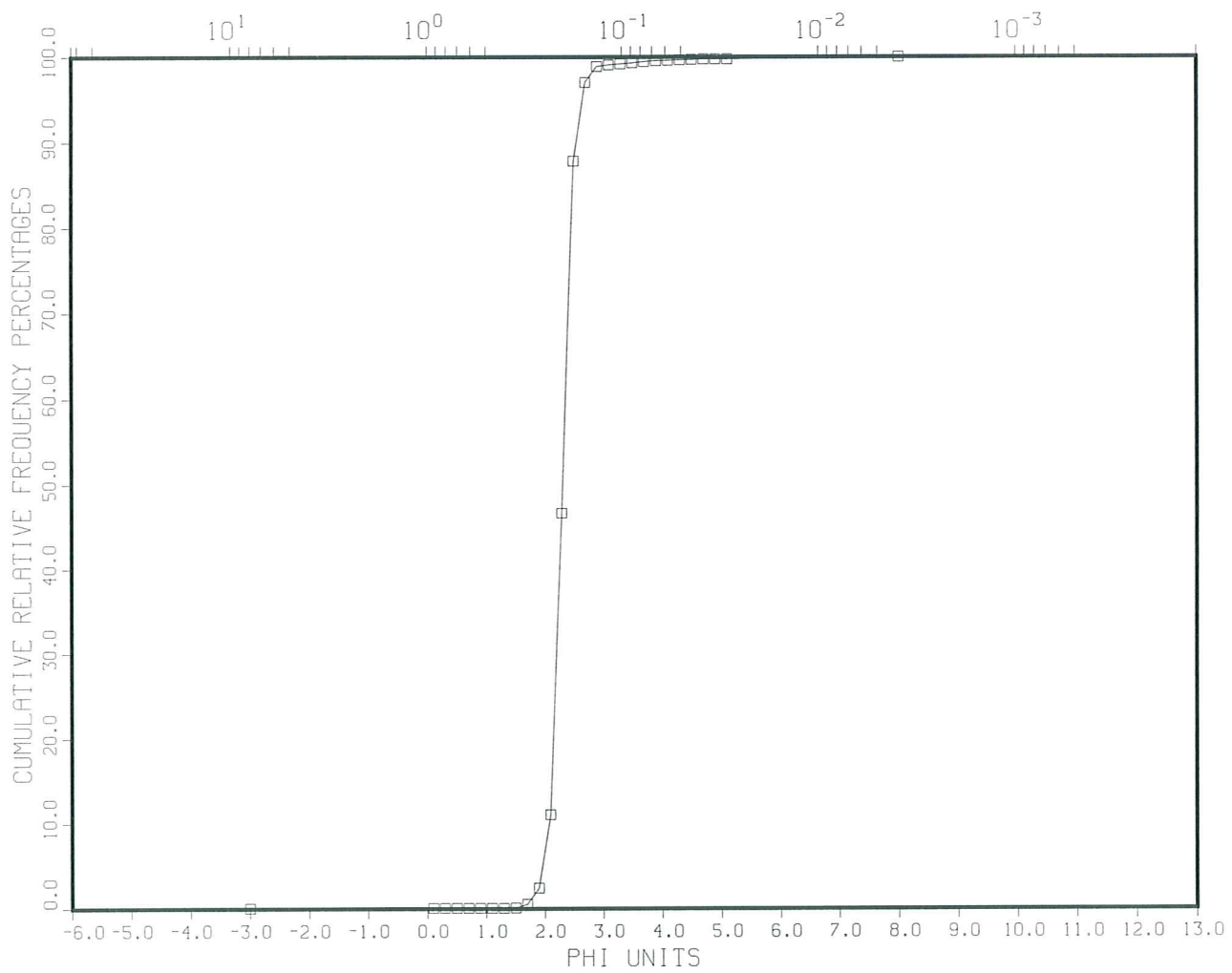
Calculation Results for
The Sample with the Identifier:

V4.0
24:10:1997
11290
29
97RUSTICO-008-R8
97RUSTICO
960030
DR. CARL AMOS
SYRINGE CORE, RUSTICO BAY, PEI
RD011290
SWF00409
0.00000000000000E+0000
0.00000000000000E+0000
0
0
0
0
0
0
0
0
53110
008-R8
008-R8
SYRINGE
CORE
46:26.10
-63:18.10
6.00
n lines for future expansion
#

Results

Midpoints		Relative	Cumulative
		Frequency	Frequency
MM	PHI	Percentages	Percentages
8.00e+00	-3.00	0.07	0.07
9.33e-01	0.10	0.00	0.07
8.12e-01	0.30	0.00	0.07

7.07e-01	0.50	0.00	0.07
6.16e-01	0.70	0.00	0.07
5.36e-01	0.90	0.00	0.07
4.67e-01	1.10	0.00	0.07
4.06e-01	1.30	0.00	0.07
3.54e-01	1.50	0.03	0.10
3.08e-01	1.70	0.44	0.54
2.68e-01	1.90	1.89	2.43
2.33e-01	2.10	8.61	11.04
2.03e-01	2.30	35.56	46.61
1.77e-01	2.50	41.22	87.82
1.54e-01	2.70	9.22	97.04
1.34e-01	2.90	1.87	98.91
1.17e-01	3.10	0.19	99.10
1.02e-01	3.30	0.10	99.20
8.84e-02	3.50	0.12	99.31
7.69e-02	3.70	0.16	99.47
6.70e-02	3.90	0.09	99.56
5.83e-02	4.10	0.04	99.60
5.08e-02	4.30	0.06	99.66
4.42e-02	4.50	0.03	99.69
3.85e-02	4.70	0.07	99.76
3.35e-02	4.90	0.00	99.76
2.92e-02	5.10	0.00	99.76
3.91e-03	8.00	0.24	100.00
2.44e-04	12.00	0.00	100.00

Grain Size Breakdown

% Gravel	% Sand	% Silt	% Clay	% Mud
0.07	99.49	0.44	0.00	0.44

Statistical Measures

Mean (PHI)	Standard Deviation (PHI)	Kurtosis (No Dim.)	Skewness (No Dim.)
2.42	0.38	137.98	5.77

97RUSTICO-009-R9,RD011291,   DR. CARL AMOS
  # ,00409,   SYRINGE CORE, RUSTICO BAY, PEI
                        MILLIMETER EQUIVALENTS
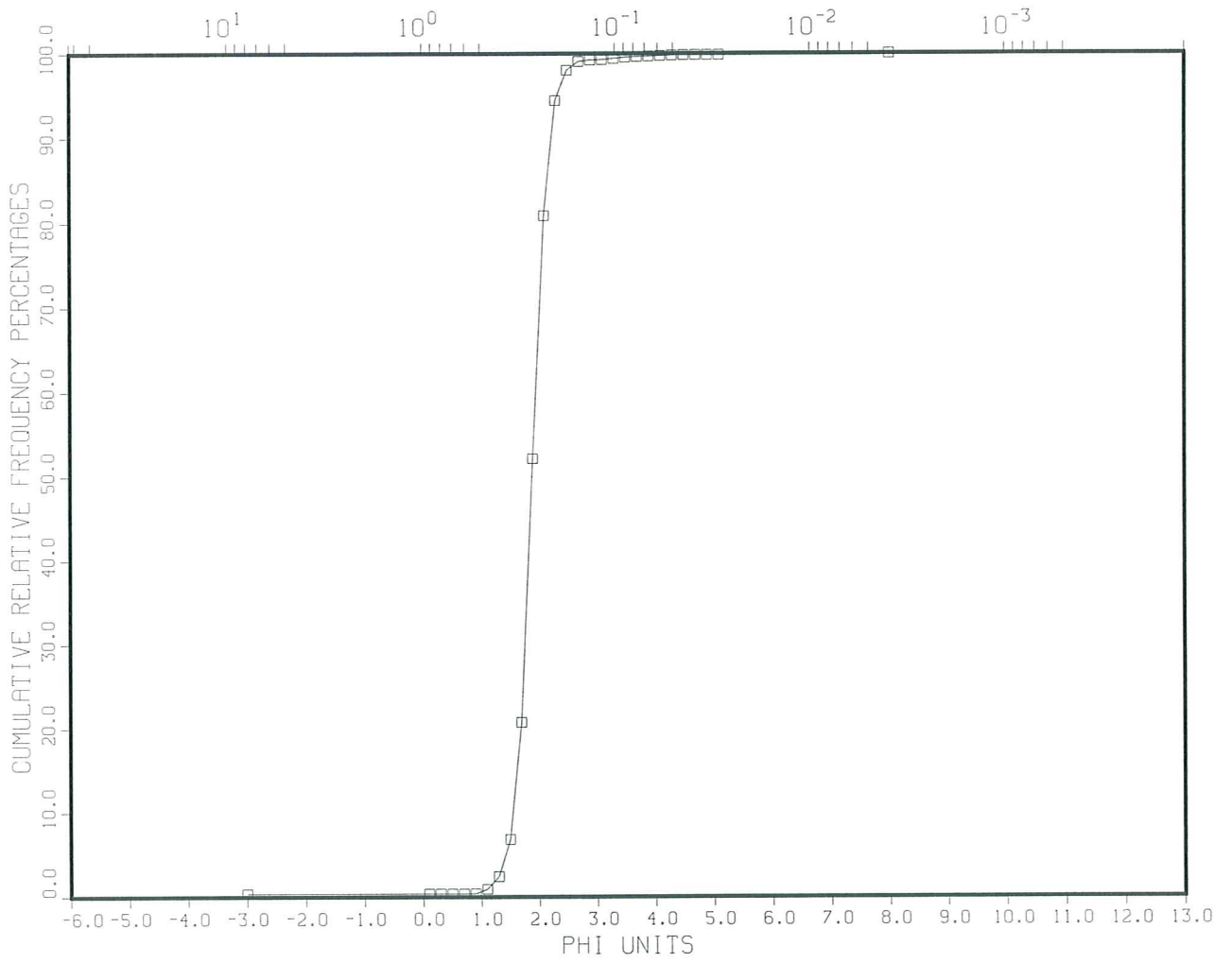
Calculation Results for
The Sample with the Identifier:

V4.0
24:10:1997
11291
29
97RUSTICO-009-R9
97RUSTICO
960030
DR. CARL AMOS
SYRINGE CORE, RUSTICO BAY, PEI
RD011291
SWF00409
0.00000000000000E+0000
0.00000000000000E+0000
0
0
0
0
0
0
0
0
53111
009-R9
009-R9
SYRINGE
CORE
46:26.58
-63:16.51
4.50
n lines for future expansion
#

Results

Midpoints		Relative	Cumulative
		Frequency	Frequency
MM	PHI	Percentages	Percentages
8.00e+00	-3.00	0.38	0.38
9.33e-01	0.10	0.00	0.38
8.12e-01	0.30	0.00	0.38

7.07e-01	0.50	0.00	0.38
6.16e-01	0.70	0.00	0.38
5.36e-01	0.90	0.01	0.39
4.67e-01	1.10	0.54	0.93
4.06e-01	1.30	1.50	2.43
3.54e-01	1.50	4.39	6.82
3.08e-01	1.70	13.91	20.73
2.68e-01	1.90	31.39	52.13
2.33e-01	2.10	28.72	80.85
2.03e-01	2.30	13.59	94.44
1.77e-01	2.50	3.60	98.04
1.54e-01	2.70	1.04	99.07
1.34e-01	2.90	0.17	99.24
1.17e-01	3.10	0.05	99.29
1.02e-01	3.30	0.13	99.42
8.84e-02	3.50	0.14	99.56
7.69e-02	3.70	0.07	99.63
6.70e-02	3.90	0.05	99.67
5.83e-02	4.10	0.06	99.74
5.08e-02	4.30	0.05	99.78
4.42e-02	4.50	0.05	99.83
3.85e-02	4.70	0.02	99.84
3.35e-02	4.90	0.00	99.84
2.92e-02	5.10	0.00	99.84
3.91e-03	8.00	0.16	100.00
2.44e-04	12.00	0.00	100.00

Grain Size Breakdown

% Gravel	% Sand	% Silt	% Clay	% Mud
0.38	99.29	0.33	0.00	0.33

Statistical Measures

Mean (PHI)	Standard Deviation (PHI)	Kurtosis (No Dim.)	Skewness (No Dim.)
1.99	0.49	78.69	-0.81

97RUSTICO-O1O-R1O,RDO11292, DR. CARL AMOS
,OO409, SYRINGE CORE, RUSTICO BAY, PEI
MILLIMETER EQUIVALENTS
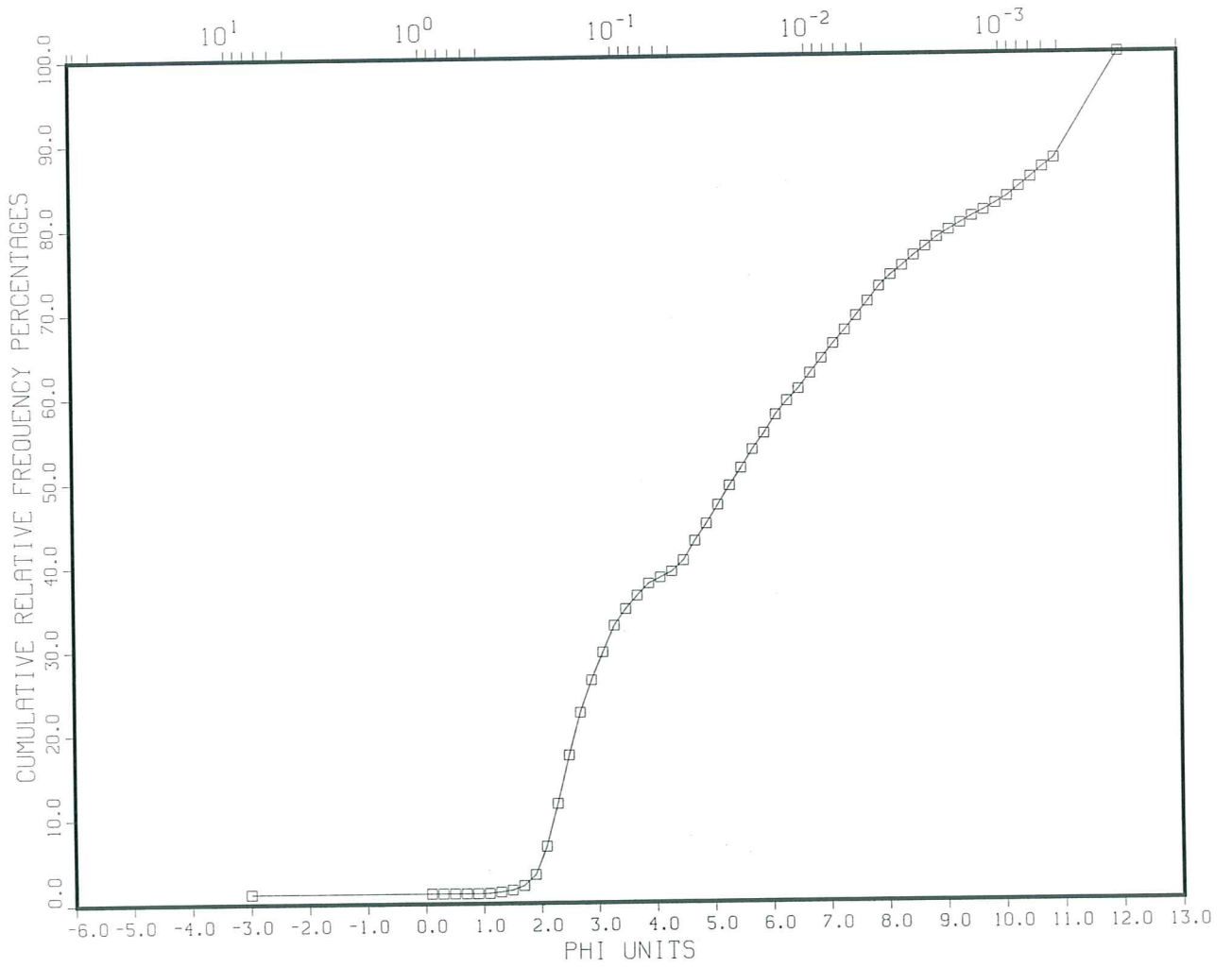
Calculation Results for
The Sample with the Identifier:

V4.0
24:10:1997
11292
57
97RUSTICO-010-R10
97RUSTICO
960030
DR. CARL AMOS
SYRINGE CORE, RUSTICO BAY, PEI
RD011292
SWF00409
0.00000000000000E+0000
0.00000000000000E+0000
0
0
0
0
0
0
0
0
53112
010-R10
010-R10
SYRINGE
CORE
46:25.97
-63:18.95
4.50
n lines for future expansion
#

Results

Midpoints		Relative	Cumulative
		Frequency	Frequency
MM	PHI	Percentages	Percentages
8.00e+00	-3.00	1.18	1.18
9.33e-01	0.10	0.00	1.18
8.12e-01	0.30	0.00	1.18

7.07e-01	0.50	0.00	1.18
6.16e-01	0.70	0.00	1.18
5.36e-01	0.90	0.00	1.18
4.67e-01	1.10	0.03	1.21
4.06e-01	1.30	0.15	1.35
3.54e-01	1.50	0.20	1.55
3.08e-01	1.70	0.51	2.06
2.68e-01	1.90	1.28	3.34
2.33e-01	2.10	3.30	6.64
2.03e-01	2.30	5.04	11.68
1.77e-01	2.50	5.68	17.36
1.54e-01	2.70	5.06	22.42
1.34e-01	2.90	3.84	26.26
1.17e-01	3.10	3.35	29.61
1.02e-01	3.30	3.18	32.78
8.84e-02	3.50	1.93	34.72
7.69e-02	3.70	1.59	36.31
6.70e-02	3.90	1.44	37.75
5.83e-02	4.10	0.71	38.46
5.08e-02	4.30	0.70	39.17
4.42e-02	4.50	1.30	40.46
3.85e-02	4.70	2.28	42.74
3.35e-02	4.90	2.03	44.77
2.92e-02	5.10	2.22	46.99
2.54e-02	5.30	2.30	49.29
2.21e-02	5.50	2.11	51.39
1.92e-02	5.70	2.16	53.56
1.67e-02	5.90	1.93	55.49
1.46e-02	6.10	2.15	57.65
1.27e-02	6.30	1.63	59.28
1.10e-02	6.50	1.39	60.67
9.62e-03	6.70	1.81	62.49
8.37e-03	6.90	1.75	64.24
7.29e-03	7.10	1.75	65.99
6.35e-03	7.30	1.58	67.57
5.52e-03	7.50	1.67	69.24
4.81e-03	7.70	1.69	70.93
4.19e-03	7.90	1.76	72.69
3.64e-03	8.10	1.33	74.02
3.17e-03	8.30	1.09	75.11
2.76e-03	8.50	1.20	76.31
2.40e-03	8.70	1.03	77.34
2.09e-03	8.90	1.10	78.44
1.82e-03	9.10	0.85	79.29
1.59e-03	9.30	0.80	80.09

1.38e-03	9.50	0.80	80.89
1.20e-03	9.70	0.69	81.59
1.05e-03	9.90	0.79	82.37
9.11e-04	10.10	0.83	83.20
7.93e-04	10.30	1.14	84.35
6.91e-04	10.50	1.07	85.42
6.01e-04	10.70	1.18	86.60
5.23e-04	10.90	1.03	87.63
2.44e-04	12.00	12.37	100.00

Grain Size Breakdown

% Gravel	% Sand	% Silt	% Clay	% Mud
1.18	36.58	34.93	27.31	62.25

Statistical Measures

Mean (PHI)	Standard Deviation (PHI)	Kurtosis (No Dim.)	Skewness (No Dim.)
5.98	3.42	2.32	0.32

97RUSTICO-011-R11,RDO11293,   DR. CARL AMOS
,00409,   SYRINGE CORE, RUSTICO BAY, PEI
                    MILLIMETER EQUIVALENTS
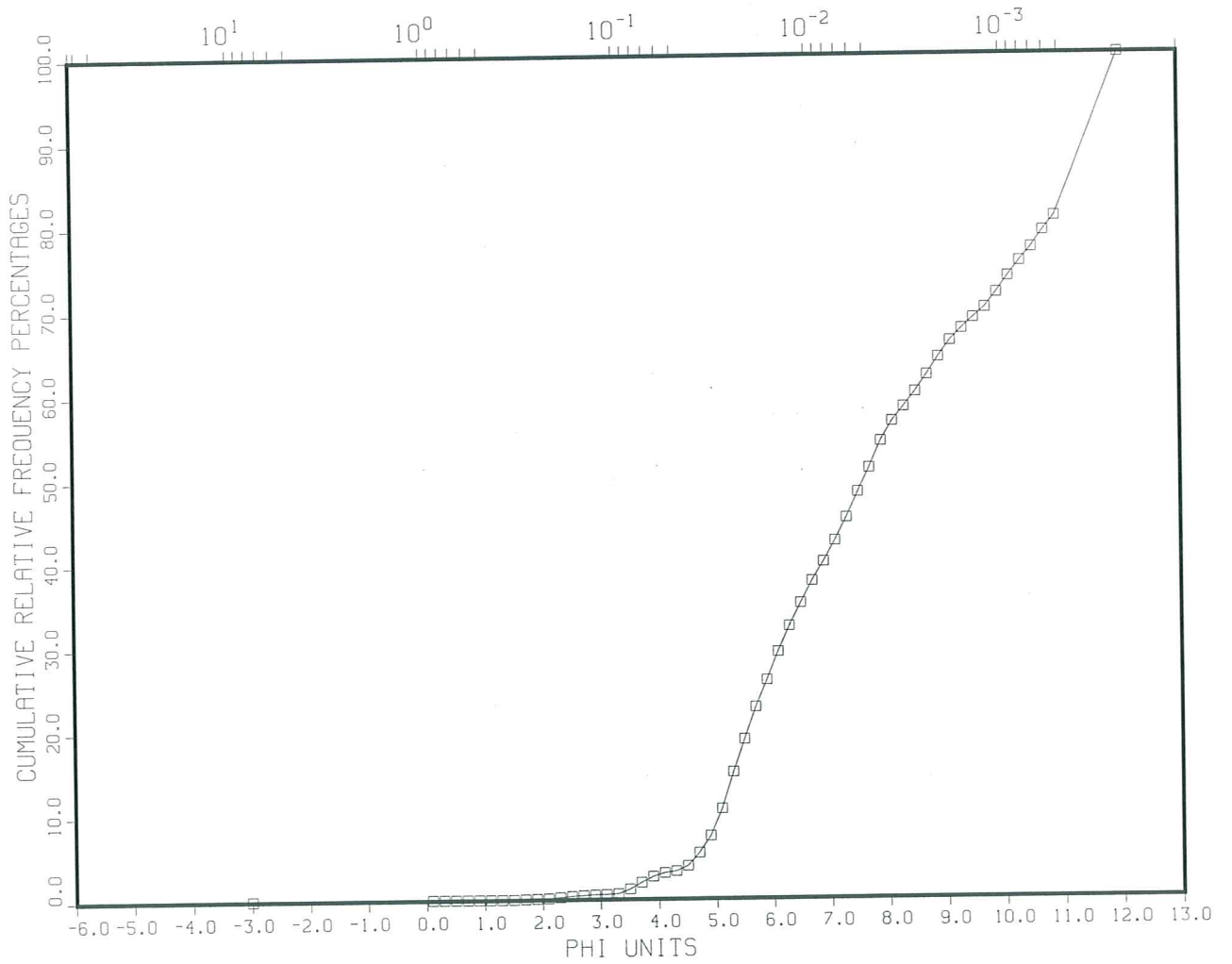
Calculation Results for
The Sample with the Identifier:

V4.0
24:10:1997
11293
57
97RUSTICO-011-R11
97RUSTICO
960030
DR. CARL AMOS
SYRINGE CORE, RUSTICO BAY, PEI
RD011293
SWF00409
0.00000000000000E+0000
0.00000000000000E+0000
0
0
0
0
0
0
0
0
53113
011-R11
011-R11
SYRINGE
CORE
46:25.33
-63:13.27
3.00
n lines for future expansion
#

Results

Midpoints		Relative	Cumulative
		Frequency	Frequency
MM	PHI	Percentages	Percentages
8.00e+00	-3.00	0.06	0.06
9.33e-01	0.10	0.00	0.06
8.12e-01	0.30	0.00	0.06

7.07e-01	0.50	0.00	0.06
6.16e-01	0.70	0.00	0.06
5.36e-01	0.90	0.00	0.06
4.67e-01	1.10	0.00	0.06
4.06e-01	1.30	0.00	0.06
3.54e-01	1.50	0.00	0.06
3.08e-01	1.70	0.02	0.08
2.68e-01	1.90	0.04	0.13
2.33e-01	2.10	0.06	0.18
2.03e-01	2.30	0.11	0.29
1.77e-01	2.50	0.12	0.42
1.54e-01	2.70	0.09	0.51
1.34e-01	2.90	0.06	0.56
1.17e-01	3.10	0.04	0.60
1.02e-01	3.30	0.08	0.68
8.84e-02	3.50	0.53	1.21
7.69e-02	3.70	0.78	1.99
6.70e-02	3.90	0.69	2.68
5.83e-02	4.10	0.44	3.12
5.08e-02	4.30	0.20	3.32
4.42e-02	4.50	0.62	3.94
3.85e-02	4.70	1.54	5.47
3.35e-02	4.90	2.00	7.48
2.92e-02	5.10	3.22	10.70
2.54e-02	5.30	4.36	15.06
2.21e-02	5.50	3.87	18.93
1.92e-02	5.70	3.82	22.75
1.67e-02	5.90	3.18	25.93
1.46e-02	6.10	3.37	29.29
1.27e-02	6.30	3.07	32.36
1.10e-02	6.50	2.74	35.10
9.62e-03	6.70	2.61	37.71
8.37e-03	6.90	2.30	40.00
7.29e-03	7.10	2.47	42.47
6.35e-03	7.30	2.75	45.21
5.52e-03	7.50	3.06	48.27
4.81e-03	7.70	2.86	51.14
4.19e-03	7.90	3.17	54.31
3.64e-03	8.10	2.35	56.66
3.17e-03	8.30	1.68	58.34
2.76e-03	8.50	1.77	60.10
2.40e-03	8.70	1.98	62.08
2.09e-03	8.90	2.09	64.17
1.82e-03	9.10	1.93	66.10
1.59e-03	9.30	1.41	67.51

1.38e-03	9.50	1.26	68.77
1.20e-03	9.70	1.20	69.97
1.05e-03	9.90	1.75	71.72
9.11e-04	10.10	1.92	73.64
7.93e-04	10.30	1.77	75.41
6.91e-04	10.50	1.59	77.00
6.01e-04	10.70	1.97	78.97
5.23e-04	10.90	1.70	80.67
2.44e-04	12.00	19.33	100.00

Grain Size Breakdown

%	%	%	%	%
Gravel	Sand	Silt	Clay	Mud
0.06	2.62	51.62	45.69	97.32

Statistical Measures

Mean (PHI)	Standard Deviation (PHI)	Kurtosis (No Dim.)	Skewness (No Dim.)
8.13	2.56	2.03	0.17

97RUSTICO-O12-R12,RD011294,   DR. CARL AMOS
,00409,   SYRINGE CORE, RUSTICO BAY, PEI
                        MILLIMETER EQUIVALENTS
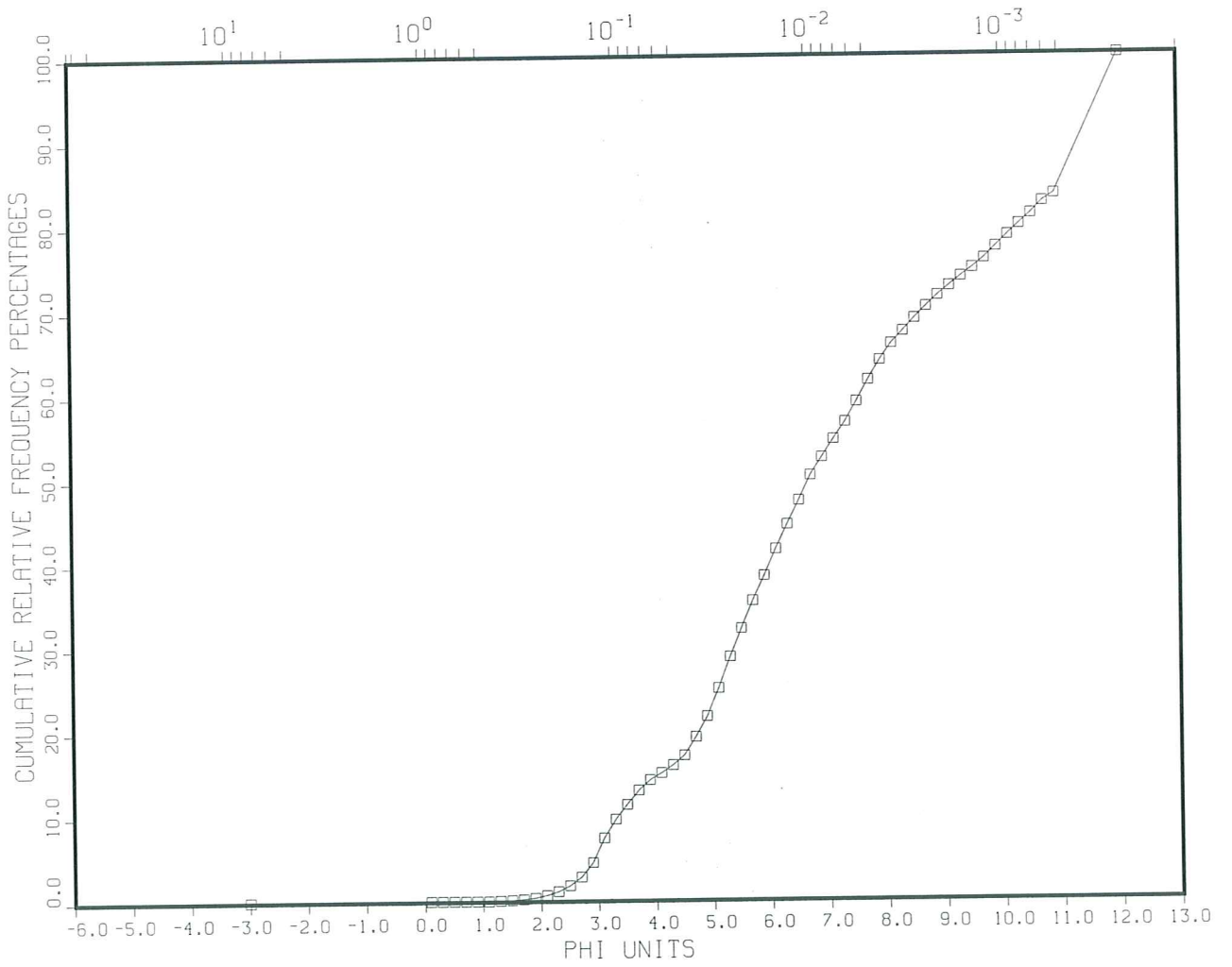
Calculation Results for
The Sample with the Identifier:

V4.0
27:10:1997
11294
57
97RUSTICO-012-R12
97RUSTICO
960030
DR. CARL AMOS
SYRINGE CORE, RUSTICO BAY, PEI
RD011294
SWF00409
0.00000000000000E+0000
0.00000000000000E+0000
0
0
0
0
0
0
0
0
53114
012-R12
012-R12
SYRINGE
CORE
46:26.01
-63:18.55
2.50
n lines for future expansion
#

Results

Midpoints		Relative Frequency	Cumulative Frequency
MM	PHI	Percentages	Percentages
8.00e+00	-3.00	0.10	0.10
9.33e-01	0.10	0.00	0.10
8.12e-01	0.30	0.00	0.10

7.07e-01	0.50	0.00	0.10
6.16e-01	0.70	0.00	0.10
5.36e-01	0.90	0.00	0.10
4.67e-01	1.10	0.00	0.10
4.06e-01	1.30	0.04	0.14
3.54e-01	1.50	0.06	0.20
3.08e-01	1.70	0.09	0.29
2.68e-01	1.90	0.16	0.46
2.33e-01	2.10	0.29	0.75
2.03e-01	2.30	0.45	1.20
1.77e-01	2.50	0.68	1.88
1.54e-01	2.70	1.00	2.88
1.34e-01	2.90	1.72	4.60
1.17e-01	3.10	2.90	7.50
1.02e-01	3.30	2.18	9.69
8.84e-02	3.50	1.74	11.43
7.69e-02	3.70	1.68	13.11
6.70e-02	3.90	1.23	14.33
5.83e-02	4.10	0.81	15.14
5.08e-02	4.30	0.91	16.05
4.42e-02	4.50	1.14	17.19
3.85e-02	4.70	2.17	19.36
3.35e-02	4.90	2.44	21.80
2.92e-02	5.10	3.31	25.11
2.54e-02	5.30	3.75	28.86
2.21e-02	5.50	3.35	32.20
1.92e-02	5.70	3.28	35.48
1.67e-02	5.90	3.00	38.49
1.46e-02	6.10	3.18	41.66
1.27e-02	6.30	2.91	44.58
1.10e-02	6.50	2.85	47.43
9.62e-03	6.70	2.98	50.41
8.37e-03	6.90	2.15	52.57
7.29e-03	7.10	2.16	54.73
6.35e-03	7.30	2.03	56.76
5.52e-03	7.50	2.39	59.15
4.81e-03	7.70	2.54	61.69
4.19e-03	7.90	2.33	64.02
3.64e-03	8.10	1.97	65.99
3.17e-03	8.30	1.45	67.43
2.76e-03	8.50	1.50	68.93
2.40e-03	8.70	1.37	70.31
2.09e-03	8.90	1.28	71.59
1.82e-03	9.10	1.12	72.71
1.59e-03	9.30	1.08	73.79

```
1.38e-03   9.50     1.00     74.79
1.20e-03   9.70     1.11     75.91
1.05e-03   9.90     1.37     77.28
9.11e-04  10.10     1.37     78.64
7.93e-04  10.30     1.27     79.91
6.91e-04  10.50     1.23     81.13
6.01e-04  10.70     1.42     82.56
5.23e-04  10.90     0.89     83.45
2.44e-04  12.00    16.55    100.00
```

Grain Size Breakdown

% Gravel	% Sand	% Silt	% Clay	% Mud
0.10	14.24	49.69	35.98	85.67

Statistical Measures

Mean (PHI)	Standard Deviation (PHI)	Kurtosis (No Dim.)	Skewness (No Dim.)
7.29	2.91	2.11	0.24

97RUSTICO-013-R13,RDO11295,   DR. CARL AMOS
,00409,   SYRINGE CORE, RUSTICO BAY, PEI
                    MILLIMETER EQUIVALENTS
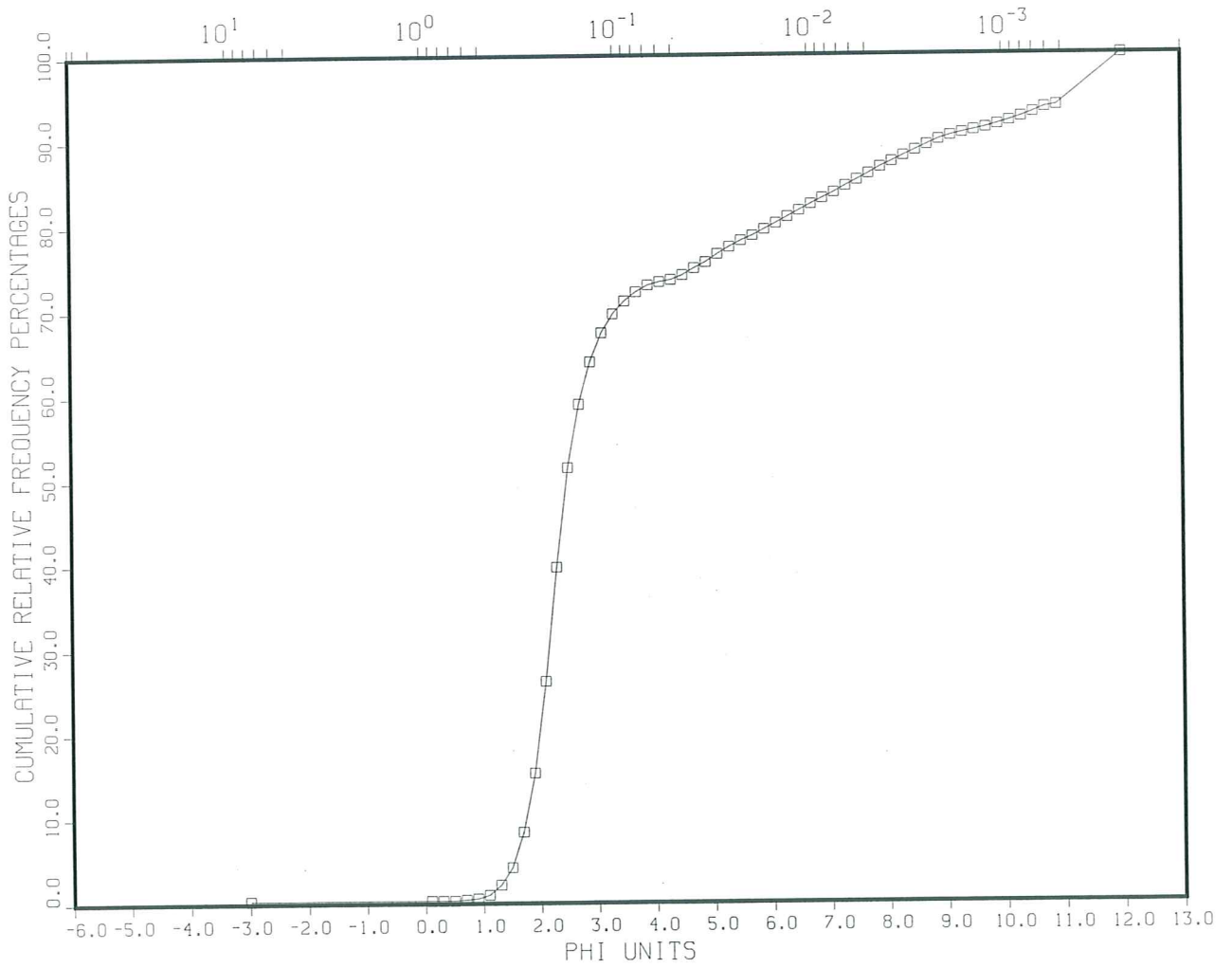
Calculation Results for
The Sample with the Identifier:

V4.0
27:10:1997
11295
57
97RUSTICO-013-R13
97RUSTICO
960030
DR. CARL AMOS
SYRINGE CORE, RUSTICO BAY, PEI
RD011295
SWF00409
0.00000000000000E+0000
0.00000000000000E+0000
0
0
0
0
0
0
0
0
53115
013-R13
013-R13
SYRINGE
CORE
46:26.24
-63:18.34
3.00
n lines for future expansion
#

Results

| Midpoints | | Relative | Cumulative |
MM	PHI	Frequency Percentages	Frequency Percentages
8.00e+00	-3.00	0.34	0.34
9.33e-01	0.10	0.00	0.34
8.12e-01	0.30	0.00	0.34

7.07e-01	0.50	0.00	0.34
6.16e-01	0.70	0.09	0.43
5.36e-01	0.90	0.14	0.58
4.67e-01	1.10	0.41	0.99
4.06e-01	1.30	1.17	2.16
3.54e-01	1.50	2.05	4.21
3.08e-01	1.70	4.18	8.38
2.68e-01	1.90	7.01	15.40
2.33e-01	2.10	10.84	26.24
2.03e-01	2.30	13.46	39.70
1.77e-01	2.50	11.82	51.52
1.54e-01	2.70	7.50	59.02
1.34e-01	2.90	4.96	63.98
1.17e-01	3.10	3.41	67.39
1.02e-01	3.30	2.19	69.58
8.84e-02	3.50	1.51	71.09
7.69e-02	3.70	1.05	72.14
6.70e-02	3.90	0.79	72.93
5.83e-02	4.10	0.38	73.31
5.08e-02	4.30	0.24	73.55
4.42e-02	4.50	0.54	74.09
3.85e-02	4.70	0.80	74.89
3.35e-02	4.90	0.71	75.60
2.92e-02	5.10	0.94	76.55
2.54e-02	5.30	0.83	77.37
2.21e-02	5.50	0.74	78.11
1.92e-02	5.70	0.59	78.70
1.67e-02	5.90	0.73	79.43
1.46e-02	6.10	0.73	80.16
1.27e-02	6.30	0.74	80.90
1.10e-02	6.50	0.74	81.64
9.62e-03	6.70	0.75	82.39
8.37e-03	6.90	0.69	83.08
7.29e-03	7.10	0.68	83.76
6.35e-03	7.30	0.75	84.51
5.52e-03	7.50	0.70	85.21
4.81e-03	7.70	0.72	85.93
4.19e-03	7.90	0.78	86.71
3.64e-03	8.10	0.63	87.34
3.17e-03	8.30	0.68	88.01
2.76e-03	8.50	0.63	88.65
2.40e-03	8.70	0.64	89.28
2.09e-03	8.90	0.62	89.90
1.82e-03	9.10	0.44	90.35
1.59e-03	9.30	0.33	90.68

1.38e-03	9.50	0.29	90.97
1.20e-03	9.70	0.30	91.27
1.05e-03	9.90	0.38	91.65
9.11e-04	10.10	0.41	92.07
7.93e-04	10.30	0.46	92.53
6.91e-04	10.50	0.51	93.04
6.01e-04	10.70	0.58	93.62
5.23e-04	10.90	0.23	93.84
2.44e-04	12.00	6.16	100.00

Grain Size Breakdown

%	%	%	%	%
Gravel	Sand	Silt	Clay	Mud
0.34	72.59	13.78	13.29	27.07

Statistical Measures

Mean (PHI)	Standard Deviation (PHI)	Kurtosis (No Dim.)	Skewness (No Dim.)
3.97	3.01	4.25	1.51

97RUSTICO-014-R14,RDO11296,   DR. CARL AMOS
,00409,   SYRINGE CORE, RUSTICO BAY, PEI
                             MILLIMETER EQUIVALENTS
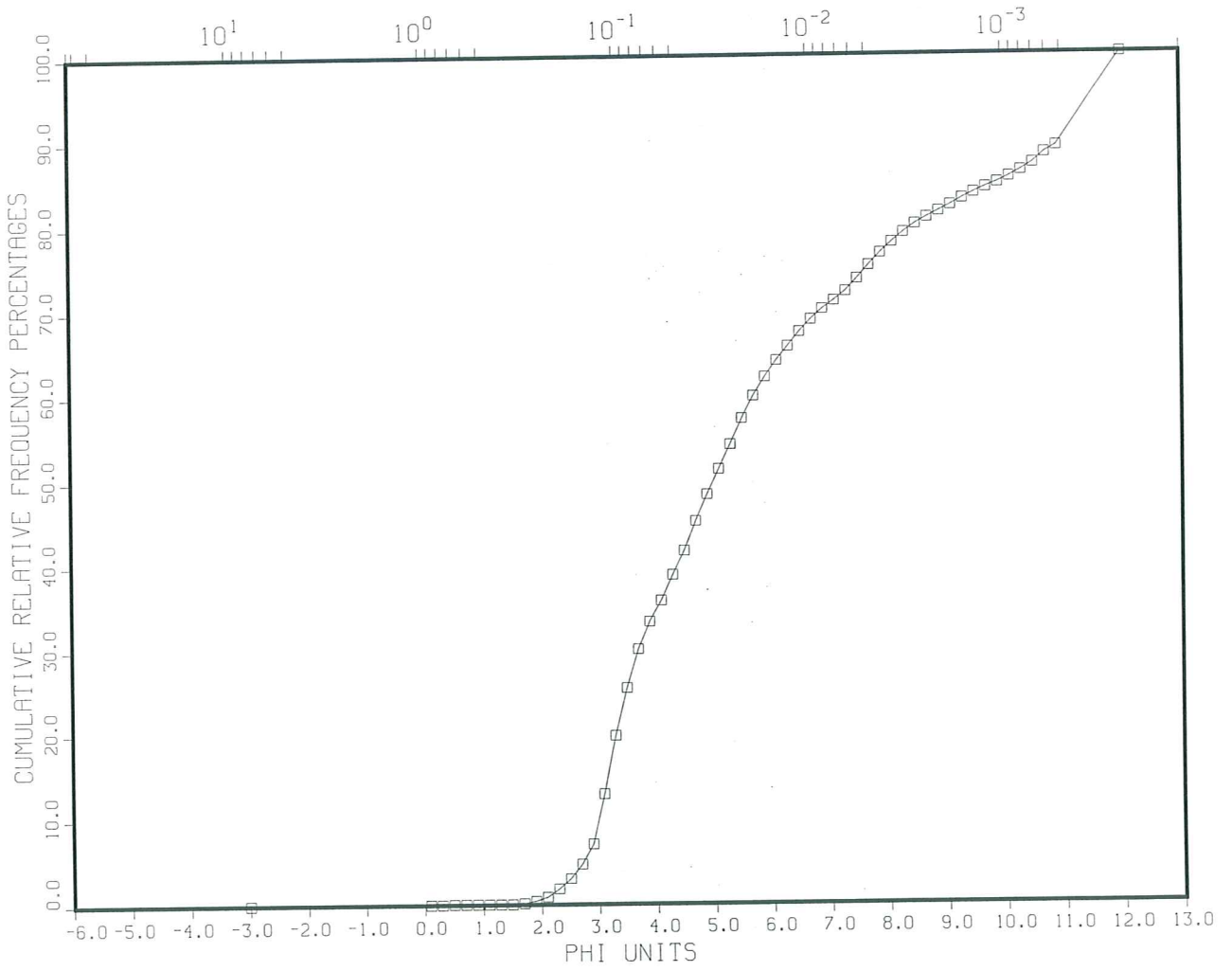
Calculation Results for
The Sample with the Identifier:

V4.0
27:10:1997
11296
57
97RUSTICO-014-R14
97RUSTICO
960030
DR. CARL AMOS
SYRINGE CORE, RUSTICO BAY, PEI
RD011296
SWF00409
0.00000000000000E+0000
0.00000000000000E+0000
0
0
0
0
0
0
0
0
53116
014-R14
014-R14
SYRINGE
CORE
46:26.83
-63:18.11
3.00
n lines for future expansion
#

Results

Midpoints		Relative	Cumulative
		Frequency	Frequency
MM	PHI	Percentages	Percentages
8.00e+00	-3.00	0.00	0.00
9.33e-01	0.10	0.00	0.00
8.12e-01	0.30	0.01	0.01

7.07e-01	0.50	0.04	0.05
6.16e-01	0.70	0.00	0.05
5.36e-01	0.90	0.00	0.05
4.67e-01	1.10	0.00	0.05
4.06e-01	1.30	0.00	0.05
3.54e-01	1.50	0.00	0.05
3.08e-01	1.70	0.11	0.16
2.68e-01	1.90	0.27	0.43
2.33e-01	2.10	0.47	0.89
2.03e-01	2.30	0.97	1.86
1.77e-01	2.50	1.19	3.05
1.54e-01	2.70	1.68	4.73
1.34e-01	2.90	2.35	7.09
1.17e-01	3.10	5.88	12.97
1.02e-01	3.30	6.84	19.80
8.84e-02	3.50	5.67	25.47
7.69e-02	3.70	4.64	30.11
6.70e-02	3.90	3.25	33.36
5.83e-02	4.10	2.48	35.85
5.08e-02	4.30	3.04	38.89
4.42e-02	4.50	2.83	41.72
3.85e-02	4.70	3.51	45.23
3.35e-02	4.90	3.17	48.40
2.92e-02	5.10	2.99	51.39
2.54e-02	5.30	2.88	54.27
2.21e-02	5.50	3.07	57.33
1.92e-02	5.70	2.62	59.95
1.67e-02	5.90	2.25	62.21
1.46e-02	6.10	1.94	64.15
1.27e-02	6.30	1.69	65.83
1.10e-02	6.50	1.69	67.52
9.62e-03	6.70	1.43	68.95
8.37e-03	6.90	1.23	70.18
7.29e-03	7.10	0.99	71.17
6.35e-03	7.30	1.07	72.24
5.52e-03	7.50	1.49	73.73
4.81e-03	7.70	1.55	75.28
4.19e-03	7.90	1.43	76.71
3.64e-03	8.10	1.25	77.97
3.17e-03	8.30	1.13	79.09
2.76e-03	8.50	0.98	80.08
2.40e-03	8.70	0.77	80.85
2.09e-03	8.90	0.71	81.56
1.82e-03	9.10	0.71	82.27
1.59e-03	9.30	0.76	83.03

1.38e-03	9.50	0.67	83.70
1.20e-03	9.70	0.60	84.30
1.05e-03	9.90	0.54	84.84
9.11e-04	10.10	0.65	85.49
7.93e-04	10.30	0.73	86.22
6.91e-04	10.50	0.86	87.08
6.01e-04	10.70	1.19	88.27
5.23e-04	10.90	0.78	89.05
2.44e-04	12.00	10.95	100.00

Grain Size Breakdown

% Gravel	% Sand	% Silt	% Clay	% Mud
0.00	33.36	43.35	23.29	66.64

Statistical Measures

Mean (PHI)	Standard Deviation (PHI)	Kurtosis (No Dim.)	Skewness (No Dim.)
6.01	2.94	2.54	0.86

97RUSTICO-O15-R15,RDO11297,   DR. CARL AMOS
\# ,OO409,   SYRINGE CORE, RUSTICO BAY, PEI
                        MILLIMETER EQUIVALENTS
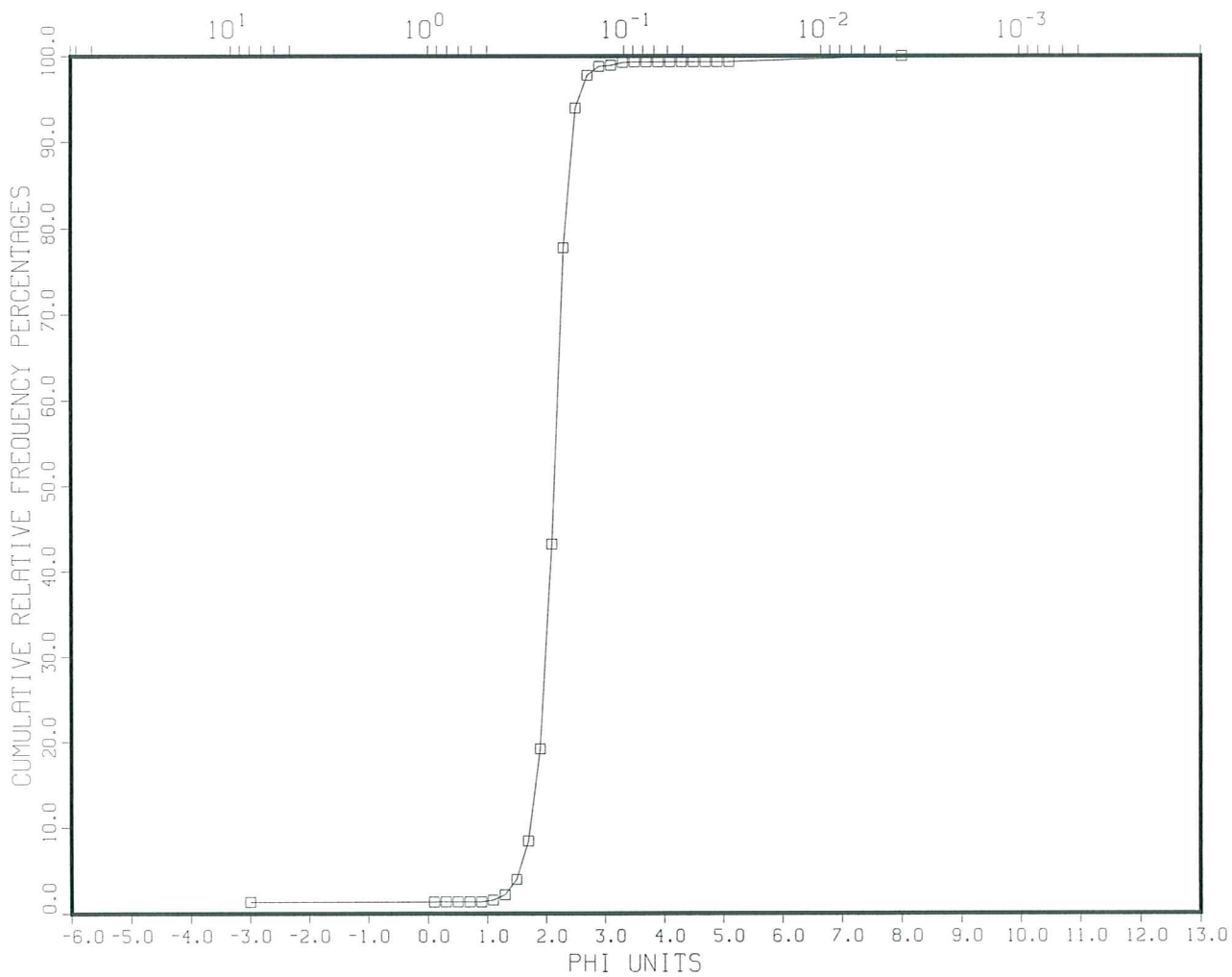
Calculation Results for
The Sample with the Identifier:

V4.0
27:10:1997
11297
29
97RUSTICO-015-R15
97RUSTICO
960030
DR. CARL AMOS
SYRINGE CORE, RUSTICO BAY, PEI
RD011297
SWF00409
0.00000000000000E+0000
0.00000000000000E+0000
0
0
0
0
0
0
0
0
53117
015-R15
015-R15
SYRINGE
CORE
46:27.19
-63:17.70
1.50
n lines for future expansion
#

Results

Midpoints		Relative	Cumulative
		Frequency	Frequency
MM	PHI	Percentages	Percentages
8.00e+00	-3.00	1.32	1.32
9.33e-01	0.10	0.01	1.33
8.12e-01	0.30	0.02	1.35

7.07e-01	0.50	0.00	1.35
6.16e-01	0.70	0.00	1.35
5.36e-01	0.90	0.00	1.35
4.67e-01	1.10	0.20	1.55
4.06e-01	1.30	0.61	2.16
3.54e-01	1.50	1.78	3.94
3.08e-01	1.70	4.48	8.42
2.68e-01	1.90	10.75	19.17
2.33e-01	2.10	24.00	43.17
2.03e-01	2.30	34.57	77.74
1.77e-01	2.50	16.20	93.94
1.54e-01	2.70	3.83	97.77
1.34e-01	2.90	1.02	98.80
1.17e-01	3.10	0.12	98.92
1.02e-01	3.30	0.32	99.24
8.84e-02	3.50	0.09	99.33
7.69e-02	3.70	0.00	99.33
6.70e-02	3.90	0.00	99.33
5.83e-02	4.10	0.00	99.33
5.08e-02	4.30	0.00	99.33
4.42e-02	4.50	0.00	99.33
3.85e-02	4.70	0.00	99.33
3.35e-02	4.90	0.00	99.33
2.92e-02	5.10	0.00	99.33
3.91e-03	8.00	0.67	100.00
2.44e-04	12.00	0.00	100.00

Grain Size Breakdown

% Gravel	% Sand	% Silt	% Clay	% Mud
1.32	98.01	0.67	0.00	0.67

Statistical Measures

Mean (PHI)	Standard Deviation (PHI)	Kurtosis (No Dim.)	Skewness (No Dim.)
2.19	0.81	39.35	-0.98